

Inaugural dissertation
for
obtaining the doctoral degree
of the
Combined Faculty of Mathematics, Engineering and Natural Sciences
of the
Ruprecht - Karls - University
Heidelberg

Presented by
M.Sc. Malte Simon
born in: Stuttgart, Germany
Oral examination: 12th of July, 2022

Identification of epigenetic T cell traits
in murine and human tissues
under homeostasis

Referees: Prof. Dr. Benedikt Brors
Prof. Dr. Markus Feuerer

Abstract

T cells have a major role in the adaptive immune response, where they eliminate infectious agents and malignant cells by specific recognition of non-self antigens. Besides this general function in the immune response, T cells also have diverse tissue-specific functions. This has been well described for regulatory T cells, which are not only essential for the control of the immune response, but are also involved in maintaining tissue homeostasis. However, most evidence comes from bulk experiments in mice resulting in limited resolution of T cell subsets and it is unknown whether Treg cells with a similar tissue adaptation program also exist in humans. Especially epigenetic adaptations underlying observed transcriptional changes in T cells from lymphoid and peripheral tissues remain incompletely understood.

In this work, I analyzed single cell ATAC sequencing data of flow-sorted CD4⁺ and CD8⁺ T cells from lymphoid and non-lymphoid tissues to investigate the molecular programs driving T cell adaptation to peripheral tissues. The availability of both human and murine samples allowed me to describe commonalities and differences in their T cell biology. In addition, I used these T cell atlases under homeostasis together with several T cell datasets from tumors to gain insights on shared chromatin accessibility changes in the tumor microenvironment.

My analysis showed the presence of human tissue Treg cells that have many commonalities with their murine counterparts. These include a conserved epigenetic signature with enriched footprint of transcription factor BATF. I further identified potential tissue Treg precursor cells in human peripheral blood and mouse spleen sharing increased chromatin accessibility at the locus encoding chemokine receptor CCR8. While murine tissue Treg cells are T helper 2 cell-biased, human Treg cells in peripheral tissues more closely resemble T follicular helper cells in their ATAC profile. Within the CD8⁺ T cell compartment, I showed that murine and human peripheral tissues harbor a population of PD1⁺TOX⁺ CD8⁺ T cells with epigenomes denoting a concurrent activation and exhaustion state. PD1⁺TOX⁺ CD8⁺ T cells shared chromatin features of tissue adaptation and BATF dependence with tissue Treg cells. I further contextualized epigenetic adaptation observed in tissue-repair associated Treg cells in a comprehensive view on immune cells that suggests commonalities not only with CD8⁺ T cells and innate lymphoid cells, but also with several myeloid cell subsets. Eventually, through comparison of T cells from healthy and tumor tissues, I showed that Treg and PD1⁺TOX⁺ CD8⁺ T cells from tumors also maintain a tissue adaptation program.

Zusammenfassung

T-Zellen spielen durch ihre gezielte Erkennung und Eliminierung körperfremder Antigene eine fundamentale Rolle in der adaptiven Immunantwort. Daneben erfüllen sie verschiedene Funktionen zur Aufrechterhaltung der Gewebekomöostase. Dies trifft insbesondere auf regulatorische T-Zellen zu, für die eine Vielzahl gewebespezifischer Funktionen neben ihrer allgemeinen immunsuppressiven Funktion gefunden wurde. Bisherige Forschungsarbeit zu T-Zellen unter Homöostase basiert jedoch hauptsächlich auf Bulk-Sequenzierungsdaten von Mäusen, welche eine limitierte Auflösung zellulärer Untergruppen aufweisen. Zudem ist bisher unbekannt, wie ähnlich epigenetische Anpassungen an periphere Gewebe zwischen murinen und humanen regulatorischen T-Zellen sind.

Diese Arbeit untersucht anhand von ATAC-Sequenzierungsdaten epigenetische Programme von $CD4^+$ und $CD8^+$ T-Zellen, welche deren Anpassung an periphere Gewebe steuern. Durch die Verfügbarkeit von humanen und murinen Proben konnte ich Gemeinsamkeiten und Unterschiede in deren T-Zell-Biologie beschreiben. Darüber hinaus konnte ich durch einen Vergleich von T-Zellen unter Homöostase und Tumor-T-Zellen Erkenntnisse über gemeinsame Veränderungen der Chromatinverfügbarkeit gewinnen.

In dieser Arbeit konnte ich menschliche Gewebe-Treg-Zellen charakterisieren, die eine gemeinsame epigenetische Signatur und Aktivität des Transkriptionsfaktors BATF mit Maus-Gewebe-Treg-Zellen teilen. Weiterhin habe ich potenzielle Vorläufer von Gewebe-Treg-Zellen im peripheren Blut des Menschen und in der Milz von Mäusen identifiziert, die sich unter anderem durch eine erhöhte Chromatinverfügbarkeit im Chemokinrezeptor CCR8-Lokus auszeichnen. Gewebe-Treg-Zellen der Maus ähneln in ihrem Chromatinprofil Typ-2-T-Helferzellen, wohingegen menschliche Treg-Zellen eine höhere Übereinstimmung zum ATAC-Profil von follikulären T-Helferzellen aufweisen. Eine Analyse des peripheren $CD8^+$ T-Zellkompartiments ergab, dass beide Spezies eine Population von $PD1^+TOX^+$ $CD8^+$ T-Zellen beherbergen, deren Epigenom auf einen gleichzeitigen Aktivierungs- und Erschöpfungszustand hindeutet. $PD1^+TOX^+$ $CD8^+$ T-Zellen teilen sowohl Chromatinmerkmale der Gewebeanpassung als auch Abhängigkeit von Transkriptionsfaktor BATF mit Gewebe-Treg-Zellen. Durch die Betrachtung von Einzelzell-Atlanten humaner und muriner Immunzellen konnte ich zeigen, dass auch verschiedene Zelltypen des myeloischen Kompartiments ein epigenetisches Anpassungsprogramm an einen Aufenthalt in peripherem Gewebe vorweisen. Schließlich ergab ein Vergleich von T-Zellen aus gesundem und Tumorgewebe, dass Treg- und $PD1^+TOX^+$ $CD8^+$ T-Zellen aus Tumoren ihre epigenetische Adaptation an Gewebe beibehalten.

Contents

1	Introduction	1
1.1	The immune system	1
1.1.1	Innate immunity	1
1.1.2	Adaptive immunity	2
1.2	Regulation of the immune system	4
1.2.1	CD4 ⁺ regulatory T cells	4
1.2.2	CD8 ⁺ regulatory T cells	6
1.2.3	Role of regulatory T cells in tumor tissue	7
1.3	Origin and development of the immune system	8
1.3.1	The hematopoietic tree	8
1.3.2	T cell education	9
1.3.3	Epigenetics and the role of chromatin accessibility	11
1.3.4	Development of Treg cells	13
1.3.5	T cell exhaustion	14
1.4	Tissue-specific functions of immune cells	15
1.4.1	Klrg1 ⁺ ST2 ⁺ tissue Treg population	17
1.5	Single-cell sequencing	18
1.5.1	Single-cell chromatin accessibility sequencing	20
1.6	Aims of the thesis	21
2	Methods	25
2.1	scATAC-seq of murine and human immune cells	25
2.2	Preprocessing of scATAC-seq data	26
2.3	Gene activity scores	28
2.4	Peak and gene activity module scores	28
2.5	chromVAR transcription factor activity	29
2.6	Cell clustering	29
2.7	Peak calling	30
2.8	Detection of differential chromatin accessibility	30
2.9	Generation of bigWig tracks	30
2.10	Homer transcription factor motif analysis	30
2.11	Trajectory analysis	31
2.12	Peak region liftOver and cross-species comparison	31
2.13	Comparison of scATAC-seq and ChIP-seq data	32
2.14	Reference-based cell annotation	32
3	Results	33
3.1	Characterization of CD4 ⁺ regulatory T cells in humans and mice	33
3.1.1	Identification of tisTregST2 cells in healthy murine tissues	34

3.1.2	Dependence of tisTreg cells in the colon on microbiota	38
3.1.3	tisTreg cells in healthy human tissues show Tfh-bias	41
3.1.4	Determination of a conserved tisTreg epigenetic signature	45
3.1.5	tisTreg cell development and identification of precursor cells	47
3.1.6	Treg cells in tumors also have a tisTreg phenotype	51
3.2	Chromatin accessibility landscape of murine and human CD8 ⁺ T cells	53
3.2.1	Effector-like PD1 ⁺ TOX ⁺ CD8 ⁺ T cells share features with tisTreg cells in healthy murine tissues	53
3.2.2	PD1 ⁺ TOX ⁺ CD8 ⁺ T cell activation program is independent of microbiota in the colon	56
3.2.3	Effector-like PD1 ⁺ TOX ⁺ CD8 ⁺ T cells are present in healthy human tissues	57
3.2.4	Comparison of PD1 ⁺ TOX ⁺ CD8 ⁺ T cells between human healthy and tumor tissue	60
3.3	Expanding the view: an immune cell atlas of tissue-specific programs	63
3.3.1	tisTreg signature identifies innate immune cells with potential repair function in healthy murine tissues	63
3.3.2	Characterization of immune cells with potential tissue-specific roles in healthy human tissues	67
4	Discussion	71
4.1	scATAC-seq confirms tisTregST2 phenotype in mice	71
4.2	tisTregST2 cells develop independently from microbiota in the colon	72
4.3	Identification and characterization of human tisTreg cells	72
4.4	<i>CCR8</i> expression identifies tisTreg cells and their precursors	74
4.5	Clinical significance of Treg cells in the tumor	75
4.6	PD1 ⁺ TOX ⁺ CD8 ⁺ T cells share tissue-adaptation features with tisTreg cells	76
4.7	Comparison of PD1 ⁺ TOX ⁺ CD8 ⁺ T cells with reported CD8 ⁺ T cell subsets	77
4.8	Tissue regenerative potential of CD8 ⁺ T cells	78
4.9	PD1 ⁺ TOX ⁺ CD8 ⁺ T cells from tumors and healthy peripheral tissues are similar	79
4.10	Immune cell atlas reveals shared features of tissue adaptation	80
4.11	Role of BATF in immune cell development	81
4.12	Limitations	82
4.13	Outlook	84
5	References	86
6	Supplement	100
6.1	Supplementary Figures	100
6.2	Supplementary Tables	121

7	List of Abbreviations	125
8	Acknowledgment	128

List of Figures

1	Treg cell inhibitory mechanisms	6
2	The hematopoietic tree	9
3	T cell development in the thymus	11
4	Epigenetic regulation of the <i>FOXP3</i> gene locus	13
5	Dysfunctional differentiation model	15
6	Non-immunological functions of the immune system	17
7	Increase in throughput of scRNA-seq technologies over time	19
8	Single-cell strategies for ATAC-seq	21
9	Project overview	23
10	Cross-species region comparison	32
11	Mouse CD4 ⁺ T cell atlas	36
12	Mouse tisTregST2 peakset	37
13	Mouse gnotobiotic CD4 ⁺ T cell atlas	39
14	tisTregST2 evolve independently from microbiota	40
15	Human CD4 ⁺ T cell atlas	43
16	Human tisTreg peakset	44
17	Human Tfh-like Treg cells support wound healing	45
18	Species-conserved tisTreg signature	47
19	tisTreg development	50
20	Treg cells in tumors share similarity with tisTregST2 cells in healthy tissues	52
21	Mouse CD8 ⁺ T cell atlas	55
22	PD1 ⁺ TOX ⁺ CD8 ⁺ T cells are independent from microbiota	57
23	Human CD8 ⁺ T cell atlas	59
24	Human HCC T cell atlas	61
25	Signature comparison	62
26	Mouse immune cell atlas	65
27	Core tisTregST2 signature peak accessibility	66
28	Confirmation of tisTregST2 marker <i>Ccr8</i>	67
29	Human immune cell atlas	69
S1	Mouse SPF CD4 ⁺ T cell quality control	100
S2	Mouse SPF CD4 ⁺ T cell markers and signatures	101
S3	Mouse gnotobiotic CD4 ⁺ T cell quality control	102
S4	Mouse gnotobiotic CD4 ⁺ T cell markers and signatures	103
S5	Human CD4 ⁺ T cell quality control	104
S6	Human CD4 ⁺ T cell marker genes	105
S7	Th2 transcription factor gene activity	106
S8	Mouse SPF CD8 ⁺ T cell quality control	107
S9	Mouse SPF CD8 ⁺ T cell markers	108

S10	Mouse gnotobiotic CD8 ⁺ T cell quality control	109
S11	Independence of effector CD8 ⁺ T cells from microbiota	110
S12	Human CD8 ⁺ T cell quality control	111
S13	Human CD8 ⁺ T cell markers and cell type annotations	112
S14	Human HCC CD3 ⁺ T cell quality control	113
S15	Human HCC CD3 ⁺ T cell markers and cell type annotations	114
S16	CD8 ⁺ T cell ATAC-profiles at exhaustion marker genes	115
S17	Mouse immune cell atlas quality control	116
S18	Confirmation of <i>Ccr8</i> ⁺ Treg cell marker in the mouse	117
S19	Mouse immune cell atlas cell type annotation and markers	118
S20	Human immune cell atlas quality control	119
S21	Human immune cell atlas cell type annotation and markers	120

List of Tables

S1	Dataset overview	121
S2	Software used for data analysis	123
S3	R packages used for data analysis	123
S4	Embeddings and resolutions per dataset	124

1 Introduction

1.1 The immune system

Vertebrates are under a constant threat stemming from foreign antigens such as microbes, viruses and toxins, from which they need to defend themselves effectively to maintain homeostasis (Marshall et al., 2018). Besides anatomical barriers such as skin and mucosa, there is a complex system of cells and molecules, collectively referred to as the immune system, which is dedicated to clear foreign antigens and limit the damage they are causing to the body. On a broad scale, the immune system can be divided into two major arms, the innate immunity and the adaptive immunity (Marshall et al., 2018). If there is a breach in the anatomical barrier, the innate immune system is the first to react to invading pathogens. Innate immune cells as well as a set of plasma proteins called the complement system together respond immediately but in a non-adaptive way. With some delay, the cells of the adaptive immune system are activated, which are able to respond to the encountered foreign antigens in a highly specific manner (Murphy and Weaver, 2018, p. 8). Innate and adaptive immunity work in a complementary fashion that allows efficient clearance of pathogens (Turvey and Broide, 2010; Bonilla and Oettgen, 2010).

1.1.1 Innate immunity

Innate immunity is composed of four layers, each of which impedes pathogenic infections. First, epithelial cells present on all body surfaces form a tight anatomic barrier that prevents foreign antigens from entering the organism. Second, physiologic processes including temperature regulation, acidic pH and molecules such as complement proteins inhibit or kill pathogens. On the third level, certain immune cells are able to phagocytose and degrade microbes. Finally, an inflammatory barrier is formed through leakage of vascular fluid in infected areas, which contains proteins with antibacterial activity (Marshall et al., 2018; Turvey and Broide, 2010; Bonilla and Oettgen, 2010).

The cellular component of innate immunity is able to mount a rapid defense response to invading pathogens. This is achieved by pattern recognition receptors (PRRs) present on innate immune cells, which recognize a range of molecular structures that are frequently present on pathogens, but not on cells of the own body. An example of pathogen-associated molecular patterns are lipopolysaccharides, which are part of bacterial cell walls and not employed by eukaryotic cells (Marshall et al., 2018). Furthermore, PRRs recognize several molecules such as ATP which are not present in extracellular space under homeostatic conditions (Murphy and Weaver, 2018, p. 9). Of note, PRRs are germline-encoded and do not change throughout the lifespan of an organism resulting in a limited capacity to encounter foreign antigens (Medzhitov and Janeway, 2000; Lanier, 2005). Dependent on the cell type, activation of PRRs entails processes such as phagocytosis,

cytokine production or cell locomotion (Netea et al., 2020).

Cells of the innate immune response comprise monocytes, macrophages, granulocytes, innate lymphoid cells (ILCs) and dendritic cells. Monocytes differentiate into macrophages or dendritic cells once they enter tissues from the bloodstream. Monocytes, macrophages, dendritic cells and granulocytes are also referred to as phagocytes due to their ability to ingest and kill pathogens (Murphy and Weaver, 2018, pp. 9, 97). Besides phagocytosis, macrophages and dendritic cells act as important messengers to the adaptive immune system via antigen presentation (Turvey and Broide, 2010). Granulocytes are further subdivided into neutrophils, eosinophils, basophils and mast cells. Neutrophils can release granules of bactericidal proteins while eosinophils are well known for their ability to destroy parasites, which are too big to ingest via phagocytosis. Basophils and mast cells both have important roles in the initiation of acute inflammation. Mast cells further release cytokines attracting other immune cells in an early state of infection (Marshall et al., 2018). Eventually, ILCs can be divided into NK cells, which function in the destruction of infected cells or cancer cells, and several other ILC subsets performing immune-regulatory functions via cytokine release (Marshall et al., 2018).

Cytokines are proteins acting as messengers in cell-cell communication. The release of cytokines by innate immune cells is paramount in the attraction of other immune cells to the site of inflammation, their activation, and the initiation of fever (Marshall et al., 2018; Murphy and Weaver, 2018, p. 33).

1.1.2 Adaptive immunity

The adaptive immune system consists of T and B lymphocytes. There are two major differences that set cells from the adaptive immune system apart from innate immune cells. On the one hand, receptors with a huge diversity in their recognized antigens are generated in a process called somatic recombination. This is in sharp contrast to the limited set of germline-encoded PRRs employed by the innate immune response (Medzhitov and Janeway, 2000; Medzhitov, 2009). On the other hand, maintenance of a population of antigen-specific lymphocytes after clearance of a foreign antigen results in an immunologic memory.

T cells are responsible for cell-mediated immunity and can be divided into cytotoxic T cells ($CD8^+$ T cells) and T-helper (Th) cells ($CD4^+$ T cells). Each cell expresses a T-cell receptor (TCR) with unique antigen recognition capability. To become activated, the interaction of the TCR with its cognate antigen presented on a major histocompatibility complex (MHC) molecule is required. There are two known classes of MHC: MHC class I molecules are found on all nucleated cells and present intracellular peptides, thereby reporting the cellular state. MHC class II molecules are only expressed by antigen-presenting cells

including dendritic cells, macrophages and B cells. They present extracellular peptides derived from phagocytosed antigens (Bonilla and Oettgen, 2010; Murphy and Weaver, 2018, pp. 19, 36). While $CD8^+$ T cells are restricted to MHC class I molecules, $CD4^+$ T cells recognize MHC class II molecules (Schmidl et al., 2018). Upon activation, which additionally requires proper signaling via co-stimulatory molecules, naive T cells perform a clonal expansion and differentiate into effector and memory T cells (Fan and Rudensky, 2016; Hwang et al., 2020).

Effector $CD8^+$ T cells contribute to clearance of pathogens in multiple ways: they trigger apoptosis in cells presenting their cognate antigen on the MHC I complex, since these cells likely represent cancer cells or are infected with pathogens such as viruses. Besides, they also activate phagocytes, which can subsequently ingest pathogens and cell debris. Further, they pass on signals to nearby cells via release of cytokines (Bonilla and Oettgen, 2010). While effector $CD8^+$ T cells are short-lived, memory $CD8^+$ T cells persist for a long time even after the infection is resolved. These memory cells allow a fast and efficient response to repeated challenges with the same antigen thus providing long-term protection (Bonilla and Oettgen, 2010; Murphy and Weaver, 2018, pp. 614-615).

On the other hand, naive $CD4^+$ T cells differentiate into various kinds of Th subsets depending on stimulation of their TCR, co-stimulatory molecules, and the cytokine milieu (Schmidl et al., 2018). They do not directly kill pathogens, but rather support and regulate other immune cells through release of specific cytokines. The most abundant and well-described subsets are Th1, Th2 and Th17. The cytokines required for their differentiation are interferon γ ($IFN\gamma$) and interleukin (IL) 12 (Th1 cells), IL-4 (Th2 cells) and transforming growth factor β ($TGF\beta$) (Th17 cells) (Richards et al., 2015). Th1 cells themselves release $IFN\gamma$, which mainly increases phagocytic activity of macrophages and anti-viral responses in other cells and promotes B cell differentiation. Together, these effects support the defense against intracellular pathogens. Th2 cells are specialized in directing immune responses against parasitic infections. They release interleukins 4, 5, and 13 resulting in the attraction of eosinophils and mast cells and immunoglobulin (Ig) E production in B cells. The release of IL-17 marks the Th17 response, which has pro-inflammatory effects such as proliferation and recruitment of neutrophils and is geared towards eradication of extracellular pathogens (Marshall et al., 2018; Weaver et al., 2013). Similar to $CD8^+$ T cells, a small population of memory $CD4^+$ T cells persists after an infection, whereas effector $CD4^+$ T cells die.

B cells form the second pillar of adaptive immunity by conferring humoral immunity. Like T cells, they also have receptors with unique antigen-recognition capability. However, B cells can directly interact with antigens without the need for mediating antigen-presenting cells. Once activated, B cells proliferate and differentiate into plasma cells or memory B cells. The former is able to produce large amounts of antibodies, which bind to ex-

tracellular pathogen epitopes. This not only impedes the pathogen's function, but also marks it for destruction. Opsonization improves pathogen clearance by triggering complement activation, phagocytosis and destruction through immune effector cells. Memory B cells can quickly proliferate and differentiate into antibody-producing plasma cells during subsequent exposures to their cognate antigen (Bonilla and Oettgen, 2010; Murphy and Weaver, 2018, pp. 34-35).

1.2 Regulation of the immune system

A tight regulation of the immune system is essential to avoid disease. Overreactions of the immune system (hypersensitivity), targeting self-antigens (autoimmunity), or insufficient reactions (immunodeficiency) can all stem from misregulation. Examples include allergies, which are caused by immune responses against harmless environmental antigens such as pollen; type I diabetes, an autoimmune reaction of the immune system against pancreatic beta cells; or the inability to destroy a tumor due to downregulation of the immune response in the tumor microenvironment (Kay, 2000). Misguided immune responses are also the cause for many chronic inflammatory diseases such as rheumatoid arthritis and asthma (Marshall et al., 2018).

During maturation of adaptive immune cells, autoimmunity is prevented by a strict selection process for lymphocytes that well discriminate self from non-self antigens. In the case of $CD4^+$ T cells, a fraction of self-reactive cells can also develop into regulatory T (Treg) cells with an important role in immune regulation (Kronenberg and Rudensky, 2005). Similarly, populations of other immune cell types with regulatory function have been described (Mauri and Bosma, 2012; Shimokawa et al., 2020; Fleming and Mosser, 2011).

1.2.1 $CD4^+$ regulatory T cells

Treg cells have a key role in immune regulation: they inhibit excessive immune responses and prevent autoimmunity by suppressing immune activity against self-antigens. Besides central tolerance, they also establish peripheral tolerance to harmless foreign antigens (Marshall et al., 2018). Treg cells are characterized by the expression of the transcription factor forkhead box P3 (FOXP3), which is essential for their development, maintenance and function (Fontenot et al., 2003). Their importance has been shown in scurfy mice, which lack a functional *Foxp3* gene entailing Treg cell deficiency, overreactive $CD4^+$ T cells, and development of fatal immune dysregulation (Brunkow et al., 2001; Clark et al., 1999). A similar phenotype is observed in humans that suffer from X-linked neonatal diabetes mellitus, enteropathy and endocrinopathy syndrome (Wildin et al., 2001).

To date, four major mechanism have been described, by which Treg cells exert their

inhibitory function (Vignali et al., 2008; Scott et al., 2021). These are summarized in Figure 1: first, they can release molecules such as IL-10, IL-35 or TGF β , which inhibit effector T cells and suppress their proliferation (Vignali et al., 2008; Collison et al., 2007). Second, Treg cells can trigger apoptosis of effector T cells and NK cells in a perforin and granzyme-dependent mode (Grossman et al., 2004). Third, generation or deprivation of certain molecules by Treg cells causes metabolic disruption. This includes formation of extracellular adenosine by the CD39/CD73 pathway, which leads to suppression of effector T cells by activation of adenosine receptor 2A on their surface (Deaglio et al., 2007). Moreover, cyclic adenosine monophosphate (cAMP) generation and subsequent transfer through gap junctions of responder T cells inhibits their proliferation and IL-2 synthesis (Bopp et al., 2007). IL-2 is a pleiotropic molecule that supports differentiation, maintenance and expansion of multiple immune cell types (Sakaguchi et al., 2008). Since Treg cells express high-affinity IL-2 receptor α -chain (CD25), they also outcompete effector immune cells for IL-2 (Vignali et al., 2008; Ross and Cantrell, 2018). Treg cells also directly modulate dendritic cell (DC) functions: specifically, interaction of CD80/CD86 on DCs with cytotoxic T-lymphocyte antigen-4 (CTLA-4) on Treg cells induces expression of the enzyme indoleamine 2,3-dioxygenase (IDO) in DCs, which has immunosuppressive effects (Fallarino et al., 2003). Eventually, Liang et al. (2008) showed that interaction of lymphocyte-activation gene 3 (LAG3) with MHC class II molecules on DCs prevents their maturation and reduces their immunostimulatory function.

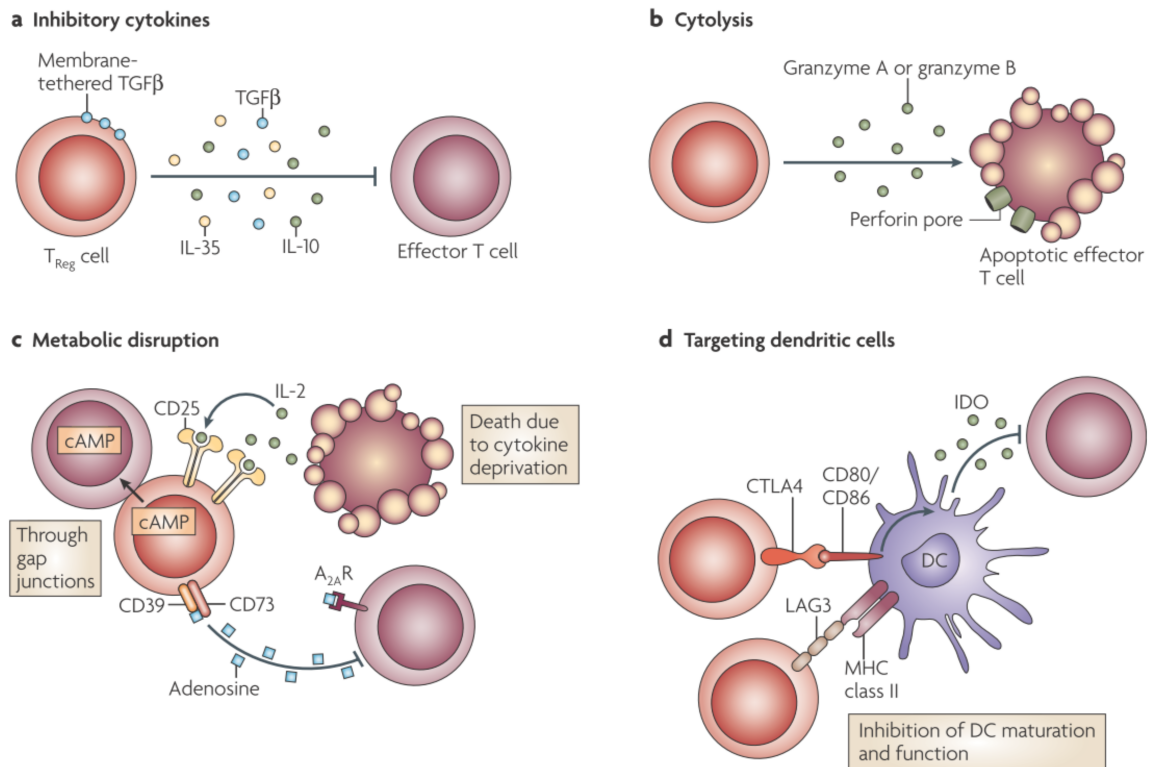


Figure 1: Treg cell inhibitory mechanisms. Treg cells have several functions that result in downregulation of the immune system. **a** Release of inhibitory cytokines. **b** Direct killing of other immune cells through release of perforins and granzymes. **c** Deprivation of molecules required for immune effector cell function and survival such as IL-2, cAMP and adenosine receptor 2A-mediated inhibition. **d** Modulation of DC development and function through inhibitory receptors such as LAG3 or induction of immunosuppressive IDO. Reprinted from Vignali et al. (2008), Copyright © 2008 provided by Springer Nature and Copyright Clearance Center.

Several Treg cell subsets have been described including thymus-derived (tTreg), peripheral (pTreg) and induced (iTreg) Treg cells. These subsets mainly differ in their developmental paths. While tTreg cells fully mature in the thymus, pTreg cells differentiate from conventional $CD4^+$ T (Tconv) cells in peripheral tissues. Together, tTreg and pTreg cells are also called natural Treg cells due to their natural occurrence, which sets them apart from iTreg cells that can be induced from Tconv cells *in-vitro*. Although iTreg cells have many similarities with natural Treg cells, their phenotype is less stable (Ohkura and Sakaguchi, 2020).

1.2.2 $CD8^+$ regulatory T cells

Besides Treg cells, there are other immune cells with immune-regulatory functions. Among murine $CD8^+$ T cells, a population of $CD122^+$ (IL-2 receptor β) cells with both memory and regulatory phenotype has been described (Rifa'i et al., 2004; Akane et al., 2016; Liu et al., 2015). Similar to Treg cells, $CD8^+CD122^+$ T cells can prevent autoimmunity and alloimmune responses. For example, in a rodent type I diabetes model, it has recently

been shown that $CD8^+CD122^+$ T cells, but not Treg cells, suppress the autoimmune disease (Shimokawa et al., 2020). In resemblance to Treg cells, $CD8^+CD122^+$ T lymphocytes rely on multiple suppressive mechanisms including production of inhibitory molecules (IL-10, $TGF\beta 1$), induction of apoptosis via Fas-FasL interaction, or modification of other T cells such as control of IL-17 production in $CD4^+$ T cells (Liu et al., 2015; Akane et al., 2016). The human counterpart to murine $CD8^+CD122^+$ T cells are $CD8^+CXCR3^+$ T cells (Shi et al., 2009). To date it is still unclear in which situations these cells function as regulatory T cells, and whether they can be induced *in-vitro* similarly to iTreg cells (Liu et al., 2015).

1.2.3 Role of regulatory T cells in tumor tissue

Next to pathogens, cancer cells can serve as another source of foreign antigen, since alterations in their genome can lead to expression of aberrant proteins or ectopic expression. Peptides presented by these cells may represent neoantigens that can be detected by the immune system. Since this causes their destruction by effector immune cells, a selective pressure is applied to cancer cells towards mechanisms evading immune surveillance. One such mechanism is the recruitment of Treg cells through production of chemokines. In multiple tumor types, increased CCL5 expression by tumor cells has been observed. This results in preferential recruitment of nTreg cells, which have high expression of the corresponding receptor CCR5 (Velasco-Velázquez et al., 2014; Singh et al., 2018; Chang et al., 2012). Another mechanism involves elevated IL-10 and $TGF\beta$ levels in the tumor microenvironment (TME) promoting pTreg cell differentiation from peripheral naive $CD4^+$ T cells (Sato et al., 2011; Mocellin et al., 2001; Neel et al., 2012).

In most cases, high tumor Treg cell infiltration is associated with poor prognosis (Chen et al., 2011; De Simone et al., 2016; Flammiger et al., 2013; Togashi et al., 2019). In murine tumor models, Treg cell depletion results in tumor rejection, but causes lethal autoimmunity (Bos et al., 2013; Shimizu et al., 1999; Kim et al., 2007).

Tumor Treg cells apply similar mechanisms as described in section 1.2.1 to control the immune response. Additionally, Xiong et al. (2015) showed that Treg cells support metastasis by facilitating epithelium-to-mesenchymal transition. Also, they likely promote differentiation of fibroblasts into cancer-associated fibroblasts. These cells release high amounts of fibronectin and collagen into the tumor stroma, thereby reducing T cell motility (Turley et al., 2015). Eventually, tumor Treg cells have also been reported to support tumor growth by producing vascular endothelial growth factor resulting in angiogenesis (Li et al., 2019b; Facciabene et al., 2011).

1.3 Origin and development of the immune system

The immune system consists of a multitude of highly specialized cell types. All of these originate from a single cell type - hematopoietic stem cells (HSCs). Due to the short viability of most mature blood cells, it is estimated that more than 10^{11} blood cells need to be replenished each day in an adult human. To allow the maintenance of sufficient blood cell production throughout the life of an organism while also ensuring adequate proportions of specialized cell subsets, hematopoiesis needs to be tightly regulated both on a genetic and epigenetic level (Catlin et al., 2011; Orkin and Zon, 2008).

1.3.1 The hematopoietic tree

Since its start over 150 years ago, research on hematopoiesis has constantly revised the hematopoietic tree, a hierarchy blood cells follow through during their differentiation process (Watcham et al., 2019). With the exception of some tissue-resident immune cell populations that develop in the yolk sac or fetal liver during embryonic development, immune cells originate from the bone marrow (Murphy and Weaver, 2018, p. 5). In the classic view, the hematopoietic tree can be divided into three compartments based on cell potency (Figure 2A).

At the top of the tree reside HSCs – multipotent cells that act as the source of all other immune cells. Another crucial characteristic besides multipotency is self-renewal that allows maintenance of a steady pool of HSCs throughout lifetime (Seita and Weissman, 2010). HSCs can be divided by decreasing self-renewal capacity into long-term HSCs (LT-HSCs), short-term HSCs (ST-HSCs) and multipotent progenitor (MPP) cells (King and Goodell, 2011). MPPs are still multipotent, but have lost self-renewal capacity. They further differentiate into one of the lineage-defining oligopotent common lymphoid progenitor (CLP) or common myeloid progenitor (CMP) cells. CLPs eventually give rise to mature unipotent lymphoid cell types including B cells, T cells and NK cells. On the other hand, CMPs define the myeloid lineage and differentiate into megakaryocyte-erythroid progenitor cells and granulocyte-monocyte progenitor (GMP) cells. The former is committed to megakaryocyte or erythrocyte differentiation while monocytes, granulocytes or mast cells are progeny of the latter. Dendritic cells are a special case in the hematopoietic tree, since they can arise from progenitor cells of the lymphoid and myeloid lineage (Manz et al., 2001; Watcham et al., 2019; Seita and Weissman, 2010).

This classic view of hematopoiesis has been refined by the discovery of new cell subsets such as multiple MPP subpopulations in the HSC compartment (Watcham et al., 2019). For example, lymphoid-primed MPPs (LMPPs) have been discovered that are primed towards the lymphoid arm, but also have the potential to become GMPs. Most recently, the availability of single-cell omics technologies has allowed the investigation of transcriptomic and (epi)genetic profiles of large numbers of cells, which revealed further

heterogeneity among blood cells. As an example, the Human Cell Atlas Project has generated a single-cell transcriptomic dataset containing over 100,000 human hematopoietic cells (Figure 2B) (Hay et al., 2018; Regev et al., 2017). The overarching observation from these studies is that hematopoiesis is a continuous rather than a discrete process, in which branching points are difficult to pinpoint (Watcham et al., 2019; Marshall et al., 2018).

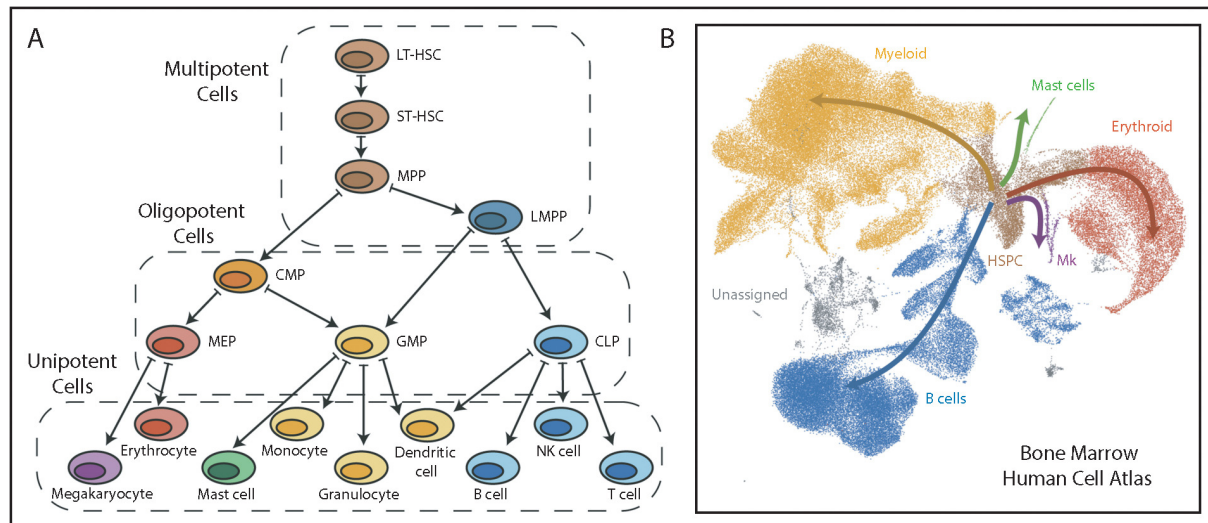


Figure 2: Hematopoietic tree diagram and corresponding scRNA atlas. **A** Diagram of the classic view on the hematopoietic tree with discrete cellular states. Cells are ordered in a hierarchy of increasing specialization and decreasing potency, as indicated by dashed boxes. **B** UMAP of single-cell transcriptomics landscape from human bone marrow mononuclear cells. Rather than discrete cellular states, continuous differentiation trajectories are observed. Arrows show the direction of differentiation. Adapted from Watcham et al. (2019), Copyright © 2019 provided by Elsevier and Copyright Clearance Center.

1.3.2 T cell education

In mammals, B cells and NK cells differentiate and mature from CLPs in the bone marrow. In contrast, CLPs constantly migrate to the thymus, where they become thymocytes and give rise to T cells (Serwold et al., 2009). The thymus can be divided into two major regions, the outer cortex and the central medulla. It consists of a network of thymic epithelial cells (TECs), macrophages, DCs and thymocytes, which collectively form the thymic stroma, a specialized microenvironment for T cell maturation (Murphy and Weaver, 2018, pp. 403-405). T cell education starts in the thymic cortex with early thymic progenitor cells, which neither express CD4 nor CD8 co-receptors and are thus double-negative (DN) (Figure 3). Epithelial cells in the cortex of the thymus then interact with these DN1 thymocytes via Notch-signaling. This induces transcription factors that determine their T cell fate, a developmental path that becomes irreversible in following DN2 stage. Of note, lineage commitment steps during T cell development also entail genome-wide epigenetic changes (Johnson et al., 2018; Hu et al., 2018; Schmidl et al.,

2018). In the second DN stage, T cell receptor rearrangement is initiated at the gene loci encoding TCR β , TCR γ , and TCR δ (Koch and Radtke, 2011). The transition from DN2 to DN3 marks the first bifurcation step, in which thymocytes further develop into $\gamma\delta$ or $\alpha\beta$ T cells. The larger fraction of thymocytes follows $\alpha\beta$ T cell fate, and only cells that express a functional pre-TCR complex in DN3 stage move on to the last DN stage. The pre-TCR complex consists of the TCR β chain together with an invariant pT α chain as well as CD3 molecules, which are the signaling components of the TCR. CD3 signaling then induces a transition to DN4, in which cells rapidly proliferate and subsequently express both CD4 and CD8 coreceptors, turning them into double-positive (DP) thymocytes (Koch and Radtke, 2011; Murphy and Weaver, 2018, pp. 405-409). DP cells rearrange their TCR α chain and present their complete TCR $\alpha\beta$ complex on their surface to enter a rigorous selection process, which is only passed by 2–4% of thymocytes ensures that T cells are neither over- nor underreactive. First, they need to pass positive selection, in which only cells with a TCR with intermediate avidity for self peptide:self-MHC molecules on DCs, cortical TECs and fibroblasts receive positive survival signals. Subsequently, a second lineage choice takes place by continuation of either CD4 or CD8 coreceptor expression resulting in single-positive (SP) thymocytes. SP thymocytes then migrate from the thymic cortex to the medulla, where negative selection takes place. Through presentation of a large compendium of self-antigens on MHC complexes of DCs and medullary TECs, potentially autoreactive SP thymocytes are identified and deleted through apoptosis. Mature naive T cells that have completed thymic education are self-tolerant and self-MHC restricted. They then migrate from the thymus into the blood, from where they reach peripheral lymphatic tissues including the spleen, lymph nodes, and mucosa-associated lymphatic tissues. Lymphocytes patrol between the blood and these secondary lymphoid structures until they get activated by a cognate antigen (Koch and Radtke, 2011; Murphy and Weaver, 2018, pp. 22, 407-427).

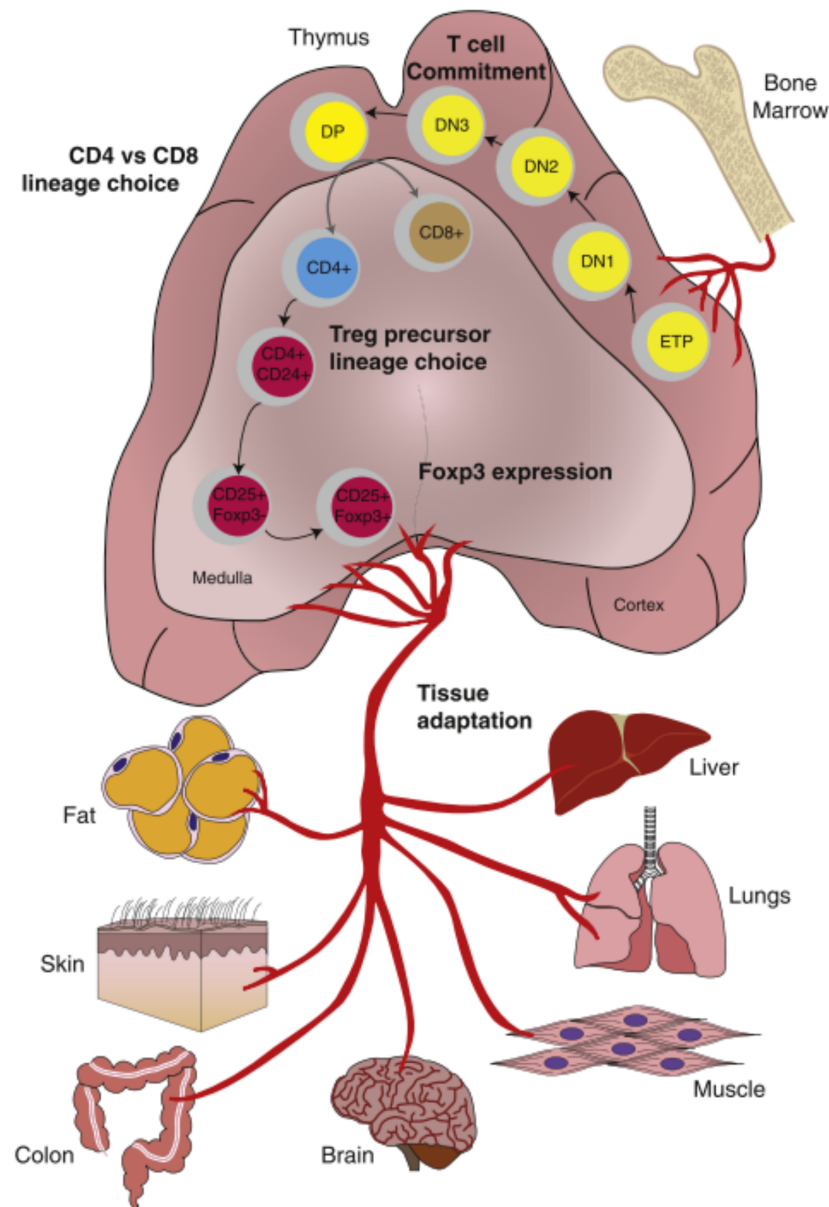


Figure 3: T cell development in the thymus. The steps during T cell development in the thymus are illustrated based on the Treg cell lineage. CLPs migrate from the bone marrow into the thymus, where they undergo a series of differentiation steps in the cortex that determine T cell commitment and result in CD4 versus CD8 lineage choice. In the medulla, further selective processes take place and a subset of CD4 SP thymocytes enters the Treg lineage through upregulation of the transcription factor FOXP3. Finally, mature naive Treg cells leave the thymus to migrate into other tissues via the circulation, where further adaptation occurs. Reprinted from Schmidl et al. (2018), Copyright © 2018 provided by Elsevier and Copyright Clearance Center.

1.3.3 Epigenetics and the role of chromatin accessibility

Eukaryotic DNA is organized together with DNA-binding proteins in a compact structure called chromatin (Luger et al., 1997). This structure ensures genome integrity and regulates transcription. Specifically, gene expression is controlled by DNA regulatory elements

including promoters, enhancers and silencers that can be bound by transcription factors, their cofactors and repressors. While actively transcribed genes are typically found within regions of accessible chromatin (euchromatin, ‘open’), RNA-polymerase cannot transcribe genetic information within condensed regions of chromatin (heterochromatin, ‘closed’) (Klemm et al., 2019; Mellor, 2005). Chromatin accessibility is modulated by epigenetic modifications, which encompasses heritable changes in the function of genes, which are not encoded in the genetic code of the DNA (Wu and Morris, 2001). Epigenetic regulation of gene expression is particularly relevant during developmental processes such as cell differentiation (Allis and Jenuwein, 2016). There are several mechanisms of epigenetic regulation including DNA methylation, histone modification and reorganization, non-coding RNAs and nucleosome remodeling (Sharma et al., 2010; Allis and Jenuwein, 2016).

One gene with well-described epigenetic regulation is *FOXP3* (Figure 4) (Huehn et al., 2009; Floess et al., 2007; Colamatteo et al., 2020). Stable *FOXP3* expression is required for a Treg phenotype, whereas its expression is suppressed in conventional T cells (Fontenot et al., 2003; Hori et al., 2003). There are multiple species-conserved genomic loci involved in its regulation: first, transcription factors downstream of TCR activation such as NFAT and AP1 are required to bind to the *FOXP3* promoter. A prerequisite for transcription factor binding is the demethylation of CpG sites in this region, which entails a relaxation of chromatin accessibility. Additionally, signals passed on through cytokine-receptor γ -chain from cytokines such as IL-2 impact promoter activation (Huehn et al., 2009; Janson et al., 2008). Second, *FOXP3* expression depends on accessible chromatin within an enhancer element called TGF β sensor. Here, the decompaction of chromatin is mainly mediated by another epigenetic mark—an increase in histone H4 acetylation. As the name of this enhancer indicates, TGF β signaling is required for the restructuring of chromatin and binding of NFAT and SMAD transcription factors in this region (Huehn et al., 2009). Lastly, the Treg-cell-specific demethylated region (TSDR) is another enhancer element that is active in Treg cells. It contains a number of CpG sites, which are demethylated specifically in Treg cells. Additional activating histone marks allow an increase in chromatin accessibility through nucleosome remodeling and subsequent binding of transcription factors that most likely stabilize *FOXP3* expression (Huehn et al., 2009; Floess et al., 2007). In the meantime, even more conserved non-coding regions affecting *FOXP3* gene expression have been described demonstrating the complexity of epigenetic gene regulation (Colamatteo et al., 2020; Delacher et al., 2017).

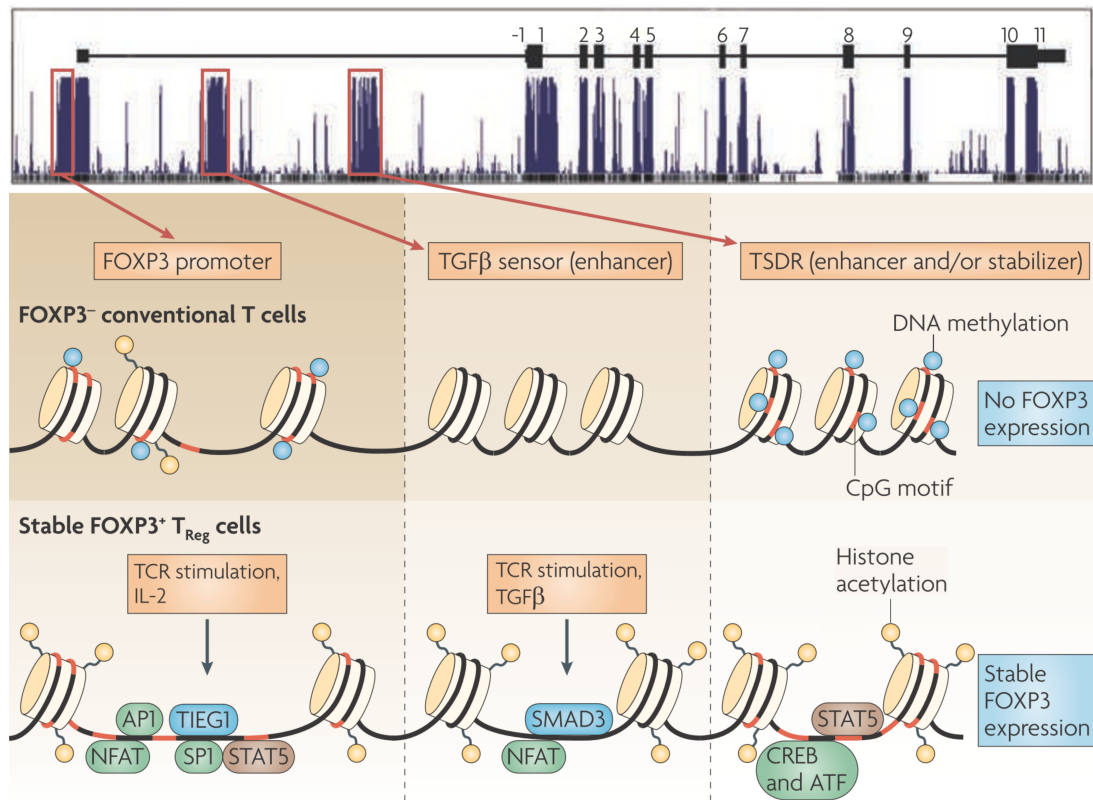


Figure 4: Epigenetic regulation of the *FOXP3* gene locus. The top panel shows the *FOXP3* locus on the X chromosome as an interspecies-conservation plot. Epigenetic modifications including DNA methylation and histone acetylation within three well-known regulatory regions that affect *FOXP3* expression are shown in comparison between FOXP3⁻ conventional T cells and stable FOXP3⁺ Treg cells. Upstream signals and transcription factors required for *FOXP3* expression are indicated. TSDR, Treg-cell-specific demethylated region. Adapted from Huehn et al. (2009), Copyright © 1969 provided by Springer Nature and Copyright Clearance Center.

1.3.4 Development of Treg cells

Not all T cells that are reactive to self-peptide:self-MHC molecules are eliminated in the thymus. tTreg cells mainly develop from a subset of DP or CD4 SP thymocytes with self-reactive TCRs (Figure 3). Specifically, TCR stimulation at higher intensity but below the threshold causing negative selection induces expression of CD25 and the master transcription factor FOXP3 (Ohkura et al., 2013). Additionally, interaction of CD28 with its ligands on TECs and a cytokine milieu mainly including IL-2 and TGFβ is required to start the Treg differentiation program (Richards et al., 2015). Treg cells leave the thymus in a mature state and subsequently circulate through secondary lymphoid tissues or migrate into nonlymphoid tissues via the blood (Sakaguchi et al., 2008).

Epigenetic processes also play an important role during Treg cell generation. Above all, a Treg-associated DNA demethylation pattern is established, which is triggered by TCR stimulation in the thymus and seems to be FOXP3-independent (Ohkura et al., 2012). The study by Ohkura et al. (2012) further showed that only FOXP3 expression and this

hypomethylation pattern resulted in stable Treg cells with full suppressive activity. Accordingly, while induction of Treg cells from Tconv cells by FOXP3 expression confers suppressive activity, the majority of Treg signature genes is not induced (Fontenot et al., 2003; Hill et al., 2007). Epigenetic changes do not only occur during development in the thymus, but also in peripheral tissues, where further adaptations of Treg cells towards tissue-specific functions are required (Delacher et al., 2017). Thus, a total of five epigenetic reprogramming steps is observed in Treg cell development: T cell lineage commitment, CD4 and Treg lineage choice, establishment of Foxp3 expression, and tissue adaptation (Schmidl et al., 2018).

A second route of Treg cell development is the conversion from Tconv cells in the periphery. This route mainly occurs in mucosal tissues, where DCs present environmental antigens such as food antigens and further triggers including TGF β are present. Since chronic exposure at low dosage to non-self antigens promotes the conversion to pTreg cells, it is assumed that pTreg cells are responsible for establishing peripheral tolerance to harmless foreign antigens such as commensal bacteria (Lee and Lee, 2018). Although the developmental origin of Treg cells is difficult to determine and markers are still controversial, the transcription factors HELIOS and ROR γ t have been proposed as markers for tTreg and pTreg cells, respectively (Thornton et al., 2010; Himmel et al., 2013).

1.3.5 T cell exhaustion

When T cells are constantly activated by antigens they transition into a hyporesponsive state, which is also known as T cell exhaustion. Persistent antigen exposure and accompanying T cell exhaustion can occur during chronic infections or in the tumor microenvironment. Chronic stimulation of the TCR results in upregulation of inhibitory receptors, i.e. PD-1, TIM-3, TIGIT and LAG-3, and epigenetic and transcriptomic changes. Together, these alterations lead to reduced effector function and the inability of cytotoxic T cells to control or clear the infection or tumor. In detail, dysfunctional CD8⁺ T cells produce less effector cytokines (IFN γ , TNF α , IL-2) and cytotoxic molecules (granzymes and perforin) and have reduced proliferative activity (Zhang et al., 2020; Philip and Schietinger, 2021; Thommen and Schumacher, 2018). In the tumor microenvironment, several cell types additionally contribute to immune suppression. For example, tumor cells and stromal cells may express PD ligands that downregulate cytotoxic T cells via PD-1/PD-L interactions and Treg cells can produce the suppressive cytokines IL-10 and TGF β (Zhang et al., 2020).

Recently, a more fine-grained distinction between different states of T cell dysfunction has evolved (Figure 5). Mainly, progenitor exhausted T cells arise from chronic antigen exposure. While effector functions are already reduced, this state is still reversible. The reprogramming of these cells is the aim of many immunotherapeutic strategies such as

PD-1 inhibitors, which shield PD-1 receptors from activation and improve their effector function. With ongoing antigen exposure and inhibitory signaling, progenitors gradually become terminally exhausted T cells. In contrast to early stages of dysfunction, terminal dysfunction is not reversible. Main differences of these cells compared to progenitor exhausted T cells include specific epigenetic changes and upregulation of CD39, TIM3, transcription factor TOX and simultaneous downregulation of TCF1 (Philip and Schietinger, 2021; Thommen and Schumacher, 2018).

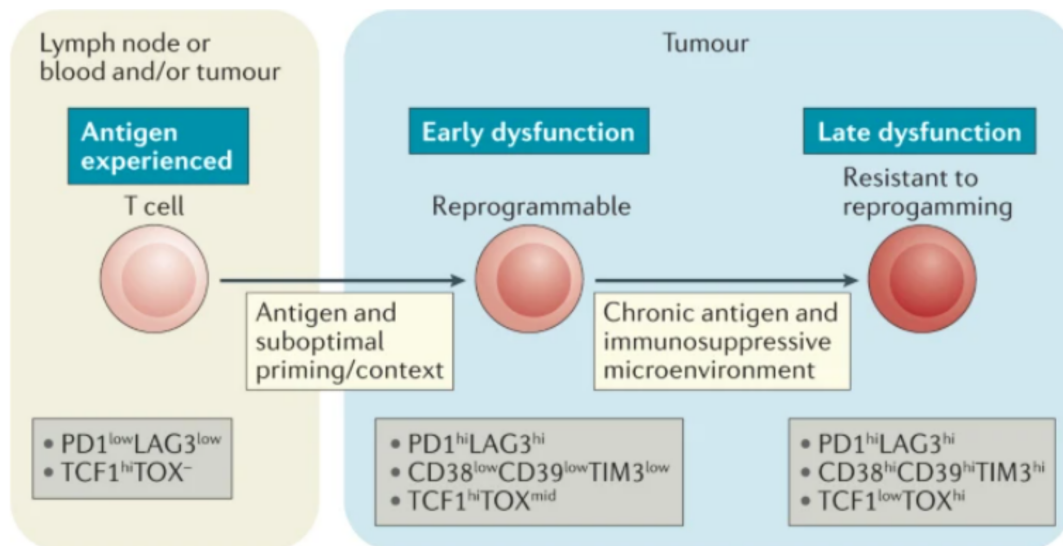


Figure 5: T cell dysfunctional model. Functional antigen-experienced T cells are characterized by low PD-1 and LAG-3 expression, absence of TOX expression, and high TCF1 activity. Persistent antigen exposure and suboptimal conditions for T cell activation as encountered in the tumor microenvironment result in a reversible state of early T cell dysfunction. Further antigen exposure and inhibitory signals eventually cause late dysfunction without reprogramming capability. In contrast to functional and early dysfunction states, late dysfunction is characterized by low TCF-1 and high TOX expression. The figure is modified from Philip and Schietinger (2021), Copyright © 2021 provided by Springer Nature and Copyright Clearance Center.

1.4 Tissue-specific functions of immune cells

Immune cells do not only protect the host against invading pathogens, but are also involved in the maintenance of tissue homeostasis (Figure 6). For example, multiple, mostly innate immune cell types have been described to regulate adipose tissue homeostasis, thermogenesis, innervation and expansion (Trim and Lynch, 2021). A major role in preventing obesity and diabetes has been attributed to macrophages, which are able to alter lipid metabolism through adjusting insulin sensitivity and modulating lipolysis (Odegaard et al., 2007; Lumeng et al., 2007). Invariant natural killer T (iNKT) cells, $\gamma\delta$ T cells, mast cells and DCs have the ability to promote proliferation of adipocyte progenitors. Additionally, iNKT cells may induce adipocyte apoptosis, $\gamma\delta$ T cells can upregulate pathways related to tissue remodeling and fat metabolism in adipocytes, and mast cells are in-

volved in fibroblast activation and tissue fibrosis. Moreover, macrophages, iNKT cells, $\gamma\delta$ T cells, ILCs, Treg cells, mast cells and eosinophils together control adipocyte browning and thermogenesis (Trim and Lynch, 2021).

Tissue-resident memory T (Trm) cells reside in non-lymphoid tissues, where they can quickly respond to foreign antigens. This sets them apart from central memory (Tcm) and effector memory T (Tem) cells, both of which circulate between lymphoid and non-lymphoid tissues via the blood. Within adipose tissue, Trm cells have been shown to balance antimicrobial defense and lipid metabolism (Han et al., 2017; Sasson et al., 2020).

In barrier tissues including epithelia of the skin, intestines and the lung, macrophages have been shown to support wound healing. Mechanistically, expression of growth factors such as $TGF\beta 1$ and PDGF promotes differentiation and proliferation of fibroblasts and epithelial cells (Barron and Wynn, 2011). In addition, macrophages regulate extracellular matrix turnover through secretion of metalloproteinases or their inhibitors (Wynn, 2008; Murray and Wynn, 2011). Similar to macrophages, tissue-resident lymphocytes can sense tissue damage and respond by release of tissue-protective factors such as IL-22 and amphiregulin (AREG) in different organs (Fan and Rudensky, 2016). AREG is a ligand of the epidermal growth factor receptor (EGFR) and stimulates differentiation and proliferation of target cells, e.g. epithelial cells, fibroblasts and immune cells, thereby promoting tissue repair. To date, AREG production and involvement in wound healing has been demonstrated for many cell types including T cells, ILCs, basophils and mast cells (Zaiss et al., 2015; Rankin and Artis, 2018).

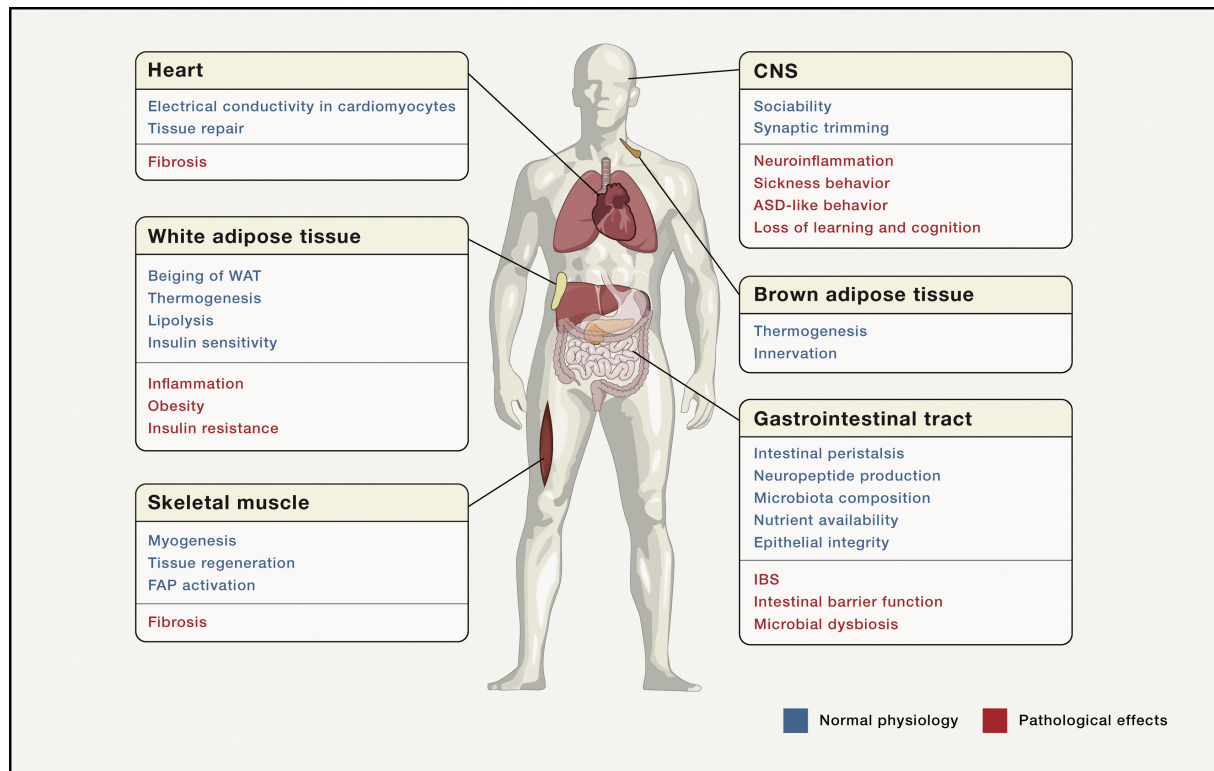


Figure 6: Non-immunological functions of the immune system. Immune cells contribute to tissue homeostasis in various organs, where they regulate processes such as tissue repair and regeneration, thermogenesis and metabolic functions. A spectrum of diseases and medical conditions has been associated with dysregulation of the immune system. ASD, autism spectrum disorder; FAP, fibroadipogenic precursor; IBS, irritable bowel syndrome; WAT, white adipose tissue. Reprinted from Rankin and Artis (2018), Copyright © 2018 provided by Elsevier and Copyright Clearance Center.

1.4.1 $\text{Klrg1}^+\text{ST2}^+$ tissue Treg population

Treg cells do not only have the potential to regulate other immune cells but additionally have an important role in maintaining homeostasis in non-lymphoid tissues. Tissue-adapted Treg populations were first described by Feuerer et al. (2009) in visceral adipose tissue (VAT). Here, they highly express peroxisome proliferator-activated receptor- γ (PPAR- γ), the master transcription factor of adipocyte differentiation, which is required for their accumulation and acquisition of a VAT-specific transcriptomic profile. Treg cells maintain insulin sensitivity of adipocytes (Cipolletta et al., 2012). Skin Treg cells are recruited both by migration into the skin and peripheral induction (Richards et al., 2015). They can produce AREG, which stimulates keratinocyte proliferation and induces expression of antimicrobial peptides (Johnston et al., 2011; Berasain and Avila, 2014). Also, tissue damage arising from infections of the lung or muscle injuries is remedied by tissue-resident Treg cells that suppress excessive inflammation and release AREG to induce wound healing (Burzyn et al., 2013; Arpaia et al., 2015). Most pTreg cells arise in the gut, where they provide tolerance to food antigens and commensal bacteria and

maintain epithelial integrity together with tTreg cells. As an example, intestinal Treg cells were shown to support stem-cell renewal via release of IL-10 (Biton et al., 2018; Cosovanu and Neumann, 2020).

In 2017, Delacher et al. (2017) characterized murine Treg cells isolated from lymph nodes and different non-lymphoid tissues on an epigenetic level using tagmentation-based whole-genome bisulfite sequencing. This led to the discovery of a conserved DNA methylation profile among tissue-resident Treg cells. Corresponding to their epigenetic programming, these cells also had a unique gene expression signature, which was dominated by Th2 cell-specific genes. Compared to Tconv cells from the same tissues, these tissue-resident Treg cells showed hypomethylation and concordant upregulation at several marker genes including *Il1rl1* (encoding the cytokine IL-33 receptor ST2), the differentiation marker killer cell lectin-like receptor subfamily G1 (*Klrg1*), transcription factor *Gata3* and the immune receptor *Tigit* and were thus termed ‘tissue Treg (tisTreg) ST2 cells’ (tisTregST2 cells). Moreover, AREG and IL-10 expression as well as dependence on transcription factor Basic leucine zipper transcription factor, ATF-like (BATF) and IL-33 were described as common features of tisTregST2 cells. In adult mice, the Treg population consists of 80–90% tisTregST2 cells in the VAT, 50–60% in the skin, 30% in the colon, 10%–20% in the lungs, liver and bone marrow and below 5% in lymphoid organs (Delacher et al., 2017). A subsequent interrogation of chromatin accessibility and single-cell transcriptomes identified two tisTregST2 precursor stages that were detected in lymphoid tissues. Using the gene nuclear factor, interleukin 3 regulated (*Nfil3*) as a reporter, development from *Klrg1⁻Nfil3⁻* over *Klrg1⁻Nfil3⁺* towards *Klrg1⁺Nfil3⁺* Treg cells could be observed in the spleen and lymph nodes (Delacher et al., 2020). In line with these results, priming of non-lymphoid Treg cells within lymphoid tissues has been described (Miragaia et al., 2019; Li et al., 2018). Importantly, BATF was shown to be the driver of the tisTregST2 tissue-adaptation program. Interestingly, it has also been shown that the PPAR- γ locus is accessible in all tisTregST2 cells independent of their tissue location (Delacher et al., 2020).

1.5 Single-cell sequencing

In 2009, Tang et al. (2009) published the first study on single-cell transcriptome sequencing (scRNA-seq) using next-generation sequencing technologies. Since then, there has been a vast increase in available protocols and sequencing strategies, which improved cell throughput by several orders of magnitude (Figure 7). Recently, a method for single cell transcriptome sequencing scaling to millions of nuclei in a single experiment has been reported (Datlinger et al., 2021).

Besides scRNA-seq, other types of omic layers can be assayed on a single-cell level, either alone or in different combinations. These include single-cell genomes, epigenomes and

proteomes (Angerer et al., 2017).

The main advantage of single-cell sequencing compared to conventional bulk-based methods is the detection of heterogeneity within the assayed population. This allows the characterization of rare cell populations or cell states that would otherwise be masked by the major cell type(s) present in the sample. The constant increase in cell throughput and sensitivity not only improves the resolution of cell subsets, but also allows the inference of continuous developmental processes and their regulatory landscapes (Hwang et al., 2018; Kharchenko, 2021).

A common challenge encountered in single-cell data analysis is the sparsity of measurements due to low amounts of input material and limited capture rates. For example, high-throughput methods in scRNA-seq only capture between 5–20% of transcript molecules present in each cell. Thus, special models accounting for under-sampling of mRNA transcripts, so-called ‘dropouts’, are required (Ding et al., 2020).

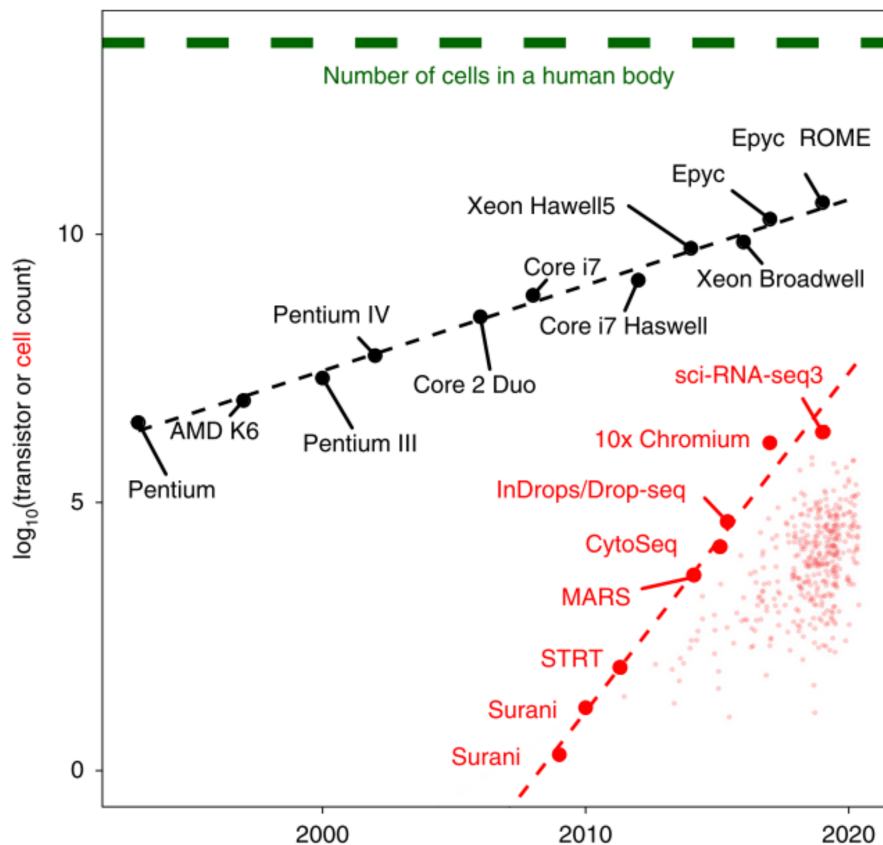


Figure 7: Increase in throughput of scRNA-seq technologies over time. The number of sequenced single-cell transcriptomes is shown for selected datasets (red line) in comparison to the advancement in available CPU transistor counts (black line) and the estimated number of cells in the human body (green line). The size of single-cell datasets is increasing faster than computing performance, which requires development of efficient data processing methods. The figure is taken from Kharchenko (2021), Copyright © 2021 provided by Springer Nature and Copyright Clearance Center.

1.5.1 Single-cell chromatin accessibility sequencing

To understand genotype-to-phenotype relationships it is important to investigate epigenetic attributes of the DNA (Klemm et al., 2019; Mellor, 2005). Buenrostro et al. (2013) developed an assay for transposase-accessible chromatin using sequencing (ATAC-seq), which is an efficient method to obtain information about chromatin accessibility (Figure 8). Mechanistically, it relies on a hyperactive Tn5 transposase that is able to simultaneously cleave DNA and insert short DNA sequences in a process called ‘tagmentation’. Since Tn5 transposase can only target open chromatin regions, this results in the generation of tagged DNA fragments representing the accessible part of the genome. Prior to high-throughput sequencing, the DNA fragments can then be amplified using polymerase chain reaction (PCR) to increase input material. Compared to other methods assaying chromatin accessibility such as DNase-seq or FAIRE-seq, ATAC-seq requires fewer cells as input material and is less complex and costly (Buenrostro et al., 2013; Baek and Lee, 2020).

Several methods have adapted ATAC-seq for single cell applications. They can be broadly categorized into split-and-pool combinatorial cellular indexing approaches and microfluidics approaches. In the former, cells are repeatedly pooled and sorted into wells containing transposases with unique barcodes, which results in a library of cell-specific tagged DNA fragments. The latter employ microfluidic devices to separate cells into reaction chambers. These can be either wells in plate-based methods such as Fluidigm IFC or droplets in droplet-based methods.

The first study presenting a commercial droplet-based platform was published in 2019 by Satpathy (2019), who generated chromatin profiles of more than 200,000 cells. In their workflow, transposition of DNA is performed in a bulk suspension of nuclei. Subsequently, a microfluidic device called “10x Chromium controller” is used to encapsulate single nuclei together with barcoded gel beads and chemical reagents within nanoliter-sized droplets. Linear amplification results in the attachment of barcodes to the DNA fragments, thereby uniquely mapping fragments to each cell. Eventually, the emulsion is broken, and a common PCR step is applied to further amplify the fragment pool for high-throughput sequencing (Satpathy, 2019).

scATAC-seq allows the identification of cell types and their regulatory elements. It can be used to uncover *de novo* transcription factor motifs and estimate transcription factor activity. Further, the single-cell resolution allows the delineation of smooth transitions in chromatin accessibility making scATAC-seq a useful method for the inference of developmental trajectories.

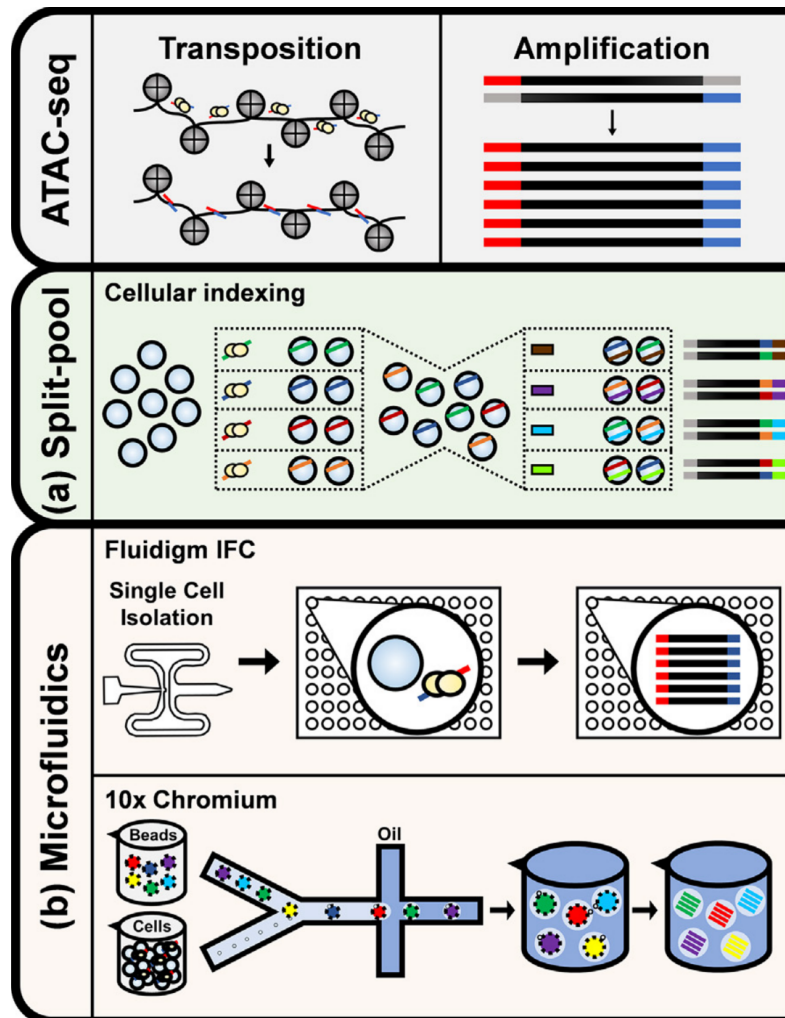


Figure 8: Single-cell strategies for ATAC-seq. The ATAC-seq protocol involves a transposition step, in which Tn5 transposase fragments and tags accessible DNA and an amplification step to increase the input material for sequencing. In a single-cell setting, cell-specific barcodes can be introduced by split-pool approaches (a) or using microfluidics (b). Adapted from Baek and Lee (2020), Copyright © 2020 by the authors under the CC BY-NC-ND license.

1.6 Aims of the thesis

It is becoming increasingly clear that many immune cells fulfill tissue-specific functions besides their protective role for the host. In mice, *tisTregST2* cells have been previously described to be involved in tissue regeneration (Delacher et al., 2017, 2020). However, it is not well defined whether these findings also apply to humans and other types of immune cells may also have such a tissue repair program.

In this thesis, three projects are presented that employ scATAC-seq to map immune cell epigenomes at single cell resolution and deepen the current understanding of tissue-specific immune functions (Figure 9).

In Chapter 3.1, $CD4^+$ T cells from healthy murine and human tissues are analyzed with

a focus on Treg cells. The main research questions are whether human Treg cells in peripheral tissues with similar characteristics to murine tisTregST2 cells can be identified, and what their epigenetic commonalities and differences are. Moreover, the single cell epigenomes are used to gain insights into the developmental steps towards a tisTreg phenotype and the underlying driving transcription factors. Sequencing of CD4⁺ T cells from gnotobiotic mice aims to answer whether the repair phenotype of Treg cells in the colon can be established independently from microbiota. Eventually, Treg cells from healthy peripheral tissues are compared to those from tumor tissues to define differences between homeostasis and challenged conditions.

In Chapter 3.2, the focus is shifted towards the CD8⁺ T cell compartment. The project is based on multiple datasets containing CD8⁺ T cells extracted from healthy murine and human tissues as well as human solid tumors. Specifically, comparisons with tisTregST2 cells based on chromatin accessibility are performed to determine whether CD8⁺ T cells also have tissue-regenerative potential in addition to their effector function. If similar characteristics to tisTregST2 cells are found, an in-depth analysis including differential accessibility, pseudotime and transcription factor activity analysis equivalent to Chapter 3.1 is done. This includes the identification and comparison of CD8⁺ T cells with tissue-adapted phenotype in healthy murine and human tissues, the determination of their possible developmental paths, assessment of microbiota-dependence in the colon, and comparisons between healthy and tumor tissue. Importantly, tissue-regenerative CD8⁺ T cells are contextualized in the current CD8⁺ T cell classification and known effector states such as T cell exhaustion.

The third project presented in Chapter 3.3 expands the view of tissue-specific roles by performing a pan-leukocyte analysis. Murine and human scATAC-seq datasets containing both innate and adaptive immune cells from healthy tissues are evaluated with respect to their tissue-repair potential, thereby validating and extending the findings from the T cell compartment. This project aims to obtain a more holistic view on tissue-adaptation of immune cells.

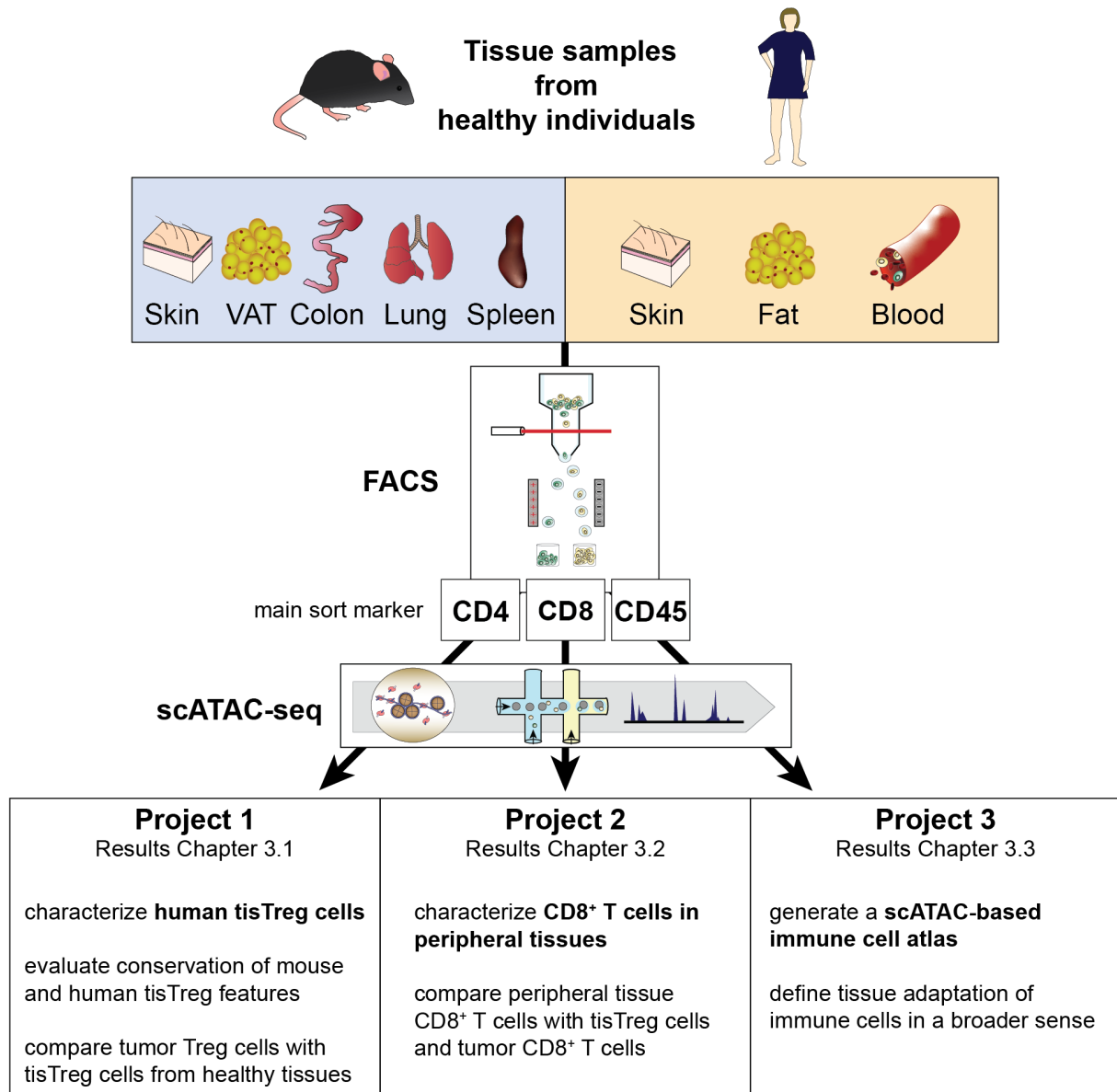


Figure 9: Project overview and aims. Summary of the experimental strategy and aims of the three projects presented in this thesis.

2 Methods

I applied similar methods to analyze data from Projects 1 (tisTreg cell analysis, Results Chapter 3.1) and 2 (Tissue CD8⁺ T cell analysis, Results Chapter 3.2). For Project 3 (Immune cell atlas, Results Chapter 3.3), I changed the analysis workflow to ensure the use of most up-to-date data processing methods. An overview of all samples analyzed in this work is given in Supplementary Table S1. Supplementary Tables S2 and S3 list the computational tools I employed for data analysis.

2.1 scATAC-seq of murine and human immune cells

In Project 1 and 2, specific-pathogen-free (SPF) male C57BL/6 mice of at least 10 weeks of age and germ-free male wild type C57BL/6 mice of at least 9 weeks of age were used to obtain tissue samples. In Project 3, male C57BL/6 mice of 48–50 weeks of age were used. Additionally, tumor tissue samples of murine breast cancer were obtained from BALB-NeuT transgenic mice (Hosseini et al., 2016).

Murine and human tissue samples were dissociated to obtain single cell suspensions, which were enriched for immune cells using column-based magnetic purification and fluorescence-activated cell sorting (FACS). For Project 1, T cells were magnetically enriched using anti-CD4 or anti-CD25 antibodies. Subsequently, cells were sorted with a BD FACSAriaTmII or BD FACSFusionTm cell sorter. Treg cells from the murine spleen were sorted as CD45⁺Dead⁻CD19⁻CD3⁺TCR β ⁺CD8⁻CD4⁺CD25⁺. Additionally, cells from the spleen, colon, skin, lung and VAT were sorted for CD45⁺Dead⁻CD19⁻CD3⁺TCR β ⁺CD8⁻CD4⁺ to enrich CD4⁺ T cells. The same sorting strategy was applied to tissues from germ-free animals and HER2-transgenic tumor bearing animals. From human peripheral blood of two independent donors, CD3⁺Dead⁻CD19⁻TCR β ⁺CD8⁻CD4⁺ CD4⁺ T cells and CD3⁺Dead⁻CD19⁻TCR β ⁺CD8⁻CD4⁺CD25⁺CD127⁻ Treg cells were sorted. Using the same sorting gates, CD4⁺ T cells were sorted from subcutaneous fat of donor 3, 4 and 5, skin of donor 4 and 5 and Treg cells were sorted from subcutaneous fat of donor 3 and 5. For Project 2, anti-CD8 antibodies were used for pre-enrichment of T cells from healthy tissues with column-based magnetic separation. CD45⁺Dead⁻CD19⁻CD3⁺TCR β ⁺CD4⁻CD8⁺ sort gates were then used to sort CD8⁺ T cells from the murine spleen, colon, skin, VAT (SPF and germ-free mice) and lung (SPF mice only). CD3⁺Dead⁻CD19⁻TCR β ⁺CD4⁻CD8⁺ T cells were sorted from peripheral blood of healthy human donors 1 and 2. Additionally, sorting was done for CD45⁺Dead⁻CD14⁻CD19⁻CD3⁺TCR β ⁺CD4⁻CD8⁺ for fat tissue from donors 3, 4 and 5 and skin of donors 4 and 5. Cells from liver cancer donor 6 were sorted with CD45⁺Dead⁻CD3⁺TCR β ⁺ or CD45⁺Dead⁻CD14⁻CD19⁻CD3⁺TCR β ⁺CD4⁻CD8⁺ to obtain T cells or CD8⁺ T cells, re-

spectively. Similarly, T cells were sorted from liver cancer donor 7. Eventually, CD8⁺ T cells and CD45⁺Dead⁻CD3⁺TCR β ⁺CD4⁺CD8⁻CD25⁺CD127⁻ Treg cells were sorted from liver cancer donor 8. In Project 3, anti-CD45 microbeads were used to magnetically purify immune cells from dissociated murine tissue samples. Then, anti-CD45 antibody staining was performed on murine and human cell suspensions and CD45⁺ immune cells were sorted with a BD FACSFusionTm cell sorter.

Subsequently, nuclei were prepared and the transposition reaction was performed before loading the mix on a 10x Chromium Next GEM Chip H for library generation with the 10x Chromium Controller. After PCR-based library amplification, sequencing was performed on an Illumina NextSeqTm 550.

For the basal cell carcinoma T cell dataset from (Satpathy, 2019), processed data files were obtained from GSE129785. The peak matrix, Cicero gene activity scores (Pliner et al., 2018) and meta data provided by the authors were used for analyses in Project 1.

2.2 Preprocessing of scATAC-seq data

The software Cell Ranger atac (version 1.1.0) was used to process scATAC-seq raw data. Read filtering, alignment, peak calling and count matrix generation were done using the command ‘cellranger-atac count’. The 10x Genomics reference genome assemblies ‘refdata-cellranger-atac-mm10-1.1.0’ and ‘refdata-cellranger-atac-hg19-1.1.0’ were used for mouse and human data, respectively. Gel bead and barcode multiplets were identified with a custom script (‘clean_barcode_multiplets_1.1.py’) provided by 10x Genomics. Barcodes were subsequently annotated as cells when they passed the following filters:

- minimum of 5,000 read-pairs passing Cell Ranger atac read filters
- less than 20% read-pairs with poor mapping behavior (reads with mapq below 30, chimeric and unmapped reads)
- less than 90% read-pair duplicates
- less than 10% mitochondrial DNA read-pairs
- no annotation as gel bead or barcode multiplet

A merged peak-barcode matrix including barcodes annotated as cells from all samples was generated with the command ‘cellranger-atac aggr –normalize=none’. For further processing, the merged matrix was loaded into R (version 3.6.0) using the package Seurat (version 3.2.1, (Stuart et al., 2019)). As another important quality control measure, the transcription start site score was calculated for each cell as previously described (Satpathy, 2019). In short, transcription start sites (TSS) were obtained from the R annotation

packages TxDb.Mmusculus.UCSC.mm10.knownGene (version 3.4.7, murine samples) or TxDb.Hsapiens.UCSC.hg19.knownGene (version 3.2.2, human samples). Then, the per-base coverage in a 1 kb region around each TSS was calculated and normalized by division by the mean coverage of the 100 bp flanks of each region. Subsequently, the normalized coverage was smoothed over a window of 50 bp and the maximum smoothed value was defined as TSS score. All cells with a TSS score smaller than 8 were filtered out.

In Project 1, the influence of cells with high count depth on downstream analyses was reduced by randomly subsampling fragments to 50,000 unique fragments per cell. In Project 2, instead an approach with synthetic doublet generation was chosen to identify and remove potential cell doublets. For each sample, 20% of cells were randomly selected and sorted into pairs. For each pair, the peak counts were summed up and binarized, resulting in a synthetic cell doublet. All synthetic doublets were then merged with the original peak-barcode matrix. The cells in this matrix were then projected into a low dimensional space using the R package Signac (Stuart et al., 2021, version 1.0.0). Briefly, TF-IDF transformation was applied to the matrix using the function ‘RunTFIDF(method=1)’ followed by singular value decomposition (‘RunSVD’) based on the upper quartile of accessible peaks (FindTopFeatures(min.cutoff = ‘q75’). Secondary dimensionality reduction was applied to the first 20 SVD components with the command ‘RunUMAP(dims=20, metric = ‘euclidean’)). Then, the two-dimensional UMAP embeddings were used to count the number of synthetic doublets for each cell among its 50 nearest neighbours. Finally, all cells with more than 10 synthetic doublets in their neighbourhood were excluded from further analysis.

Peaks on chromosomes Y, M or random were removed. Additionally, peaks overlapping with regions from the Signac blacklists ‘blacklist_mm10’ and ‘blacklist_hg19’ were filtered out from the murine and human peak-barcode matrix, respectively. Moreover, peaks with a total binary count below 10 across all cells were excluded.

The binary peak-barcode matrix was subjected to normalization (‘RunTFIDF(method=1)’ and dimensionality reduction based on the upper quartile of accessible peaks using the functions ‘FindTopFeatures(min.cutoff = ‘q75’ and ‘RunSVD’. Batch effects present in the SVD space due to donors in the human and sample pooling in the murine datasets were corrected with Harmony (version 1, (Korsunsky et al., 2019)) using the command ‘HarmonyMatrix’ with sigma=1 for human and sigma=0.3 for murine data, respectively. Finally, the first 20 components from SVD or Harmony embeddings were passed to ‘RunUMAP(metric=‘euclidean’ for secondary dimensionality reduction with UMAP.

In Project 3, the following changes were introduced to preprocessing: Cell Ranger atac version 2.0.0 was used, which includes bead and barcode multiplet detection in its pipeline. Moreover, refdata-cellranger-arc-mm10-2020-A-2.0.0 and refdata-cellranger-arc-GRCh38-

2020-A-2.0.0 were used for alignment of murine and human reads, respectively. Subsequent analyses were performed with the R package ArchR (Granja et al., 2021, version 1.0.1). First, the fragment files ('fragments.tsv') generated by the Cell Ranger atac pipeline were converted into Arrow files using the command 'createArrowFiles(minTSS=0, minFrag=1000, maxFrag=10000) and bundled into an ArchR project ('ArchRProject'). Then, all barcodes with less than 3000 fragments or a ArchR TSS score below 6 were filtered out. Subsequently, doublet enrichment scores were calculated for each Arrow file using 'addDoubletScores' and potential doublets were filtered out by exclusion of all barcodes with DoubletEnrichment score above 2. Eventually, all barcodes annotated by the Cell Ranger ATAC pipeline as gel bead doublet, low-targeting barcode, or barcode multiplet were removed.

Further, dataset-specific filtering of barcodes was required in Project 3. In short, a group of cells clustering into the barcode multiplet region in UMAP space was removed in the mouse dataset. The human dataset was split by donor, and one cluster likely representing cell doublets was excluded for donor 11. Dimensionality reduction was performed with iterative semantic indexing (addIterativeLSI) followed by 'addUMAP(nNeighbors=30, minDist=0.5)' for secondary dimensionality reduction with UMAP.

2.3 Gene activity scores

Gene activity scores were calculated as a proxy for mRNA expression levels. In Projects 1 and 2, coordinates of gene bodies were obtained by running the R GenomicFeatures commands 'genes(TxDb.Mmusculus.UCSC.mm10.knownGene)' and 'genes(TxDb.Hsapiens.UCSC.hg19.knownGene)' for annotation of murine and human datasets, respectively. The coordinates were pruned to standard chromosomes (keepStandardChromosomes(pruning.mode='coarse')) and extended by 2 kb upstream of the TSS to cover promoter regions (Extend(upstream=2,000)). Subsequently, these regions were used as input features for the 'FeatureMatrix' command from the Signac package to count the number of fragments per feature for each cell. These gene activity scores were normalized and scaled using 'NormalizeData(normalization.method='LogNormalize', scale.factor=median(nCount_Reads))' for visualization purposes.

In Project 3, gene activity scores were automatically added during Arrow file generation.

2.4 Peak and gene activity module scores

To summarize accessibility within a set of regions of interest, the frequency of each peak in the binary peak-cell matrix of the dataset was quantified by dividing the sum of counts for the peak through the total sum of counts for all peaks. Then, all peaks from the

dataset overlapping with the regions of interest (signature peaks) were identified and the number of signature peaks was summed up for each cell. To estimate the size of random overlap while accounting for cell count depth, cells with increasing peak count (step size 1,000 peaks for normal tissue datasets, step size 5,000 for tumor T cells from Satpathy (2019) were simulated. For each of these simulated cells, the respective number of peaks was randomly drawn from the dataset with probabilities set to the previously determined peak frequencies. Subsequently, the number of signature peaks in this random peak set was calculated. This procedure was repeated 48 times and the average number of signature peaks + 1 pseudocount was set as expected background match number with the set of regions of interest for a given count depth. Finally, a module score was assigned for each cell by dividing the number of signature peaks +1 through the background match number of the simulated cell with closest count depth.

In Project 3, regions of interest were first added to the ArchR project using the ‘addPeakAnnotations’ function. Then, chromVAR deviation z-scores (Schep et al., 2017) for this set were calculated (‘addDeviationsMatrix’) and used as module scores.

Gene activity module scores were calculated with the function ‘AddModuleScore(nbin=10, ctrl=200)’ from the Seurat R package. The ‘pool’ parameter was set to a sample of 2,000 randomly chosen genes from the gene activity matrix.

2.5 chromVAR transcription factor activity

In Projects 1 and 2, transcription factor activity was estimated for each cell using chromVAR deviation z-scores (Schep et al., 2017). Position weight matrices from known transcription factor motifs provided by the Homer software package (<http://homer.ucsd.edu/homer/custom.motifs>) were used to construct a motif-peak matrix with the Signac function ‘CreateMotifMatrix’. As reference genomes, BSgenome.Mmusculus.UCSC.mm10 and BSgenome.Hsapiens.UCSC.hg19 were used for mouse and human data, respectively. The matrix was added to the Seurat object (CreateMotifObject, AddMotifObject) and annotated with base composition statistics for each peak (RegionStats). Eventually, deviation z-scores were calculated using ‘RunChromVAR’.

In Project 3, the ArchR functions ‘addPeakAnnotations’ and ‘addDeviationsMatrix’ were used to access chromVAR functionalities in a similar way.

2.6 Cell clustering

Starting from SVD or Harmony embeddings, a shared nearest neighbour graph was generated using Seurat (FindNeighbours(dims=1:20)). The graph was then used to identify cell clusters with the function ‘FindClusters’ at various resolutions. The partitionings selected

for visualization and further analyses are summarized in Supplementary Table S4. In Project 3, the function ‘addClusters(maxClusters=Inf)’ was used as a wrapper to Seurat’s clustering workflow based on the embeddings from iterative LSI.

2.7 Peak calling

In Project 3, MACS2 (Zhang et al., 2008, <https://github.com/macs3-project/MACS>) was used for peak calling. First, datasets were clustered at resolution 0.1. Subsequently, the coverage for each group was determined with the function ‘addGroupCoverages(groupBy=‘Clusters_0.1’)’. Eventually, 501 bp fixed-width peaks were added for each cluster, and iteratively aggregated into a common peak set using the function ‘addReproduciblePeakSet(groupBy=‘Clusters_0.1’)’.

2.8 Detection of differential chromatin accessibility

Seurat was used to detect differentially accessible peak regions. Briefly, a logistic regression model was constructed for each peak and compared to a null model with a likelihood ratio test. The count depth per cell was introduced as latent variable (FindMarkers(test.use = ‘LR’, latent.vars=‘n_peaks’, min.pct=0.1, logfc.threshold=0.25). In Project 3, markers were identified with a Wilcoxon rank sum test using the ArchR function ‘getMarkerFeatures(bias=c(“TSSEnrichment”, “log10(nFragments)”)’). TSS score and count depth were specified as biases, which are factored in during null group selection.

2.9 Generation of bigWig tracks

The Sinto toolkit (<https://github.com/timoast/sinto>) was used to extract reads from a barcode selection from sample-level bam files as generated by Cell Ranger atac. Reads from different samples were merged into a common bam files using ‘samtools merge’ (Li et al., 2009) and the coverage within bins was calculated with ‘bamCoverage’ from deepTools (Ramírez et al., 2016).

2.10 Homer transcription factor motif analysis

To answer whether known or de novo transcription factor motifs are enriched within a set of marker peaks, Homer (Heinz et al., 2010) was applied. Position weight matrices available on the Homer website (<http://homer.ucsd.edu/homer/custom.motifs>) were used as reference for transcription factor database to run the command ‘findMotifsGenome.pl peaks.bed hg19 -mask -size given -len 8,10,12,14’.

Transcription factor footprints for clusters of cells were generated by sorting their reads into a cluster-level bam file. Then, ‘makeTagDirectory’ was used to convert these bam files

into tag directories. Finally, peaks from the respective dataset were centered around the selected transcription factor motif (`annotatePeaks.pl -center -mask -size -1000,1000`) and tags within 2,000 bp around centered peaks were quantified (`annotatePeaks.pl -fragLength 1 -size -1000,1000 -hist 1`).

2.11 Trajectory analysis

Monocle (Trapnell et al., 2014) was used to order cells along a possible developmental trajectory. First, clusters of cells from presumably different developmental steps were extracted from the complete dataset and normalization as well as dimensionality reduction were done as described in section 2.2. For the human CD4⁺ T cell dataset, the peak-barcode matrix was subsetting to a random sample of 5,000 cells from each cluster to reduce computational burden. Next, it was reduced to the 3,000 peaks with highest accessibility across all cells and the number of peaks per cell was counted (`detectGenes`). Subsequently, size factors were estimated (`estimateSizeFactors`) and dimensionality reduction with `DDRTree` was performed (`reduceDimensions(reduction_method='DDRTree', residualModelFormulaStr='~num_genes_expressed')`). In a final step, cells were mapped into the trajectory using `'orderCells'`.

2.12 Peak region liftOver and cross-species comparison

To compare peaksets between mouse and human, regions were transferred from mm10 to hg19 genome coordinates using the UCSC liftOver tool (Kuhn et al., 2013) together with a matching chain file (`mm10ToHg19.over.chain.gz`, available at <http://hgdownload.cse.ucsc.edu/goldenpath/>). The lifted regions were additionally transferred back to mm10 with the `hg19ToMm10.over.chain.gz` file. In both cases, the `'minMatch'` argument was set to 0.2 to ensure high DNA sequence conservation between murine and human regions. Only regions with an overlap above 90% and width difference below 40% with the original regions after mm10-hg19-mm10 liftover sequence were kept. Then, original and hg19-liftover regions were annotated with the symbols of overlapping genes as well as their closest gene using the gene references described in section 2.3. To include promoter regions, all gene regions were extended by 2 kb upstream of their transcription start site. After translation of MGI symbols to HGNC symbols with biomart (Durinck et al., 2009), mm10 region - hg19 liftover region pairs without any matching symbols were filtered out. The procedure to derive a species-conserved tisTreg peak signature is summarized in Figure 10.

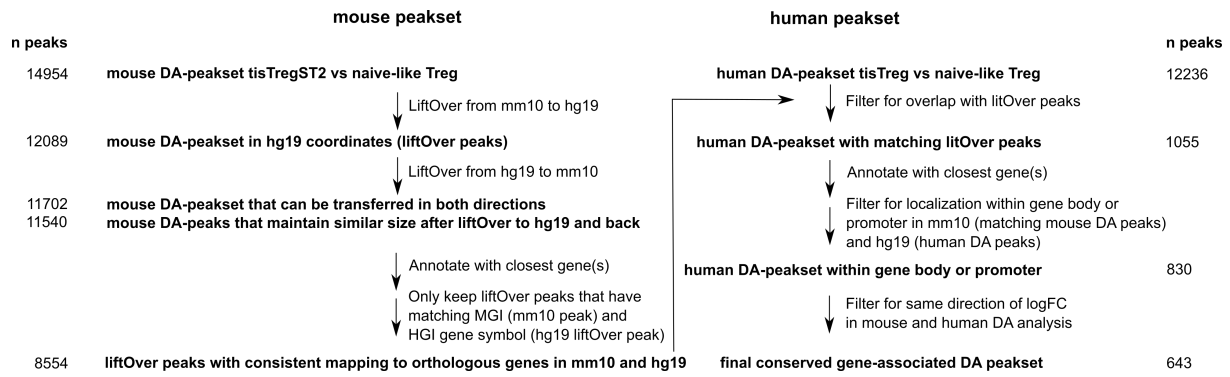


Figure 10: Cross-species region comparison. Steps done to derive a tisTreg signature conserved between mouse and human. The number of available peaks in each step is indicated.

2.13 Comparison of scATAC-seq and ChIP-seq data

Chromatin immunoprecipitation following sequencing (ChIP-seq) data for transcription factor BATF was obtained from replicate 2 of GSM803538 (Pope et al., 2014). Subsequently, the number of peaks from the conserved tisTreg signature overlapping with at least one BATF ChIP-seq peak was counted to assess the extent of BATF binding.

2.14 Reference-based cell annotation

Reference-based cell annotation was done with SingleR using reference datasets from the cellDex R package (Aran et al., 2019). For mouse and human data, the ImmGen and Monaco immune reference atlases were chosen, respectively (Monaco et al., 2019; Heng et al., 2008). Prior to annotation, reference samples were reduced to the cell types present in the query dataset. Annotation was performed based on the normalized gene activity matrix using the command 'SingleR' with default settings.

3 Results

In Chapter 3.1, I present analyses of several murine and human CD4⁺ T cell datasets that resulted in the epigenetic characterization of human tissue regulatory T (tisTreg) cells. Chapter 3.2 summarizes results from similarly composed datasets of CD8⁺ T cells and defines peripheral tissue PD1⁺TOX⁺ CD8⁺ T cells with a shared activation and intermediate exhaustion phenotype. Finally, I give an outlook on tissue adaptation programs in a pan-immune cell context by introducing a murine and human scATAC-seq immune cell atlas in Chapter 3.3.

The projects presented in this thesis are the result of collaborative work between the Chair of Immunology at the Leibniz Institute for Immunotherapy in Regensburg headed by Prof. Dr. Markus Feuerer and the Division of Applied Bioinformatics at the German Cancer Research Center (DKFZ) in Heidelberg headed by Prof. Dr. Benedikt Brors. Prof. Dr. Markus Feuerer and Prof. Dr. Michael Delacher (Chair of Immunology at the Leibniz Institute for Immunotherapy and Institute of Immunology, University Medical Center Mainz) conceptualized the projects. All wet-lab experiments, sequencing and data demultiplexing were performed at the Leibniz Institute for Immunotherapy. Dr. Charles Imbusch (Division of Applied Bioinformatics, DKFZ) analyzed scRNA- and scTCR datasets. Bulk RNA-seq analysis was performed by Dr. Agnes Hotz-Wagenblatt (Core Facility Omics IT and Data management, DKFZ). I (Division of Applied Bioinformatics, DKFZ) performed the bioinformatic analysis of all scATAC-seq datasets generated for these projects.

3.1 Characterization of CD4⁺ regulatory T cells in humans and mice

In this project, I analyzed several scATAC-seq datasets of sorted CD4⁺ T cells from murine and human tissues. This confirmed the presence of a previously identified Treg cell population with regenerative capacity (termed tisTregST2 cells) in murine peripheral tissues and led to the identification of human tisTreg cells with similar characteristics (Delacher et al., 2017, 2020). A cross-species comparison of chromatin accessibility allowed the identification of a conserved tisTreg epigenetic program. Further, transcription factor footprinting indicated a strong regulatory role of basic leucine zipper transcription factor, ATF-like (BATF) in this program. Importantly, we identified the chemokine receptor CCR8 as a common marker for murine and human tisTreg cells which is also useful to detect their precursor cells in the blood. In contrast to these commonalities, I showed that human tisTreg cells share a T follicular helper (Tfh)-like differentiation program, which differs from the T-helper 2 (Th2)-like tisTregST2 program observed in Treg cells within murine peripheral tissues. In a comparison of tisTreg cells from healthy tissues with tu-

mor Treg cells I further revealed that several features which were previously thought to be tumor-specific rather depict tissue adaptations, which are also present under homeostatic conditions.

Results from this analysis were published in:

Single-cell chromatin accessibility landscape identifies tissue repair program in human regulatory T cells (Delacher, M., Simon, M., Sanderink, L., Hotz-Wagenblatt, A., Wuttke, M., Schambeck, K., Schmidleithner, L., Bittner, S., Pant, A., Ritter, U., Hehlhans, T., Riegel, D., Schneider, V., Groeber-Becker, F. K., Eigenberger, A., Gebhard, C., Strieder, N., Fischer, A., Rehli, M., Hoffmann, P., Edinger, M., Strowig, T., Huehn, J., Schmidl, C., Werner, J., Prantl, L., Brors, B., Imbusch, C., Feuerer, M., 2021, *Immunity*).

3.1.1 Identification of tisTregST2 cells in healthy murine tissues

To investigate chromatin accessibility in Treg cells under homeostasis on a single-cell level, my collaborators Prof. Dr. Markus Feuerer and Prof. Dr. Michael Delacher generated a scATAC-seq dataset of murine CD4⁺ T cells. Briefly, CD4⁺ and CD4⁺CD25⁺ T cells were extracted from tissues pooled from several specific-pathogen-free (SPF) mice including spleen, colon, skin, visceral adipose tissue (VAT) and lung and subjected to droplet-based single-cell assay for transposase-accessible chromatin using sequencing (scATAC-seq) using the 10x Genomics Chromium Single Cell ATAC library preparation and Illumina Next-Generation Sequencing (Supplementary Table S1, details described in Methods Chapter 2.1).

I processed demultiplexed FASTQ files using the Cell Ranger ATAC pipeline, which includes quality control steps on reads and barcodes, read alignment and peak calling. Subsequently, I annotated barcodes as cells if they passed several quality control criteria (Supplementary Figure S1A). These included a sufficient number of detected fragments (unique sequenced reads of pieces of DNA resulting from two adjacent Tn5 transposase integration events) for downstream analyses. Furthermore, I calculated the enrichment of reads around transcription start sites over their flanking regions, which is expected to be high for high-quality single-cell libraries. Eventually, I confirmed successful ATAC library preparation by plotting the distribution of fragment sizes, which showed a clear periodicity representing nucleosome positioning (Supplementary Figure S1B) (Buenrostro et al., 2015). After quality control a dataset of 26,002 cells with a median of 20,397 fragments per cell was obtained. I then generated a low-dimensional representation of the data using latent semantic indexing (LSI) and UMAP (Deerwester et al., 1990; McInnes et al., 2018), which is shown colored by originating tissue in Figure 11A. After batch-correction against the pool of mice using Harmony (Korsunsky et al., 2019), I clustered cells in the obtained low-dimensional space (Figure 11B, Supplementary Figure 11C). Cells in the

UMAP space arranged according to library sizes within clusters, but count depth did not strongly influence the overall clustering (Supplementary Figure 11D). To identify cell types in this CD4⁺ T cell atlas, I calculated gene activities by summing up reads within genes and their promoter regions for known marker genes. Treg cell clusters were highlighted by gene activity of their master regulator FOXP3, killer cell lectin-like receptor subfamily G1 (KLRG1) and effector molecules AREG and IL-10 (Figure 11C, Supplementary Figure S2A). Proliferator-activated receptor γ (PPAR- γ), which was identified as an important transcription factor for fat Treg cell accumulation but also accessible in tisTregST2 cells in general, had the highest gene activity in fat Treg cells, thereby supporting these previous findings (Cipolletta et al., 2012; Delacher et al., 2020). On the other hand, accessibility at the *Il2*, *Tbx21* and *Ifng* loci identified FOXP3-negative conventional T (Tconv) cells in peripheral tissues. *Sell* (CD62L) gene activity was high in the majority of cells derived from the spleen (e.g. clusters 0, 3, 4, 7) and marked the localization of naive T cells.

In addition to marker gene activity, I also employed previously established ATAC signatures to identify tisTregST2 cells (Delacher et al., 2020). The core tisTregST2 signature contains peaks conserved in tisTregST2 cells among multiple tissues and includes several regions at gene loci encoding tisTregST2 key regulators or effector molecules. It clearly highlighted Treg cells in peripheral tissues, as shown in Figure 11D. Moreover, tisTregST2 signatures separately derived for each tissue also had the highest overlap in tisTregST2 cells from the respective tissue in our dataset, thereby confirming their tissue specificity (Supplementary Figure S2B). Potential precursor Treg cells from the spleen were highlighted by the early and late tisTregST2 progenitor signatures (Delacher et al., 2020). Based on these analyses, I annotated tisTregST2 cells in the VAT (cluster 23), skin (16) and colon (10, 19). Treg cells from the spleen were found in clusters 0, 3, 5, 11, 14, 18 and 22. I further annotated effector CD4⁺ T cells in peripheral tissues including the VAT (2, 17, 21), skin (12, 20) and colon (6).

To derive a tisTregST2-specific peakset based on our scATAC-seq data, I performed a differential accessibility analysis via comparison of skin and VAT tisTregST2 clusters 16 and 23, which showed the highest overlap with the core tisTregST2 signature, against spleen naive Treg cell clusters 0, 3 and 14. This resulted in a signature of 14,594 peaks, half of which (7,655 peaks) were significantly more accessible in tisTregST2 cells. Closer examination revealed a stronger fold-change in accessibility for the majority of these peaks within tisTregST2 cells from the skin as compared to the VAT (Figure 12, left). To show the specificity of these results, I annotated the closest genes to the peaks and confirmed the presence of known tisTregST2 marker genes (*Klrg1*, *Pparg*, *Il10*) (Figure 12, right) (Tsukumo et al., 2013; Delacher et al., 2020).

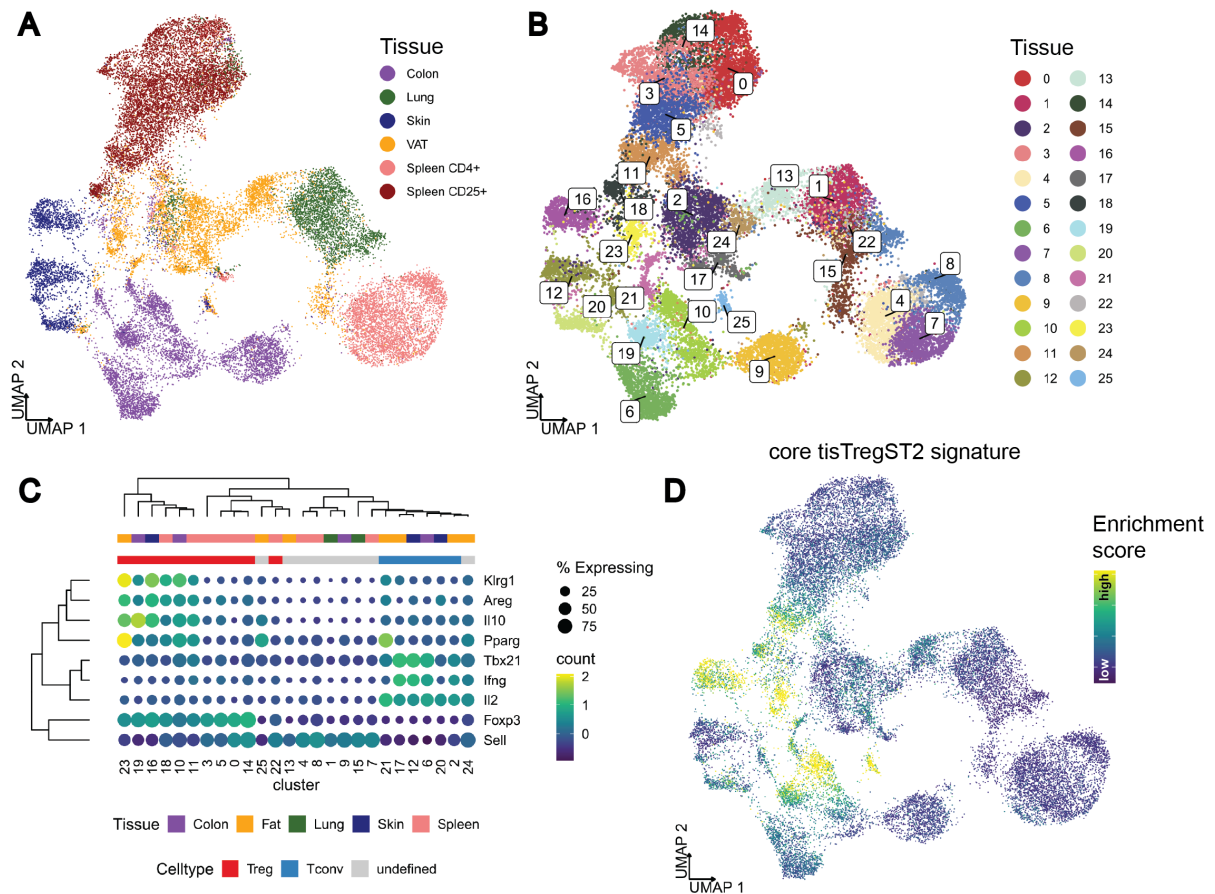


Figure 11: Mouse CD4⁺ T cell atlas. scATAC-seq data of CD4⁺ T cells sorted from different murine tissues. UMAP colored by **A** originating tissue and defining FACS marker, **B** clusters obtained from graph-based clustering. **C** Dotplot of marker gene activity showing the percentage of cells with detected activity and scaled number of fragments per cluster. The top annotation shows the main tissue of origin and cell type for each cluster. Columns and rows are clustered using Euclidean distances and complete linkage. **D** UMAP colored by enrichment of core tisTregST2 signature peaks within each cell. Modified from Delacher et al. (2021).

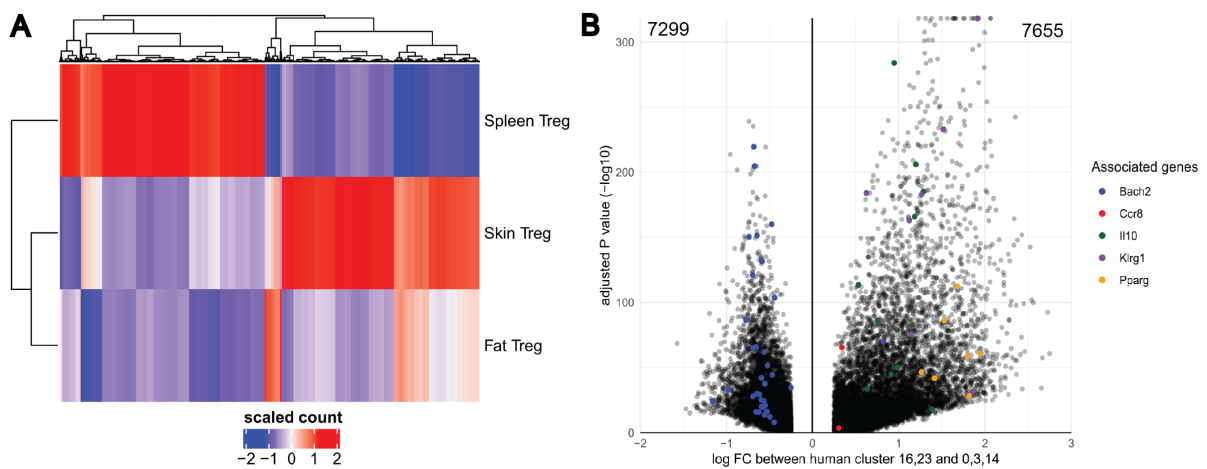


Figure 12: Mouse tisTregST2 peakset. **A** Heatmap of scaled accessibility within peak regions resulting from the differential comparison of murine skin and fat tisTregST2 cells against naive Treg cells from the spleen. Columns show differentially accessible peaks and are clustered using Euclidean distances and complete linkage. **B** The volcano plot is showing log-fold change and adjusted P-values of the differential accessible peaks between tisTregST2 cells (cluster 16, 23) and naive Treg cells (cluster 0, 3, 14). The number of differentially accessible peaks is indicated and gene symbols of several peak-associated genes with important role in Treg biology are highlighted (tisTregST2 marker genes *Klrg1*, *Pparg*, *Il10*; naive T cell transcription factor *Bach2*; chemokine receptor *Ccr8*). Modified from Delacher et al. (2021).

3.1.2 Dependence of tisTreg cells in the colon on microbiota

To investigate whether the maturation and maintenance of the colonic tisTregST2 population depends on microbiota, my collaboration partners generated a dataset similar to Chapter 3.1.1 using gnotobiotic mice. I processed the data and performed quality control (Supplementary Figure S3), which resulted in a dataset of 31,124 cells with 8,562 median fragments per cell. Subsequently, I reduced the dimensionality of the data by running LSI and UMAP and clustered the cells in LSI space. A UMAP representation of the data colored by originating tissue and cluster annotation is shown in Figure 13A-B. Similar to the previous analysis, I used gene activities and bulk ATAC tisTregST2 signatures to annotate clusters (Figure 13C-D, Supplementary Figure S4). Cluster 9 mainly contained tisTregST2 cells from the colon, but also from the VAT, whereas cluster 13 represented skin tisTregST2 cells. Moreover, spleen-derived cluster 6 was identified as tisTregST2 precursor population and clusters 1, 5, 15 and 17 contained naive Treg cells. Eventually, several Tconv cell clusters were annotated (clusters 3, 11, 12, 19, 20).

To further investigate the influence of microbiota on Treg cells in the colon, I next filtered the scATAC-seq data from SPF and gnotobiotic mice to the subset of colon-derived cells and repeated dimensionality reduction (Figure 14). Subsequently, I plotted marker gene activities and the core tisTregST2 signature to identify tisTregST2 cells. In both datasets, a population of cells with high *Foxp3*, *Klrg1* and *Ikzf2* and low *Rorc* chromatin accessibility was detected corresponding to tisTregST2 cells of thymic origin (tTreg cells). In contrast, peripheral Treg (pTreg) cells with high *Foxp3* and *Rorc* but low *Ikzf2* gene activity were only detected in the colon of SPF mice but not in germ-free mice in line with previous studies (Atarashi et al., 2013; Sawa et al., 2011; Sefik et al., 2015). The tTreg fractions had high gene activity of *Areg* and *Il10*. My collaboration partners confirmed the protein expression of these genes in KLRG1⁺ Treg cells isolated from the skin of SPF and gnotobiotic mice (data not shown).

Together, this analysis showed that tisTregST2 cells of thymic origin, but not pTreg cells, populate the colon without interaction with microbiota-derived antigens and express tisTregST2 effector molecules AREG and IL-10.

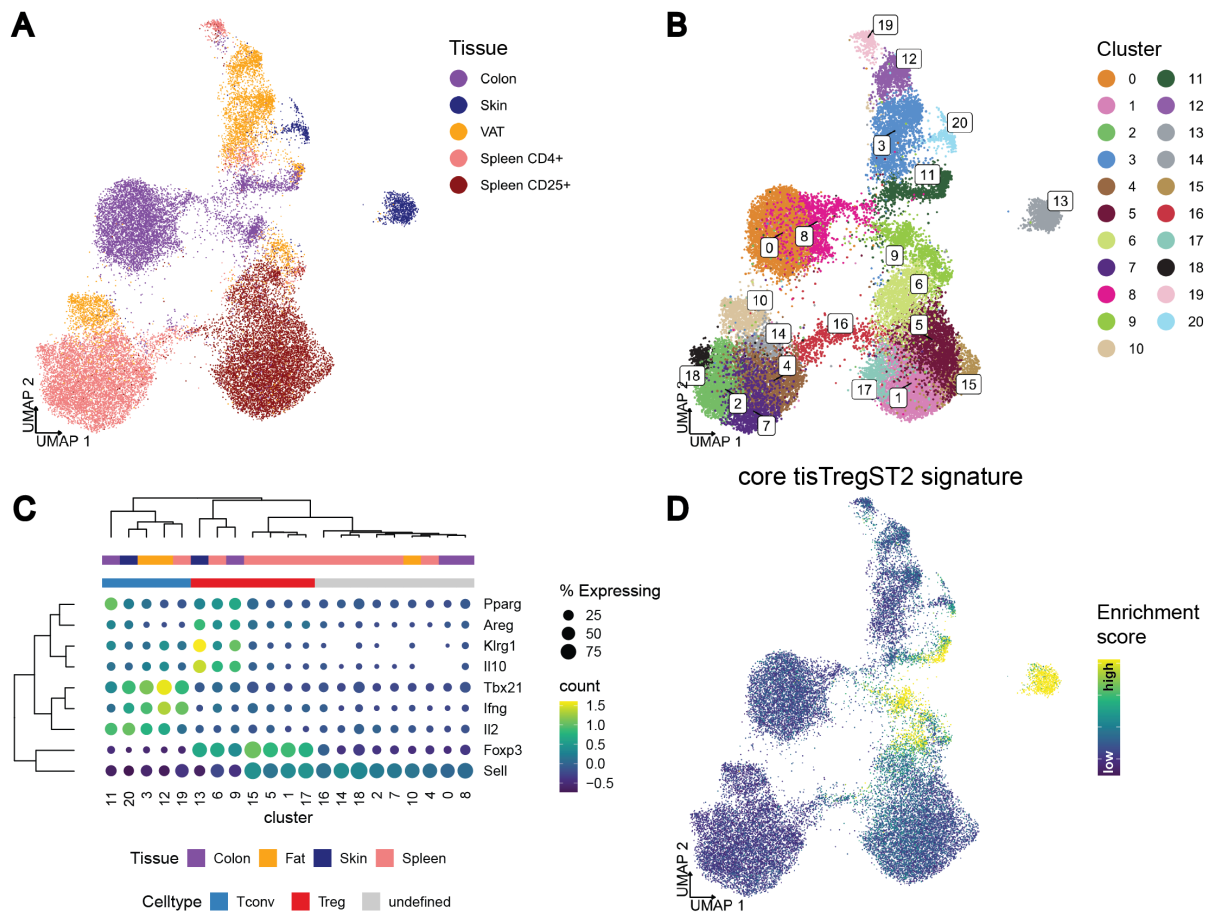


Figure 13: Mouse gnotobiotic CD4⁺ T cell atlas. UMAP of scATAC-seq data from gnotobiotic mice colored by **A** tissue and sort marker and **B** results from graph-based clustering. **C** Dotplot of marker gene accessibility showing the percentage of cells and scaled number of fragments per cluster. The top annotation shows the main tissue of origin and cell type for each cluster. Rows and columns are clustered using Euclidean distances and complete linkage. **D** Core tisTregST2 signature enrichment. Modified from Delacher et al. (2021).

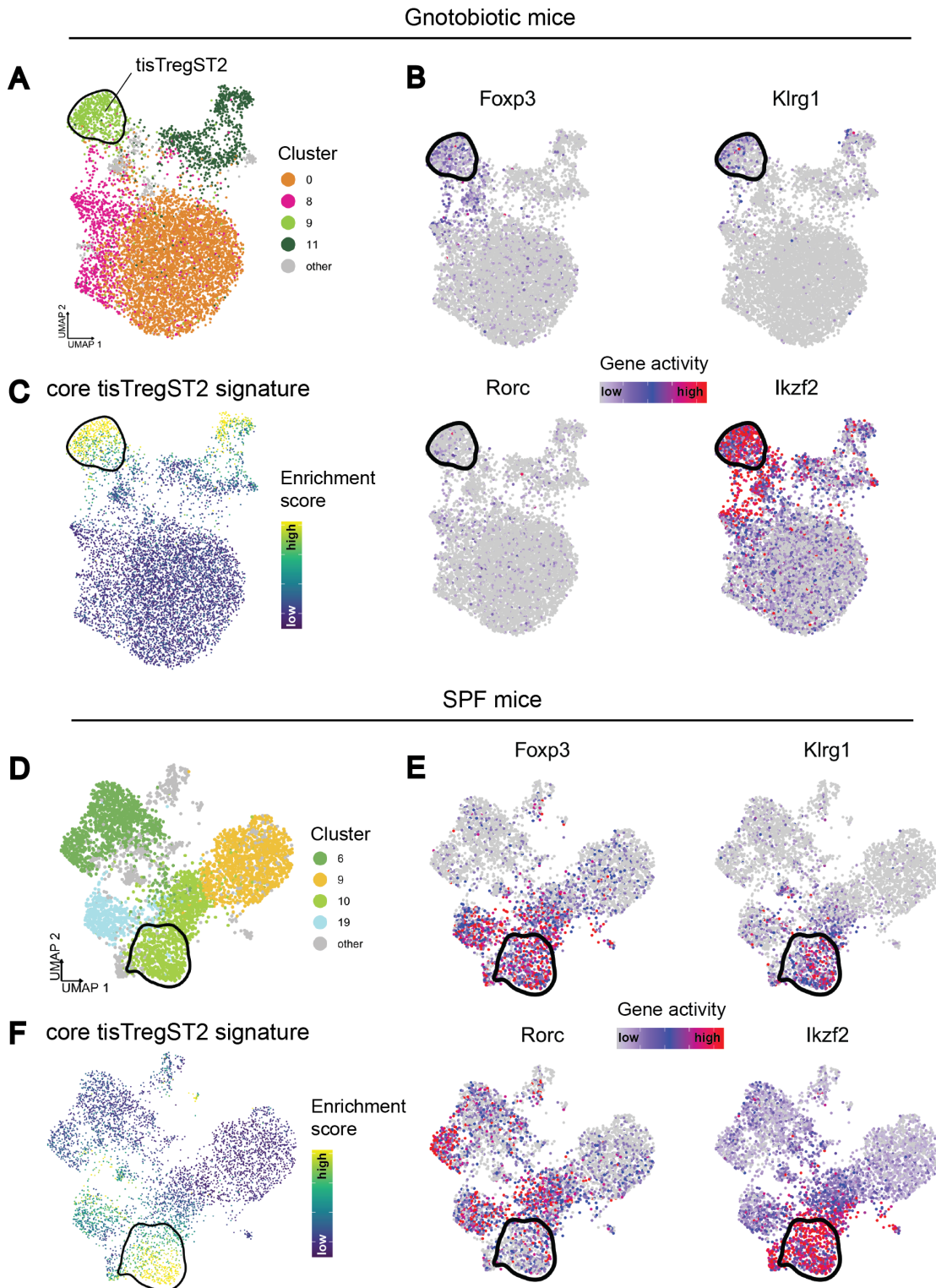


Figure 14: *tisTregST2* evolve independently from microbiota. UMAP representation of colon-derived CD4⁺ T cells selected from the gnotobiotic mice colored by **A** cluster annotation from Figure 13B, **B** gene activity of *Foxp3*, *Klrg1*, *Rorc* and *Ikzf2* and **C** enrichment of core *tisTregST2* signature peaks. Equivalently, a UMAP representation of colon-derived CD4⁺ T cells selected from SPF mice colored by **D** cluster annotation from Figure 11B, **E** gene activity and **F** core *tisTregST2* signature enrichment is shown. The *tisTregST2* populations of thymic origin are circled. Additionally, a pTreg population is detected in cluster 19 of SPF mice. Modified from Delacher et al. (2021).

3.1.3 tisTreg cells in healthy human tissues show Tfh-bias

In the previous chapters, I have shown that scATAC-seq is a suitable method to characterize Treg cells and was able to confirm previous results on tisTregST2 cells (Delacher et al., 2020, 2017). Since it is unclear whether a population similar to murine tisTregST2 cells also exists in humans, my collaboration partners generated a scATAC-seq dataset of sorted CD4⁺ T cells from blood, fat and skin tissue of healthy human donors. Based on the established metrics, I evaluated the quality of the sequenced samples and performed filtering on the barcodes resulting in a final dataset of 83,267 cells with a median number of 12,989 fragments per cell (Supplementary Figure S5A-B). Since the cells clustered by donor, I performed a Harmony integration of the data using the donor as batch variable (Supplementary Figure S5C). I also used the corrected embedding for graph-based clustering into 16 clusters and UMAP dimensionality reduction (Figure 15A-B and Supplementary Figure S5C-D). Subsequently, I annotated cells based on gene activities of lineage-defining genes (Figure 15C and Supplementary Figure S6). Specifically, accessibility in the human Treg marker genes *FOXP3*, *CTLA4* and *ENTPD1* (CD39) was observed in clusters 1, 3, 7, 8, 9 and 11. These cells also had high *IKZF2* gene activity supporting a tTreg differentiation path. The murine tisTregST2 marker gene *KLRG1* had very low accessibility in human Treg cells indicating the need to further investigate differences between murine and human Treg cells. Low *FOXP3* but high gene activity of genes encoding Th effector molecules including *IL2* and *IFNG* was found in clusters 0, 2, 4, 10, 12, 14, which I annotated as Tconv cells. Eventually, high *SELL* gene activity and low accessibility within genes encoding activation-associated molecules marked naive Tconv (6, 13) and Treg (7) cell clusters. While murine tisTregST2 cells have been shown to be Th2-biased, loci encoding Th2 key transcription factors including *GATA3* and *IRF4* did not have increased accessibility in human tisTreg cells (Supplementary Figure S7) (Delacher et al., 2017, 2020; Tindemans et al., 2014). However, I showed that human tisTreg cells share many chromatin regulatory features with Tfh cells by generating a Tfh peak signature from a public human T cell scATAC-seq dataset (Satpathy, 2019). I then tested for its enrichment in our dataset of healthy human CD4⁺ T cells (Figure 15D). The overlap with this signature increased from naive (cluster 7) over memory (cluster 1) towards Treg cells in the fat and skin (cluster 3) indicating a possible developmental path (Figure 15E).

Since cluster 3 was the only one containing Treg cells from peripheral tissues including fat and skin, I performed a differential accessibility analysis between these tissue Treg cells and blood naive Treg cluster 7 to derive a human tisTreg peak signature. This resulted in 12,236 differential accessible peaks including 4,416 tisTreg-specific peaks. Among these, I observed both shared and tissue-specific increases in accessibility (Figure 16, left). Several naive Treg-associated peaks were in close proximity to *BACH2*, whereas increased

accessibility in tisTreg cells was found nearby *CTLA4* and *ENTPD1*, thereby supporting the validity of the signature (Figure 16, right).

To provide evidence that the human Tfh-biased tisTreg population represents cells with tissue-regenerative capacity, my collaboration partners performed an *in-vitro* wound-healing experiment (Figure 17A-B). First, they treated naive Treg cells either with a cytokine cocktail inducing Tfh differentiation or only Il-2 to maintain the Treg phenotype for 6 days. Supernatant from these cells was collected and applied to a wound-healing assay, in which the closing of a scratched layer of keratinocytes was observed over time. As a result, wounds treated with supernatant from Tfh-like Treg cells closed significantly faster compared to those treated with supernatant from Il2-only Treg cells or without supernatant. They next performed bulk ATAC-seq of *in-vitro* Tfh-like Treg cells and Il-2-only Treg cells and compared them against each other to define differentially accessible peaks (*in-vitro* Tfh-like Treg signature, 12,622 Tfh-like Treg-specific peaks). To evaluate the similarity of *in-vitro* Tfh-like Treg cells with tissue Treg cells, I annotated the closest gene to each peak in the human tissue Treg signature, the Tfh-like signature and the *in-vitro* Tfh-like Treg signature and calculated intersection sizes (Figure 17C). Approximately half of the peak-associated genes in both the human tissue Treg signature (784/1,633 genes) and the Tfh-like signature (826/1,675 genes) overlapped with those from the *in-vitro* Tfh-like signature. This was well above the expected overlap of 23% (5,361/22,955 genes) for a random selection of genes from the human CD4⁺ dataset. In addition, my collaboration partners compared *in-vitro* induced Tfh-like Treg cells with ex-vivo human CCR8⁺ Treg cells on the transcriptomic level, which resulted in 228 common upregulated genes including several transcription factors and tissue-repair-associated genes such as *BATF*, *BCL6*, *PDGFA* and *GRN* (data not shown) (Bateman et al., 2018; Bowen-Pope et al., 1989).

Together, these experiments confirmed the tissue-regenerative capacity of human tisTreg cells and showed that a similar population can be generated *in-vitro* from naive Treg cells by applying a Tfh-inducing cytokine mixture.

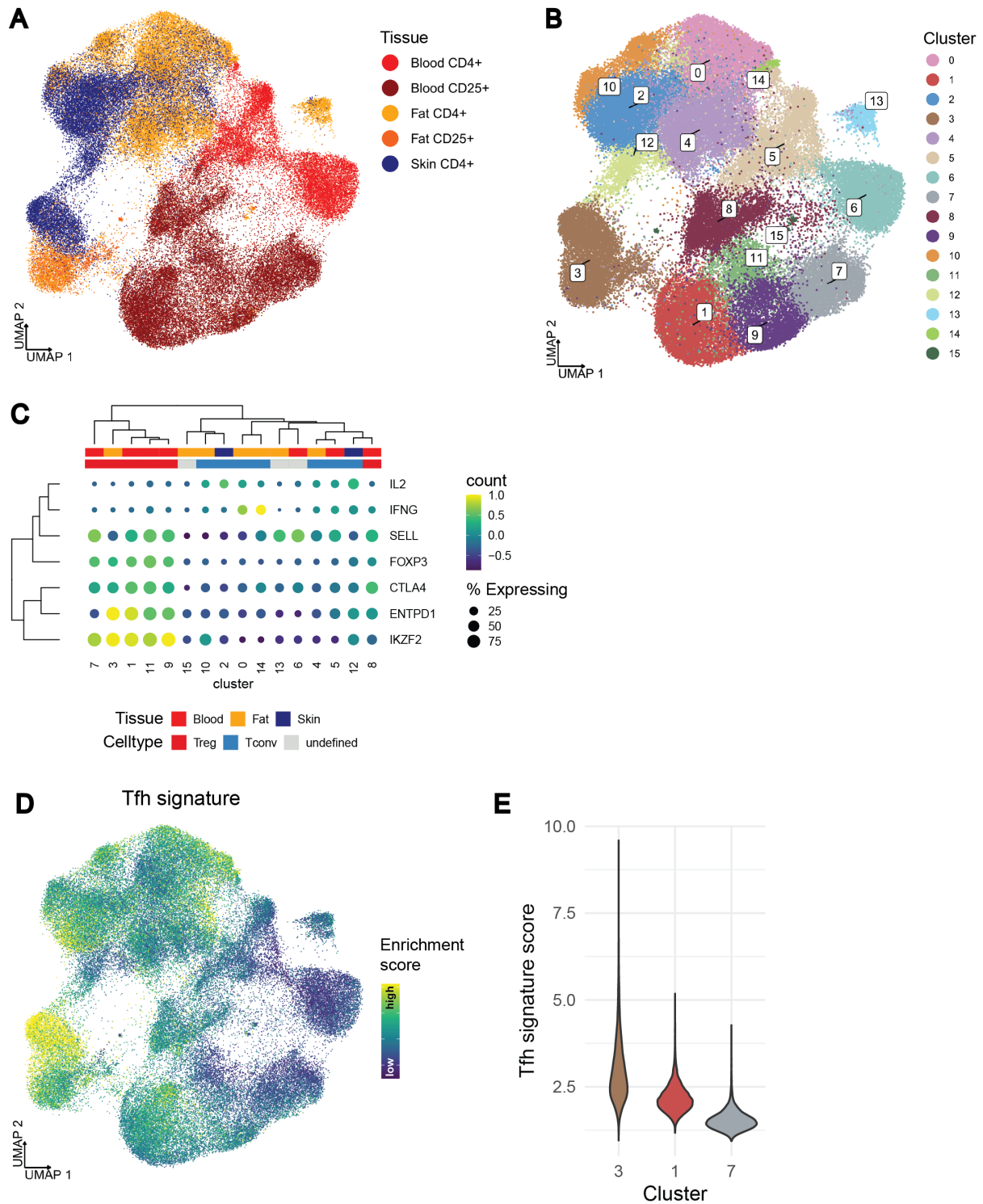


Figure 15: Human CD4⁺ T cell atlas. **A** UMAP representation colored by tissue of origin and the defining sort marker. **B** Cell grouping into 16 clusters based on graph-based clustering. **C** Dotplot showing scaled gene activity and percentage of cells with detected activity per cluster. The top annotation shows main tissue per cluster and annotated cell types. Rows and columns are clustered using Euclidean distances and complete linkage. Enrichment scores of Tfh-associated peaks **D** in the UMAP space and **E** as violin plot for Treg clusters 1, 3 and 7. Modified from Delacher et al. (2021).

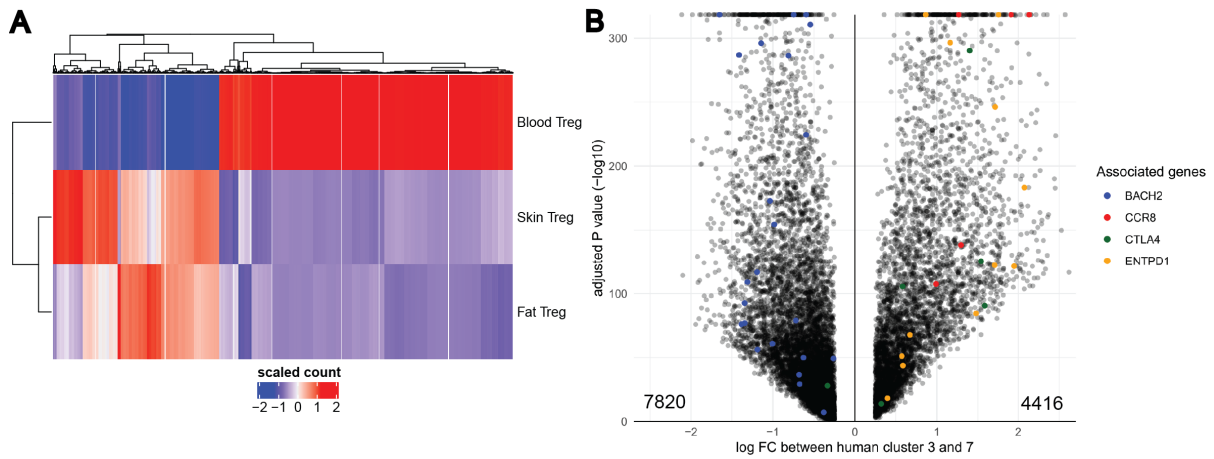


Figure 16: Human tisTreg peakset. A human tisTreg-specific peakset was derived by comparing fat and skin Treg cluster 3 against naive Treg cluster 7 resulting in 12,236 differential peaks. **A** Heatmap of scaled accessibility of tisTreg signature peaks in skin, fat and blood Treg cells. Columns show differential peaks and are clustered using Euclidean distances and complete linkage. **B** The volcano plot is showing log-fold changes and adjusted P-values of peaks from the differential accessibility analysis. Numbers of differentially accessible peaks for the respective clusters are indicated and *BACH2*-, *CCR8*-, *CTLA4*- and *ENTPD1*-associated peaks are highlighted. Modified from Delacher et al. (2021).

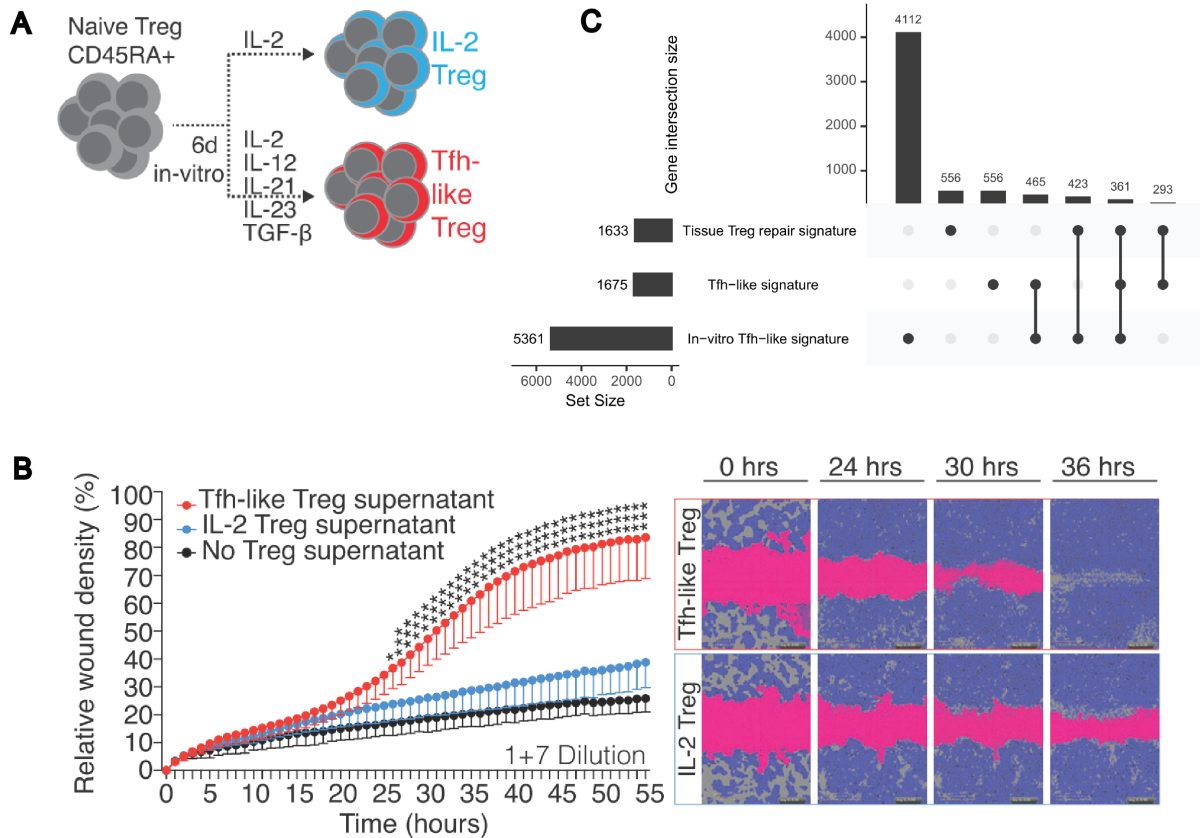


Figure 17: Human Tfh-like Treg cells support wound healing. **A** Scheme of the experimental setup. Naive Treg cells were treated either with IL-2 only or a cytokine cocktail (IL-2, IL-12, IL-21, IL-23 and TGF β), which is known to induce Tfh differentiation over 6 days. **B** Diluted supernatants including factors secreted by the IL-2 Treg cells or Tfh-like Treg cells were applied to a wound-healing assay, in which closing of a wounded HaCaT cell monolayer was tracked over time ($n = 5$, unpaired t test, adjustment of p-values with Holm-Sidak test). **C** Upset plot showing intersection sizes between the human tissue Treg signature ('Tissue Treg repair signature'), the Tfh-like signature and the *in-vitro* Tfh-like signature. For each signature peak, the closest gene was annotated. Subsequently, unique genes were compared between the sets. Subfigures A and B were prepared by Prof. Dr. Michael Delacher. Modified from Delacher et al. (2021).

3.1.4 Determination of a conserved tisTreg epigenetic signature

Having defined mouse and human tisTreg peaksets based on scATAC-seq data, I was wondering whether these chromatin states are conserved between species. Therefore I developed an approach to perform a cross-species comparison of genomic regions based on the UCSC genome liftOver tool (described in Methods Chapter 2.12) (Kuhn et al., 2013). Briefly, the mouse tisTregST2 signature with 14,954 peaks was transferred to the human genome and tested for robustness resulting in 8,554 peaks transferred from mm10 to hg19. Subsequently, I searched for overlaps of the liftOver peaks with the human tisTreg peakset (12,236 peaks) and determined 1,055 matches. A final conserved tisTreg signature with 643 peaks was obtained by filtering for peak pairs within gene bodies or promoter regions that have a consistent direction of change in chromatin accessibility in

the mouse and human differential accessibility analysis (Figure 18A). Annotation of the closest genes showed that species-conserved tisTreg peaks are located within transcription factors (*BATF*, *GATA3*, *TOX*), surface receptors (*CCR2*, *CCR5*, *CCR6*, *CCR8*), and members of the TNF receptor superfamily (*TNFRSF8*, *TNFRSF9*). A low accessibility compared to naive Treg cells was observed for tisTreg cells at the loci encoding transcription factor *BACH2* and surface receptor *CCR7*.

I next approached the question whether there are common transcription factors regulating tisTreg development. First, I used HOMER to search for de-novo motifs in the human tisTreg peakset (4,416 skin and fat Treg-specific peaks). This revealed a DNA pattern similar to the basic leucine zipper (bZIP) domain transcription factor family motif as top enriched sequence (Figure 18B, top) (Heinz et al., 2010). As transcription factor BATF belongs to this family and was also among the conserved genes gaining chromatin accessibility within tisTreg cells, I quantified the accessibility around BATF binding motifs throughout the human genome. This showed high coverage within cells from tisTreg cell cluster 3, somewhat lower coverage in memory Treg cell cluster 1 and lowest coverage in naive Treg cell cluster 7 (Figure 18B, bottom). I found further evidence for the importance of BATF in tisTreg development by searching for overlaps between the conserved tisTreg signature peaks with publicly available BATF chromatin immunoprecipitation following sequencing (ChIP-seq) data (Gene Expression Omnibus accession code GSM803538). This revealed BATF binding sites within more than half of the tisTreg-specific peaks, whereas less than a quarter of conserved naive Treg peaks had confirmed BATF binding sites (summarized as piecharts in Figure 18A).

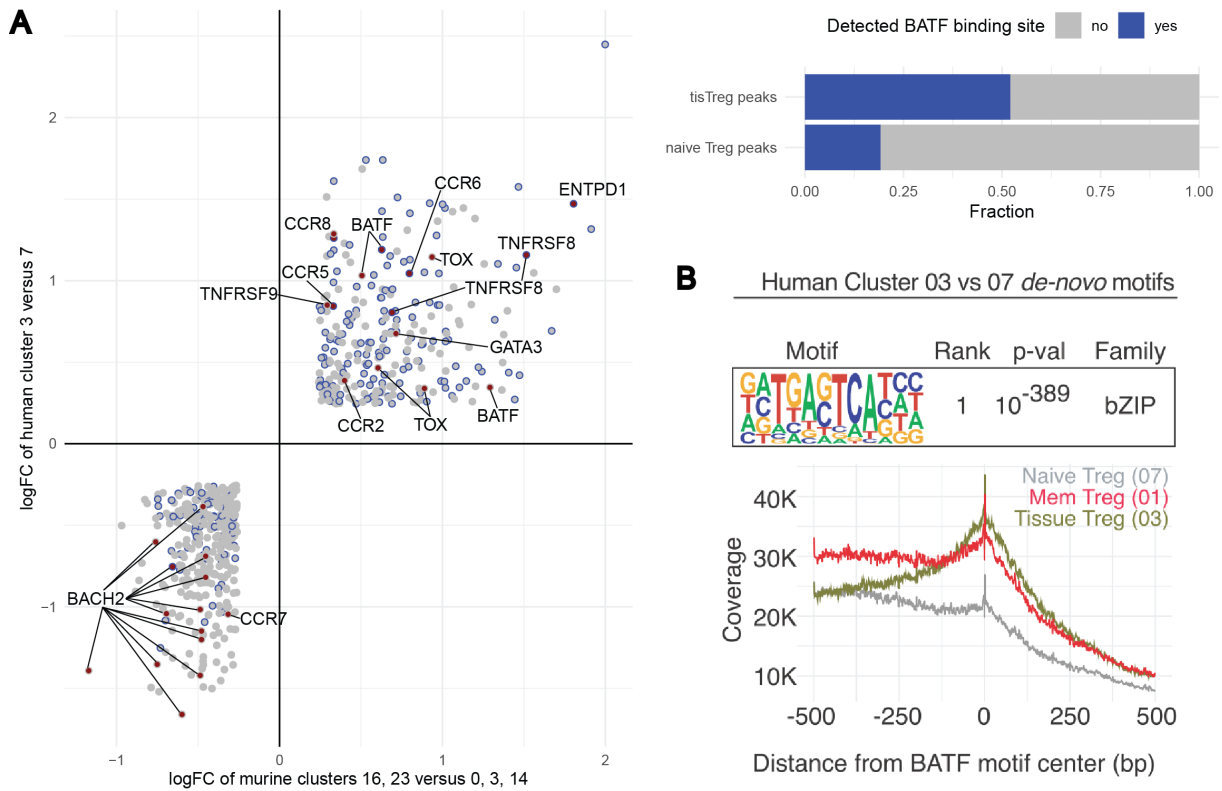


Figure 18: Species-conserved tisTreg signature. **A** Left, scatter plot of 643 conserved tisTreg-specific peaks in mouse and humans. Log-fold changes are shown from the human and murine cluster comparison of tisTreg cells against naive Treg cells. Genes of interest are highlighted and ATAC peaks overlapping with peaks from a BATF ChIP-seq experiment (GSM803538) are encircled in blue. Right, barplot summarizing the number of peaks with BATF ChIP-seq overlaps for tisTreg- and naive Treg-specific peaks. **B** Top, most enriched motif from the HOMER de-novo motif analysis on human tisTreg-associated peaks and most similar transcription factor family. Bottom, transcription factor footprint for the BATF motif that summarizes the coverage around BATF binding sites for human Treg clusters 1, 3 and 7. Modified from Delacher et al. (2021).

3.1.5 tisTreg cell development and identification of precursor cells

A fundamental question in the characterization of tisTreg cells is how they develop from naive T cells. It was previously shown that murine tisTregST2 cells have two precursor stages, which can be detected in lymphoid tissues including the spleen and lymph nodes (Delacher et al., 2020). Building on these results, I performed pseudotime analyses using Monocle (Trapnell et al., 2014). First, I extracted Treg cell clusters from the SPF mouse CD4⁺ T cell dataset and used the most accessible peaks to order cells along a pseudotime trajectory (Figure 19A). This showed a developmental path starting from naive Treg cell cluster 0 over clusters 5 and 11 towards tisTregST2 clusters from the colon (10), skin (16) and VAT (23) (Supplementary Figure S2B). Clusters 5 and 11 also shared a high overlap with the early and late tisTregST2 progenitor signature, respectively. Overall, the obtained trajectory confirmed a development with multiple precursor steps (Delacher et al., 2020). Moreover, an increase in BATF transcription factor ac-

tivity was observed over pseudotime supporting its role in tisTregST2 development. I applied the same procedure to order Treg cells from the gnotobiotic mice along a possible developmental path. Similar to the SPF mouse dataset, this resulted in a trajectory from naive Treg cells (cluster 01), over early and late precursor stages (cluster 6) towards tisTregST2 cells from peripheral tissues (clusters 9, 13) with a steady increase in BATF activity (Figure 19B).

I investigated whether a similar differentiation sequence is obtained in humans by subjecting Treg cells from the human CD4⁺ T cell dataset to trajectory inference with Monocle. As shown in Figure 19C, pseudotime increased from naive Treg cells (cluster 7) over memory Treg cells (cluster 1) from the blood towards the common skin and fat tisTreg cluster 3, again accompanied by an increase in BATF activity. Besides an increase in BATF chromVAR score (Schep et al., 2017), the chromatin accessibility within the BATF gene locus also increased from naive over memory Treg towards tisTreg cells.

In summary, pseudotime analysis showed that BATF is an important transcription factor in both mouse and human tisTreg development. Since BATF is also known to be involved in Tfh cell development in humans (Ise et al., 2011) the observed overlap with the Tfh signature within the tisTreg cluster described earlier in Chapter 3.1.3 supports a major role of BATF in tisTreg development.

To identify potential tisTreg precursor cells in mice and humans, I searched for unifying marker genes within the conserved tisTreg signature (presented in Chapter 3.1.4). One such gene was the surface receptor *CCR8* (Figure 18A, in addition also highlighted in Figures 12 and 16). I used BATF ChIP-seq data to confirm a BATF binding site in its promoter region. Chromatin accessibility at this site and other regions in the promoter and gene body of *CCR8* increased from naive and progenitor Treg cells to tisTreg cells in both species making it a promising gene to track tisTreg progenitors early during their development (Figure 19D-E). My collaboration partners did two additional experiments to confirm *CCR8* as useful marker gene for tisTreg cells and their precursors in mice and humans: first, RNA-seq of flow-sorted murine tisTregST2 and their precursor populations showed that high *Ccr8* transcript numbers are detected in peripheral tisTregST2 cells and *Klrg1⁺Nfil3⁺* late tisTregST2 precursors (Figure 19F). *Klrg1⁻Nfil3⁺* early precursors had an intermediate *Ccr8* gene expression, which was still significantly higher than the expression level in *Klrg1⁻Nfil3⁻* naive Treg cells. This analysis showed that the observed increase in chromatin accessibility of *Ccr8* during tisTregST2 development entails an increase in *Ccr8* mRNA transcript levels. Second, additional scATAC-seq of flow-sorted CCR8⁺ Treg cells from human blood was performed to evaluate *CCR8* as a marker gene for tisTreg precursors in human blood. I integrated these data into the human CD4⁺ T cell atlas and repeated pseudotime analysis on the Treg cell compartment including blood CCR8⁺ Treg cells (Figure 19G, top). As expected, blood CCR8⁺ Treg cells aligned in

between naive Treg (cluster 7) and tisTreg (cluster 3) cells at a pseudotime similar to the blood memory Treg cells (cluster 1). I employed the human tisTreg peak signature presented in Figure 16 to further measure the similarity of blood CCR8⁺ Treg cells to tisTreg cells from the fat and skin. This signature was refined by correcting for Tconv-associated peaks. In detail, differential peaks from the comparison of Tconv clusters 0, 2, 4, 10, 12, 14 against cluster 7 from the human CD4⁺ T cell dataset were excluded resulting in 2,678 tisTreg-specific peaks (human tisTreg signature). The overlap with the human tisTreg signature was quantified in all Treg populations and showed that the CCR8⁺ Treg cells from the blood are most similar to tisTreg cells from peripheral tissues (Figure 19G, bottom). Eventually, I searched for differential peaks between fat and skin tisTreg cells from human cluster 3 and calculated their enrichment within the CCR8⁺ Treg population. This highlighted largely different subsets of cells indicating a commitment of precursors towards one specific tissue or possibly the presence of recirculating tisTreg cells from fat and skin (Figure 19H).

In summary, tisTreg cells develop from naive Treg cells via precursor populations present in the murine spleen and human blood. These can be detected using CCR8 as a common marker.

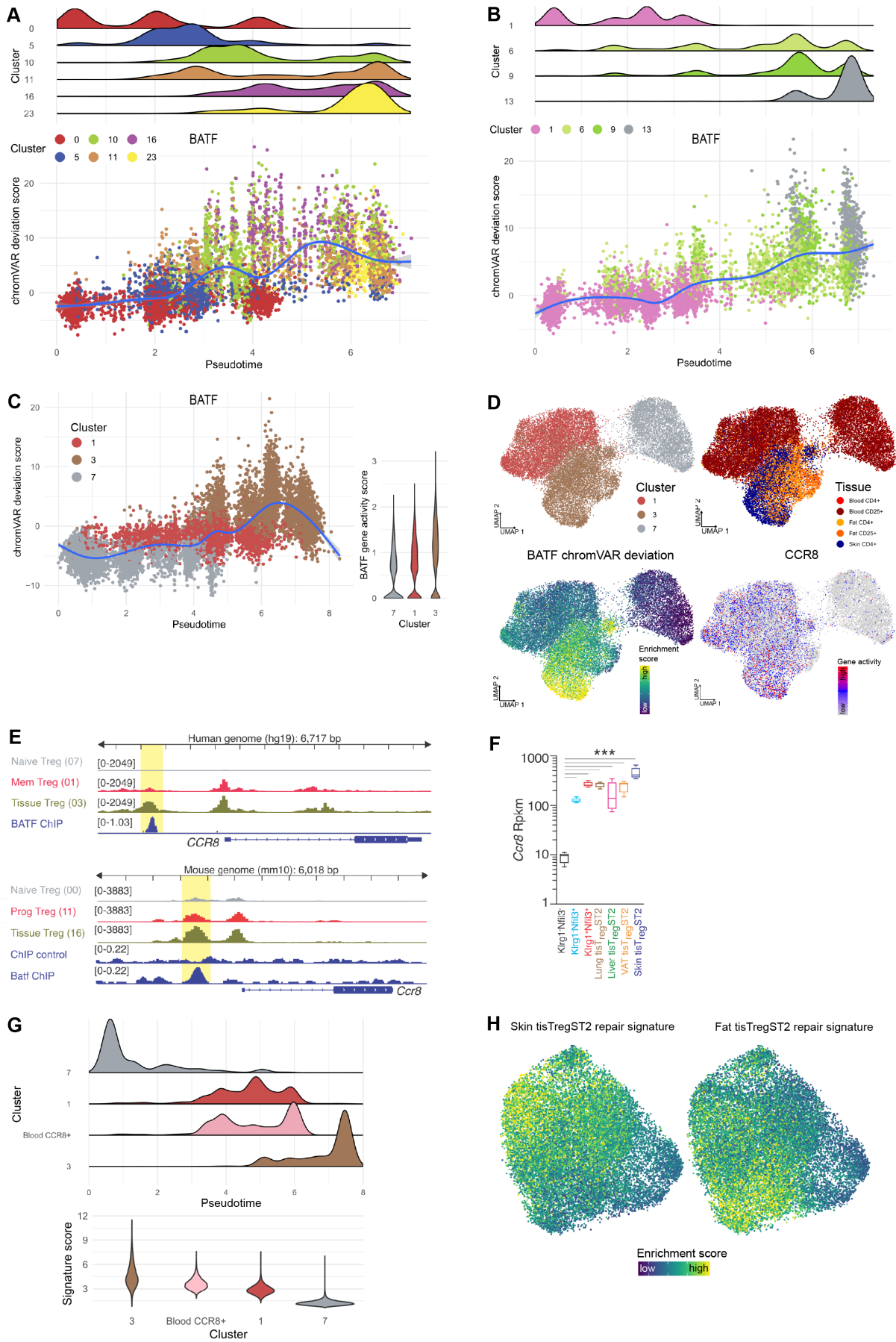


Figure 19: tisTreg development. (Legend continued.)

3.1.6 Treg cells in tumors also have a tisTreg phenotype

High expression of *CCR8* in Treg cells within tumor tissue has been described in several studies (De Simone et al., 2016; Plitas et al., 2016). Since I was interested in comparing tisTreg cells from healthy peripheral tissues to tumor-resident Treg cells, I downloaded and analyzed a publicly available scATAC-seq dataset containing cells from tumor biopsies of several basal cell carcinoma patients (Satpathy, 2019). I extracted the CD4⁺ T cell subset from the data using the authors' annotations and visualized the cells in UMAP space (Figure 20A). Treg cells indeed had high gene activity of *CCR8*. High accessibility within the *IKZF2* gene locus classified these cells as tTreg. Importantly, the previously defined human tissue Treg signature was enriched within the majority of tumor Treg and Tfh cells. To confirm this result, I searched for differentially accessible peaks of tumor Treg cells in comparison to other CD4⁺ T cells in the tumor dataset (Tumor Treg signature). The tisTreg cells (cluster 3) from the healthy human CD4⁺ T cell dataset had the highest overlap with the tumor Treg signature, and an intermediate overlap was found in the tisTreg precursor/recirculating tisTreg cluster 1 (Figure 20B).

In addition to looking at the human tumor T cells, my collaboration partners also generated a scATAC-seq dataset of sorted CD4⁺ and CD25⁺ T cells from mammary tumors of BALB-neuT mice (Hosseini et al., 2016). After processing these data, I demonstrated that a subset of CD25⁺ Treg cells is enriched for peaks from the previously defined murine core tisTregST2 signature (Figure 20C). Similar to human Treg cells, these cells also had high *Ccr8* and *Ikzf2* chromatin accessibility.

Together, this analysis revealed that many tumor CCR8⁺ Treg-associated chromatin features are also found in tisTreg cells under homeostatic conditions.

Figure 19: tisTreg development. Density of cells from Treg clusters and Batf chromVAR score against pseudotime for the **A** SPF mouse dataset, **B** gnotobiotic mouse dataset and the **C** human dataset. Additionally, BATF gene activity per cluster is shown. **D** UMAP representation of human Treg cells colored by cluster annotation, tissue of origin, BATF chromVAR deviation score and *CCR8* gene activity. **E** Aggregated chromatin accessibility signal for human (top) and murine (bottom) Treg cell clusters at the *CCR8* gene locus. The bottom track shows the ChIP-seq signal for BATF (GSM803538). The yellow bar highlights a BATF binding site in the *CCR8* promoter region that increases in chromatin accessibility during development of tisTreg cells. **F** *Ccr8* mRNA expression in murine tisTregST2 cells from the lung, liver, VAT and skin and their precursors from the spleen (n=5, DeSeq2 (Love et al., 2014)). **G** Density of human Treg cells from Monocle trajectory as shown in C (blood naive Treg cluster 7, blood memory Treg cluster 1, skin and fat tissue Treg cluster 3), but including the sorted blood CCR8⁺ Treg population. Below, violin plot of enrichment scores for the human tisTreg signature. **H** UMAP plot showing the enrichment of the human skin Treg and fat Treg peak signatures in the human blood CCR8⁺ Treg population. Subfigures E and F were prepared by Prof. Dr. Michael Delacher. Modified from Delacher et al. (2021).

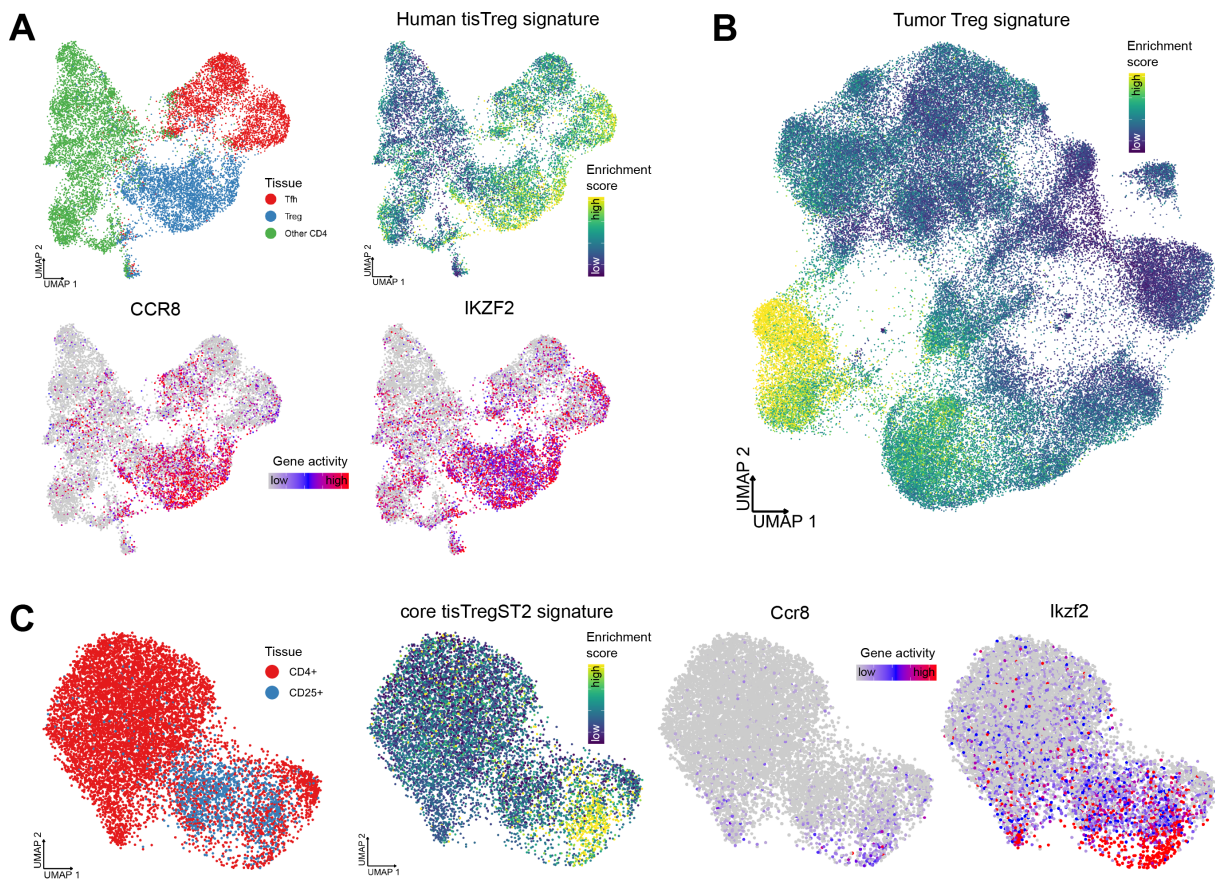


Figure 20: Treg cells in tumors share similarity with tisTregST2 cells in healthy tissues. **A** UMAP of CD4⁺ T cell subset from Satpathy (2019) colored by cell type annotation, enrichment of the human tisTreg signature and gene activity scores of *CCR8* and *IKZF2*. **B** Enrichment of tumor Treg-specific peaks generated from A in the human CD4⁺ T cell dataset. **C** UMAP of CD4⁺ T cells isolated from murine mammary tumors colored by sort marker, enrichment of core tisTregST2 signature peaks and *Ccr8* and *Ikzf2* gene activity score. Modified from Delacher et al. (2021).

3.2 Chromatin accessibility landscape of murine and human CD8⁺ T cells

Following a close characterization of Treg cells in murine and human tissues, we proceeded with investigations on the chromatin accessibility landscape of CD8⁺ T cells. One major question that we aimed to answer is whether CD8⁺ T cells are also involved in tissue regeneration. Previously, supportive and obstructive roles of CD8⁺ T cells in tissue regeneration have been reported in different mouse models (Zhang et al., 2014; Dudek et al., 2021; Liang et al., 2020; Linehan et al., 2018). Since little is known on tissue-regenerative roles of CD8⁺ T cells in humans and it is unclear, how tissue regeneration is regulated in CD8⁺ T cells, we performed scATAC-seq of CD8⁺ T cells sorted from different healthy murine and human tissues and human tumor tissue. In this analysis, we found that CD8⁺ T cells in healthy peripheral murine and human tissues show both characteristics of effector and exhaustion state. These cells share similarities with tisTregST2 cells – above all they also participate in tissue repair and are controlled by transcription factor BATF. This population was also present in human hepatocellular carcinoma (HCC) tumor tissue highlighting a new facet of tumor immunology.

We are currently revising a manuscript with results from this analysis under the title:

Single-cell chromatin accessibility landscape reveals tissue-repair potential of human effector CD8 T cells (Delacher, M., Simon, M., Schmidleithner, L., Stüve, P., Sanderink, L., Hotz-Wagenblatt, A., Wuttke, M., Schambeck, K., Ruhland, B., Hofmann, V., Bittner, S., Pant, A., Eigenberger, A., Menevse, A., Gebhard, C., Strieder, N., Abken, H., Rehli, M., Schmidl, C., Beckhove, P., Strowig, T., Huehn, J., Hehlhans, T., Prantl, L., Werner, J., Brors, B., Imbusch, C., Feuerer, M.)

3.2.1 Effector-like PD1⁺TOX⁺ CD8⁺ T cells share features with tisTreg cells in healthy murine tissues

To reveal the chromatin landscape of murine CD8⁺ T cells, my collaborators generated a scATAC-seq data set of sorted CD8⁺ T cells from murine VAT, skin, colon, lung and spleen. After processing these data, I performed quality control and obtained a final dataset of 11,755 cells with a median of 21,457 fragments per cell (Supplementary Figure S8). I then generated a low-dimensional representation and determined graph-based clusters (Figure 21A-B). Interestingly, I observed that several genes reported in the context of T cell exhaustion (*Havcr2*, *Pdcd1*, *Lag3*, *Tigit*) or effector activity (*Gzmb*, *Areg*, *Ifng*, *Tnf*) were also accessible in CD8⁺ T cells from healthy peripheral tissues including the skin (cluster 11), VAT (clusters 3, 10, 16) and colon (clusters 14, 15) (Figure 21C and Supplementary Figure S9A). To further characterize cellular states, I performed annotation with SingleR using the CD8⁺ T cell subset from the Immgen dataset as reference (Heng

et al., 2008; Aran et al., 2019). This confirmed the effector identity of the aforementioned clusters and revealed a segmentation by differentiation status in addition to the tissue of origin within the UMAP space (Figure 21D, Supplementary Figure S9B). Next, I used Monocle to order cells along a trajectory to gain insights about possible developmental paths (Figure 21E). Effector CD8⁺ T cell clusters positioned at the end of this trajectory and had increased BATF activity, as seen previously during tisTregST2 cell development. I defined a CD8 activation signature by comparison of effector CD8⁺ T cell clusters 3, 10, 11, 14-16 against all other clusters (3,321 effector CD8⁺ T cell-specific peaks). Additionally, the top de novo enriched motif based on this CD8 activation signature was most similar to motifs from the bZIP transcription factor family further supporting a role of BATF in the development of effector CD8⁺ T cells. My collaboration partners validated this finding by flow cytometry of T cells obtained from the spleen, lung, and VAT of BATF-deficient mice, which confirmed a low abundance of CD62L⁻PD1⁺TOX⁺ CD8⁺ T cells (data not shown).

In short, we identified CD8⁺ T cells in healthy murine peripheral tissues with effector and exhaustion phenotype and high BATF activity (subsequently termed PD1⁺TOX⁺ CD8⁺ T cells).

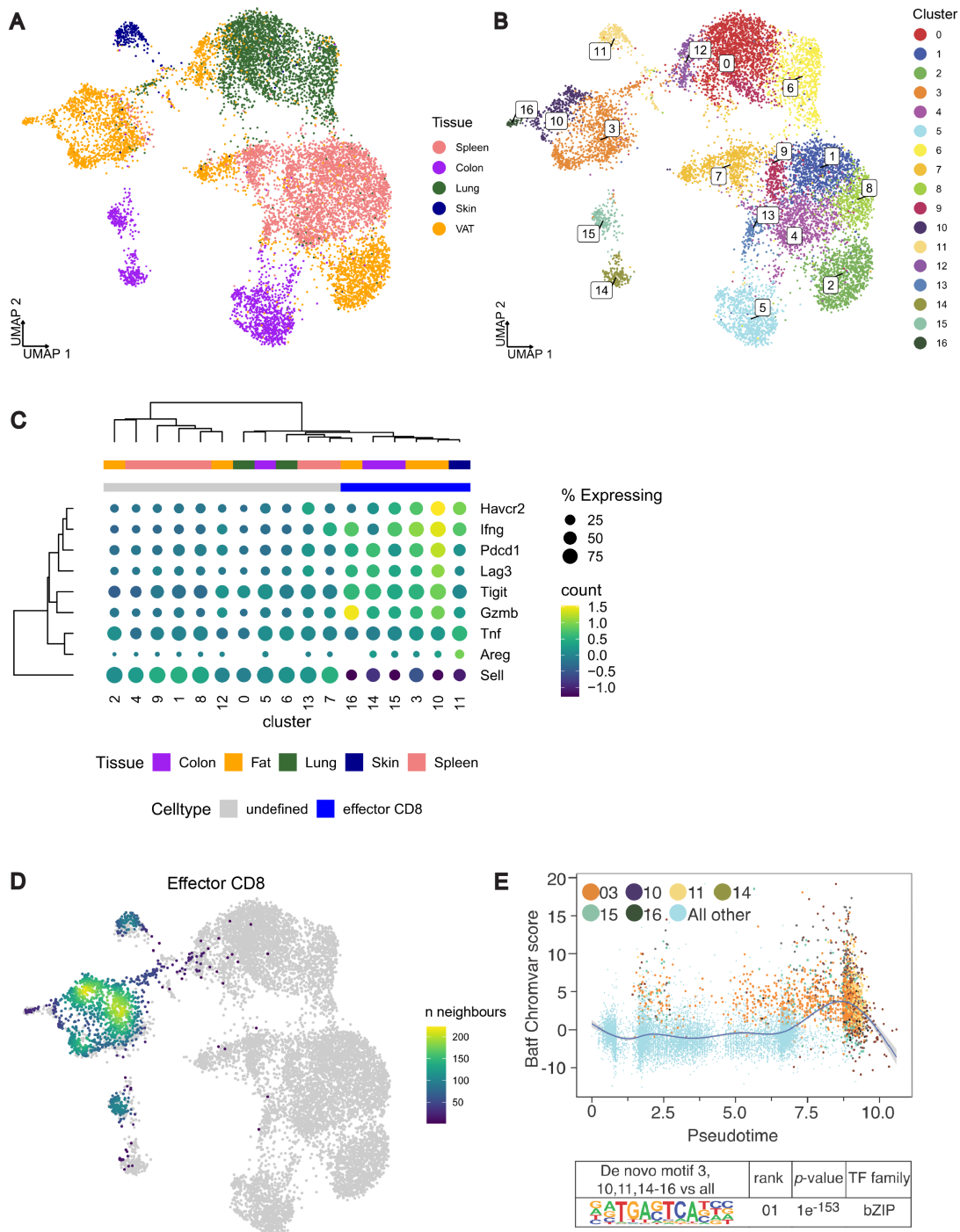


Figure 21: Mouse CD8⁺ T cell atlas. scATAC-seq data of CD8⁺ T cells sorted from different healthy murine tissues. UMAP of CD8⁺ T cells colored by **A** originating tissue and **B** clusters obtained from graph-based clustering. **C** Dotplot of scaled gene activity and fraction of cells with detected fragments for CD8⁺ T cell activation and exhaustion marker genes summarized by clusters. The top rows show the main tissue of origin and effector CD8 annotation by cluster. Rows and columns are clustered using Euclidean distances and complete linkage. **D** Localization of cells annotated as effector CD8⁺ T cells by SingleR. The number of nearest neighbors with effector CD8 annotation is encoded by color, gray values indicate a different annotation. **E** BATF chromVAR deviation score plotted against pseudotime (top). Effector CD8⁺ T cell clusters are highlighted by their cluster color, and cells from other clusters are colored in light blue. (Bottom) Top-ranking de novo motif from the HOMER motif discovery analysis based on CD8 activation signature peaks. Modified from Delacher et al. (nd).

3.2.2 PD1⁺TOX⁺ CD8⁺ T cell activation program is independent of microbiota in the colon

Similar to the establishment of the tisTregST2 program, we were interested whether PD1⁺TOX⁺ CD8⁺ T cells arise independent from microbiota. Therefore I processed and analyzed a newly generated scATAC-seq dataset of sorted CD8⁺ T cells from healthy tissues of gnotobiotic mice. After quality control, the dataset contained 16,258 cells with a median number of 9,414 fragments per cell (Supplementary Figure S10). Similar to the CD8⁺ T cells from SPF mice, effector CD8⁺ T cells were found in the VAT, skin and colon (Figure 22A-B, Supplementary Figure S11A). I then calculated the enrichment for the CD8 activation signature in cells from the mouse SPF and gnotobiotic datasets. The effector CD8⁺ T cell populations in both datasets showed a similar overlap with the signature and there was a high correlation of the colon effector CD8⁺ T cell clusters from both datasets based on their gene activities (Figure 22C, Supplementary Figure S11B-C).

Together, these results indicated independence of PD1⁺TOX⁺ CD8⁺ T cells from microbiota.

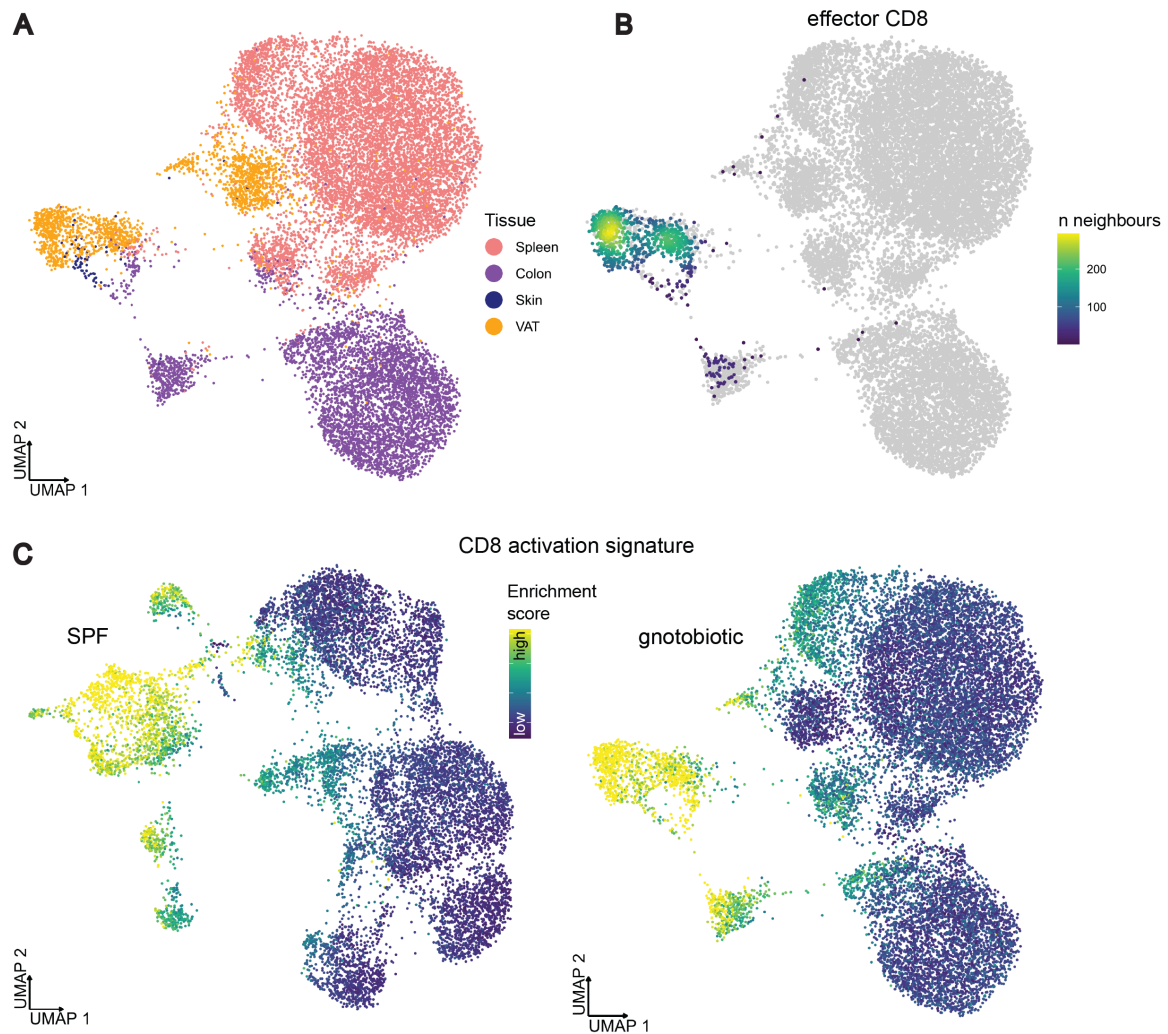


Figure 22: PD1⁺TOX⁺ CD8⁺ T cells are independent from microbiota. UMAP of CD8⁺ T cells from gnotobiotic mice colored by **A** originating tissue and **B** SingleR annotation of effector CD8⁺ T cells. **C** CD8 activation signature enrichment score shown on UMAP of the SPF (left) and gnotobiotic (right) mouse dataset.

3.2.3 Effector-like PD1⁺TOX⁺ CD8⁺ T cells are present in healthy human tissues

We next performed a close characterization of human CD8⁺ T cells to reveal commonalities and differences to murine PD1⁺TOX⁺ CD8⁺ T cells. My collaborators generated a scATAC-seq dataset of sorted CD8⁺ T cells from the fat, skin and blood of healthy human donors. I processed these data and tested its quality resulting in a dataset of 37,013 cells with a median of 13,974 fragments per cell (Supplementary Figure S12). As before, I then performed dimensionality reduction, batch correction with Harmony, graph-based clustering, and reference-based cell annotation with SingleR (Figure 23A-C, Supplementary Figure S13A-B). Using this approach together with marker gene activities, I annotated clusters 3, 4 and 10 as naive CD8⁺ T cells (high *SELL* gene activity), clusters 2 and 5 as mucosal-associated invariant (MAIT) cells (high *KLRB1* gene activity) and the remain-

ing cells as central or effector memory CD8⁺ T cells. I also quantified the enrichment for the previously established human tisTreg signature, which highlighted memory CD8⁺ T cells from the fat (cluster 9), skin (cluster 11) and blood (cluster 6) (Figure 23D). Interestingly, these cells were accessible in exhaustion-associated genes including *TOX*, *PDCD1*, *LAG3*, *TIGIT* and *ENTPD1*. I confirmed this observation by including peak signatures from a recent ATAC-based analysis of CD8⁺ T cell dysfunctional states, which showed enrichment of exhaustion-associated peaks in clusters 9 and 11 (Supplementary Figure S13C) (Pritykin et al., 2021). These clusters also had low gene activity in *S1PR1* and *CCR7* indicating tissue-resident behavior (data not shown) (Kok et al., 2021). I further characterized cells from clusters 9 and 11 by comparing their chromatin accessibility against naive CD8⁺ T cells and MAIT cells. De-novo motif discovery analysis on the common 263 differential peaks gaining accessibility in the memory CD8⁺ T cells resulted in BATF as transcription factor with the highest similarity to the top-enriched motif. As previously observed, there was an increase in the BATF chromVAR deviation score from naive over blood-based intermediates towards tissue-resident effector CD8⁺ T cells over pseudotime (Figure 23E).

Increased expression of the above-mentioned exhaustion-associated genes and BATF in fat and skin PD1⁺TOX⁺ CD8⁺ T cells from healthy human donors was confirmed on scRNA-seq data by my collaboration partners (data not shown). They also performed an *in-vitro* wound healing assay to study whether TOX⁺ effector CD8⁺ T cells also support wound healing similar to induced Tfh-like Treg cells. Specifically, my collaborators used a system with three different cell lines including influenza-specific TOX⁺ effector CD8⁺ T cells, HLA-A2⁺ fibroblasts presenting influenza-peptide and HLA-A2⁻ epithelial cells (data not shown). With increasing concentrations of influenza peptide, TOX⁺ effector CD8⁺ T cell activation and cell-mediated killing of fibroblasts increased as expected. However, they also observed a simultaneous dose-dependent growth of epithelial cells, which persisted when applying cell-free supernatant from the system to an *in-vitro* wound healing assay with epithelial cells. Mechanistically, concentrations of the EGFR ligands TGF α and AREG increased dependent on influenza peptide dose and the presence of epithelial cells. Moreover, activated CD8⁺ T cells directly supported wound healing via release of TNF and IFN γ . This experiment showed that interactions of activated TOX⁺ effector CD8⁺ T cells with fibroblasts and epithelial cells promote wound healing via release of tissue-regenerative factors (Delacher et al., nd).

In short, human tissue-resident CD8⁺ T cells have an activation and exhaustion-like chromatin state with a predominant footprint of transcription factor BATF. Similar to their murine counterparts, PD1⁺TOX⁺ CD8⁺ T cells also exist in human peripheral tissues. They support wound healing by inducing the expression of tissue-regenerative molecules.

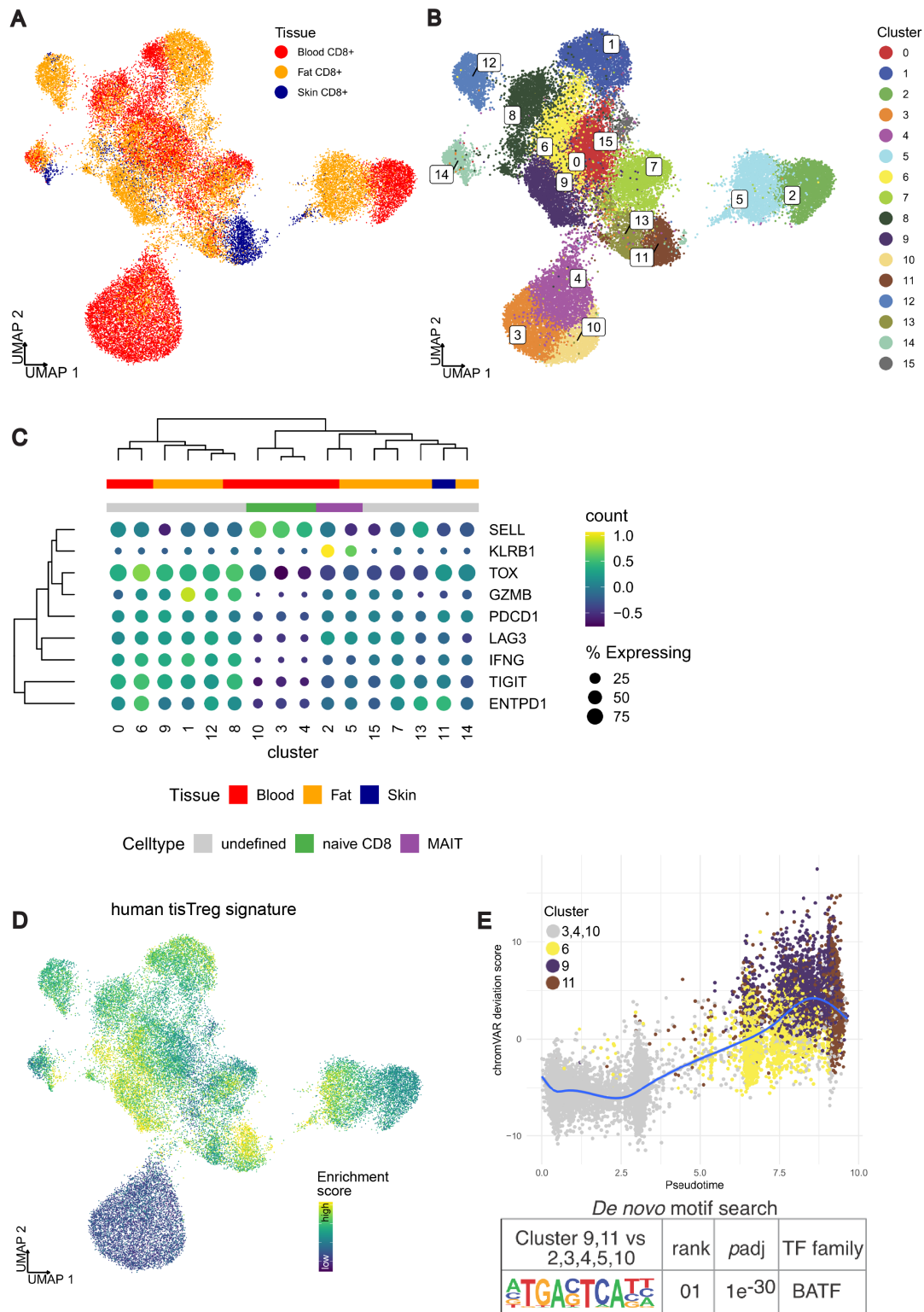


Figure 23: Human CD8⁺ T cell atlas. scATAC-seq data of CD8⁺ T cells sorted from healthy human tissues. UMAP of CD8⁺ T cells colored by **A** originating tissue and **B** 16 clusters obtained from graph-based clustering. **C** Dotplot of scaled marker gene activity and fraction of cells with detected gene activity by cluster with major originating tissue and cell type annotation shown in the top rows. **D** Enrichment score for human tisTreg signature presented in Chapter 3.1.5. **E** Top de-novo motif search result from HOMER based on the tisTreg signature-positive memory CD8⁺ T cell clusters 9 and 11 against naive CD8⁺ T cells and MAIT cells (clusters 2, 3, 4, 5, 10) (top) and scatter plot of BATF transcription factor activity against pseudotime colored by cluster. Modified from Delacher et al. (nd).

3.2.4 Comparison of PD1⁺TOX⁺ CD8⁺ T cells between human healthy and tumor tissue

Since PD1⁺TOX⁺ CD8⁺ T cells are known in the context of exhaustion within tumor tissue, we next compared these cells between healthy and tumor tissue. My collaborators sequenced CD3⁺ T cells isolated from tumors of three human hepatocellular carcinoma patients. I processed these scATAC-seq data and performed quality control, after which I obtained 36,555 cells with 7,503 median fragments per cell (Supplementary Figure S14). Since the low-dimensional representation of the data was influenced by the donor, I calculated a batch-corrected dimensionality reduction using Harmony (Supplementary Figure S14C). To obtain a segmentation into CD4⁺ and CD8⁺ T cells, I then smoothed *CD4* and *CD8A* gene activities among neighboring cells and assigned the cell type for each cell based on the bigger value (Figure 24A). Next, I performed graph-based clustering to enable a cluster-level mapping of cell types and states (Figure 24B). I further annotated cells by inspection of marker gene activities, calculation of a gene activity module score based on a previously published RNA CD8⁺ T cell exhaustion signature (Miao et al., 2020) and reference-based annotation with SingleR (Figure 24C-D, Supplementary Figure S15). Using these approaches, I assigned clusters 1 and 4 as Treg cells, cluster 10 as MAIT cells and cluster 2 and 7 as Tconv cells. Among the SingleR-annotated effector CD8⁺ T cell clusters (5, 6, 8, 9, 11, 12), clusters 5, 9, 11 and 12 had the highest scores of the RNA CD8 exhaustion signature. Since they also had high gene activity of *ENTPD1*, a marker for terminal exhaustion of CD8⁺ T cells (Gupta et al., 2015), I annotated these clusters as terminally-exhausted CD8⁺ T cells (CD8exh). Concordant with the intermediate exhaustion phenotype of memory CD8⁺ T cells in healthy peripheral human tissues, the effector CD8⁺ T cell clusters 6 and 8 had intermediate CD8⁺ T cell exhaustion signature scores.

To compare PD1⁺TOX⁺ CD8⁺ T cells from healthy tissues with exhausted CD8⁺ T cells from tumor tissue I first derived an ATAC-based CD8⁺ T cell exhaustion signature by comparing CD8exh cells (cluster 5, 9, 11, 12) against the remaining CD8⁺ T cells (clusters 6, 8, 14) and MAIT cells (10) (ATAC CD8 exhaustion signature, 1,895 CD8exh-specific peaks). Subsequently, I quantified the enrichment for the RNA and ATAC-based CD8 exhaustion signatures in the human healthy CD8⁺ T cell dataset and compared it with the human tisTreg signature (Figure 25). The exhaustion and tisTreg signatures had similar score distributions between the clusters: fat and skin memory CD8⁺ T cells ranged at the upper end and blood naive CD8⁺ T cells at the lower end. To take a more detailed look at CD8⁺ T cell exhaustion-associated genes (*PDCD1*, *ENTPD1*, *TOX*, *TIGIT*) I summarized the fragment coverage within genomic windows for selected clusters (Supplementary Figure S16). While *ENTPD1* was only accessible in tumor CD8exh cells, memory CD8⁺ T cells from healthy fat, skin and blood had high similarity to CD8exh

cells in their accessibility profiles for the remaining genes. Naive CD8⁺ T cells from the blood were inaccessible in these markers, and tumor effector CD8⁺ T cells had similar gene accessibility in *PDCD1* and *TIGIT* but low *TOX* gene accessibility.

These analyses show that, although not being identical in their chromatin landscapes, there are many shared features between tumor CD8^{exh} and healthy tissue PD1⁺TOX⁺ CD8⁺ T cells.

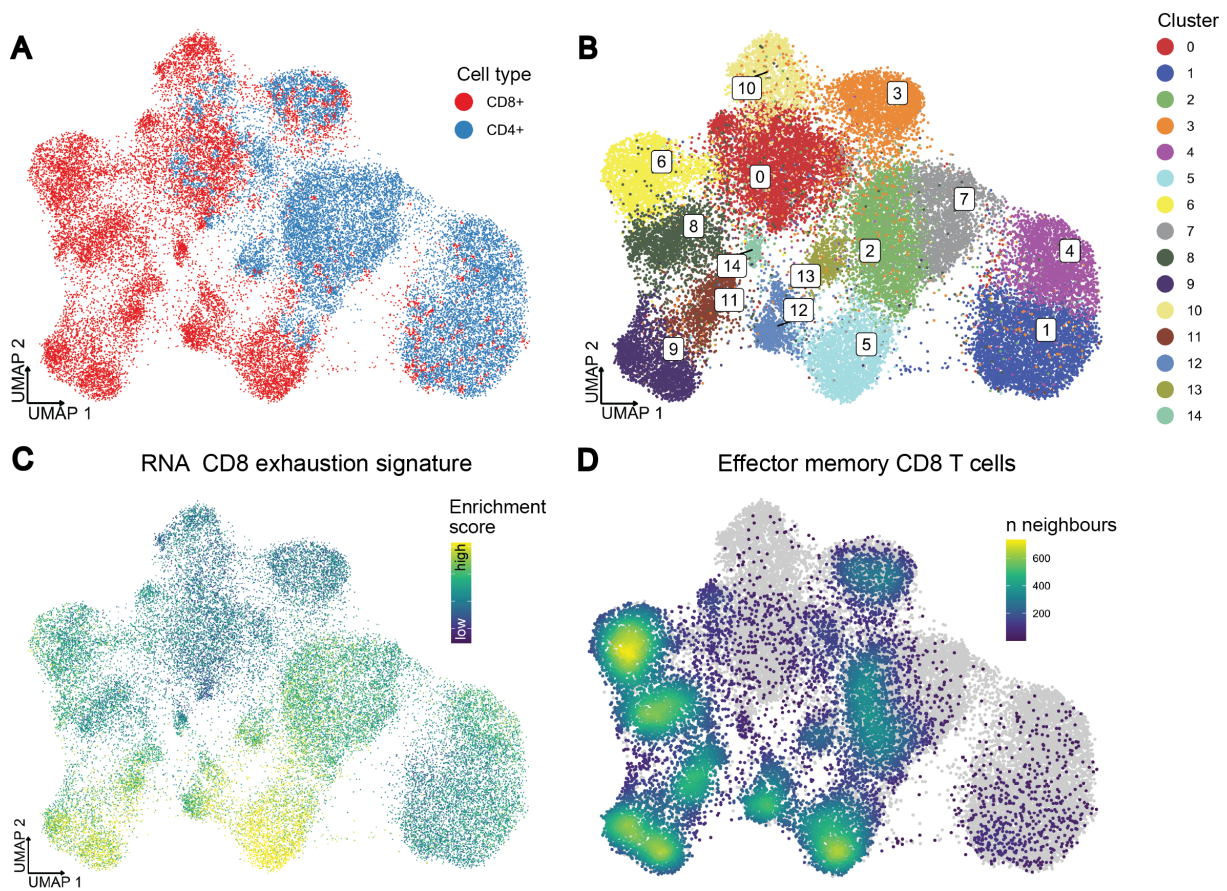


Figure 24: Human HCC T cell atlas. scATAC-seq data of T cells from hepatocellular tumors. UMAP of T cells colored by **A** annotation the CD4⁺ and CD8⁺ T cell compartment, **B** assignment to 15 clusters by graph-based clustering, **C** RNA-based CD8⁺ T cell exhaustion gene signature score, and **D** density of cells annotated as effector memory CD8⁺ T cell by SingleR. Modified from Delacher et al. (nd).

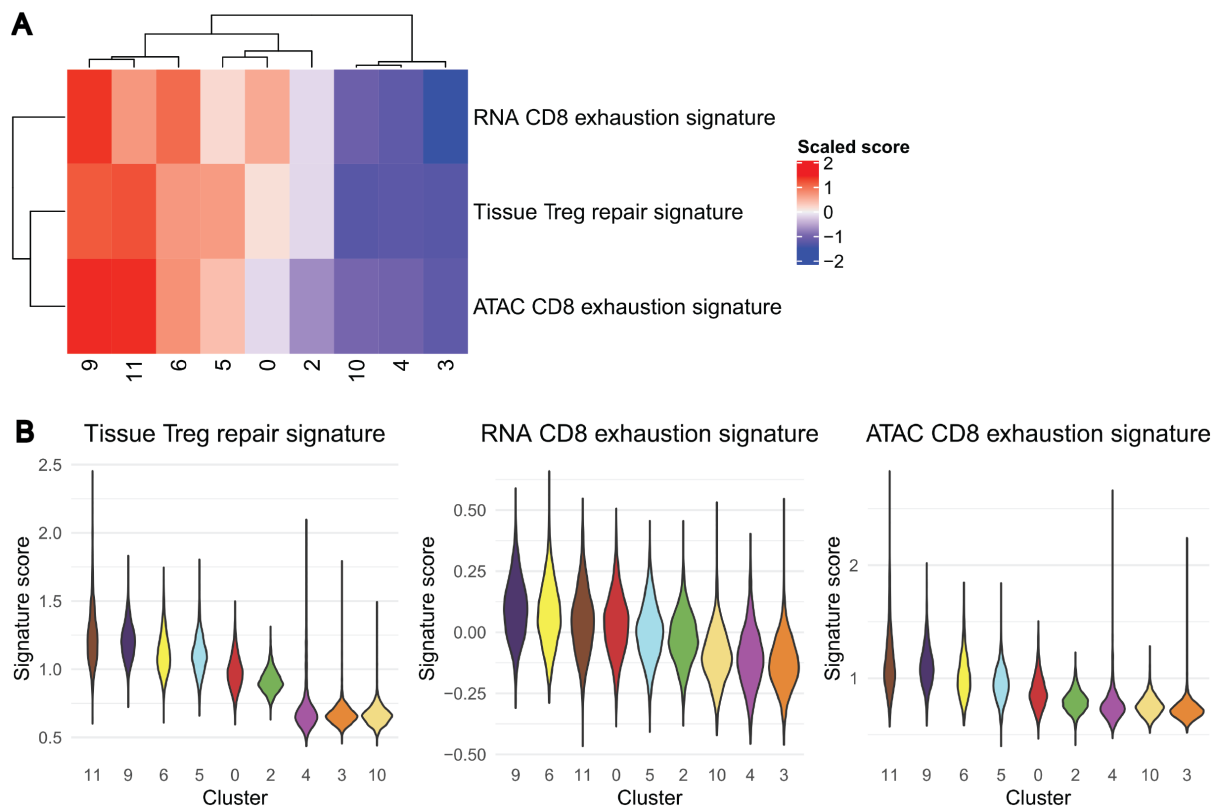


Figure 25: Signature comparison. **A** Heatmap of scaled scores for the human tisTreg signature and RNA-based and ATAC-based CD8 exhaustion signatures for clusters from the human CD8⁺ T cell dataset. Rows and columns are clustered using Euclidean distances and complete linkage. **B** The violin plots are showing the distribution of signature scores by cluster from A. Modified from Delacher et al. (nd).

3.3 Expanding the view: an immune cell atlas of tissue-specific programs

Following the in-depth characterization of the chromatin states of murine and human T cells with tissue-regenerative potential, we broadened the view to the whole immune cell landscape. To investigate tissue repair programs in other immune cell types, my collaboration partners generated two additional scATAC-seq datasets from flow-sorted CD45⁺ immune cells of different healthy murine and human tissues. As before, my contribution is to process and analyze these datasets.

Although this project is still ongoing, I included some of the preliminary results in this thesis: within the Treg cell subset, I confirmed the tisTregST2 marker *Ccr8* that can already be detected in tisTregST2 precursor cells from the spleen. Above all, my analysis showed that many of the tisTregST2 cell-associated chromatin features are not exclusive to T cells but are also present in other immune cell types including ILC2 cells, monocytes, macrophages and dendritic cells.

3.3.1 tisTreg signature identifies innate immune cells with potential repair function in healthy murine tissues

To generate a murine immune cell chromatin accessibility atlas, my collaboration partners sorted CD45⁺ immune cells from skin, VAT, colon and spleen tissue pooled from several healthy mice and subjected them to scATAC-seq. I then processed these data and performed quality control, which resulted in a collection of 44,192 cells with a median of 8,710 fragments per cell (Supplementary Figure S17). Next, I reduced the dimensionality of the dataset, did graph-based clustering and annotated the resulting clusters based on marker gene activities and reference-based annotation with SingleR (Figure 26A-D, Supplementary Figure S19A and C). To verify these annotations, I compared the obtained immune cell type fractions per tissue with annotations from published datasets (Supplementary Figure S19B). Consistent with previous studies, more than 50% of immune cells from the spleen were B lymphocytes, and T lymphocytes represented the second largest fraction of immune cells (The Tabula Muris Consortium et al., 2018; Han et al., 2018; Chen et al., 2018).

I calculated an enrichment score for the core tisTregST2 signature with chromVAR to localize cells sharing commonalities with tisTregST2 cells (Figure 26E) (Schep et al., 2017). The score indicated a strong enrichment of signature peaks in macrophages (clusters 18-21, 23) and monocytes (22), and an intermediate enrichment in DCs (24-28), granulocytes (16, 17), and a subset of ILCs largely consisting of ILC2 cells (9). tisTregST2 cells from the VAT, skin and colon (11) had the highest enrichment score within the lymphoid compartment. However, they had a lower overlap with the signature compared to myeloid

cells. As expected, naive T cells (13) ranged among the cells with lowest enrichment of coreTisTregST2 signature peaks. Similarly, I observed that there was a high predicted transcription factor activity of BATF in cell clusters with high core tisTregST2 signature scores (core tisTregST2 signature z-score - BATF chromVAR z-score Pearson correlation = 0.63), especially within a subset of monocytes and macrophages (20-22) (Figure 26F). On the other hand, BATF activity was low in naive B and T cell clusters 5, 6 and 13.

To disentangle, which peaks of the core tisTregST2 signature contribute to the high enrichment within myeloid cells, I counted the number of fragments within each peak region per cell and then summarized the mean fragment number per cluster (Figure 27). Partitioning of the peaks into four clusters using k-means clustering showed that approximately half of the signature peaks (k-means peak clusters 2-4) had high accessibility within macrophages, monocytes and DCs (clusters 18-28), but comparatively low accessibility within tisTregST2 cluster 11. On the other hand, the remaining regions from peak cluster 1 were most accessible in tisTregST2 cells and ILC clusters 2 and 9. This indicated that the peaks in the core tisTregST2 signature are only partially exclusive to tisTregST2 cells when evaluated in a pan-immune cell context.

I confirmed our findings presented in Chapter 3.1.5 on the detection of tisTregST2 precursor cells by *Ccr8* expression using the naive CD4⁺ T cell and Treg cell subset from the mouse immune cell atlas. First, I recalculated a dimensionality reduction and graph-based clusters (Figure 28A). I then used *Ccr8* gene activity as a proxy for its mRNA expression level and compared it with the enrichment of the murine tisTregST2 tissue and progenitor signatures and additional marker genes (Figure 28B-D, Supplementary Figure S18). *Ccr8* gene activity was low in the naive CD4⁺ T cell/naive Treg cluster 1 and increased towards late tisTregST2 progenitor cells within cluster 5, which were also accessible in the murine tisTregST2 precursor marker genes *Nfil3* and *Klrg1* (Delacher et al., 2020). Eventually, highest *Ccr8* gene activity was obtained in tisTregST2 cells from the colon (cluster 3), VAT (4) and skin (2). On the other hand, the colonic pTreg cluster 6, as identified by high *Rorc* and low *Ikzf2* gene activity, had low chromatin accessibility at the *Ccr8* locus. These results confirmed *Ccr8* as marker for tisTregST2 cells and their progenitors.

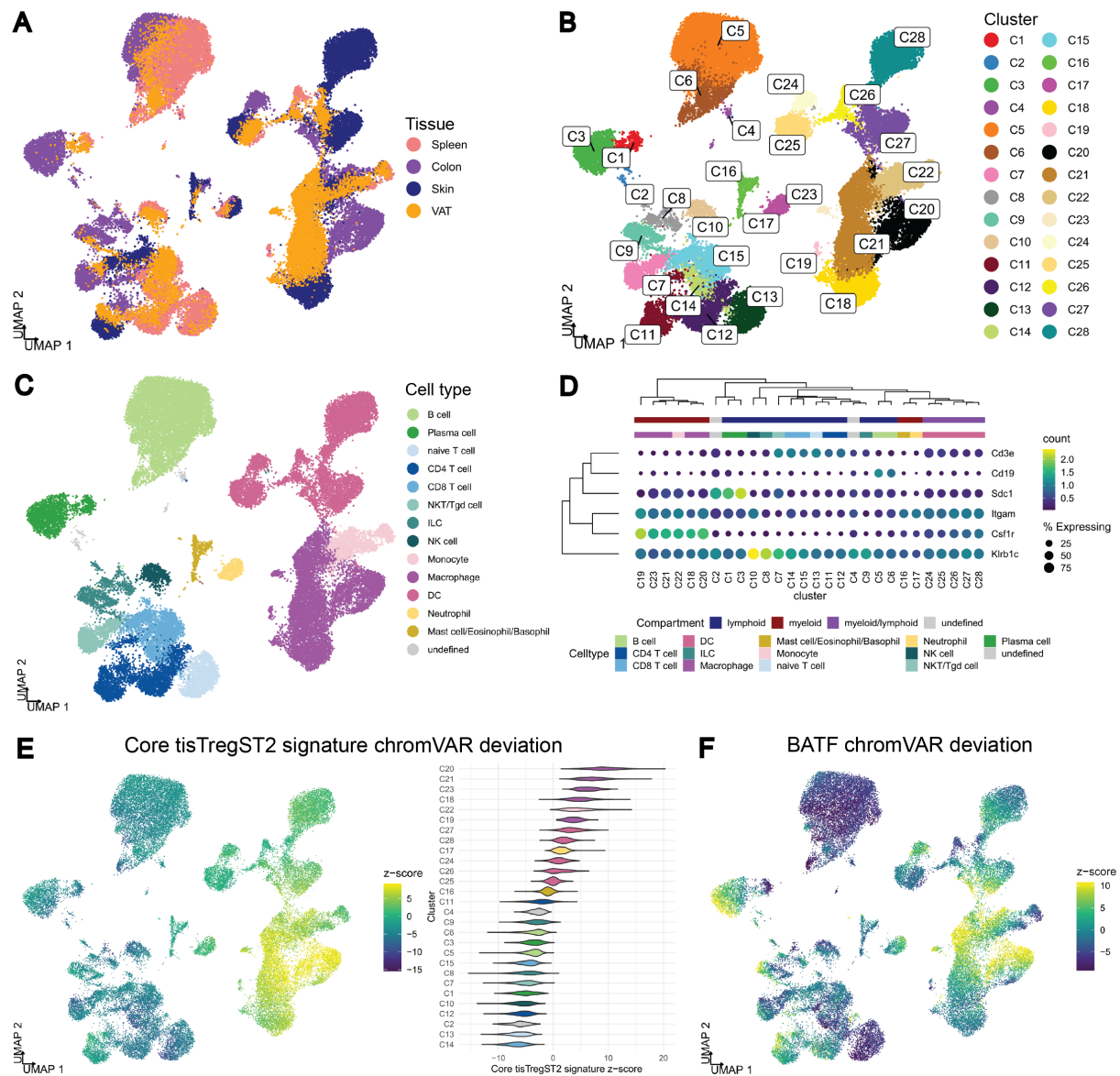


Figure 26: Mouse immune cell atlas. scATAC-seq data of CD45⁺ immune cells sorted from different murine tissues. UMAP colored by **A** originating tissue, **B** 28 clusters from graph-based clustering and **C** mapping of clusters to cell types. **D** Dotplot showing scaled gene activities and fraction of cells with detected activity per cluster. The column annotations indicate the major compartment and cell type, respectively. Markers for T cells (*Cd3e*), B cells (*Cd19*), plasma cells (*Sdc1*), myeloid cells (*Itgam*), macrophages (*Csf1r*) and NK cells (*Klr1c*) are shown. Rows and columns are clustered using Euclidean distances and complete linkage. chromVAR deviation z-scores visualized on UMAP for **E** the core tisTregST2 peak signature and **F** BATF transcription factor activity.

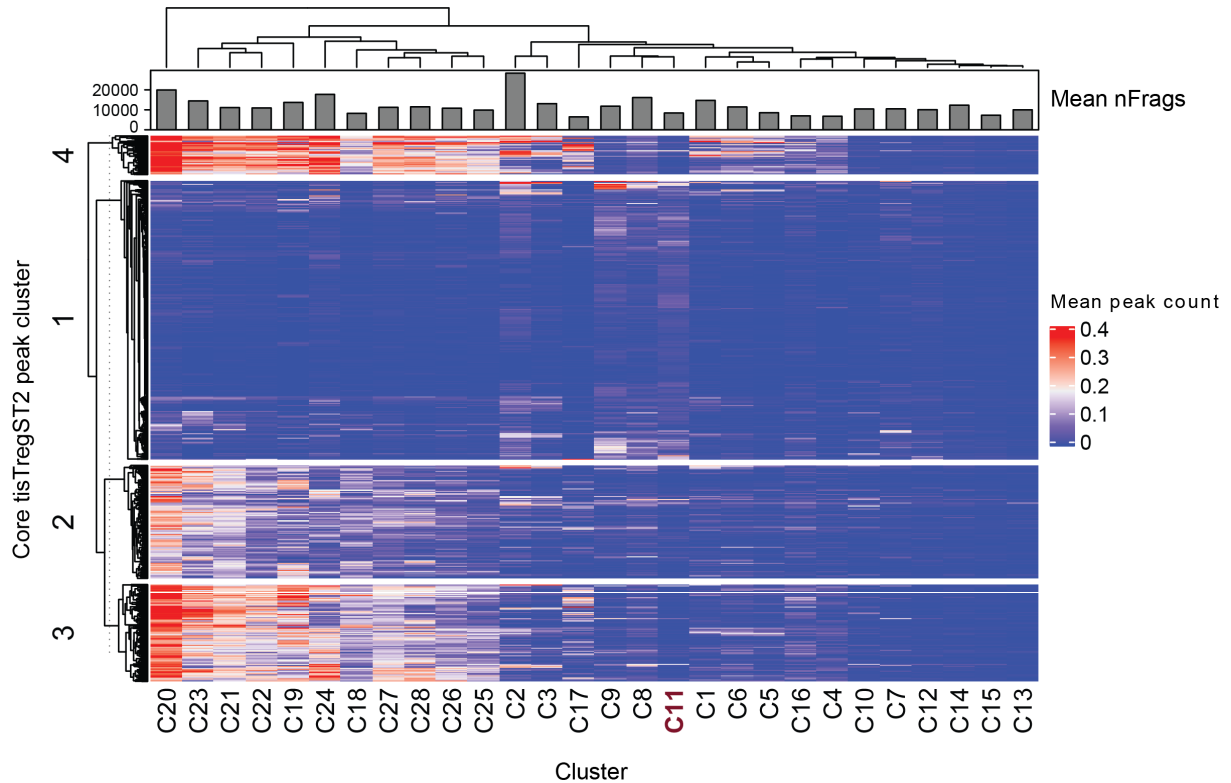


Figure 27: Core tisTregST2 signature peak accessibility. Heatmap of the mean number of fragments per cell summarized by clusters from the murine immune cell atlas (Figure 26B). The columns indicate clusters and rows represent peaks from the core tisTregST2 signature (2,267 peaks). Rows were partitioned into four peak clusters using k-means clustering. Within each subset, hierarchical clustering based on Euclidean distances with complete linkage was applied. Similarly, columns were grouped using hierarchical clustering. The top annotation summarizes the mean total fragment number per cell in the respective cluster. tisTregST2 cluster 11 is highlighted in red.

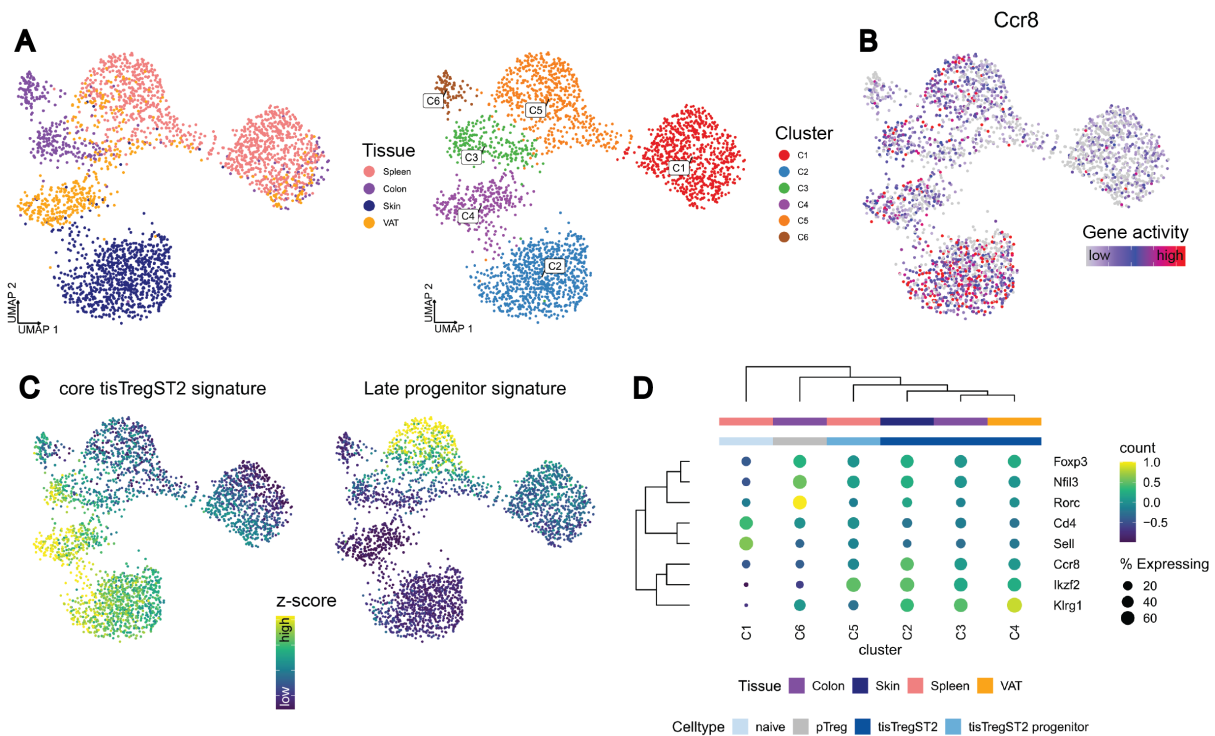


Figure 28: Confirmation of tisTregST2 marker *Ccr8*. UMAP of the Treg and naive T cell subset from the murine immune cell atlas colored by **A** originating tissue and clusters from graph-based clustering, **B** *Ccr8* gene activity score and **C** chromVAR deviation z-scores highlighting enrichment of the core tisTregST2 and late tisTregST2 progenitor signature peaks. **D** Dotplot of scaled gene activities and fraction of cluster cells with detected activity for key genes characterizing tisTregST2 development. The main originating tissues and developmental steps are annotated above the dotplot for the clusters from A. Rows and columns are clustered using Euclidean distances and complete linkage.

3.3.2 Characterization of immune cells with potential tissue-specific roles in healthy human tissues

Analogous to the murine data, my collaboration partners prepared cells for a human immune cell atlas by flow-sorting $CD45^+$ immune cells from fat, skin and blood of a healthy donor and subsequent scATAC-seq. I processed these data and filtered out low-quality barcodes. This resulted in a dataset of 38,783 cells with a median of 7,207 fragments per cell (Supplementary Figure S20). In Figure 29A-B, tissue and cluster annotations of the cells in UMAP space are shown. As before, I annotated cells using SingleR and gene activities of selected cell type markers (Figure 29C-D, Supplementary Figure S21). According to this annotation, $CD4^+$ T cells dominate the immune cell composition of blood and skin. B cells, $CD8^+$ T cells, MAIT cells and neutrophils were almost exclusively detected in the blood, whereas macrophages and DCs were only found in the fat and skin.

I next used the previously defined human tisTreg signature to compute a peak enrichment score for each cell. A high z-score was obtained for Treg cells from the fat and skin (subset

of cluster 9) and a fraction of non-naive blood Treg cells (subset of 14), thereby confirming its specificity to highlight tisTreg cells and their precursors. In addition, high scores within the blood were obtained for CD8⁺ T cells (16), a subset of NK cells (subset of 19) and B cells (6). Within fat and skin, the signature was highly enriched in a fraction of cells from clusters 4 and 5 (monocytes/macrophages/DCs) and another non-Treg cell subset of cluster 9 (Figure 29E). These immune cell subsets from the peripheral tissues also had the highest BATF transcription factor activity scores (human tisTreg signature z-score - BATF chromVAR z-score Pearson correlation = 0.58) (Figure 29F).

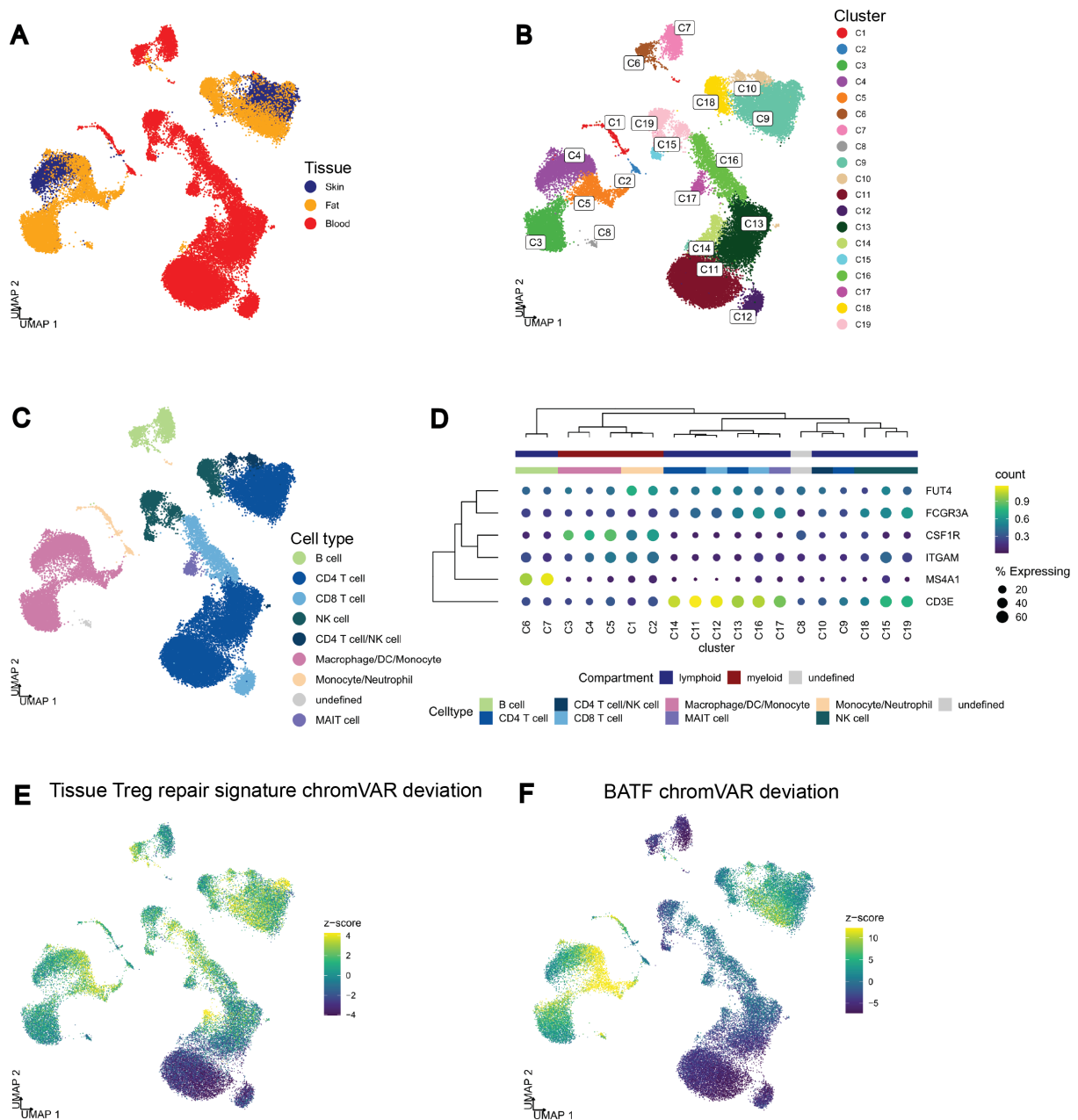


Figure 29: Human immune cell atlas. scATAC-seq data of $CD45^+$ immune cells sorted from the fat, skin and blood of a healthy human donor. UMAP colored by **A** originating tissue, **B** 19 clusters obtained by graph-based clustering, **C** cell type annotation of clusters from B. **D** Dotplot of scaled marker gene activity and fraction of cells with detected activity by cluster defining major compartments and cell types. The column annotations represent the major compartment and cell type, respectively. Markers for neutrophils (*FUT4*), NK cells (*FCGR3A*), myeloid cells (*ITGAM*), macrophages (*CSF1R*), B cells (*MSA1*) and T cells (*CD3E*) are shown. Rows and columns are clustered using Euclidean distances and complete linkage. UMAP colored by chromVAR deviation z-scores for **E** the human tisTreg signature and **F** BATF transcription factor activity.

4 Discussion

4.1 scATAC-seq confirms tisTregST2 phenotype in mice

The data presented in Chapter 3.1 provides the first scATAC-seq atlas of CD4⁺ T cells from healthy murine and human lymphoid and non-lymphoid tissues. Previous publications involving scATAC-seq were either assaying a broad spectrum of tissue cells without focus on the immune cell compartment, generating immune cell profiles from the blood only or investigating certain disease conditions such as basal cell carcinoma (Cusanovich et al., 2018; Domcke et al., 2020; Zheng et al., 2020; Satpathy, 2019; Yu et al., 2020). My analysis provided a detailed view on epigenetic changes and their underlying regulatory factors occurring within immune cells during tissue adaptation under homeostasis. Importantly, the single-cell resolution provided the means to identify differences between cellular subsets and the inference of developmental trajectories. Both would not have been possible with bulk sequencing approaches.

Delacher et al. (2017) previously used a combination of whole-genome bisulfite sequencing and RNA-seq to characterize a murine population of tissue-resident Treg cells termed ‘tisTregST2’ cells. These cells secrete the tissue-regenerative factor AREG and IL-10, and have a defined transcriptional and DNA methylation landscape. In particular, they have high expression of Th2 cell-associated genes including *Il1rl1* (IL-33 receptor ST2) and *Gata3*, and were shown to depend on transcription factor BATF. In addition, two murine tisTregST2 precursor stages were identified in the spleen and lymph nodes using scRNA-seq (Delacher et al., 2020). The authors further derived chromatin accessibility signatures based on ATAC-seq of sorted tisTregST2 cells from peripheral tissues including the skin, VAT, colon and lung and determined a ‘core tisTregST2’ signature, which is shared among all tisTregST2 populations (Delacher et al., 2020).

In this work, I projected the tisTregST2 signatures on the scATAC-seq dataset of mouse CD4⁺ T cells and was able to identify clusters representing tisTregST2 cells. Fractions of tisTregST2 cells within the Treg compartment were concordant with previous results, where tisTregST2 cells constituted the majority of Treg cells in fat and skin, but were only present in low fractions within the lung and lymphoid tissues including the spleen (Delacher et al., 2020). I found an increase in the enrichment of precursor signature peaks along the developmental trajectory from spleen naive Treg cells towards peripheral tisTregST2 cells. The cell ordering in my pseudotime analysis is therefore in line with the results from Delacher et al. (2020). BATF transcription factor activity assessed for each cell showed an increase along this trajectory confirming its importance for tisTregST2 cell development. Importantly, the single-cell resolution of the dataset allowed a precise annotation of tisTregST2 cells, which is in contrast to the lower cell type purity obtained from bulk sequencing data (Sicherman et al., 2021; Delacher et al., 2020). I used this

advantage to derive a refined tisTregST2-specific peak signature.

Together, my analysis showed that tisTregST2 cells can be successfully identified and characterized using scATAC-seq. Pseudotime analysis confirmed the previously proposed developmental steps with early and late precursor stages in the spleen and supported a major role of BATF in driving this development.

4.2 tisTregST2 cells develop independently from microbiota in the colon

In the colon, two subsets of FOXP3⁺ Treg cells have been described. They differ by their origin: thymus-derived Treg (tTreg) cells and peripheral Treg (pTreg) cells. pTreg cells are induced from Tconv cells in mucosal tissues to mediate tolerance against self-antigens and harmless foreign antigens (Shevach and Thornton, 2014; Yadav et al., 2013). I annotated colon Treg cell subsets in our scATAC-seq data generated from SPF and gnotobiotic mice and showed that pTreg cells were absent in the gnotobiotic mice. This was in line with previous results describing the dependency of pTreg cell induction on microbial antigens (Atarashi et al., 2011; Geuking et al., 2011; Yadav et al., 2013). In accordance with their development originating in lymphoid tissues, tisTregST2 cells made up the tTreg fraction in the colon of SPF mice, but were different from pTreg cells, which only had a low-to-intermediate enrichment of tisTregST2 signature peaks. The tisTregST2 cells in the colon of SPF and gnotobiotic mice had high gene activity of tisTreg effector molecules AREG and IL-10 (Burzyn et al., 2013; Cipolletta et al., 2012). My collaboration partners further confirmed their protein expression in skin KLRG1⁺ Treg cells from SPF and gnotobiotic mice (Delacher et al., 2021).

In short, these analyses showed that functional tisTregST2 cells colonize the colon independent from microbiota. Consequently, tTreg cells do not only mediate peripheral tolerance in the colon, but are also capable to produce tissue-regenerating factors. Whether the same holds true for pTreg cells is subject to further investigations. The specific depletion of the tTreg lineage in mice combined with a wound-healing assay would be an option to address this question.

4.3 Identification and characterization of human tisTreg cells

Previous evidence on tisTregST2 cells is based on research conducted on mice (Delacher et al., 2017, 2020). It was an unanswered question whether Treg cells with tissue-regenerative capacity also exist in humans. The main finding of my analysis in Chapter 3.1 is the identification of tisTreg cells in human peripheral tissues including fat and skin (Figure 15). I performed an in-depth comparison between human and murine tisTreg cells elaborating on their commonalities and differences. This analysis is especially valu-

able since the transferability of knowledge gained from mouse models to humans is a major concern in the development of new treatments (Leenaars et al., 2019).

Regarding commonalities, I found a set of tisTreg-specific open chromatin regions, which was present in both species (Figure 18). Peaks in this conserved tisTreg signature were associated with the transcription factors *BATF*, *GATA3* and *TOX*, and multiple surface and TNF superfamily receptors. The signature also contained *ENTPD1* among its associated genes, which encodes the ectonucleotidase CD39 known to play an important role in the suppressive function of Treg cells in mice and humans (Antonioli et al., 2013). In addition, multiple regions associated with *BACH2*, a transcription factor responsible for maintenance of a naive T cell state, became consistently inaccessible in mouse and human tisTreg cells (Tsukumo et al., 2013). The conserved signature was strongly enriched for BATF binding sites supporting its fundamental role for the tisTreg program in both species (Hayatsu et al., 2017; Mijnheer et al., 2021; Vasanthakumar et al., 2015; Ise et al., 2011).

Treg cells were shown to mirror transcriptional programs of specific Th cell subsets to allow their effective regulation (Duhén et al., 2012; Cretney et al., 2013). A well-described property of murine tisTregST2 cells is their polarization towards a Th2 cell phenotype (Delacher et al., 2017). Indeed, murine tisTregST2 cells in our scATAC-seq data had high gene activity of the Th2 transcription factors *Gata3* and *Irf4*. However, this was not the case in their human counterparts, which instead showed enrichment of peaks associated with Tfh cells. Type 2 immune responses mounted by Th2 cells are directed against helminths and support tissue repair, but are also involved in allergy and other diseases with a chronic inflammatory component (Walker and McKenzie, 2018). Tfh cells, on the other hand, regulate B cell maturation within germinal centers and B cell follicles (Zaretsky et al., 2009; Crotty, 2014). This difference in polarization between mouse and human tisTreg cells shows that their epigenetic program is only partly conserved. It raises the question, why Treg cells in peripheral tissues have a Tfh bias although Tfh cells are primarily present in lymphoid tissues (Crotty, 2019). Of note, a close relationship between the Th2 and Tfh lineage has been reported, i.e. both cell types having the ability to produce Il-4, the Th2 signature cytokine (Zaretsky et al., 2009; Sahoo et al., 2016).

Murine tisTreg cells have been shown to support wound healing in multiple tissues including the skin, muscle and lung via release of amphiregulin (Burzyn et al., 2013; Arpaia et al., 2015; Johnston et al., 2011; Berasain and Avila, 2014). To provide evidence that the human tisTreg cells have similar capacity my collaboration partners induced Tfh-like Treg cells from naive Treg cells *in-vitro*. Supernatant from these cells accelerated wound closure in an *in-vitro* wound-healing assay suggesting that human tisTreg cells indeed produce tissue-regenerative factors. I compared *in-vitro* induced Tfh-like Treg cells and true tisTreg cells on the epigenetic level: approximately half of the peak-associated

genes from the human tisTreg scATAC-seq-based peakset overlapped with genes associated with Tfh-like Treg ATAC-peaks, thus showing considerable similarity between the populations. Additionally, a comparison of transcriptomes from *in-vitro* induced Tfh-like Treg cells and ex-vivo human $CCR8^+$ Treg cells showed consistent log-fold change for the majority of their differentially-expressed genes. It included upregulation of transcription factors *BATF* and *BCL6* and several wound-healing associated genes (Delacher et al., 2021). While we were able to provide strong evidence for the tissue-repair functionality of human tisTreg cells, a definite proof would be the use of bona fide human tisTreg cells for the wound healing assay. However, it is only possible to extract a few thousand tisTreg cells from human skin and fat tissue samples. This is not sufficient for the assay, which requires approximately 100 times more cells. Another possibility would be the *in-vitro* expansion of $CCR8^+$ Treg cells isolated from human blood, however, protocols to achieve this are yet to be established.

4.4 *CCR8* expression identifies tisTreg cells and their precursors

An important aspect in the characterization of tisTreg cells is the understanding of their developmental path and the underlying driving transcription factors. Delacher et al. (2020) showed that early and late tisTregST2 precursor cells can be identified in the murine spleen using the marker genes *Klrg1* and *Nfil3*. However, these markers were not accessible in human Treg cells, thus requiring the definition of new human markers. I used Monocle to align human and mouse Treg cells from lymphoid and non-lymphoid tissues along pseudotime trajectories (Figure 19). In all cases, I observed a development from naive Treg cells over intermediates in the spleen or blood towards tisTreg cells, which was accompanied by an increase in accessibility of tisTreg-specific peaks and *BATF* transcription factor activity.

I identified *CCR8* among the associated genes in the species-conserved tisTreg signature. Its localization on the cell surface and the gradual increase of *CCR8* gene activity along the pseudotime trajectories in both species make it a promising new marker for tisTreg precursor cells. *CCR8* encodes the C-C motif chemokine receptor 8, which is involved in cell migration and increases suppressive activity and survival of Treg cells. In mouse and humans, it is expressed in Treg cells and to lesser extent in Th2 cells, NK cells and monocytes (Barsheshet et al., 2017; Soler et al., 2006; Coghil et al., 2013). To further validate *CCR8* as a marker for the identification of tisTreg cells and their precursors, my collaboration partners showed its increase in mRNA abundance from *Klrg1⁻Nfil3⁻* Treg cells over early precursors towards the late precursors and tisTregST2 cells in peripheral tissues of the mouse. In addition, human $CCR8^+$ Treg cells were sorted from the blood and assayed by scATAC-seq. I found that these cells align between blood-based intermediates

and tisTreg cells within the human tisTreg developmental trajectory. Moreover, there was a differential enrichment of skin- or fat-specific tisTreg peaks within the $CCR8^+$ Treg pool indicating a priming of these cells for the respective tissue. In Delacher et al. (2021), additional paired scRNA- and scTCR-seq showed that there was a considerable clonal overlap between tisTreg cells and blood $CCR8^+$ Treg cells. This observation strengthened the suitability of *CCR8* as marker to identify tisTreg precursor cells. In mouse experiments, Kolodin et al. (2015) previously showed that there is only little recirculation of Treg cells between fat and the spleen. Instead, tTreg cells clonally expanded within the fat based on TCR sequencing data. Therefore, although my analysis does not provide definite evidence that human blood $CCR8^+$ Treg cells are tisTreg precursors directly originating from lymphoid organs, it is unlikely that they contain a large fraction of recirculating tisTreg cells from fat or skin.

A comparison of the human $CCR8^+$ Treg population with Treg cell subsets described in the literature shows that they share similarity with the highly suppressive effector/activated Treg cell fraction described by Tanaka and Sakaguchi (2017), which is defined by high FOXP3 and CD25 expression and low CD45RA surface protein abundance. Povolieri et al. (2018) further described a $CD161^+$ Treg population with tissue-regenerative and high suppressive capacity found in human blood and the intestinal mucosa. Despite sharing functional similarity with tisTreg cells, they represent another cell subset: $CD161^+$ Treg cells are induced by microbiota-derived retinoic acid and therefore belong to the pTreg fraction whereas tisTreg cells originate from the thymus (tTreg). The difference between these Treg cell subsets becomes further evident by the lack of *KLRB1* (CD161) gene accessibility and mRNA expression in tisTreg cells.

4.5 Clinical significance of Treg cells in the tumor

Selective pressure posed by the host's immune system frequently results in tumor-mediated recruitment of Treg cells, which subsequently suppress the immune response and thereby avoid the destruction of cancer cells. Consequently, the presence of Treg cells in tumors is mostly associated with poor survival rates (Chen et al., 2011; De Simone et al., 2016; Flammiger et al., 2013; Togashi et al., 2019). In previous studies, $CCR8^+$ expression was described as specific feature of tumor Treg cells and had a negative correlation with overall and disease free survival of patients (Plitas et al., 2016; De Simone et al., 2016). Recently, Wang et al. (2019) proposed that $CCR8^+$ Treg cells in peripheral blood of breast cancer patients represent precursors of tumor Treg cells. According to my analysis, $CCR8^+$ Treg cells are not tumor-specific, but reside in peripheral tissues of healthy donors as well. Moreover, blood-based $CCR8^+$ Treg cells are a subset of effector/memory Treg cells most likely constituting tisTreg precursors.

The similarity of tumor-resident Treg cells with tisTreg cells in our data suggests that

they also share most of their functional properties including the production of tissue-regenerative molecules. This would constitute an additional, more direct way to support tumor growth besides mediating immune suppression. While this hypothesis still needs to be experimentally verified, previous studies reported a related mechanism: tumor Treg cells released VEGF, which increased angiogenesis within the tumor tissue (Li et al., 2019b; Facciabene et al., 2011).

Based on their supportive role in tumor growth and their negative impact on patient survival, targeting tumor Treg cells is of high clinical interest. However, targeted therapies are required since systemic Treg depletion results in severe autoimmunity (Sakaguchi et al., 1995; Kim et al., 2007). Most recently, monoclonal antibodies directed against CCR8 were used to deplete CCR8⁺ Treg cells in mice bearing breast, colon or renal carcinoma. This resulted in a durable anti-tumor immune response and a strong inhibition of tumor growth (Kidani et al., 2022; Villarreal et al., 2018). Interestingly, the authors did not observe immunopathologies in anti-CCR8 treated mice even though such side effects would be likely based on my analysis showing the presence of CCR8⁺ Treg cells in healthy peripheral tissues. They hypothesized that tumor de-novo antigens might have higher antigenicity compared to self-antigens from normal tissue. Therefore, partial tumor Treg depletion suffices to restore the immune response against the tumor, whereas autoimmunity only arises at close to complete depletion of Treg cells (Kidani et al., 2022; Shimizu et al., 1999). Together, CCR8-targeted treatment, either alone or in combination with other immunotherapy agents that lead to synergistic effects, may be a promising future treatment approach (Kidani et al., 2022; Villarreal et al., 2018). In 2021, one phase I clinical trial involving anti-CCR8 monoclonal antibody treatment in patients with advanced solid tumors has been started (NCT05007782, registered on ClinicalTrials.gov¹). This trial will provide new data on autoimmunity and other possible side effects of CCR8⁺ Treg depletion in humans.

4.6 PD1⁺TOX⁺ CD8⁺ T cells share tissue-adaptation features with tisTreg cells

In Chapter 3.1, I performed a close characterization of the chromatin accessibility landscape of mouse and human tisTreg cells. Insights from this study are also useful to evaluate other immune cell types with respect to the tisTreg program and potential regenerative capacity. In Chapter 3.2, my collaboration partners generated scATAC-seq of sorted CD8⁺ T cells from the same tissues as the previously analyzed CD4⁺ T cells, which allowed a direct comparison with known features of tisTreg cells. Similar to the collection of CD4⁺ T cell datasets, this resulted in a scATAC-seq atlas of CD8⁺ T cells from healthy

¹<https://clinicaltrials.gov/ct2/show/NCT05007782>, last visited on 04/20/2022

and diseased mouse and human tissues. I used these data to define epigenetic features of CD8⁺ T cells in nonlymphoid tissues. This analysis allows the interpretation of previous publications on tumor CD8⁺ T cells in a new context – tissue adaptation (Satpathy, 2019; Pritykin et al., 2021).

My analysis identified CD8⁺ T cells in peripheral mouse and human tissues that share both characteristics of effector and exhaustion status (Figures 21 and 23). For instance, I observed high chromatin accessibility in the effector-associated genes *GZMB* and *IFNG* and exhaustion-associated genes *TOX*, *PDCD1* and *TIGIT*. Therefore, these cells were termed PD1⁺TOX⁺ CD8⁺ T cells. A subsequent comparison of PD1⁺TOX⁺ CD8⁺ T cells with tisTreg cells revealed several similarities including an increase in BATF transcription factor activity during their development towards a tissue CD8 phenotype, presence in germ-free mice, conservation of tisTreg-associated peaks and importantly, capability to promote tissue repair. BATF dependence was validated by my collaboration partners in BATF^{-/-} mice that almost completely lacked the PD1⁺TOX⁺ CD8⁺ T cell fraction in multiple tissues. Finally, CD8⁺ T cells with high conservation of chromatin features specific for PD1⁺TOX⁺ CD8⁺ T cells from healthy peripheral tissues were also detected in tumor tissue, indicating that their tissue adaptation program is preserved even in a disease setting.

4.7 Comparison of PD1⁺TOX⁺ CD8⁺ T cells with reported CD8⁺ T cell subsets

Based on TCR activation status and localization, T cells are frequently classified as naive (antigen-inexperienced), effector (activated and proliferating after exposure to a cognate antigen) or memory (previous antigen experience) cell. Within the memory fraction, there is a further distinction between central/effector memory (circulating) and tissue-resident memory (Trm, non-circulating) cells (Szabo et al., 2019; Kok et al., 2021). In this framework, PD1⁺TOX⁺ CD8⁺ T cells are most similar to the Trm fraction based on their gene activity, and SingleR based annotation as central/effector memory CD8⁺ T cells can most likely be attributed to missing CD8⁺ Trm cell samples within the reference dataset (Monaco et al., 2019; Aran et al., 2019; Hayward et al., 2020). For example, PD-1 expression in CD8⁺ T cells under homeostasis has been described as a feature of Trm cells (Kumar et al., 2017; Hombrink et al., 2016). In addition, Trm cells represent the largest subset among memory T cells within peripheral tissues, which is in concordance with the high abundance of PD1⁺TOX⁺ CD8⁺ T cells from peripheral tissues in our datasets (Kumar et al., 2018; Thome et al., 2014; Kumar et al., 2017). My pseudo-time analysis further suggests the presence of an intermediate PD1⁺TOX⁺ CD8⁺ T cell phenotype in the blood. This is consistent with previous studies reporting that a population of T cells poised for tissue residency exist within the circulating pool of cells (Kok

et al., 2021, 2020). Additional studies such as cell tracking or parabiosis experiments would be required to test the extent of recirculation within the PD1⁺TOX⁺ CD8⁺ T cells population (Piconese et al., 2020).

There are reports about multiple subsets of CD8⁺ T cells with regulatory function, together termed CD8⁺ Treg cells (Smith and Kumar, 2008; Niederlova et al., 2021). One of the best described subsets are the murine CD8⁺CD122⁺ T cells and their human counterparts, CD8⁺CXCR3⁺ T cells (Rifa'i et al., 2004; Akane et al., 2016; Shi et al., 2009). They resemble central memory T cells and were shown to suppress auto- and alloimmune responses by direct target cell killing and production of inhibitory molecules such as IL-10 and TGF β 1 (Liu et al., 2015; Mishra et al., 2021; Akane et al., 2016). More detailed, PD-1 expression was proposed as a marker to distinguish CD8⁺CD122⁺ T cells with regulatory from those with memory phenotype (Dai et al., 2010). Since there is still controversy in this field and robust markers for CD8⁺ Treg populations are missing, it was not possible to unequivocally identify such cells in our data. Although a subset of PD1⁺TOX⁺ CD8⁺ T cells with high tisTreg signature expression also had high gene activity of published CD8⁺ Treg cell markers including *IL2RB* (CD122), *KLRA1* (mouse-specific, encoding Ly49) and *CXCR3*, further experiments such as *in-vitro* suppression assays would be required to show immune-regulatory activity of PD1⁺TOX⁺ CD8⁺ T cells (Shi et al., 2009; Rifa'i et al., 2004).

4.8 Tissue regenerative potential of CD8⁺ T cells

Support in tissue repair by CD8⁺ T cells has been described under different conditions in mice. Yu et al. (2011); Brodeur et al. (2015) showed that CD8⁺ T cells secrete factors that directly (TNF α) or indirectly (IL13-mediated stimulation of TNF α production in macrophages) increase proliferation in epithelial cells and thereby promote thyroid or lung fibrosis. Further studies revealed that CD8⁺ Trm cells recruit CD4⁺ mononuclear cells to enhance vascular regeneration after injury, whereas an obstructive role was attributed to the enrichment of effector/effector memory CD8⁺ T cells (Stabile et al., 2006; Liang et al., 2020). Similarly, promoting MCP-1 secretion and consequential attraction of macrophages was shown to stimulate myoblast proliferation in damaged muscle tissue (Zhang et al., 2014).

While wound healing capability of murine CD8⁺ T cells is well supported, there are only few reports about tissue-repair function of human CD8⁺ T cells. *In-vitro* assays performed by my collaboration partners showed that human activated TOX⁺ CD8⁺ T cells induce wound healing by release of TNF and IFN γ and interaction with epithelial cells that promotes production of TGF α and AREG. My analysis of scATAC-seq data revealed that human PD1⁺TOX⁺ CD8⁺ T cells share many chromatin features with tisTreg cells distinguishing them from naive Treg and Tconv cells. These results indicate that PD1⁺TOX⁺

CD8⁺ T cells also contribute to the maintenance of tissue homeostasis besides their cytotoxic function. To further strengthen this hypothesis, it would be important to annotate the regions within the tisTreg signature with respect to their functional impact, since it likely contains both features specific to tissue-repair and tissue-adaptation. This would allow to define whether chromatin accessibility features indicative of tissue-repair function are present in PD1⁺TOX⁺ CD8⁺ T cells as well. Above all, further studies are required to investigate the relevance of TOX⁺ CD8⁺ T mediated wound healing *in vivo*, and to clarify whether this function is restricted to the PD1⁺TOX⁺ CD8⁺ T cell subset or a general feature of activated CD8⁺ T cells.

-

4.9 PD1⁺TOX⁺ CD8⁺ T cells from tumors and healthy peripheral tissues are similar

My analysis including both published CD8⁺ T cell exhaustion signatures and a direct comparison of our own scATAC-seq data of CD8⁺ T cells from healthy peripheral and HCC tumor tissue showed that PD1⁺TOX⁺ CD8⁺ T cells from the skin and fat of healthy donors are similar to exhausted CD8⁺ T cells derived from tumor samples (Pritykin et al., 2021). Specifically, dysfunctional CD8⁺ T cell signatures showed the strongest overlap with the chromatin landscape of PD1⁺TOX⁺ CD8⁺ T cells from healthy tissues, and scores were enriched in a highly similar fashion to the human tisTreg signature. Despite this enrichment of exhaustion-associated accessible chromatin regions, it is highly unlikely that PD1⁺TOX⁺ CD8⁺ T cells from the skin and fat of healthy donors are dysfunctional, i.e. gene activity for effector-associated genes such as *IFNG*, *GZMB* or *TNF* was high. Instead, our data indicate that many features previously described as specific for T cell exhaustion in cancer or other chronic diseases rather represent tissue adaptation. This includes well-known exhaustion-associated genes such as *PDCD1*, *TOX* and *TIGIT*, all of which are also accessible and expressed at somewhat lower level in peripheral tissue CD8⁺ T cells under homeostasis (Scott et al., 2019; Wherry et al., 2007; Ostroumov et al., 2021). Given the Trm phenotype of PD1⁺TOX⁺ CD8⁺ T cells, there is supporting evidence found for this hypothesis: Corgnac et al. (2020) reported a functional population of Trm cells expressing both PD-1 and CD39. Their density correlated with improved survival rates of lung cancer patients. It is now recognized that tumor-infiltrating lymphocytes are composed of a variety of different subsets and that some of these subsets – including Trm and other memory-type T cells – express inhibitory checkpoint molecules in a fully functional state. Moreover, control or clearance of a tumor requires the presence of both effector T cells and long-lasting memory-type T cells (Han and Yoon, 2020; Schøller et al., 2021). Therefore, my results fit well in the growing body of evidence that expression of inhibitory checkpoint molecules does not imply T cell exhaustion.

To date, studies frequently include comparisons between T cells from tumor tissue and peripheral blood or lymphoid tissues, which yields both disease- and tissue-associated features (Li et al., 2019a; Cillo et al., 2020; Puram et al., 2017; Zhang et al., 2018; Azizi et al., 2018). The data presented in this chapter will thus be useful to allow a better distinction between true disease-associated changes and features occurring in T cells from healthy peripheral tissues as well in the future.

The high concordance between exhaustion- and tisTreg signature score distributions combined with the results from our *in-vitro* wound healing assays of human PD1⁺TOX⁺ CD8⁺ T cells leads to the hypothesis that CD8⁺ T cells in the tumor act like a double-edged sword: they might both kill tumor cells and support tumor cell proliferation. However, further experiments to prove tissue-repair capacity of tumor-infiltrating PD1⁺TOX⁺ CD8⁺ T cells are warranted. Meanwhile, the vast amounts of literature on positive effects of tumor CD8⁺ T cell infiltration on survival rates suggest that the cytotoxic function of CD8⁺ T cells might outweigh the effects of supporting cell proliferation (van der Leun et al., 2020; Ali et al., 2014; Fluxá et al., 2018; Oshi et al., 2020; Craven et al., 2021).

4.10 Immune cell atlas reveals shared features of tissue adaptation

Chapter 3.3 provides an outlook on tissue-specific alterations in atlases of murine and human immune cells containing both lymphoid and myeloid cells. I quantified the overlap with the tisTreg ATAC signatures for each cell. These features were enriched within the tisTreg clusters and underrepresented in naive T cell clusters, thereby confirming my previous results. However, peaks from the tisTreg signatures were also present in ILC2 cells, and had high enrichment within monocytes, macrophages and dendritic cells. To further explain this observation, I quantified the accessibility for each peak in the core tisTregST2 signature in the murine scATAC-seq atlas and found that it consists of roughly equal contributions from peaks with specificity for tisTreg cells and ILCs and peaks with high accessibility within the myeloid compartment (Figures 26 and 27). Since the core tisTregST2 signature was derived from multiple independent samples from different tissues, each of which required a distinct T cell extraction protocol, it is highly unlikely that it contains a common myeloid cell contamination (Delacher et al., 2020). Moreover, I determined a similar mixed contribution of accessible peaks for the murine and human scATAC-based tisTreg signatures from chapters 3.1.1 and 3.1.3. Due to the single-cell resolution underlying these comparisons, a contamination of myeloid cells in these analyses could be excluded. Rather, the shared peaks show that the tisTreg signatures contain a ‘tissue’ component present across multiple immune cell types, and that they are in the current state most appropriate to highlight tisTreg clusters in datasets of T lymphocytes only. The immune cell atlases now provide the opportunity to refine these signatures

to their subset of true tisTreg-specific peaks. This will not only be useful for a precise annotation of tisTreg cells in new datasets, but also give insights into tisTreg biology by interpreting genes associated with the retained features.

Another explanation for the enrichment of tisTreg signature peaks in myeloid cells is that they share chromatin features related to a tissue repair phenotype with tisTreg cells. Indeed, AREG expression and wound healing potential has been demonstrated in multiple cell types including macrophages, dendritic cells and ILCs (Meng et al., 2015; Bles et al., 2010; Zaiss et al., 2015; Rankin and Artis, 2018). For example, macrophages have confirmed tissue-reparative functions in the skin, intestines, lung and hair follicles (Barron and Wynn, 2011; Nguyen and Soulika, 2019; Yanez et al., 2017). They support proliferation of target cells such as fibroblasts and epithelial cells not only via AREG production, but also via release of other growth factors such as TGF β , PDGF and VEGF (Nguyen and Soulika, 2019; Barron and Wynn, 2011).

In summary, our immune cell atlas project has potential to advance the understanding of tissue-specific functions of immune cells by defining their common epigenetic framework and highlighting immune cell subset-specific chromatin features of tissue adaptation.

4.11 Role of BATF in immune cell development

In Chapters 3.1 and 3.2, we found that the transcription factor BATF plays an important role for Treg and PD1⁺TOX⁺ CD8⁺ T cells in their development towards peripheral tissues. In mice, this result confirmed previous studies emphasizing the requirement of BATF for tisTreg differentiation and maintenance (Delacher et al., 2017; Miragaia et al., 2019; Vasanthakumar et al., 2015; Hayatsu et al., 2017). (Mijnheer et al., 2021) described a similar population of human effector Treg cells under inflammatory conditions and proposed BATF to be a key transcriptional regulator for these cells. Similarly, the activated and suppressive effector Treg cell phenotype in human non-small-cell lung cancer tumor samples was dependent on the activity of BATF and its binding partner IRF4 (Alvisi et al., 2020).

The immune atlas data presented in Chapter 3.3 showed that there is a high correlation of BATF activity with enrichment of the tisTreg signature, and more importantly, that its activity is also high in a subset of other immune cell types such as macrophages, DCs, ILCs and plasma cells. This indicates that BATF plays a more general role in immune cell development and their adaptation towards peripheral tissues. In support of this observation, BATF was recently described as a pioneer transcription factor that initiates effector cell differentiation (Pham et al., 2019; Ciofani et al., 2012). In T cells, BATF is activated downstream of TCR signaling and induces changes in chromatin accessibility. In turn, these allow the expression of lineage-defining transcription factors such as Bcl-6,

which is considered the master regulator of Tfh cell development (Ise et al., 2011; Pham et al., 2019; Nurieva et al., 2009). Besides its role in T cells, BATF is also involved in the development and function of B cells and dendritic cells (Betz et al., 2010; Ise et al., 2011; Murphy et al., 2013; Tsao et al., 2022). Important insights were gained from BATF knockout mice, which lack Th17 cells and have impaired Th2 and Tfh cell development (Schraml et al., 2009; Betz et al., 2010). In CD8⁺ T cells, missing BATF activity results in diminished proliferation and effector cell differentiation and an aberrant cytokine production profile, whereas Treg cells acquire characteristics typical for Th2 cells (Tsao et al., 2022; Xu et al., 2021; Kurachi et al., 2014). Together, BATF has a broad spectrum of effects in the development and function of multiple immune cell lineages. While we were able to show that it is also required for acquisition of a tissue-specialized phenotype in tisTreg and PD1⁺TOX⁺ CD8⁺ T cells, a direct link to the tissue repair capacity of these cells is still missing. The interrogation of BATF binding sites at gene loci of molecules involved in wound-healing would be a good starting point to approach this question.

4.12 Limitations

Methods interrogating chromatin accessibility such as scATAC-seq yield genomic regions ('peaks') as features, which are difficult to interpret. Therefore, a common approach is to summarize chromatin accessibility within and around gene-encoding regions to obtain a gene activity score. This score can be used in a similar way as in transcriptomic analyses, e.g. to define differentially accessible genes, and annotate cell populations based on the activity of marker genes or with scRNA-based methods such as SingleR (Aran et al., 2019). A limitation of this approach is that while gene activity often represents a good proxy for the gene's expression level, chromatin accessibility has poor predictive value for mRNA transcript levels of some genes. In a comparison of bulk sequencing data, Starks et al. (2019) reported a Spearman correlation of 0.7 between ATAC-based gene activities and RNA-seq measurements from matching biological samples. Recently, multi-omic approaches have become available, in which both ATAC- and RNA-signals are captured from the same cell. Studies reported median Pearson correlations in the range of 0.4 – 0.6 between gene activity scores and mRNA transcript counts of cells from PBMC and bone marrow samples (Granja et al., 2021; Stuart et al., 2019; Granja et al., 2019). One explanation for this moderate correlation is that genes are frequently 'poised' for expression: their DNA is already accessible, but requires further activation signals such as histone modifications or transcription factor binding in order to get transcribed (DiSpirito et al., 2018; Klemm et al., 2019). Also, there is a negligible or even repressing effect of increased chromatin accessibility on gene expression in some cases (Riethoven, 2010). Several improvements in the correspondence of gene activities and mRNA

levels were achieved by incorporating distal regions in a distance-weighted fashion besides gene body and promoter region into gene activity models (Granja et al., 2021). However, there remains uncertainty about the true association of these elements with nearby genes (McLean et al., 2010). An example from our data is the *AREG* gene, which clearly shows increased mRNA expression in human fat and skin PD1⁺TOX⁺ CD8⁺ T cells compared to blood CD8⁺ T cells, whereas hardly any change is detectable in its chromatin accessibility (Delacher et al., nd). Thus, gene activity scores need to be interpreted with care and it may be beneficial to select regions incorporated in a gene activity score on an individual basis instead of using a generalized approach. In the future, the generation of cis-regulatory maps defining distal elements and their effects on genes may greatly improve the prediction of gene expression based on their chromatin accessibility.

Another limitation of our work is the requirement of additional experiments to prove the tissue-repair capacity of tisTreg and PD1⁺TOX⁺CD8⁺ T cells *in vivo*. In Chapter 3.1, we showed the similarity of *in-vitro* induced Tfh-like Treg cells with tisTreg cells, which produced factors that significantly supported wound closure. However, it is still unclear how much tisTreg cells contribute to wound healing under natural conditions in organisms including mice and humans. Currently, the number of tisTreg cells that can be isolated from peripheral tissue samples such as fat and skin is too low for applications such as wound healing assays hindering the use of ex-vivo tisTreg cells (Pijuan et al., 2019). The development of new assays with lower cell input requirements or the use of mouse models allowing selective depletion of tisTreg cells could consolidate the tissue-repair function of bonafide tisTreg cells. Similar considerations also apply to the proposed growth-promoting function of tumor CCR8⁺ Treg cells and the PD1⁺TOX⁺CD8⁺ T cells described in Chapter 3.2. Another line of evidence would be to elucidate the molecular mechanisms underlying the repair capacity of tisTreg and PD1⁺TOX⁺CD8⁺ T cells. This could be approached by generation of gene-regulatory networks linking transcription factors to genes directly involved in tissue repair, accompanied with loss-of-function experiments to validate their impact on tissue repair potential (DiSpirito et al., 2018; Cong et al., 2013).

Using pseudotime analysis, I was able to infer developmental trajectories of tisTreg and PD1⁺TOX⁺CD8⁺ T cells. These started from naive T cells in lymphoid tissues and developed via precursor stages in the spleen and blood. A caveat of scATAC-based trajectory inference with Monocle is that the direction of change is arbitrary. It was therefore not possible to unambiguously determine whether the cells with intermediate phenotypes represent precursors or recirculating cells. This is in contrast with other methods such as RNA velocity or scVelo that rely on RNA-splicing information and produce directed trajectories (Bergen et al., 2020; La Manno et al., 2018; Trapnell et al., 2014). An advantage over single-cell transcriptomic methods is that trajectory analysis based on scATAC-seq captures dynamic changes in gene regulation and transcription factor activity, thereby

providing valuable insights into the drivers of cell development.

Lastly, it remains to be clarified whether tissue repair capacity is a distinct feature of $PD1^+TOX^+ CD8^+$ T cells, which would justify to classify them as another subpopulation among $CD8^+$ T cells.

4.13 Outlook

The close epigenetic characterization of $CD4^+$ and $CD8^+$ T cells from peripheral tissues presented in Chapters 3.1 and 3.2 have led to the identification of human tisTreg cells and $PD1^+TOX^+ CD8^+$ T cells with tissue-regenerative capacity. The immune cell atlas data introduced in Chapter 3.3 will allow me to obtain a comprehensive view on chromatin accessibility in immune cells, and thereby distinguish between universal and cell type-specific alterations in chromatin accessibility. Using these data, I will not only be able to refine previous results such as the tisTreg signatures, but also generate insights on cell types such as ILCs, which are yet to be described on the epigenetic level.

Delacher et al. (2020) previously showed two precursor stages of murine tisTregST2 cells within the spleen using a combination of scRNA-seq and ATAC-seq. To better understand human tisTreg cells, an important task will be to define whether there are also multiple distinct steps during the development of human tisTreg cells. In this context, it would also be relevant to distinguish between tisTreg precursors and tisTreg cells that have egressed from peripheral tissues. Parabiosis experiments, cell tracking protocols or bioinformatic approaches that yield directed graphs of development such as RNA velocity might be useful to investigate this aspect (La Manno et al., 2018; Piconese et al., 2020). Also, recent development of multi-omic single-cell approaches such as SHARE-seq that allow simultaneous measurement of RNA transcripts and accessible chromatin allow the inference of directed developmental steps with new concepts such as ‘chromatin potential’, in which chromatin accessibility predicts future mRNA states (Ma et al., 2020).

Our analyses are therapeutically relevant in multiple aspects. First, the identification of human tisTreg cells may lead to new applications in regenerative medicine, where expansion and administration of tisTreg-like cells to patients may foster wound healing while simultaneously preventing further tissue damage caused by inflammatory reactions. Second, with their ability to promote proliferation, we revealed a potential additional mechanism of Treg cells to support tumor growth besides their suppressive effects on effector cells. It will be important to further test this hypothesis, since it might entail altered cancer immunotherapeutic strategies: checkpoint inhibitors could be combined with agents blocking signaling pathways that induce cell proliferation such as the EGFR pathway (Wee and Wang, 2017). On a similar note, $PD1^+TOX^+ CD8^+$ T cells may support cell proliferation and thereby also support tumor growth in some cases. A supporting ob-

ervation to this notion was reported in nonalcoholic steatohepatitis, where $CD8^+$ T cells with a $PD1^+CXCR6^+TOX^+TNF^+$ phenotype promoted tissue fibrosis and the induction of hepatocellular carcinoma (Pfister et al., 2021; Dudek et al., 2021). Third, my comparison of T cells between healthy peripheral tissues and tumor tissue showed substantial overlap in their epigenetic landscape. The data included in these analyses will therefore be useful to define changes affecting T cell epigenomes in the tumor microenvironment that do not merely represent tissue adaptation events. This may support the choice of targetable molecules in immunotherapies that specifically affect tumor T cells and minimize the risk of side effects in healthy tissues such as autoimmune reactions.

5 References

References

- Akane, K., Kojima, S., Mak, T. W., Shiku, H., and Suzuki, H. (2016). CD8+CD122+CD49dlow regulatory T cells maintain T-cell homeostasis by killing activated T cells via Fas/FasL-mediated cytotoxicity. *Proceedings of the National Academy of Sciences*, 113(9):2460–2465.
- Ali, H. R., Provenzano, E., Dawson, S.-J., Blows, F. M., Liu, B., Shah, M., Earl, H. M., Poole, C. J., Hiller, L., Dunn, J. A., Bowden, S. J., Twelves, C., Bartlett, J. M. S., Mahmoud, S. M. A., Rakha, E., Ellis, I. O., Liu, S., Gao, D., Nielsen, T. O., Pharoah, P. D. P., and Caldas, C. (2014). Association between CD8+ T-cell infiltration and breast cancer survival in 12 439 patients. *Annals of Oncology*, 25(8):1536–1543.
- Allis, C. D. and Jenuwein, T. (2016). The molecular hallmarks of epigenetic control. *Nature Reviews Genetics*, 17(8):487–500.
- Alvisi, G., Brummelman, J., Puccio, S., Mazza, E. M., Tomada, E. P., Losurdo, A., Zanon, V., Peano, C., Colombo, F. S., Scarpa, A., Alloisio, M., Vasanthakumar, A., Roychoudhuri, R., Kallikourdis, M., Pagani, M., Lopci, E., Novellis, P., Blume, J., Kallies, A., Veronesi, G., and Lugli, E. (2020). IRF4 instructs effector Treg differentiation and immune suppression in human cancer. *Journal of Clinical Investigation*, 130(6):3137–3150.
- Angerer, P., Simon, L., Tritschler, S., Wolf, F. A., Fischer, D., and Theis, F. J. (2017). Single cells make big data: New challenges and opportunities in transcriptomics. *Current Opinion in Systems Biology*, 4:85–91.
- Antonioni, L., Pacher, P., Vizi, E. S., and Haskó, G. (2013). CD39 and CD73 in immunity and inflammation. *Trends in molecular medicine*, 19(6):355–367.
- Aran, D., Looney, A. P., Liu, L., Wu, E., Fong, V., Hsu, A., Chak, S., Naikawadi, R. P., Wolters, P. J., Abate, A. R., Butte, A. J., and Bhattacharya, M. (2019). Reference-based analysis of lung single-cell sequencing reveals a transitional profibrotic macrophage. *Nature Immunology*, 20(2):163–172.
- Arpaia, N., Green, J. A., Moltedo, B., Arvey, A., Hemmers, S., Yuan, S., Treuting, P. M., and Rudensky, A. Y. (2015). A Distinct Function of Regulatory T Cells in Tissue Protection. *Cell*, 162(5):1078–1089.
- Atarashi, K., Tanoue, T., Oshima, K., Suda, W., Nagano, Y., Nishikawa, H., Fukuda, S., Saito, T., Narushima, S., Hase, K., Kim, S., Fritz, J. V., Wilmes, P., Ueha, S., Matsushima, K., Ohno, H., Olle, B., Sakaguchi, S., Taniguchi, T., Morita, H., Hattori, M., and Honda, K. (2013). Treg induction by a rationally selected mixture of Clostridia strains from the human microbiota. *Nature*, 500(7461):232–236.
- Atarashi, K., Tanoue, T., Shima, T., Imaoka, A., Kuwahara, T., Momose, Y., Cheng, G., Yamasaki, S., Saito, T., Ohba, Y., Taniguchi, T., Takeda, K., Hori, S., Ivanov, I. I., Umesaki, Y., Itoh, K., and Honda, K. (2011). Induction of colonic regulatory T cells by indigenous Clostridium species. *Science (New York, N.Y.)*, 331(6015):337–341.
- Azizi, E., Carr, A. J., Plitas, G., Cornish, A. E., Konopacki, C., Prabhakaran, S., Nainys, J., Wu, K., Kisieliovas, V., Setty, M., Choi, K., Fromme, R. M., Dao, P., McKenney, P. T., Wasti, R. C., Kadaveru, K., Mazutis, L., Rudensky, A. Y., and Pe’er, D. (2018). Single-Cell Map of Diverse Immune Phenotypes in the Breast Tumor Microenvironment. *Cell*, 174(5):1293–1308.e36.
- Baek, S. and Lee, I. (2020). Single-cell ATAC sequencing analysis: From data preprocessing to hypothesis generation. *Computational and Structural Biotechnology Journal*, 18:1429–1439.
- Barron, L. and Wynn, T. A. (2011). Fibrosis is regulated by Th2 and Th17 responses and by dynamic interactions between fibroblasts and macrophages. *American Journal of Physiology. Gastrointestinal and Liver Physiology*, 300(5):G723–728.
- Barsheshet, Y., Wildbaum, G., Levy, E., Vitenshtein, A., Akinseye, C., Griggs, J., Lira, S. A., and Karin, N. (2017). CCR8+FOXP3+ Treg cells as master drivers of immune regulation. *Proceedings of the National Academy of Sciences*, 114(23):6086–6091.
- Bateman, A., Cheung, S. T., and Bennett, H. P. J. (2018). A Brief Overview of Progranulin in Health and Disease. *Methods in Molecular Biology (Clifton, N.J.)*, 1806:3–15.
- Berasain, C. and Avila, M. A. (2014). Amphiregulin. *Seminars in Cell & Developmental Biology*, 28:31–41.

- Bergen, V., Lange, M., Peidli, S., Wolf, F. A., and Theis, F. J. (2020). Generalizing RNA velocity to transient cell states through dynamical modeling. *Nature Biotechnology*, 38(12):1408–1414.
- Betz, B. C., Jordan-Williams, K. L., Wang, C., Kang, S. G., Liao, J., Logan, M. R., Kim, C. H., and Taparowsky, E. J. (2010). Batf coordinates multiple aspects of B and T cell function required for normal antibody responses. *The Journal of Experimental Medicine*, 207(5):933–942.
- Biton, M., Haber, A. L., Rogel, N., Burgin, G., Beyaz, S., Schnell, A., Ashenberg, O., Su, C.-W., Smillie, C., Shekhar, K., Chen, Z., Wu, C., Ordovas-Montanes, J., Alvarez, D., Herbst, R. H., Zhang, M., Tirosh, I., Dionne, D., Nguyen, L. T., Xifaras, M. E., Shalek, A. K., von Andrian, U. H., Graham, D. B., Rozenblatt-Rosen, O., Shi, H. N., Kuchroo, V., Yilmaz, O. H., Regev, A., and Xavier, R. J. (2018). T Helper Cell Cytokines Modulate Intestinal Stem Cell Renewal and Differentiation. *Cell*, 175(5):1307–1320.e22.
- Bles, N., Di Pietrantonio, L., Boeynaems, J.-M., and Communi, D. (2010). ATP confers tumorigenic properties to dendritic cells by inducing amphiregulin secretion. *Blood*, 116(17):3219–3226.
- Bonilla, F. A. and Oettgen, H. C. (2010). Adaptive immunity. *Journal of Allergy and Clinical Immunology*, 125(2):S33–S40.
- Bopp, T., Becker, C., Klein, M., Klein-Hessling, S., Palmetshofer, A., Serfling, E., Heib, V., Becker, M., Kubach, J., Schmitt, S., Stoll, S., Schild, H., Staeger, M. S., Stassen, M., Jonuleit, H., and Schmitt, E. (2007). Cyclic adenosine monophosphate is a key component of regulatory T cell-mediated suppression. *The Journal of Experimental Medicine*, 204(6):1303–1310.
- Bos, P. D., Plitas, G., Rudra, D., Lee, S. Y., and Rudensky, A. Y. (2013). Transient regulatory T cell ablation deters oncogene-driven breast cancer and enhances radiotherapy. *The Journal of Experimental Medicine*, 210(11):2435–2466.
- Bowen-Pope, D. F., Hart, C. E., and Seifert, R. A. (1989). Sera and conditioned media contain different isoforms of platelet-derived growth factor (PDGF) which bind to different classes of PDGF receptor. *Journal of Biological Chemistry*, 264(5):2502–2508.
- Brodeur, T. Y., Robidoux, T. E., Weinstein, J. S., Craft, J., Swain, S. L., and Marshak-Rothstein, A. (2015). IL-21 Promotes Pulmonary Fibrosis through the Induction of Profibrotic CD8⁺ T Cells. *Journal of Immunology (Baltimore, Md.: 1950)*, 195(11):5251–5260.
- Brunkow, M. E., Jeffery, E. W., Hjerrild, K. A., Paeper, B., Clark, L. B., Yasayko, S.-A., Wilkinson, J. E., Galas, D., Ziegler, S. F., and Ramsdell, F. (2001). Disruption of a new forkhead/winged-helix protein, scurfy, results in the fatal lymphoproliferative disorder of the scurfy mouse. *Nature Genetics*, 27(1):68–73.
- Buenrostro, J. D., Giresi, P. G., Zaba, L. C., Chang, H. Y., and Greenleaf, W. J. (2013). Transposition of native chromatin for fast and sensitive epigenomic profiling of open chromatin, DNA-binding proteins and nucleosome position. *Nature Methods*, 10(12):1213–1218.
- Buenrostro, J. D., Wu, B., Litzgenburger, U. M., Ruff, D., Gonzales, M. L., Snyder, M. P., Chang, H. Y., and Greenleaf, W. J. (2015). Single-cell chromatin accessibility reveals principles of regulatory variation. *Nature*, 523(7561):486–490.
- Burzyn, D., Kuswanto, W., Kolodin, D., Shadrach, J. L., Cerletti, M., Jang, Y., Sefik, E., Tan, T. G., Wagers, A. J., Benoist, C., and Mathis, D. (2013). A special population of regulatory T cells potentiates muscle repair. *Cell*, 155(6):1282–1295.
- Catlin, S. N., Busque, L., Gale, R. E., Guttorp, P., and Abkowitz, J. L. (2011). The replication rate of human hematopoietic stem cells in vivo. *Blood*, 117(17):4460–4466.
- Chang, L.-Y., Lin, Y.-C., Mahalingam, J., Huang, C.-T., Chen, T.-W., Kang, C.-W., Peng, H.-M., Chu, Y.-Y., Chiang, J.-M., Dutta, A., Day, Y.-J., Chen, T.-C., Yeh, C.-T., and Lin, C.-Y. (2012). Tumor-Derived Chemokine CCL5 Enhances TGF- β -Mediated Killing of CD8⁺ T Cells in Colon Cancer by T-Regulatory Cells. *Cancer Research*, 72(5):1092–1102.
- Chen, K.-J., Lin, S.-Z., Zhou, L., Xie, H.-Y., Zhou, W.-H., Taki-Eldin, A., and Zheng, S.-S. (2011). Selective recruitment of regulatory T cell through CCR6-CCL20 in hepatocellular carcinoma fosters tumor progression and predicts poor prognosis. *PLoS One*, 6(9):e24671.
- Chen, Z., Quan, L., Huang, A., Zhao, Q., Yuan, Y., Yuan, X., Shen, Q., Shang, J., Ben, Y., Qin, F. X.-F., and Wu, A. (2018). seq-ImmuCC: Cell-Centric View of Tissue Transcriptome Measuring Cellular Compositions of Immune Microenvironment From Mouse RNA-Seq Data. *Frontiers in Immunology*, 9:1286.
- Cillo, A. R., Kürten, C. H. L., Tabib, T., Qi, Z., Onkar, S., Wang, T., Liu, A., Duvvuri, U., Kim, S., Soose, R. J., Oesterreich, S., Chen, W., Lafyatis, R., Bruno, T. C., Ferris, R. L., and Vignali, D. A. A. (2020). Immune Landscape of Viral- and Carcinogen-Driven Head and Neck Cancer. *Immunity*, 52(1):183–199.e9.

- Ciofani, M., Madar, A., Galan, C., Sellars, M., Mace, K., Pauli, F., Agarwal, A., Huang, W., Parkurst, C. N., Muratet, M., Newberry, K. M., Meadows, S., Greenfield, A., Yang, Y., Jain, P., Kirigin, F. K., Birchmeier, C., Wagner, E. F., Murphy, K. M., Myers, R. M., Bonneau, R., and Littman, D. R. (2012). A Validated Regulatory Network for Th17 Cell Specification. *Cell*, 151(2):289–303.
- Cipolletta, D., Feuerer, M., Li, A., Kamei, N., Lee, J., Shoelson, S. E., Benoist, C., and Mathis, D. (2012). PPAR- γ is a major driver of the accumulation and phenotype of adipose tissue Treg cells. *Nature*, 486(7404):549–553.
- Clark, L. B., Appleby, M. W., Brunkow, M. E., Wilkinson, J. E., Ziegler, S. F., and Ramsdell, F. (1999). Cellular and Molecular Characterization of the scurfy Mouse Mutant. *The Journal of Immunology*, 162(5):2546–2554.
- Coghill, J. M., Fowler, K. A., West, M. L., Fulton, L. M., van Deventer, H., McKinnon, K. P., Vincent, B. G., Lin, K., Panoskaltis-Mortari, A., Cook, D. N., Blazar, B. R., and Serody, J. S. (2013). CC chemokine receptor 8 potentiates donor Treg survival and is critical for the prevention of murine graft-versus-host disease. *Blood*, 122(5):825–836.
- Colamatteo, A., Carbone, F., Bruzzaniti, S., Galgani, M., Fusco, C., Maniscalco, G. T., Di Rella, F., de Candia, P., and De Rosa, V. (2020). Molecular Mechanisms Controlling Foxp3 Expression in Health and Autoimmunity: From Epigenetic to Post-translational Regulation. *Frontiers in Immunology*, 10.
- Collison, L. W., Workman, C. J., Kuo, T. T., Boyd, K., Wang, Y., Vignali, K. M., Cross, R., Sehy, D., Blumberg, R. S., and Vignali, D. A. A. (2007). The inhibitory cytokine IL-35 contributes to regulatory T-cell function. *Nature*, 450(7169):566–569.
- Cong, L., Ran, F. A., Cox, D., Lin, S., Barretto, R., Habib, N., Hsu, P. D., Wu, X., Jiang, W., Marraffini, L. A., and Zhang, F. (2013). Multiplex genome engineering using CRISPR/Cas systems. *Science (New York, N. Y.)*, 339(6121):819–823.
- Cornac, S., Malenica, I., Mezquita, L., Auclin, E., Voilin, E., Kacher, J., Halse, H., Grynszpan, L., Signolle, N., Dayris, T., Leclerc, M., Droin, N., de Montpréville, V., Mercier, O., Validire, P., Scoazec, J.-Y., Massard, C., Chouaib, S., Planchard, D., Adam, J., Besse, B., and Mami-Chouaib, F. (2020). CD103+CD8+ TRM Cells Accumulate in Tumors of Anti-PD-1-Responder Lung Cancer Patients and Are Tumor-Reactive Lymphocytes Enriched with Tc17. *Cell Reports Medicine*, 1(7):100127.
- Cosovanu, C. and Neumann, C. (2020). The Many Functions of Foxp3+ Regulatory T Cells in the Intestine. *Frontiers in Immunology*, 11:2710.
- Craven, K. E., Gökmen-Polar, Y., and Badve, S. S. (2021). CIBERSORT analysis of TCGA and METABRIC identifies subgroups with better outcomes in triple negative breast cancer. *Scientific Reports*, 11(1):4691.
- Cretney, E., Kallies, A., and Nutt, S. L. (2013). Differentiation and function of Foxp3+ effector regulatory T cells. *Trends in Immunology*, 34(2):74–80.
- Crotty, S. (2014). T Follicular Helper Cell Differentiation, Function, and Roles in Disease. *Immunity*, 41(4):529–542.
- Crotty, S. (2019). T Follicular Helper Cell Biology: A Decade of Discovery and Diseases. *Immunity*, 50(5):1132–1148.
- Cusanovich, D. A., Hill, A. J., Aghamirzaie, D., Daza, R. M., Pliner, H. A., Berletch, J. B., Filippova, G. N., Huang, X., Christiansen, L., DeWitt, W. S., Lee, C., Regalado, S. G., Read, D. F., Steemers, F. J., Disteche, C. M., Trapnell, C., and Shendure, J. (2018). A Single-Cell Atlas of In Vivo Mammalian Chromatin Accessibility. *Cell*, 174(5):1309–1324.e18.
- Dai, H., Wan, N., Zhang, S., Moore, Y., Wan, F., and Dai, Z. (2010). Cutting edge: programmed death-1 defines CD8+CD122+ T cells as regulatory versus memory T cells. *Journal of Immunology (Baltimore, Md.: 1950)*, 185(2):803–807.
- Datlinger, P., Rendeiro, A. F., Boenke, T., Senekowitsch, M., Krausgruber, T., Barreca, D., and Bock, C. (2021). Ultra-high-throughput single-cell RNA sequencing and perturbation screening with combinatorial fluidic indexing. *Nature Methods*, 18(6):635–642.
- Deaglio, S., Dwyer, K. M., Gao, W., Friedman, D., Usheva, A., Erat, A., Chen, J.-F., Enjyoji, K., Linden, J., Oukka, M., Kuchroo, V. K., Strom, T. B., and Robson, S. C. (2007). Adenosine generation catalyzed by CD39 and CD73 expressed on regulatory T cells mediates immune suppression. *Journal of Experimental Medicine*, 204(6):1257–1265.
- Deerwester, S., Dumais, S. T., Furnas, G. W., Landauer, T. K., and Harshman, R. (1990). Indexing by latent semantic analysis. *Journal of the American Society for Information Science*, 41(6):391–407.
- Delacher, M., Imbusch, C. D., Hotz-Wagenblatt, A., Mallm, J.-P., Bauer, K., Simon, M., Riegel, D., Rendeiro, A. F., Bittner, S., Sanderink, L., Pant, A., Schmidleithner, L., Braband, K. L., Echtenachter, B., Fischer, A., Giunchiglia, V., Hoffmann,

- P., Edinger, M., Bock, C., Rehli, M., Brors, B., Schmidl, C., and Feuerer, M. (2020). Precursors for Nonlymphoid-Tissue Treg Cells Reside in Secondary Lymphoid Organs and Are Programmed by the Transcription Factor BATF. *Immunity*, 52(2):295–312.e11.
- Delacher, M., Imbusch, C. D., Weichenhan, D., Breiling, A., Hotz-Wagenblatt, A., Träger, U., Hofer, A. C., Kägebein, D., Wang, Q., Frauhammer, F., Mallm, J. P., Bauer, K., Herrmann, C., Lang, P. A., Brors, B., Plass, C., and Feuerer, M. (2017). Genome-wide DNA-methylation landscape defines specialization of regulatory T cells in tissues. *Nature Immunology*.
- Delacher, M., Simon, M., Sanderink, L., Hotz-Wagenblatt, A., Wuttke, M., Schambeck, K., Schmidleithner, L., Bittner, S., Pant, A., Ritter, U., Hehlgans, T., Riegel, D., Schneider, V., Groeber-Becker, F. K., Eigenberger, A., Gebhard, C., Strieder, N., Fischer, A., Rehli, M., Hoffmann, P., Edinger, M., Strowig, T., Huehn, J., Schmidl, C., Werner, J. M., Prantl, L., Brors, B., Imbusch, C. D., and Feuerer, M. (2021). Single-cell chromatin accessibility landscape identifies tissue repair program in human regulatory T cells. *Immunity*, 54(4):702–720.e17.
- Delacher, M., Simon, M., Schmidleithner, L., Stüve, P., Lieke, S., Hotz-Wagenblatt, A., Wuttke, M., Schambeck, K., Ruhland, B., Hofmann, V., Bittner, S., Pant, A., Eigenberger, A., Menevse, A.-N., Gebhard, C., Strieder, N., Abken, H., Rehli, M., Schmidl, C., Beckhove, P., Strowig, T., Huehn, J., Hehlgans, T., Prantl, L., Werner, J. M., Brors, B., Imbusch, C. D., and Feuerer, M. (n.d.). Single-cell chromatin accessibility landscape reveals tissue-repair potential of human effector CD8 T cells. In preparation.
- De Simone, M., Arrighoni, A., Rossetti, G., Guarini, P., Ranzani, V., Politano, C., Bonnal, R. J. P., Provasi, E., Sarnicola, M. L., Panzeri, I., Moro, M., Crosti, M., Mazzara, S., Vaira, V., Bosari, S., Palleschi, A., Santambrogio, L., Bovo, G., Zucchini, N., Totis, M., Gianotti, L., Cesana, G., Perego, R. A., Maroni, N., Ceretti, A. P., Opocher, E., De Francesco, R., Geginat, J., Stunnenberg, H. G., Abrignani, S., and Pagani, M. (2016). Transcriptional Landscape of Human Tissue Lymphocytes Unveils Uniqueness of Tumor-Infiltrating T Regulatory Cells. *Immunity*, 45(5):1135–1147.
- Ding, J., Adiconis, X., Simmons, S. K., Kowalczyk, M. S., Hession, C. C., Marjanovic, N. D., Hughes, T. K., Wadsworth, M. H., Burks, T., Nguyen, L. T., Kwon, J. Y. H., Barak, B., Ge, W., Kedaigle, A. J., Carroll, S., Li, S., Hacohen, N., Rozenblatt-Rosen, O., Shalek, A. K., Villani, A.-C., Regev, A., and Levin, J. Z. (2020). Systematic comparison of single-cell and single-nucleus RNA-sequencing methods. *Nature Biotechnology*, 38(6):737–746.
- DiSpirito, J. R., Zemmour, D., Ramanan, D., Cho, J., Zilionis, R., Klein, A. M., Benoist, C., and Mathis, D. (2018). Molecular diversification of regulatory T cells in nonlymphoid tissues. *Science Immunology*, 3(27):eaat5861.
- Domcke, S., Hill, A. J., Daza, R. M., Cao, J., O’Day, D. R., Pliner, H. A., Aldinger, K. A., Pokholok, D., Zhang, F., Milbank, J. H., Zager, M. A., Glass, I. A., Steemers, F. J., Doherty, D., Trapnell, C., Cusanovich, D. A., and Shendure, J. (2020). A human cell atlas of fetal chromatin accessibility. *Science*, 370(6518):eaba7612.
- Dudek, M., Pfister, D., Donakonda, S., Filpe, P., Schneider, A., Laschinger, M., Hartmann, D., Hüser, N., Meiser, P., Bayerl, F., Inverso, D., Wigger, J., Sebode, M., Öllinger, R., Rad, R., Hegenbarth, S., Anton, M., Guillot, A., Bowman, A., Heide, D., Müller, F., Ramadori, P., Leone, V., Garcia-Caceres, C., Gruber, T., Seifert, G., Kabat, A. M., Mallm, J.-P., Reider, S., Effenberger, M., Roth, S., Billeter, A. T., Müller-Stich, B., Pearce, E. J., Koch-Nolte, F., Käser, R., Tilg, H., Thimme, R., Boettler, T., Tacke, F., Dufour, J.-F., Haller, D., Murray, P. J., Heeren, R., Zehn, D., Böttcher, J. P., Heikenwälder, M., and Knolle, P. A. (2021). Auto-aggressive CXCR6+ CD8 T cells cause liver immune pathology in NASH. *Nature*, 592(7854):444–449.
- Duhen, T., Duhen, R., Lanzavecchia, A., Sallusto, F., and Campbell, D. J. (2012). Functionally distinct subsets of human FOXP3+ Treg cells that phenotypically mirror effector Th cells. *Blood*, 119(19):4430–4440.
- Durinck, S., Spellman, P. T., Birney, E., and Huber, W. (2009). Mapping identifiers for the integration of genomic datasets with the R/Bioconductor package biomaRt. *Nature Protocols*, 4(8):1184–1191.
- Facciabene, A., Peng, X., Hagemann, I. S., Balint, K., Barchetti, A., Wang, L.-P., Gimotty, P. A., Gilks, C. B., Lal, P., Zhang, L., and Coukos, G. (2011). Tumour hypoxia promotes tolerance and angiogenesis via CCL28 and Treg cells. *Nature*, 475(7355):226–230.
- Fallarino, F., Grohmann, U., Hwang, K. W., Orabona, C., Vacca, C., Bianchi, R., Belladonna, M. L., Fioretti, M. C., Alegre, M.-L., and Puccetti, P. (2003). Modulation of tryptophan catabolism by regulatory T cells. *Nature Immunology*, 4(12):1206–1212.
- Fan, X. and Rudensky, A. Y. (2016). Hallmarks of Tissue-Resident Lymphocytes. *Cell*, 164(6):1198–1211.

- Feuerer, M., Herrero, L., Cipolletta, D., Naaz, A., Wong, J., Nayer, A., Lee, J., Goldfine, A. B., Benoist, C., Shoelson, S., and Mathis, D. (2009). Lean, but not obese, fat is enriched for a unique population of regulatory T cells that affect metabolic parameters. *Nature Medicine*, 15(8):930–939.
- Flammiger, A., Weisbach, L., Huland, H., Tennstedt, P., Simon, R., Minner, S., Bokemeyer, C., Sauter, G., Schlomm, T., and Trepel, M. (2013). High tissue density of FOXP3+ T cells is associated with clinical outcome in prostate cancer. *European Journal of Cancer (Oxford, England: 1990)*, 49(6):1273–1279.
- Fleming, B. D. and Mosser, D. M. (2011). Regulatory macrophages: setting the threshold for therapy. *European journal of immunology*, 41(9):2498–2502.
- Floess, S., Freyer, J., Siewert, C., Baron, U., Olek, S., Polansky, J., Schlawe, K., Chang, H.-D., Bopp, T., Schmitt, E., Klein-Hessling, S., Serfling, E., Hamann, A., and Huehn, J. (2007). Epigenetic Control of the foxp3 Locus in Regulatory T Cells. *PLOS Biology*, 5(2):e38.
- Fluxá, P., Rojas-Sepúlveda, D., Gleisner, M. A., Tittarelli, A., Villegas, P., Tapia, L., Rivera, M. T., López, M. N., Catán, F., Uribe, M., and Salazar-Onfray, F. (2018). High CD8+ and absence of Foxp3+ T lymphocytes infiltration in gallbladder tumors correlate with prolonged patients survival. *BMC Cancer*, 18(1):243.
- Fontenot, J. D., Gavin, M. A., and Rudensky, A. Y. (2003). Foxp3 programs the development and function of CD4+CD25+ regulatory T cells. *Nature Immunology*, 4(4):330–336.
- Geuking, M. B., Cahenzli, J., Lawson, M. A. E., Ng, D. C. K., Slack, E., Hapfelmeier, S., McCoy, K. D., and Macpherson, A. J. (2011). Intestinal Bacterial Colonization Induces Mutualistic Regulatory T Cell Responses. *Immunity*, 34(5):794–806.
- Granja, J. M., Corces, M. R., Pierce, S. E., Bagdatli, S. T., Choudhry, H., Chang, H. Y., and Greenleaf, W. J. (2021). ArchR is a scalable software package for integrative single-cell chromatin accessibility analysis. *Nature Genetics*, 53(3):403–411.
- Granja, J. M., Klemm, S., McGinnis, L. M., Kathiria, A. S., Mezger, A., Corces, M. R., Parks, B., Gars, E., Liedtke, M., Zheng, G. X. Y., Chang, H. Y., Majeti, R., and Greenleaf, W. J. (2019). Single-cell multiomic analysis identifies regulatory programs in mixed-phenotype acute leukemia. *Nature Biotechnology*, 37(12):1458–1465.
- Grossman, W. J., Verbsky, J. W., Tollefsen, B. L., Kemper, C., Atkinson, J. P., and Ley, T. J. (2004). Differential expression of granzymes A and B in human cytotoxic lymphocyte subsets and T regulatory cells. *Blood*, 104(9):2840–2848.
- Gupta, P. K., Godec, J., Wolski, D., Adland, E., Yates, K., Pauken, K. E., Cosgrove, C., Ledderose, C., Junger, W. G., Robson, S. C., Wherry, E. J., Alter, G., Goulder, P. J. R., Klenerman, P., Sharpe, A. H., Lauer, G. M., and Haining, W. N. (2015). CD39 Expression Identifies Terminally Exhausted CD8+ T Cells. *PLoS pathogens*, 11(10):e1005177.
- Han, J. W. and Yoon, S. K. (2020). Tissue-Resident Lymphocytes: Implications in Immunotherapy for Hepatocellular Carcinoma. *International Journal of Molecular Sciences*, 22(1):232.
- Han, S.-J., Glatman Zaretsky, A., Andrade-Oliveira, V., Collins, N., Dzutsev, A., Shaik, J., Morais da Fonseca, D., Harrison, O. J., Tamoutounour, S., Byrd, A. L., Smelkinson, M., Bouladoux, N., Bliska, J. B., Brenchley, J. M., Brodsky, I. E., and Belkaid, Y. (2017). White Adipose Tissue Is a Reservoir for Memory T Cells and Promotes Protective Memory Responses to Infection. *Immunity*, 47(6):1154–1168.e6.
- Han, X., Wang, R., Zhou, Y., Fei, L., Sun, H., Lai, S., Saadatpour, A., Zhou, Z., Chen, H., Ye, F., Huang, D., Xu, Y., Huang, W., Jiang, M., Jiang, X., Mao, J., Chen, Y., Lu, C., Xie, J., Fang, Q., Wang, Y., Yue, R., Li, T., Huang, H., Orkin, S. H., Yuan, G.-C., Chen, M., and Guo, G. (2018). Mapping the Mouse Cell Atlas by Microwell-Seq. *Cell*, 172(5):1091–1107.e17.
- Hay, S. B., Ferchen, K., Chetal, K., Grimes, H. L., and Salomonis, N. (2018). The Human Cell Atlas bone marrow single-cell interactive web portal. *Experimental Hematology*, 68:51–61.
- Hayatsu, N., Miyao, T., Tachibana, M., Murakami, R., Kimura, A., Kato, T., Kawakami, E., Endo, T. A., Setoguchi, R., Watarai, H., Nishikawa, T., Yasuda, T., Yoshida, H., and Hori, S. (2017). Analyses of a Mutant Foxp3 Allele Reveal BATF as a Critical Transcription Factor in the Differentiation and Accumulation of Tissue Regulatory T Cells. *Immunity*, 47(2):268–283.e9.
- Hayward, S. L., Scharer, C. D., Cartwright, E. K., Takamura, S., Li, Z.-R. T., Boss, J. M., and Kohlmeier, J. E. (2020). Environmental cues regulate epigenetic reprogramming of airway-resident memory CD8+ T cells. *Nature Immunology*, 21(3):309–320.

- Heinz, S., Benner, C., Spann, N., Bertolino, E., Lin, Y. C., Laslo, P., Cheng, J. X., Murre, C., Singh, H., and Glass, C. K. (2010). Simple Combinations of Lineage-Determining Transcription Factors Prime cis-Regulatory Elements Required for Macrophage and B Cell Identities. *Molecular Cell*, 38(4):576–589.
- Heng, T. S. P., Painter, M. W., and Immunological Genome Project Consortium (2008). The Immunological Genome Project: networks of gene expression in immune cells. *Nature Immunology*, 9(10):1091–1094.
- Hill, J. A., Feuerer, M., Tash, K., Haxhinasto, S., Perez, J., Melamed, R., Mathis, D., and Benoist, C. (2007). Foxp3 transcription-factor-dependent and -independent regulation of the regulatory T cell transcriptional signature. *Immunity*, 27(5):786–800.
- Himmel, M. E., MacDonald, K. G., Garcia, R. V., Steiner, T. S., and Levings, M. K. (2013). Helios+ and Helios- cells coexist within the natural FOXP3+ T regulatory cell subset in humans. *Journal of Immunology (Baltimore, Md.: 1950)*, 190(5):2001–2008.
- Hombrink, P., Helbig, C., Backer, R. A., Piet, B., Oja, A. E., Stark, R., Brassler, G., Jongejan, A., Jonkers, R. E., Nota, B., Basak, O., Clevers, H. C., Moerland, P. D., Amsen, D., and van Lier, R. A. W. (2016). Programs for the persistence, vigilance and control of human CD8+ lung-resident memory T cells. *Nature Immunology*, 17(12):1467–1478.
- Hori, S., Nomura, T., and Sakaguchi, S. (2003). Control of regulatory T cell development by the transcription factor Foxp3. *Science (New York, N.Y.)*, 299(5609):1057–1061.
- Hosseini, H., Obradović, M. M. S., Hoffmann, M., Harper, K. L., Sosa, M. S., Werner-Klein, M., Nanduri, L. K., Werno, C., Ehrlich, C., Maneck, M., Patwary, N., Haunschild, G., Gužvić, M., Reimelt, C., Grauvogl, M., Eichner, N., Weber, F., Hartkopf, A. D., Taran, F.-A., Brucker, S. Y., Fehm, T., Rack, B., Buchholz, S., Spang, R., Meister, G., Aguirre-Ghiso, J. A., and Klein, C. A. (2016). Early dissemination seeds metastasis in breast cancer. *Nature*, 540(7634):552–558.
- Hu, G., Cui, K., Fang, D., Hirose, S., Wang, X., Wangsa, D., Jin, W., Ried, T., Liu, P., Zhu, J., Rothenberg, E. V., and Zhao, K. (2018). Transformation of Accessible Chromatin and 3D Nucleome Underlies Lineage Commitment of Early T Cells. *Immunity*, 48(2):227–242.e8.
- Huehn, J., Polansky, J. K., and Hamann, A. (2009). Epigenetic control of FOXP3 expression: the key to a stable regulatory T-cell lineage? *Nature Reviews Immunology*, 9(2):83–89.
- Hwang, B., Lee, J. H., and Bang, D. (2018). Single-cell RNA sequencing technologies and bioinformatics pipelines. *Experimental & Molecular Medicine*, 50(8):1–14.
- Hwang, J.-R., Byeon, Y., Kim, D., and Park, S.-G. (2020). Recent insights of T cell receptor-mediated signaling pathways for T cell activation and development. *Experimental & Molecular Medicine*, 52(5):750–761.
- Ise, W., Kohyama, M., Schraml, B. U., Zhang, T., Schwer, B., Basu, U., Alt, F. W., Tang, J., Oltz, E. M., Murphy, T. L., and Murphy, K. M. (2011). The transcription factor BATF controls the global regulators of class-switch recombination in both B cells and T cells. *Nature Immunology*, 12(6):536–543.
- Janson, P. C. J., Winerdal, M. E., Marits, P., Thörn, M., Ohlsson, R., and Winqvist, O. (2008). FOXP3 Promoter Demethylation Reveals the Committed Treg Population in Humans. *PLoS ONE*, 3(2):e1612.
- Johnson, J. L., Georgakilas, G., Petrovic, J., Kurachi, M., Cai, S., Harly, C., Pear, W. S., Bhandoola, A., Wherry, E. J., and Vahedi, G. (2018). Lineage-Determining Transcription Factor TCF-1 Initiates the Epigenetic Identity of T Cells. *Immunity*, 48(2):243–257.e10.
- Johnston, A., Gudjonsson, J. E., Aphale, A., Guzman, A. M., Stoll, S. W., and Elder, J. T. (2011). EGFR and IL-1 Signaling Synergistically Promote Keratinocyte Antimicrobial Defenses in a Differentiation-Dependent Manner. *Journal of Investigative Dermatology*, 131(2):329–337.
- Kay, A. B. (2000). Overview of ‘Allergy and allergic diseases: with a view to the future’. *British Medical Bulletin*, 56(4):843–864.
- Kharchenko, P. V. (2021). The triumphs and limitations of computational methods for scRNA-seq. *Nature Methods*, 18(7):723–732.
- Kidani, Y., Nogami, W., Yasumizu, Y., Kawashima, A., Tanaka, A., Sonoda, Y., Tona, Y., Nashiki, K., Matsumoto, R., Hagiwara, M., Osaki, M., Dohi, K., Kanazawa, T., Ueyama, A., Yoshikawa, M., Yoshida, T., Matsumoto, M., Hojo, K., Shinonome, S., Yoshida, H., Hirata, M., Haruna, M., Nakamura, Y., Motooka, D., Okuzaki, D., Sugiyama, Y., Kinoshita, M., Okuno, T., Kato, T., Hatano, K., Uemura, M., Imamura, R., Yokoi, K., Tanemura, A., Shintani, Y., Kimura, T., Nonomura, N., Wada, H., Mori, M., Doki, Y., Ohkura, N., and Sakaguchi, S. (2022). CCR8-targeted specific depletion

- of clonally expanded Treg cells in tumor tissues evokes potent tumor immunity with long-lasting memory. *Proceedings of the National Academy of Sciences*, 119(7).
- Kim, J. M., Rasmussen, J. P., and Rudensky, A. Y. (2007). Regulatory T cells prevent catastrophic autoimmunity throughout the lifespan of mice. *Nature Immunology*, 8(2):191–197.
- King, K. Y. and Goodell, M. A. (2011). Inflammatory modulation of HSCs: viewing the HSC as a foundation for the immune response. *Nature Reviews Immunology*, 11(10):685–692.
- Klemm, S. L., Shipony, Z., and Greenleaf, W. J. (2019). Chromatin accessibility and the regulatory epigenome. *Nature Reviews Genetics*, 20(4):207–220.
- Koch, U. and Radtke, F. (2011). Mechanisms of T Cell Development and Transformation. *Annual Review of Cell and Developmental Biology*, 27(1):539–562.
- Kok, L., Dijkgraaf, F. E., Urbanus, J., Bresser, K., Vredevoogd, D. W., Cardoso, R. F., Perić, L., Beltman, J. B., and Schumacher, T. N. (2020). A committed tissue-resident memory T cell precursor within the circulating CD8⁺ effector T cell pool. *The Journal of Experimental Medicine*, 217(10):e20191711.
- Kok, L., Masopust, D., and Schumacher, T. N. (2021). The precursors of CD8⁺ tissue resident memory T cells: from lymphoid organs to infected tissues. *Nature Reviews Immunology*, pages 1–11.
- Kolodin, D., van Panhuys, N., Li, C., Magnuson, A. M., Cipolletta, D., Miller, C. M., Wagers, A., Germain, R. N., Benoist, C., and Mathis, D. (2015). Antigen- and cytokine-driven accumulation of regulatory T cells in visceral adipose tissue of lean mice. *Cell Metabolism*, 21(4):543–557.
- Korsunsky, I., Millard, N., Fan, J., Slowikowski, K., Zhang, F., Wei, K., Baglaenko, Y., Brenner, M., Loh, P.-r., and Raychaudhuri, S. (2019). Fast, sensitive and accurate integration of single-cell data with Harmony. *Nature Methods*, 16(12):1289–1296.
- Kronenberg, M. and Rudensky, A. (2005). Regulation of immunity by self-reactive T cells. *Nature*, 435(7042):598–604.
- Kuhn, R. M., Haussler, D., and Kent, W. J. (2013). The UCSC genome browser and associated tools. *Briefings in Bioinformatics*, 14(2):144–161.
- Kumar, B. V., Connors, T. J., and Farber, D. L. (2018). Human T Cell Development, Localization, and Function throughout Life. *Immunity*, 48(2):202–213.
- Kumar, B. V., Ma, W., Miron, M., Granot, T., Guyer, R. S., Carpenter, D. J., Senda, T., Sun, X., Ho, S.-H., Lerner, H., Friedman, A. L., Shen, Y., and Farber, D. L. (2017). Human Tissue-Resident Memory T Cells Are Defined by Core Transcriptional and Functional Signatures in Lymphoid and Mucosal Sites. *Cell Reports*, 20(12):2921–2934.
- Kurachi, M., Barnitz, R. A., Yosef, N., Odorizzi, P. M., DiIorio, M. A., Lemieux, M. E., Yates, K., Godec, J., Klatt, M. G., Regev, A., Wherry, E. J., and Haining, W. N. (2014). The transcription factor BATF operates as an essential differentiation checkpoint in early effector CD8⁺ T cells. *Nature Immunology*, 15(4):373–383.
- La Manno, G., Soldatov, R., Zeisel, A., Braun, E., Hochgerner, H., Petukhov, V., Lidschreiber, K., Kastrioti, M. E., Lönnerberg, P., Furlan, A., Fan, J., Borm, L. E., Liu, Z., van Bruggen, D., Guo, J., He, X., Barker, R., Sundström, E., Castelo-Branco, G., Cramer, P., Adameyko, I., Linnarsson, S., and Kharchenko, P. V. (2018). RNA velocity of single cells. *Nature*, 560(7719):494–498.
- Lanier, L. L. (2005). NK cell recognition. *Annual Review of Immunology*, 23:225–274.
- Lee, W. and Lee, G. R. (2018). Transcriptional regulation and development of regulatory T cells. *Experimental & Molecular Medicine*, 50(3):e456–e456.
- Leenaars, C. H. C., Kouwenaar, C., Staffleu, F. R., Bleich, A., Ritskes-Hoitinga, M., De Vries, R. B. M., and Meijboom, F. L. B. (2019). Animal to human translation: a systematic scoping review of reported concordance rates. *Journal of Translational Medicine*, 17(1):223.
- Li, C., DiSpirito, J. R., Zemmour, D., Spallanzani, R. G., Kuswanto, W., Benoist, C., and Mathis, D. (2018). TCR Transgenic Mice Reveal Stepwise, Multi-site Acquisition of the Distinctive Fat-Treg Phenotype. *Cell*, 174(2):285–299.e12.
- Li, H., Handsaker, B., Wysoker, A., Fennell, T., Ruan, J., Homer, N., Marth, G., Abecasis, G., and Durbin, R. (2009). The Sequence Alignment/Map format and SAMtools. *Bioinformatics*, 25(16):2078–2079.

- Li, H., van der Leun, A. M., Yofe, I., Lubling, Y., Gelbard-Solodkin, D., van Akkooi, A. C., van den Braber, M., Rozeman, E. A., Haanen, J. B., Blank, C. U., Horlings, H. M., David, E., Baran, Y., Bercovich, A., Lifshitz, A., Schumacher, T. N., Tanay, A., and Amit, I. (2019a). Dysfunctional CD8 T Cells Form a Proliferative, Dynamically Regulated Compartment within Human Melanoma. *Cell*, 176(4):775–789.e18.
- Li, X., Li, D., Shi, Q., Huang, X., and Ju, X. (2019b). Umbilical cord blood-derived Helios-positive regulatory T cells promote angiogenesis in acute lymphoblastic leukemia in mice via CCL22 and the VEGFA-VEGFR2 pathway. *Molecular Medicine Reports*, 19(5):4195–4204.
- Liang, B., Workman, C., Lee, J., Chew, C., Dale, B. M., Colonna, L., Flores, M., Li, N., Schweighoffer, E., Greenberg, S., Tybulewicz, V., Vignali, D., and Clynes, R. (2008). Regulatory T Cells Inhibit Dendritic Cells by Lymphocyte Activation Gene-3 Engagement of MHC Class II. *The Journal of Immunology*, 180(9):5916–5926.
- Liang, C., Yang, K. Y., Chan, V. W., Li, X., Fung, T. H., Wu, Y., Tian, X. Y., Huang, Y., Qin, L., Lau, J. Y., and Lui, K. O. (2020). CD8+ T-cell plasticity regulates vascular regeneration in type-2 diabetes. *Theranostics*, 10(9):4217–4232.
- Linehan, J. L., Harrison, O. J., Han, S.-J., Byrd, A. L., Vujkovic-Cvijin, I., Villarino, A. V., Sen, S. K., Shaik, J., Smelkinson, M., Tamoutounour, S., Collins, N., Bouladoux, N., Dzutsev, A., Rosshart, S. P., Arbuckle, J. H., Wang, C.-R., Kristie, T. M., Rehermann, B., Trinchieri, G., Brenchley, J. M., O’Shea, J. J., and Belkaid, Y. (2018). Non-classical Immunity Controls Microbiota Impact on Skin Immunity and Tissue Repair. *Cell*, 172(4):784–796.e18.
- Liu, J., Chen, D., Nie, G. D., and Dai, Z. (2015). CD8+CD122+ T-Cells: A Newly Emerging Regulator with Central Memory Cell Phenotypes. *Frontiers in Immunology*, 6.
- Love, M. I., Huber, W., and Anders, S. (2014). Moderated estimation of fold change and dispersion for RNA-seq data with DESeq2. *Genome Biology*.
- Luger, K., Mäder, A. W., Richmond, R. K., Sargent, D. F., and Richmond, T. J. (1997). Crystal structure of the nucleosome core particle at 2.8 Å resolution. *Nature*, 389(6648):251–260.
- Lumeng, C. N., Bodzin, J. L., and Saltiel, A. R. (2007). Obesity induces a phenotypic switch in adipose tissue macrophage polarization. *The Journal of Clinical Investigation*, 117(1):175–184.
- Ma, S., Zhang, B., LaFave, L. M., Earl, A. S., Chiang, Z., Hu, Y., Ding, J., Brack, A., Kartha, V. K., Tay, T., Law, T., Lareau, C., Hsu, Y.-C., Regev, A., and Buenrostro, J. D. (2020). Chromatin Potential Identified by Shared Single-Cell Profiling of RNA and Chromatin. *Cell*, 183(4):1103–1116.e20.
- Manz, M. G., Traver, D., Miyamoto, T., Weissman, I. L., and Akashi, K. (2001). Dendritic cell potentials of early lymphoid and myeloid progenitors. *Blood*, 97(11):3333–3341.
- Marshall, J. S., Warrington, R., Watson, W., and Kim, H. L. (2018). An introduction to immunology and immunopathology. *Allergy, Asthma & Clinical Immunology*, 14(S2):49.
- Mauri, C. and Bosma, A. (2012). Immune Regulatory Function of B Cells. *Annual Review of Immunology*, 30(1):221–241.
- McInnes, L., Healy, J., and Melville, J. (2018). UMAP: Uniform Manifold Approximation and Projection for Dimension Reduction. *arXiv:1802.03426 [cs, stat]*.
- McLean, C. Y., Bristor, D., Hiller, M., Clarke, S. L., Schaar, B. T., Lowe, C. B., Wenger, A. M., and Bejerano, G. (2010). GREAT improves functional interpretation of cis-regulatory regions. *Nature Biotechnology*, 28(5):495–501.
- Medzhitov, R. (2009). Approaching the Asymptote: 20 Years Later. *Immunity*, 30(6):766–775.
- Medzhitov, R. and Janeway, C. (2000). Innate immune recognition: mechanisms and pathways. *Immunological Reviews*, 173:89–97.
- Mellor, J. (2005). The Dynamics of Chromatin Remodeling at Promoters. *Molecular Cell*, 19(2):147–157.
- Meng, C., Liu, G., Mu, H., Zhou, M., Zhang, S., and Xu, Y. (2015). Amphiregulin may be a new biomarker of classically activated macrophages. *Biochemical and Biophysical Research Communications*, 466(3):393–399.
- Miao, Y.-R., Zhang, Q., Lei, Q., Luo, M., Xie, G.-Y., Wang, H., and Guo, A.-Y. (2020). ImmuCellAI: A Unique Method for Comprehensive T-Cell Subsets Abundance Prediction and its Application in Cancer Immunotherapy. *Advanced Science*, 7(7):1902880.
- Mijnheer, G., Lutter, L., Mokry, M., van der Wal, M., Scholman, R., Fleskens, V., Pandit, A., Tao, W., Wekking, M., Vervoort, S., Roberts, C., Petrelli, A., Peeters, J. G. C., Knijff, M., de Roock, S., Vastert, S., Taams, L. S., van

- Loosdregt, J., and van Wijk, F. (2021). Conserved human effector Treg cell transcriptomic and epigenetic signature in arthritic joint inflammation. *Nature Communications*, 12(1):2710.
- Miragaia, R. J., Gomes, T., Chomka, A., Jardine, L., Riedel, A., Hegazy, A. N., Whibley, N., Tucci, A., Chen, X., Lindeman, I., Emerton, G., Krausgruber, T., Shields, J., Haniffa, M., Powrie, F., and Teichmann, S. A. (2019). Single-Cell Transcriptomics of Regulatory T Cells Reveals Trajectories of Tissue Adaptation. *Immunity*, 50(2):493–504.e7.
- Mishra, S., Srinivasan, S., Ma, C., and Zhang, N. (2021). CD8+ Regulatory T Cell – A Mystery to Be Revealed. *Frontiers in Immunology*, 12.
- Mocellin, S., Wang, E., and Marincola, F. M. (2001). Cytokines and Immune Response in the Tumor Microenvironment. *Journal of Immunotherapy*, 24(5):392–407.
- Monaco, G., Lee, B., Xu, W., Mustafah, S., Hwang, Y. Y., Carré, C., Burdin, N., Visan, L., Ceccarelli, M., Poidinger, M., Zippelius, A., Pedro de Magalhães, J., and Larbi, A. (2019). RNA-Seq Signatures Normalized by mRNA Abundance Allow Absolute Deconvolution of Human Immune Cell Types. *Cell Reports*, 26(6):1627–1640.e7.
- Murphy, K. and Weaver, C. (2018). *Janeway Immunobiologie*. Springer Spektrum, Berlin, Germany.
- Murphy, T. L., Tussiwand, R., and Murphy, K. M. (2013). Specificity through cooperation: BATF–IRF interactions control immune-regulatory networks. *Nature Reviews Immunology*, 13(7):499–509.
- Murray, P. J. and Wynn, T. A. (2011). Protective and pathogenic functions of macrophage subsets. *Nature Reviews Immunology*, 11(11):723–737.
- Neel, J.-C., Humbert, L., and Lebrun, J.-J. (2012). The Dual Role of TGF β in Human Cancer: From Tumor Suppression to Cancer Metastasis. *ISRN Molecular Biology*, 2012:e381428.
- Netea, M. G., Domínguez-Andrés, J., Barreiro, L. B., Chavakis, T., Divangahi, M., Fuchs, E., Joosten, L. A. B., van der Meer, J. W. M., Mhlanga, M. M., Mulder, W. J. M., Riksen, N. P., Schlitzer, A., Schultze, J. L., Stabel Benn, C., Sun, J. C., Xavier, R. J., and Latz, E. (2020). Defining trained immunity and its role in health and disease. *Nature Reviews Immunology*, 20(6):375–388.
- Nguyen, A. V. and Soulika, A. M. (2019). The Dynamics of the Skin’s Immune System. *International Journal of Molecular Sciences*, 20(8):1811.
- Niederlova, V., Tsyklauri, O., Chadimova, T., and Stepanek, O. (2021). CD8+ Tregs revisited: A heterogeneous population with different phenotypes and properties. *European Journal of Immunology*, 51(3):512–530.
- Nurieva, R. I., Chung, Y., Martinez, G. J., Yang, X. O., Tanaka, S., Matskevitch, T. D., Wang, Y.-H., and Dong, C. (2009). Bcl6 mediates the development of T follicular helper cells. *Science (New York, N.Y.)*, 325(5943):1001–1005.
- Odegaard, J. I., Ricardo-Gonzalez, R. R., Goforth, M. H., Morel, C. R., Subramanian, V., Mukundan, L., Red Eagle, A., Vats, D., Brombacher, F., Ferrante, A. W., and Chawla, A. (2007). Macrophage-specific PPAR γ controls alternative activation and improves insulin resistance. *Nature*, 447(7148):1116–1120.
- Ohkura, N., Hamaguchi, M., Morikawa, H., Sugimura, K., Tanaka, A., Ito, Y., Osaki, M., Tanaka, Y., Yamashita, R., Nakano, N., Huehn, J., Fehling, H. J., Sparwasser, T., Nakai, K., and Sakaguchi, S. (2012). T Cell Receptor Stimulation-Induced Epigenetic Changes and Foxp3 Expression Are Independent and Complementary Events Required for Treg Cell Development. *Immunity*, 37(5):785–799.
- Ohkura, N., Kitagawa, Y., and Sakaguchi, S. (2013). Development and Maintenance of Regulatory T cells. *Immunity*, 38(3):414–423.
- Ohkura, N. and Sakaguchi, S. (2020). Transcriptional and epigenetic basis of Treg cell development and function: its genetic anomalies or variations in autoimmune diseases. *Cell Research*, 30(6):465–474.
- Orkin, S. H. and Zon, L. I. (2008). Hematopoiesis: An Evolving Paradigm for Stem Cell Biology. *Cell*, 132(4):631–644.
- Oshi, M., Asaoka, M., Tokumaru, Y., Yan, L., Matsuyama, R., Ishikawa, T., Endo, I., and Takabe, K. (2020). CD8 T Cell Score as a Prognostic Biomarker for Triple Negative Breast Cancer. *International Journal of Molecular Sciences*, 21(18):E6968.
- Ostroumov, D., Duong, S., Wingerath, J., Woller, N., Manns, M. P., Timrott, K., Kleine, M., Ramackers, W., Roessler, S., Nahnsen, S., Immunoglobulin And Immunoreceptor tyrosiCzettel, n., Dittrich-Breiholz, O., Eggert, T., Kühnel, F.,

- and Wirth, T. C. (2021). Transcriptome Profiling Identifies TIGIT as a Marker of T-Cell Exhaustion in Liver Cancer. *Hepatology (Baltimore, Md.)*, 73(4):1399–1418.
- Pfister, D., Núñez, N. G., Pinyol, R., Govaere, O., Pinter, M., Szydlowska, M., Gupta, R., Qiu, M., Deczkowska, A., Weiner, A., Müller, F., Sinha, A., Friebel, E., Engleitner, T., Lenggenhager, D., Moncsek, A., Heide, D., Stirn, K., Kosla, J., Kotsiliti, E., Leone, V., Dudek, M., Yousuf, S., Inverso, D., Singh, I., Teijeiro, A., Castet, F., Montironi, C., Haber, P. K., Tiniakos, D., Bedossa, P., Cockell, S., Younes, R., Vacca, M., Marra, F., Schattenberg, J. M., Allison, M., Bugianesi, E., Ratziu, V., Pressiani, T., D'Alessio, A., Personeni, N., Rimassa, L., Daly, A. K., Scheiner, B., Pomej, K., Kirstein, M. M., Vogel, A., Peck-Radosavljevic, M., Hucke, F., Finkelmeier, F., Waidmann, O., Trojan, J., Schulze, K., Wege, H., Koch, S., Weinmann, A., Bueter, M., Rössler, F., Siebenhüner, A., De Dosso, S., Mallm, J.-P., Umansky, V., Jugold, M., Luedde, T., Schietinger, A., Schirmacher, P., Emu, B., Augustin, H. G., Billeter, A., Müller-Stich, B., Kikuchi, H., Duda, D. G., Kütting, F., Waldschmidt, D.-T., Ebert, M. P., Rahbari, N., Mei, H. E., Schulz, A. R., Ringelhan, M., Malek, N., Spahn, S., Bitzer, M., Ruiz de Galarreta, M., Lujambio, A., Dufour, J.-F., Marron, T. U., Kaseb, A., Kudo, M., Huang, Y.-H., Djouder, N., Wolter, K., Zender, L., Marche, P. N., Decaens, T., Pinato, D. J., Rad, R., Mertens, J. C., Weber, A., Unger, K., Meissner, F., Roth, S., Jilkova, Z. M., Claassen, M., Anstee, Q. M., Amit, I., Knolle, P., Becher, B., Llovet, J. M., and Heikenwalder, M. (2021). NASH limits anti-tumour surveillance in immunotherapy-treated HCC. *Nature*, 592(7854):450–456.
- Pham, D., Moseley, C. E., Gao, M., Savic, D., Winstead, C. J., Sun, M., Kee, B. L., Myers, R. M., Weaver, C. T., and Hatton, R. D. (2019). Batf Pioneers the Reorganization of Chromatin in Developing Effector T Cells via Ets1-Dependent Recruitment of Ctcf. *Cell Reports*, 29(5):1203–1220.e7.
- Philip, M. and Schietinger, A. (2021). CD8+ T cell differentiation and dysfunction in cancer. *Nature Reviews Immunology*, pages 1–15.
- Piconese, S., Campello, S., and Natalini, A. (2020). Recirculation and Residency of T Cells and Tregs: Lessons Learnt in Anacapri. *Frontiers in Immunology*, 11.
- Pijuan, J., Barceló, C., Moreno, D. F., Maiques, O., Sisó, P., Marti, R. M., Macià, A., and Panosa, A. (2019). In vitro Cell Migration, Invasion, and Adhesion Assays: From Cell Imaging to Data Analysis. *Frontiers in Cell and Developmental Biology*, 7.
- Pliner, H. A., Packer, J. S., McFaline-Figueroa, J. L., Cusanovich, D. A., Daza, R. M., Aghamirzaie, D., Srivatsan, S., Qiu, X., Jackson, D., Minkina, A., Adey, A. C., Steemers, F. J., Shendure, J., and Trapnell, C. (2018). Cicero Predicts cis-Regulatory DNA Interactions from Single-Cell Chromatin Accessibility Data. *Molecular Cell*, 71(5):858–871.e8.
- Plitas, G., Konopacki, C., Wu, K., Bos, P. D., Morrow, M., Putintseva, E., Chudakov, D., and Rudensky, A. (2016). Regulatory T Cells Exhibit Distinct Features in Human Breast Cancer. *Immunity*, 45(5):1122–1134.
- Pope, B., Ryba, T., Dileep, V., Yue, F., Wu, W., Denas, O., Vera, D., Wang, Y., Hansen, R., Canfield, T., Thurman, R., Cheng, Y., Gülsoy, G., Dennis, J., Snyder, M., Stamatoyannopoulos, J., Taylor, J., Hardison, R., Kahveci, T., Ren, B., and Gilbert, D. (2014). Topologically associating domains are stable units of replication-timing regulation. *Nature*, 515(7527):402–405.
- Povoleri, G. A. M., Nova-Lamperti, E., Scottà, C., Fanelli, G., Chen, Y.-C., Becker, P. D., Boardman, D., Costantini, B., Romano, M., Pavlidis, P., McGregor, R., Pantazi, E., Chauss, D., Sun, H.-W., Shih, H.-Y., Cousins, D. J., Cooper, N., Powell, N., Kemper, C., Pirooznia, M., Laurence, A., Kordasti, S., Kazemian, M., Lombardi, G., and Afzali, B. (2018). Human retinoic acid-regulated CD161+ regulatory T cells support wound repair in intestinal mucosa. *Nature Immunology*, 19(12):1403–1414.
- Pritykin, Y., van der Veecken, J., Pine, A. R., Zhong, Y., Sahin, M., Mazutis, L., Pe'er, D., Rudensky, A. Y., and Leslie, C. S. (2021). A unified atlas of CD8 T cell dysfunctional states in cancer and infection. *Molecular Cell*, 81(11):2477–2493.e10.
- Puram, S. V., Tirosh, I., Parikh, A. S., Patel, A. P., Yizhak, K., Gillespie, S., Rodman, C., Luo, C. L., Mroz, E. A., Emerick, K. S., Deschler, D. G., Varvares, M. A., Mylvaganam, R., Rozenblatt-Rosen, O., Rocco, J. W., Faquin, W. C., Lin, D. T., Regev, A., and Bernstein, B. E. (2017). Single-Cell Transcriptomic Analysis of Primary and Metastatic Tumor Ecosystems in Head and Neck Cancer. *Cell*, 171(7):1611–1624.e24.
- Ramírez, F., Ryan, D. P., Grüning, B., Bhardwaj, V., Kilpert, F., Richter, A. S., Heyne, S., Dündar, F., and Manke, T. (2016). deepTools2: a next generation web server for deep-sequencing data analysis. *Nucleic Acids Research*, 44.
- Rankin, L. C. and Artis, D. (2018). Beyond Host Defense: Emerging Functions of the Immune System in Regulating Complex Tissue Physiology. *Cell*, 173(3):554–567.

- Regev, A., Teichmann, S. A., Lander, E. S., Amit, I., Benoist, C., Birney, E., Bodenmiller, B., Campbell, P., Carninci, P., Clatworthy, M., Clevers, H., Deplancke, B., Dunham, I., Eberwine, J., Eils, R., Enard, W., Farmer, A., Fugger, L., Göttgens, B., Hacohen, N., Haniffa, M., Hemberg, M., Kim, S., Klenerman, P., Kriegstein, A., Lein, E., Linnarsson, S., Lundberg, E., Lundeberg, J., Majumder, P., Marioni, J. C., Merad, M., Mhlanga, M., Nawijn, M., Netea, M., Nolan, G., Pe'er, D., Phillipakis, A., Ponting, C. P., Quake, S., Reik, W., Rozenblatt-Rosen, O., Sanes, J., Satija, R., Schumacher, T. N., Shalek, A., Shapiro, E., Sharma, P., Shin, J. W., Stegle, O., Stratton, M., Stubbington, M. J. T., Theis, F. J., Uhlen, M., van Oudenaarden, A., Wagner, A., Watt, F., Weissman, J., Wold, B., Xavier, R., Yosef, N., and Human Cell Atlas Meeting Participants (2017). The Human Cell Atlas. *eLife*, 6:e27041.
- Richards, D. M., Delacher, M., Goldfarb, Y., Kägebein, D., Hofer, A.-C., Abramson, J., and Feuerer, M. (2015). Treg Cell Differentiation: From Thymus to Peripheral Tissue. In *Progress in Molecular Biology and Translational Science*, volume 136, pages 175–205. Elsevier.
- Riethoven, J.-J. M. (2010). Regulatory regions in DNA: promoters, enhancers, silencers, and insulators. *Methods in Molecular Biology (Clifton, N.J.)*, 674:33–42.
- Rifa'i, M., Kawamoto, Y., Nakashima, I., and Suzuki, H. (2004). Essential Roles of CD8+CD122+ Regulatory T Cells in the Maintenance of T Cell Homeostasis. *The Journal of Experimental Medicine*, 200(9):1123–1134.
- Ross, S. H. and Cantrell, D. A. (2018). Signaling and Function of Interleukin-2 in T Lymphocytes. *Annual Review of Immunology*, 36(1):411–433.
- Sahoo, A., Wali, S., and Nurieva, R. (2016). T helper 2 and T follicular helper cells: Regulation and Function of Interleukin-4. *Cytokine & growth factor reviews*, 30:29–37.
- Sakaguchi, S., Sakaguchi, N., Asano, M., Itoh, M., and Toda, M. (1995). Immunologic self-tolerance maintained by activated T cells expressing IL-2 receptor alpha-chains (CD25). Breakdown of a single mechanism of self-tolerance causes various autoimmune diseases. *Journal of Immunology (Baltimore, Md.: 1950)*, 155(3):1151–1164.
- Sakaguchi, S., Yamaguchi, T., Nomura, T., and Ono, M. (2008). Regulatory T Cells and Immune Tolerance. *Cell*, 133(5):775–787.
- Sasson, S. C., Gordon, C. L., Christo, S. N., Klenerman, P., and Mackay, L. K. (2020). Local heroes or villains: tissue-resident memory T cells in human health and disease. *Cellular & Molecular Immunology*, 17(2):113–122.
- Sato, T., Terai, M., Tamura, Y., Alexeev, V., Mastrangelo, M. J., and Selvan, S. R. (2011). Interleukin 10 in the tumor microenvironment: a target for anticancer immunotherapy. *Immunologic Research*, 51(2-3):170–182.
- Satpathy, A. T. (2019). Massively parallel single-cell chromatin landscapes of human immune cell development and intra-tumoral T cell exhaustion. *Nature Biotechnology*, 37:20.
- Sawa, S., Lochner, M., Satoh-Takayama, N., Dulauroy, S., Bérard, M., Kleinschek, M., Cua, D., Di Santo, J. P., and Eberl, G. (2011). RORγt+ innate lymphoid cells regulate intestinal homeostasis by integrating negative signals from the symbiotic microbiota. *Nature Immunology*, 12(4):320–326.
- Schep, A. N., Wu, B., Buenrostro, J. D., and Greenleaf, W. J. (2017). chromVAR: inferring transcription-factor-associated accessibility from single-cell epigenomic data. *Nature Methods*, 14(10):975–978.
- Schmidl, C., Delacher, M., Huehn, J., and Feuerer, M. (2018). Epigenetic mechanisms regulating T-cell responses. *Journal of Allergy and Clinical Immunology*, 142(3):728–743.
- Schraml, B. U., Hildner, K., Ise, W., Lee, W.-L., Smith, W. A.-E., Solomon, B., Sahota, G., Sim, J., Mukasa, R., Cemerski, S., Hatton, R. D., Stormo, G. D., Weaver, C. T., Russell, J. H., Murphy, T. L., and Murphy, K. M. (2009). The AP-1 transcription factor Batf controls T(H)17 differentiation. *Nature*, 460(7253):405–409.
- Schøller, A. S., Nazerai, L., Christensen, J. P., and Thomsen, A. R. (2021). Functionally Competent, PD-1+ CD8+ Trm Cells Populate the Brain Following Local Antigen Encounter. *Frontiers in Immunology*, 11.
- Scott, A. C., Dündar, F., Zumbo, P., Chandran, S. S., Klebanoff, C. A., Shakiba, M., Trivedi, P., Menocal, L., Appleby, H., Camara, S., Zamarin, D., Walther, T., Snyder, A., Femia, M. R., Comen, E. A., Wen, H. Y., Hellmann, M. D., Anandasabapathy, N., Liu, Y., Altorki, N. K., Lauer, P., Levy, O., Glickman, M. S., Kaye, J., Betel, D., Philip, M., and Schietinger, A. (2019). TOX is a critical regulator of tumour-specific T cell differentiation. *Nature*, 571(7764):270–274.
- Scott, E. N., Gocher, A. M., Workman, C. J., and Vignali, D. A. A. (2021). Regulatory T Cells: Barriers of Immune Infiltration Into the Tumor Microenvironment. *Frontiers in Immunology*, 12:2282.

- Sefik, E., Geva-Zatorsky, N., Oh, S., Konnikova, L., Zemmour, D., McGuire, A. M., Burzyn, D., Ortiz-Lopez, A., Lobera, M., Yang, J., Ghosh, S., Earl, A., Snapper, S. B., Jupp, R., Kasper, D., Mathis, D., and Benoist, C. (2015). Individual intestinal symbionts induce a distinct population of RORgamma+ regulatory T cells. *Science (New York, N.Y.)*, 349(6251):993–997.
- Seita, J. and Weissman, I. L. (2010). Hematopoietic stem cell: self-renewal versus differentiation. *WIREs Systems Biology and Medicine*, 2(6):640–653.
- Serwold, T., Ehrlich, L. I. R., and Weissman, I. L. (2009). Reductive isolation from bone marrow and blood implicates common lymphoid progenitors as the major source of thymopoiesis. *Blood*, 113(4):807–815.
- Sharma, S., Kelly, T. K., and Jones, P. A. (2010). Epigenetics in cancer. *Carcinogenesis*, 31(1):27–36.
- Shevach, E. M. and Thornton, A. M. (2014). tTregs, pTregs, and iTregs: Similarities and Differences. *Immunological reviews*, 259(1):88–102.
- Shi, Z., Okuno, Y., Rifa'i, M., Endharti, A. T., Akane, K., Isobe, K.-I., and Suzuki, H. (2009). Human CD8+CXCR3+ T cells have the same function as murine CD8+CD122+ Treg. *European Journal of Immunology*, 39(8):2106–2119.
- Shimizu, J., Yamazaki, S., and Sakaguchi, S. (1999). Induction of tumor immunity by removing CD25+CD4+ T cells: a common basis between tumor immunity and autoimmunity. *Journal of Immunology (Baltimore, Md.: 1950)*, 163(10):5211–5218.
- Shimokawa, C., Kato, T., Takeuchi, T., Ohshima, N., Furuki, T., Ohtsu, Y., Suzue, K., Imai, T., Obi, S., Ochiai, A., Izumi, T., Sakurai, M., Arakawa, H., Ohno, H., and Hisaeda, H. (2020). CD8+ regulatory T cells are critical in prevention of autoimmune-mediated diabetes. *Nature Communications*, 11(1):1922.
- Sicherman, J., Newton, D. F., Pavlidis, P., Sibille, E., and Tripathy, S. J. (2021). Estimating and Correcting for Off-Target Cellular Contamination in Brain Cell Type Specific RNA-Seq Data. *Frontiers in Molecular Neuroscience*, 14.
- Singh, S. K., Mishra, M. K., Eltoum, I.-E. A., Bae, S., Lillard, J. W., and Singh, R. (2018). CCR5/CCL5 axis interaction promotes migratory and invasiveness of pancreatic cancer cells. *Scientific Reports*, 8(1):1323.
- Smith, T. R. F. and Kumar, V. (2008). Revival of CD8+ Treg-mediated suppression. *Trends in Immunology*, 29(7):337–342.
- Soler, D., Chapman, T. R., Poisson, L. R., Wang, L., Cote-Sierra, J., Ryan, M., McDonald, A., Badola, S., Fedyk, E., Coyle, A. J., Hodge, M. R., and Kolbeck, R. (2006). CCR8 Expression Identifies CD4 Memory T Cells Enriched for FOXP3⁺ Regulatory and Th2 Effector Lymphocytes. *The Journal of Immunology*, 177(10):6940–6951.
- Stabile, E., Kinnaird, T., la Sala, A., Hanson, S. K., Watkins, C., Campia, U., Shou, M., Zbinden, S., Fuchs, S., Kornfeld, H., Epstein, S. E., and Burnett, M. S. (2006). CD8+ T Lymphocytes Regulate the Arteriogenic Response to Ischemia by Infiltrating the Site of Collateral Vessel Development and Recruiting CD4+ Mononuclear Cells Through the Expression of Interleukin-16. *Circulation*, 113(1):118–124.
- Starks, R. R., Biswas, A., Jain, A., and Tuteja, G. (2019). Combined analysis of dissimilar promoter accessibility and gene expression profiles identifies tissue-specific genes and actively repressed networks. *Epigenetics & Chromatin*, 12(1):16.
- Stuart, T., Butler, A., Hoffman, P., Hafemeister, C., Papalexi, E., Mauck, W. M., Hao, Y., Stoeckius, M., Smibert, P., and Satija, R. (2019). Comprehensive Integration of Single-Cell Data. *Cell*, 177(7):1888–1902.e21.
- Stuart, T., Srivastava, A., Madad, S., Lareau, C. A., and Satija, R. (2021). Single-cell chromatin state analysis with Signac. *Nature Methods*, 18(11):1333–1341.
- Szabo, P. A., Levitin, H. M., Miron, M., Snyder, M. E., Senda, T., Yuan, J., Cheng, Y. L., Bush, E. C., Dogra, P., Thapa, P., Farber, D. L., and Sims, P. A. (2019). Single-cell transcriptomics of human T cells reveals tissue and activation signatures in health and disease. *Nature Communications*, 10(1):4706.
- Tanaka, A. and Sakaguchi, S. (2017). Regulatory T cells in cancer immunotherapy. *Cell Research*, 27(1):109–118.
- Tang, F., Barbacioru, C., Wang, Y., Nordman, E., Lee, C., Xu, N., Wang, X., Bodeau, J., Tuch, B. B., Siddiqui, A., Lao, K., and Surani, M. A. (2009). mRNA-Seq whole-transcriptome analysis of a single cell. *Nature Methods*, 6(5):377–382.
- The Tabula Muris Consortium, Overall coordination, Logistical coordination, Organ collection and processing, Library preparation and sequencing, Computational data analysis, Cell type annotation, Writing group, Supplemental text writing group, and Principal investigators (2018). Single-cell transcriptomics of 20 mouse organs creates a Tabula Muris. *Nature*, 562(7727):367–372.

- Thome, J. J. C., Yudanin, N., Ohmura, Y., Kubota, M., Grinshpun, B., Sathaliyawala, T., Kato, T., Lerner, H., Shen, Y., and Farber, D. L. (2014). Spatial Map of Human T Cell Compartmentalization and Maintenance over Decades of Life. *Cell*, 159(4):814–828.
- Thommen, D. S. and Schumacher, T. N. (2018). T Cell Dysfunction in Cancer. *Cancer Cell*, 33(4):547–562.
- Thornton, A. M., Korty, P. E., Tran, D. Q., Wohlfert, E. A., Murray, P. E., Belkaid, Y., and Shevach, E. M. (2010). Expression of Helios, an Ikaros transcription factor family member, differentiates thymic-derived from peripherally induced Foxp3+ T regulatory cells. *Journal of Immunology (Baltimore, Md.: 1950)*, 184(7):3433–3441.
- Tindemans, I., Serafini, N., Di Santo, J. P., and Hendriks, R. W. (2014). GATA-3 Function in Innate and Adaptive Immunity. *Immunity*, 41(2):191–206.
- Togashi, Y., Shitara, K., and Nishikawa, H. (2019). Regulatory T cells in cancer immunosuppression — implications for anticancer therapy. *Nature Reviews Clinical Oncology*, 16(6):356–371.
- Trapnell, C., Cacchiarelli, D., Grimsby, J., Pokharel, P., Li, S., Morse, M., Lennon, N. J., Livak, K. J., Mikkelsen, T. S., and Rinn, J. L. (2014). The dynamics and regulators of cell fate decisions are revealed by pseudotemporal ordering of single cells. *Nature Biotechnology*, 32(4):381–386.
- Trim, W. V. and Lynch, L. (2021). Immune and non-immune functions of adipose tissue leukocytes. *Nature Reviews Immunology*.
- Tsao, H.-W., Kaminski, J., Kurachi, M., Barnitz, R. A., DiIorio, M. A., LaFleur, M. W., Ise, W., Kurosaki, T., Wherry, E. J., Haining, W. N., and Yosef, N. (2022). Batf-mediated epigenetic control of effector CD8+ T cell differentiation. *Science Immunology*, 7(68):eabi4919.
- Tsukumo, S.-i., Unno, M., Muto, A., Takeuchi, A., Kometani, K., Kurosaki, T., Igarashi, K., and Saito, T. (2013). Bach2 maintains T cells in a naive state by suppressing effector memory-related genes. *Proceedings of the National Academy of Sciences of the United States of America*, 110(26):10735–10740.
- Turley, S. J., Cremasco, V., and Astarita, J. L. (2015). Immunological hallmarks of stromal cells in the tumour microenvironment. *Nature Reviews. Immunology*, 15(11):669–682.
- Turvey, S. E. and Broide, D. H. (2010). Innate immunity. *The Journal of Allergy and Clinical Immunology*, 125(2 Suppl 2):S24–32.
- van der Leun, A. M., Thommen, D. S., and Schumacher, T. N. (2020). CD8+ T cell states in human cancer: insights from single-cell analysis. *Nature reviews. Cancer*, 20(4):218–232.
- Vasanthakumar, A., Moro, K., Xin, A., Liao, Y., Gloury, R., Kawamoto, S., Fagarasan, S., Mielke, L. A., Afshar-Sterle, S., Masters, S. L., Nakae, S., Saito, H., Wentworth, J. M., Li, P., Liao, W., Leonard, W. J., Smyth, G. K., Shi, W., Nutt, S. L., Koyasu, S., and Kallies, A. (2015). The transcriptional regulators IRF4, BATF and IL-33 orchestrate development and maintenance of adipose tissue-resident regulatory T cells. *Nature Immunology*, 16(3):276–285.
- Velasco-Velázquez, M., Xolalpa, W., and Pestell, R. G. (2014). The potential to target CCL5/CCR5 in breast cancer. *Expert Opinion on Therapeutic Targets*, 18(11):1265–1275.
- Vignali, D. A. A., Collison, L. W., and Workman, C. J. (2008). How regulatory T cells work. *Nature Reviews Immunology*, 8(7):523–532.
- Villarreal, D. O., L’Huillier, A., Armington, S., Mottershead, C., Filippova, E. V., Coder, B. D., Petit, R. G., and Princiotta, M. F. (2018). Targeting CCR8 Induces Protective Antitumor Immunity and Enhances Vaccine-Induced Responses in Colon Cancer. *Cancer Research*, 78(18):5340–5348.
- Walker, J. A. and McKenzie, A. N. J. (2018). TH2 cell development and function. *Nature Reviews. Immunology*, 18(2):121–133.
- Wang, L., Simons, D. L., Lu, X., Tu, T. Y., Solomon, S., Wang, R., Rosario, A., Avalos, C., Schmolze, D., Yim, J., Waisman, J., and Lee, P. P. (2019). Connecting blood and intratumoral Treg cell activity in predicting future relapse in breast cancer. *Nature Immunology*, 20(9):1220–1230.
- Watcham, S., Kucinski, I., and Gottgens, B. (2019). New insights into hematopoietic differentiation landscapes from single-cell RNA sequencing. *Blood*, 133(13):1415–1426.

- Weaver, C. T., Elson, C. O., Fouser, L. A., and Kolls, J. K. (2013). The Th17 Pathway and Inflammatory Diseases of the Intestines, Lungs and Skin. *Annual review of pathology*, 8:477–512.
- Wee, P. and Wang, Z. (2017). Epidermal Growth Factor Receptor Cell Proliferation Signaling Pathways. *Cancers*, 9(5):52.
- Wherry, E. J., Ha, S.-J., Kaech, S. M., Haining, W. N., Sarkar, S., Kalia, V., Subramaniam, S., Blattman, J. N., Barber, D. L., and Ahmed, R. (2007). Molecular signature of CD8+ T cell exhaustion during chronic viral infection. *Immunity*, 27(4):670–684.
- Wildin, R. S., Ramsdell, F., Peake, J., Faravelli, F., Casanova, J.-L., Buist, N., Levy-Lahad, E., Mazzella, M., Goulet, O., Perroni, L., Dagna Bricarelli, F., Byrne, G., McEuen, M., Proll, S., Appleby, M., and Brunkow, M. E. (2001). X-linked neonatal diabetes mellitus, enteropathy and endocrinopathy syndrome is the human equivalent of mouse scurfy. *Nature Genetics*, 27(1):18–20.
- Wu, C.-t. and Morris, J. R. (2001). Genes, Genetics, and Epigenetics: A Correspondence. *Science*, 293(5532):1103–1105.
- Wynn, T. (2008). Cellular and molecular mechanisms of fibrosis. *The Journal of pathology*, 214(2):199–210.
- Xiong, S., Pan, X., Xu, L., Yang, Z., Guo, R., Gu, Y., Li, R., Wang, Q., Xiao, F., Du, L., Zhou, P., and Zhu, M. (2015). Regulatory T Cells Promote β -Catenin-Mediated Epithelium-to-Mesenchyme Transition During Radiation-Induced Pulmonary Fibrosis. *International Journal of Radiation Oncology, Biology, Physics*, 93(2):425–435.
- Xu, C., Fu, Y., Liu, S., Trittipi, J., Lu, X., Qi, R., Du, H., Yan, C., Zhang, C., Wan, J., Kaplan, M. H., and Yang, K. (2021). BATF Regulates T Regulatory Cell Functional Specification and Fitness of Triglyceride Metabolism in Restraining Allergic Responses. *The Journal of Immunology*.
- Yadav, M., Bluestone, J., and Stephan, S. (2013). Peripherally Induced Tregs – Role in Immune Homeostasis and Autoimmunity. *Frontiers in Immunology*, 4.
- Yanez, D. A., Lacher, R. K., Vidyarthi, A., and Colegio, O. R. (2017). The Role of Macrophages in Skin Homeostasis. *Pflügers Archiv : European journal of physiology*, 469(3-4):455–463.
- Yu, H., Wu, H., Zheng, F., Zhu, C., Yin, L., Dai, W., Liu, D., Tang, D., Hong, X., and Dai, Y. (2020). Gene-regulatory network analysis of ankylosing spondylitis with a single-cell chromatin accessible assay. *Scientific Reports*, 10(1):19411.
- Yu, S., Fang, Y., Sharav, T., Sharp, G. C., and Braley-Mullen, H. (2011). CD8+ T cells induce thyroid epithelial cell hyperplasia and fibrosis. *Journal of Immunology (Baltimore, Md.: 1950)*, 186(4):2655–2662.
- Zaiss, D. M. W., Gause, W. C., Osborne, L. C., and Artis, D. (2015). Emerging Functions of Amphiregulin in Orchestrating Immunity, Inflammation, and Tissue Repair. *Immunity*, 42(2):216–226.
- Zaretsky, A. G., Taylor, J. J., King, I. L., Marshall, F. A., Mohrs, M., and Pearce, E. J. (2009). T follicular helper cells differentiate from Th2 cells in response to helminth antigens. *Journal of Experimental Medicine*, 206(5):991–999.
- Zhang, J., Xiao, Z., Qu, C., Cui, W., Wang, X., and Du, J. (2014). CD8 T Cells Are Involved in Skeletal Muscle Regeneration through Facilitating MCP-1 Secretion and Gr1high Macrophage Infiltration. *The Journal of Immunology*, 193(10):5149–5160.
- Zhang, L., Yu, X., Zheng, L., Zhang, Y., Li, Y., Fang, Q., Gao, R., Kang, B., Zhang, Q., Huang, J. Y., Konno, H., Guo, X., Ye, Y., Gao, S., Wang, S., Hu, X., Ren, X., Shen, Z., Ouyang, W., and Zhang, Z. (2018). Lineage tracking reveals dynamic relationships of T cells in colorectal cancer. *Nature*, 564(7735):268–272.
- Zhang, Y., Liu, T., Meyer, C. A., Eickhout, J., Johnson, D. S., Bernstein, B. E., Nussbaum, C., Myers, R. M., Brown, M., Li, W., and Liu, X. S. (2008). Model-based Analysis of CHIP-Seq (MACS). *Genome Biology*, 9(9):R137.
- Zhang, Z., Liu, S., Zhang, B., Qiao, L., Zhang, Y., and Zhang, Y. (2020). T Cell Dysfunction and Exhaustion in Cancer. *Frontiers in Cell and Developmental Biology*, 8:17.
- Zheng, Y., Liu, X., Le, W., Xie, L., Li, H., Wen, W., Wang, S., Ma, S., Huang, Z., Ye, J., Shi, W., Ye, Y., Liu, Z., Song, M., Zhang, W., Han, J.-D. J., Belmonte, J. C. I., Xiao, C., Qu, J., Wang, H., Liu, G.-H., and Su, W. (2020). A human circulating immune cell landscape in aging and COVID-19. *Protein & Cell*, 11(10):740–770.

6 Supplement

6.1 Supplementary Figures

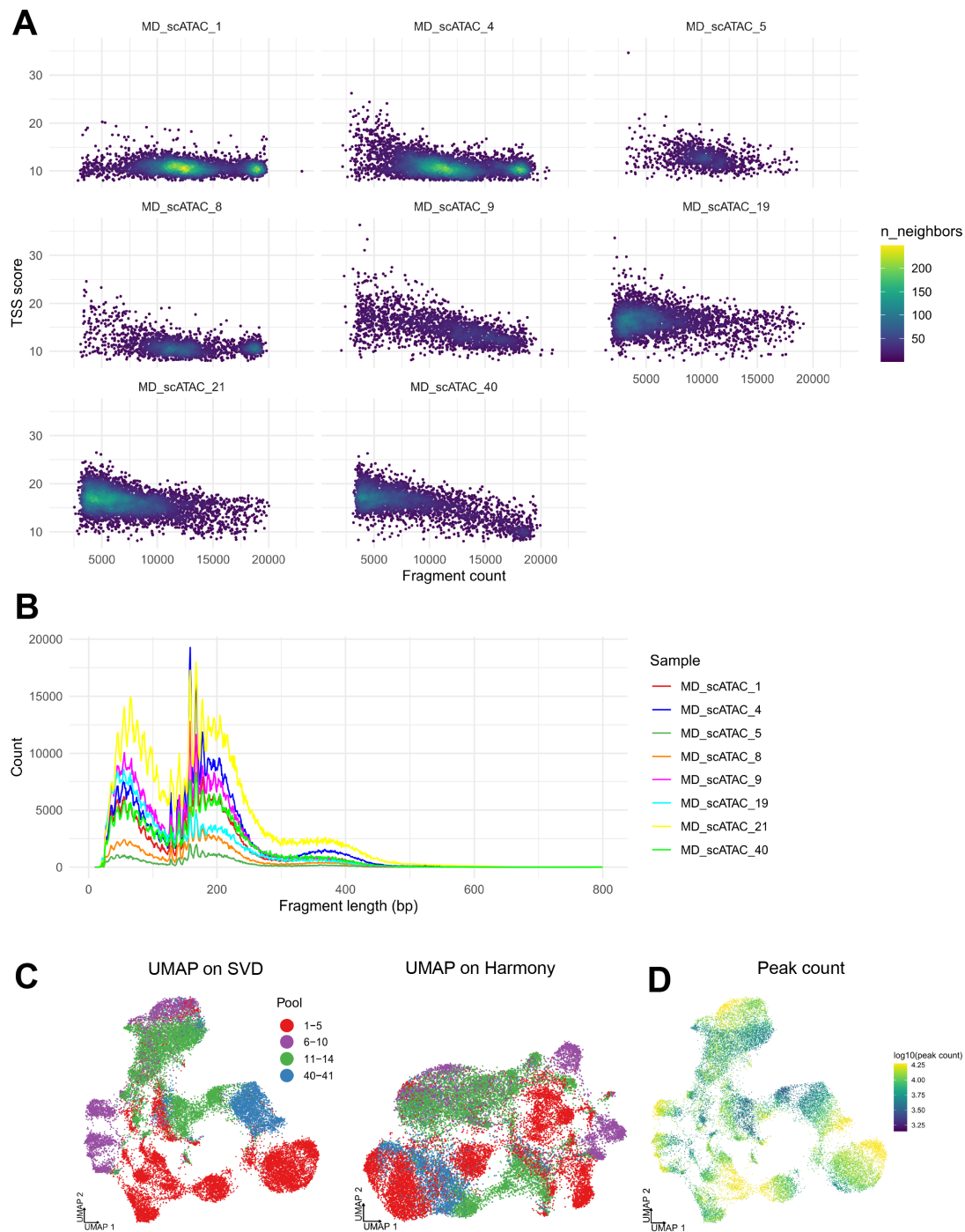


Figure S1: Mouse SPF CD4⁺ T cell quality control. **A** TSS score plotted over number of fragments for barcodes passing fragment and TSS score thresholds. Color indicates the number of nearest neighbours for each cell. **B** Fragment size distribution for each sample in the dataset. **C** UMAP representations calculated on the first 20 components of the SVD score matrix (left) and the Harmony score matrix (right) with batch correction against the pool of mice. **D** UMAP colored by peak count.

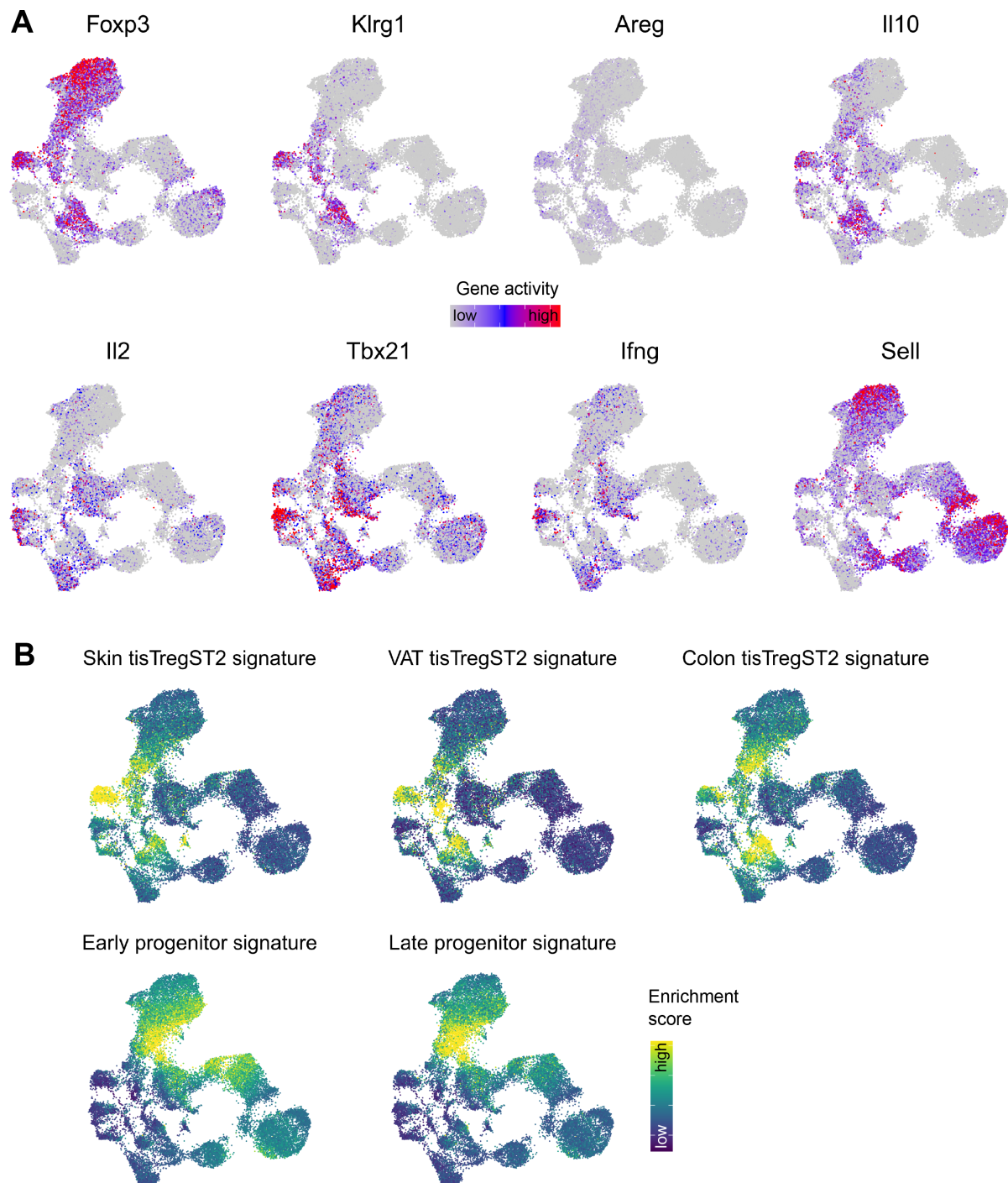


Figure S2: Mouse SPF CD4⁺ T cell markers and signatures. **A** UMAP of mouse CD4⁺ T cell dataset colored by marker gene activity scores for Treg cells (*Foxp3*), tisTregST2 cells (*Klrp1*, *Areg*, *Il10*), Tconv cells (*Il2*, *Tbx21*, *Ifng*) and naive T cells (*Sell*). **B** Signature enrichment scores of tisTregST2 signatures taken from Delacher et al. (2020).

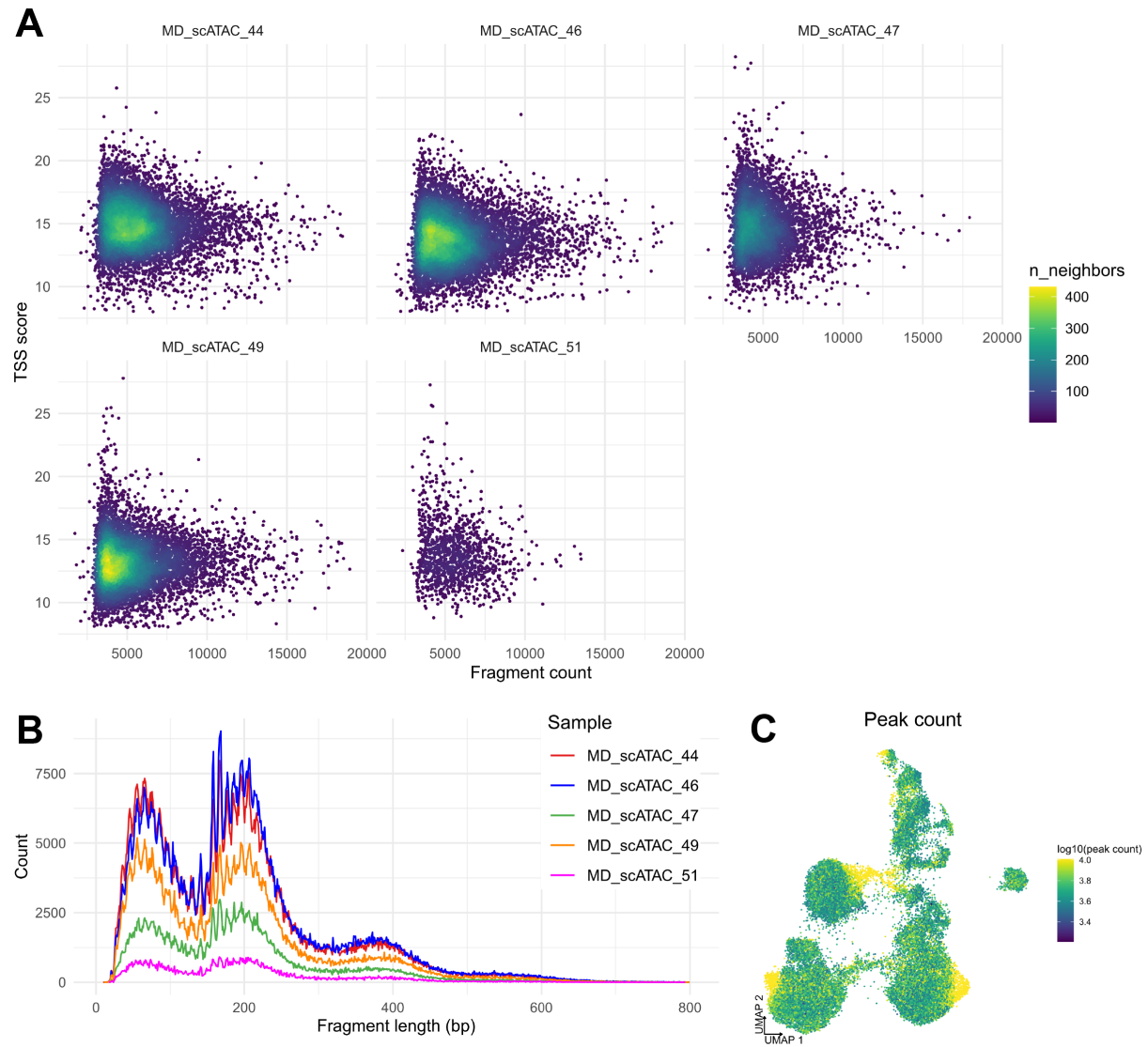


Figure S3: Mouse gnotobiotic CD4⁺ T cell quality control. **A** Scatter plot showing number of fragments and TSS score after filtering out low-quality barcodes. The number of nearest neighbors for each cell is indicated by color. **B** Fragment size distribution for each sample in the dataset. **C** UMAP colored by peak count.

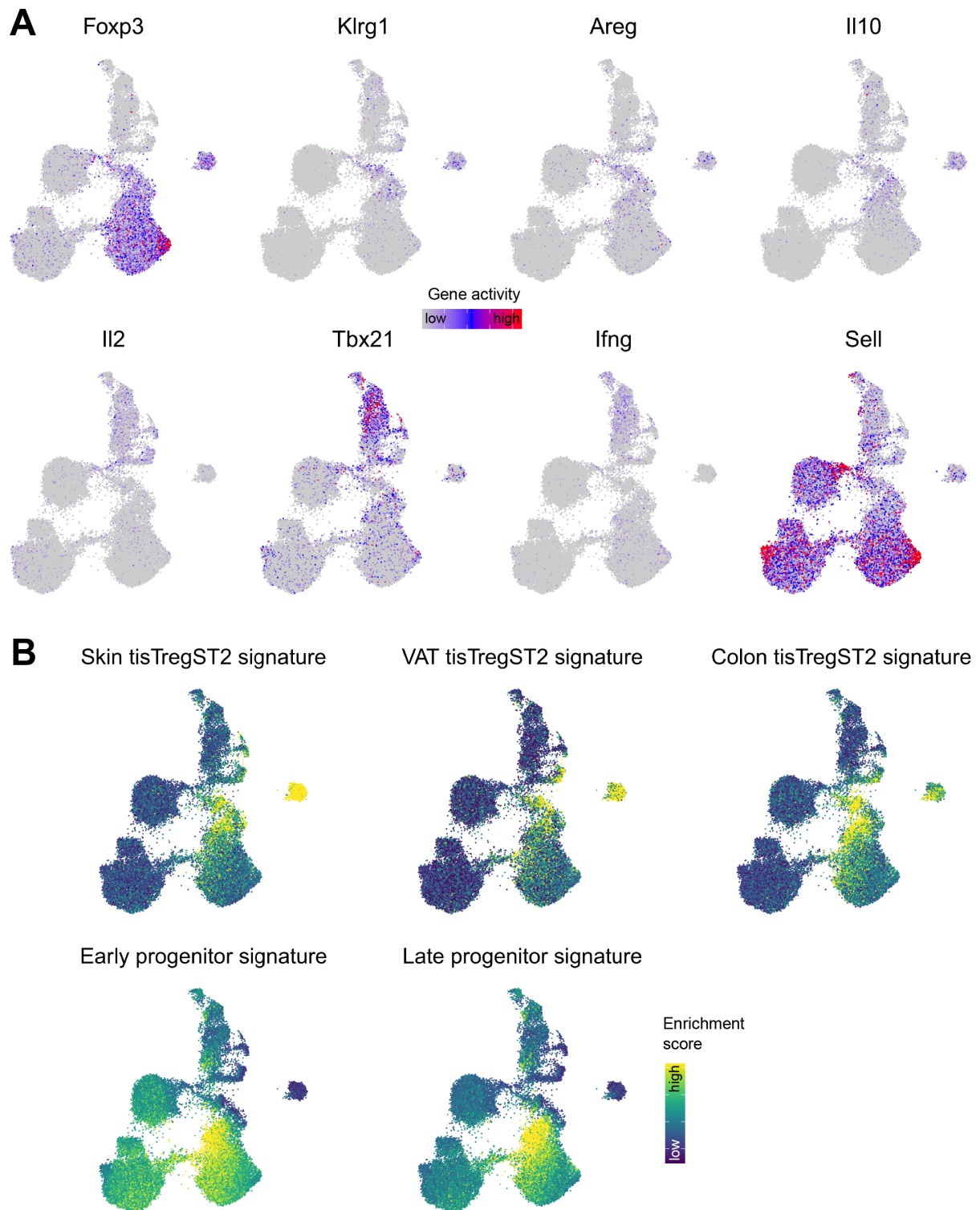
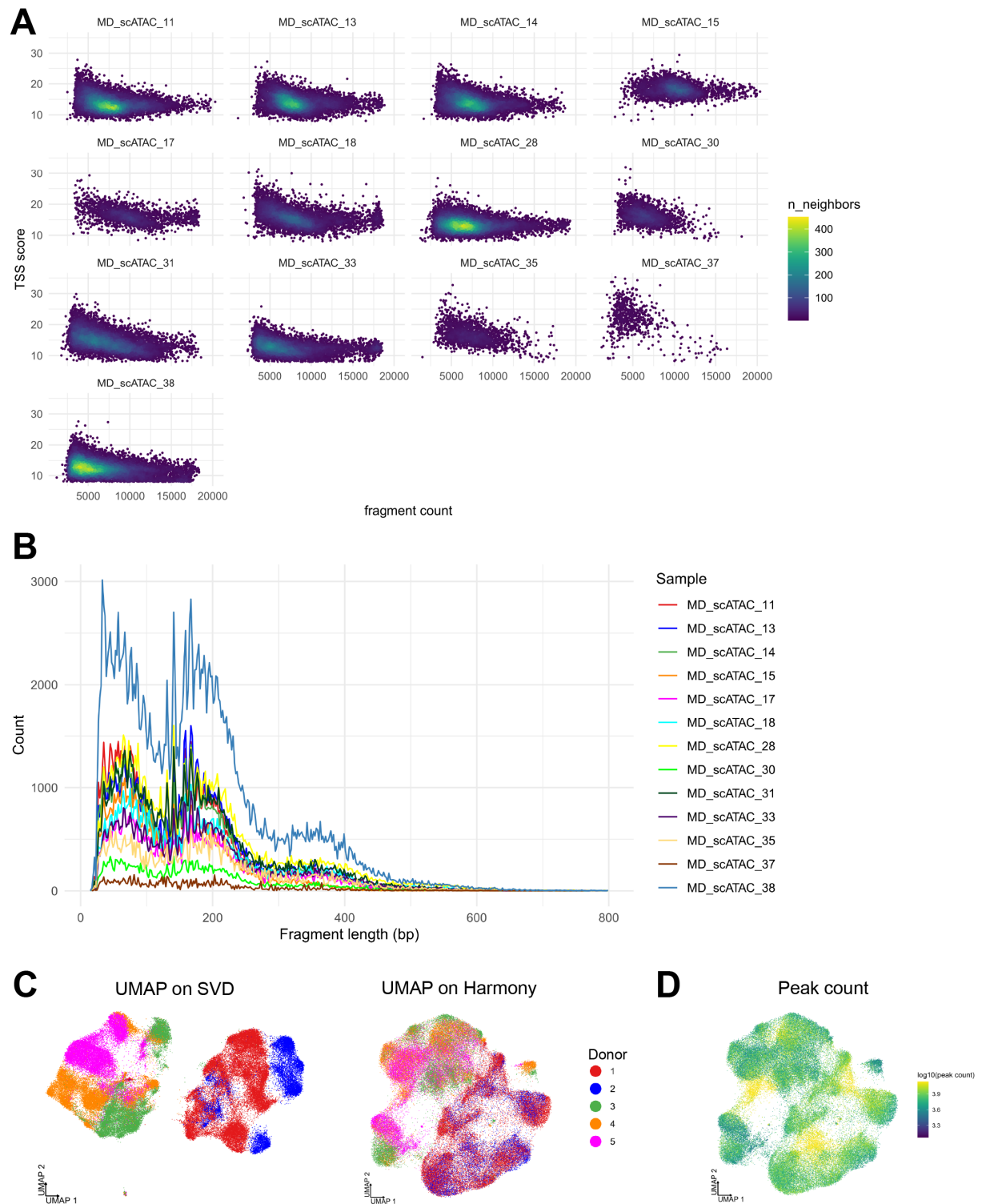


Figure S4: Mouse gnotobiotic CD4⁺ T cell markers and signatures. **A** UMAP colored by gene activities. Marker genes for Treg cells (*Foxp3*), tisTregST2 cells (*Klrp1*, *Areg*, *Il10*), Tconv cells (*Il2*, *Tbx21*, *Ifng*) and naive T cells (*Sell*) are displayed. **B** tisTregST2 signature enrichment scores plotted in UMAP space.



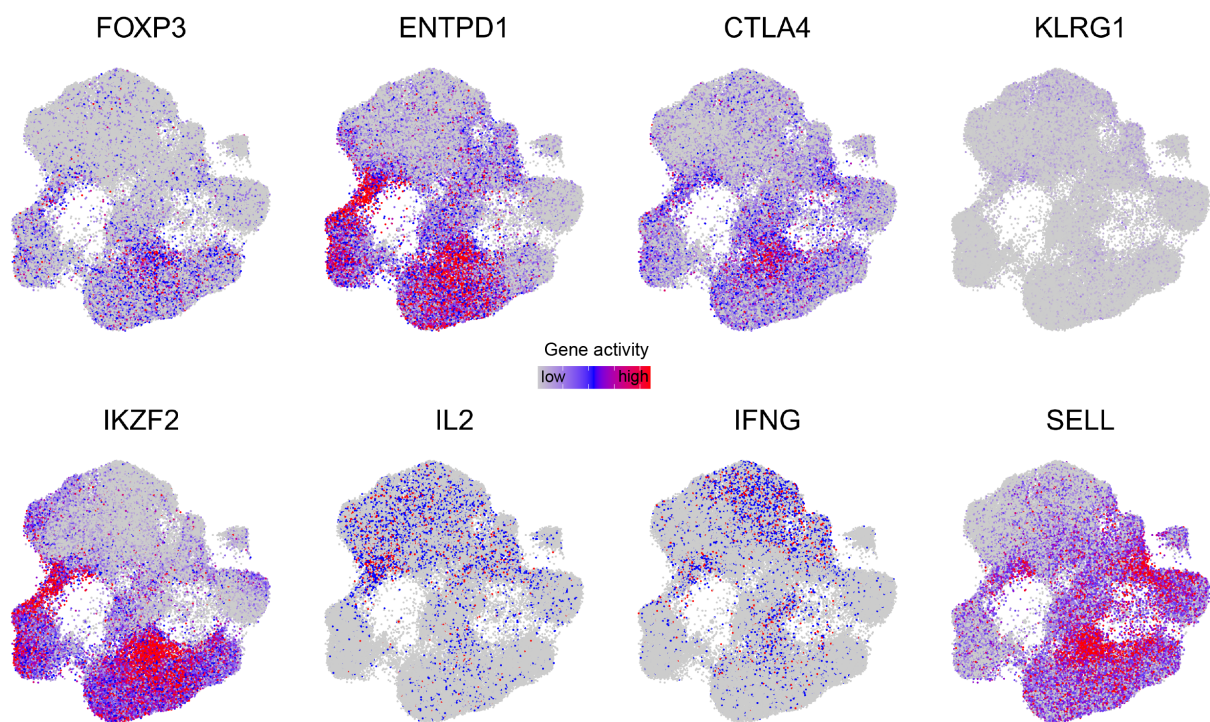


Figure S6: Human CD4⁺ T cell marker genes. UMAP colored by gene activity of selected marker genes for Treg cells (*FOXP3*, *ENTPD1*, *CTLA4*), tTreg cells (*IKZF2*), Tconv cells (*IL2*, *IFNG*) and naive T cells (*SELL*). The murine tisTregST2 marker gene *KLRG1* had low accessibility in the human dataset.

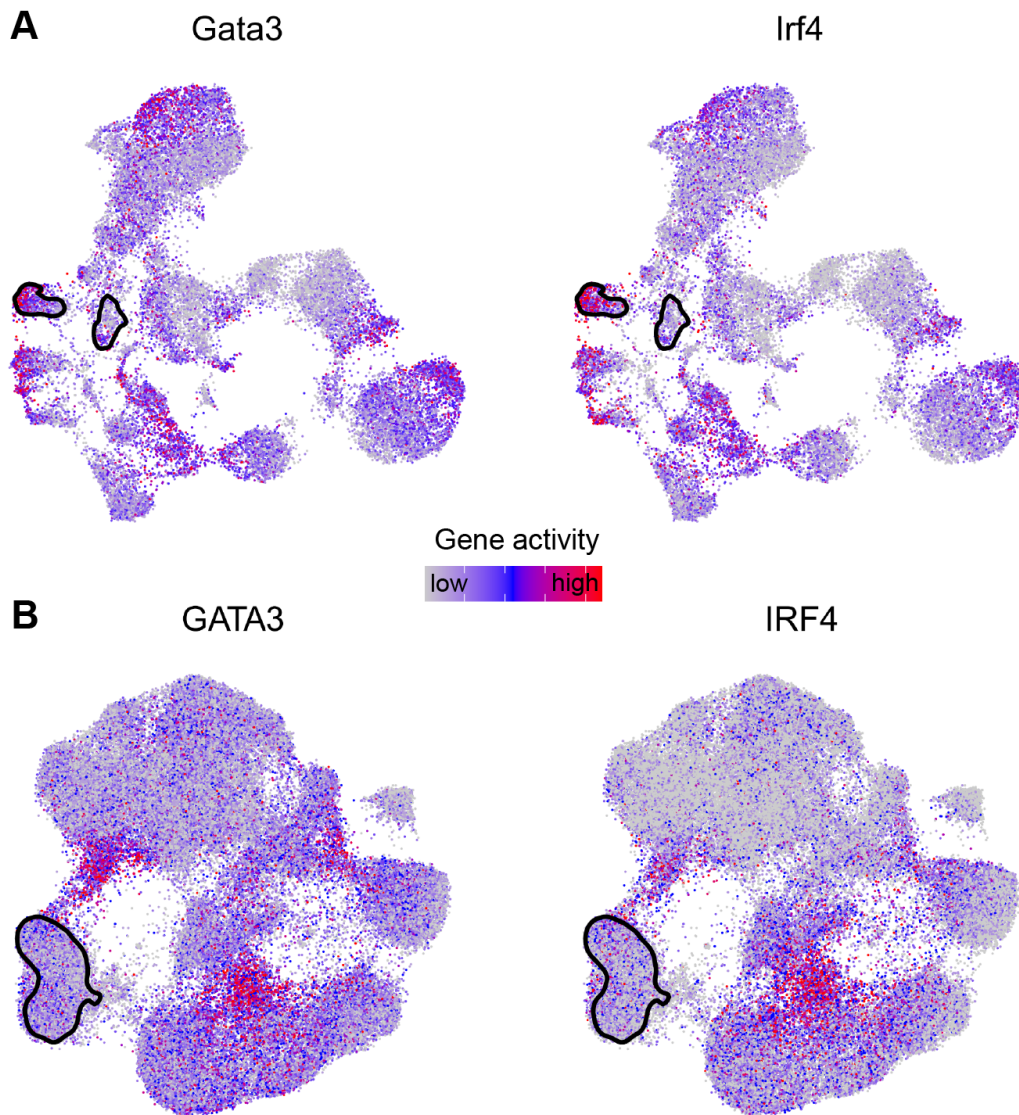


Figure S7: Th2 transcription factor gene activity. UMAP of summarized chromatin accessibility within the *Gata3* and *Irf4* gene body and promoter regions for the **A** mouse and **B** human CD4⁺ T cell dataset. Outlined fractions correspond to tisTreg cells from the fat and skin.

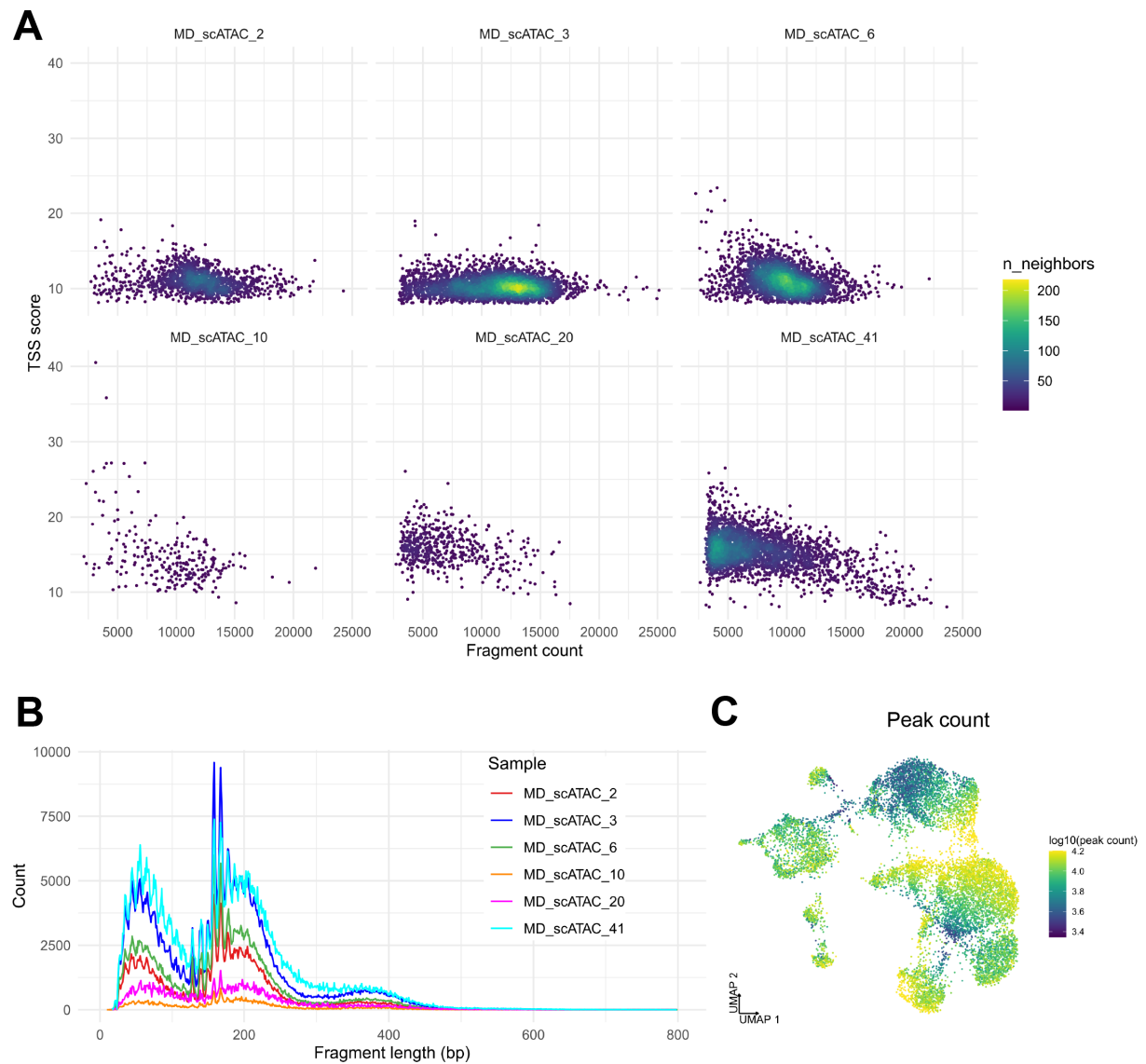


Figure S8: Mouse SPF CD8⁺ T cell quality control. **A** TSS score plotted over number of fragments after application of fragment and TSS filters. The color indicates the number of nearest neighbors for each cell. **B** Distribution of fragment sizes by sample in the dataset. **C** UMAP colored by peak count per cell.

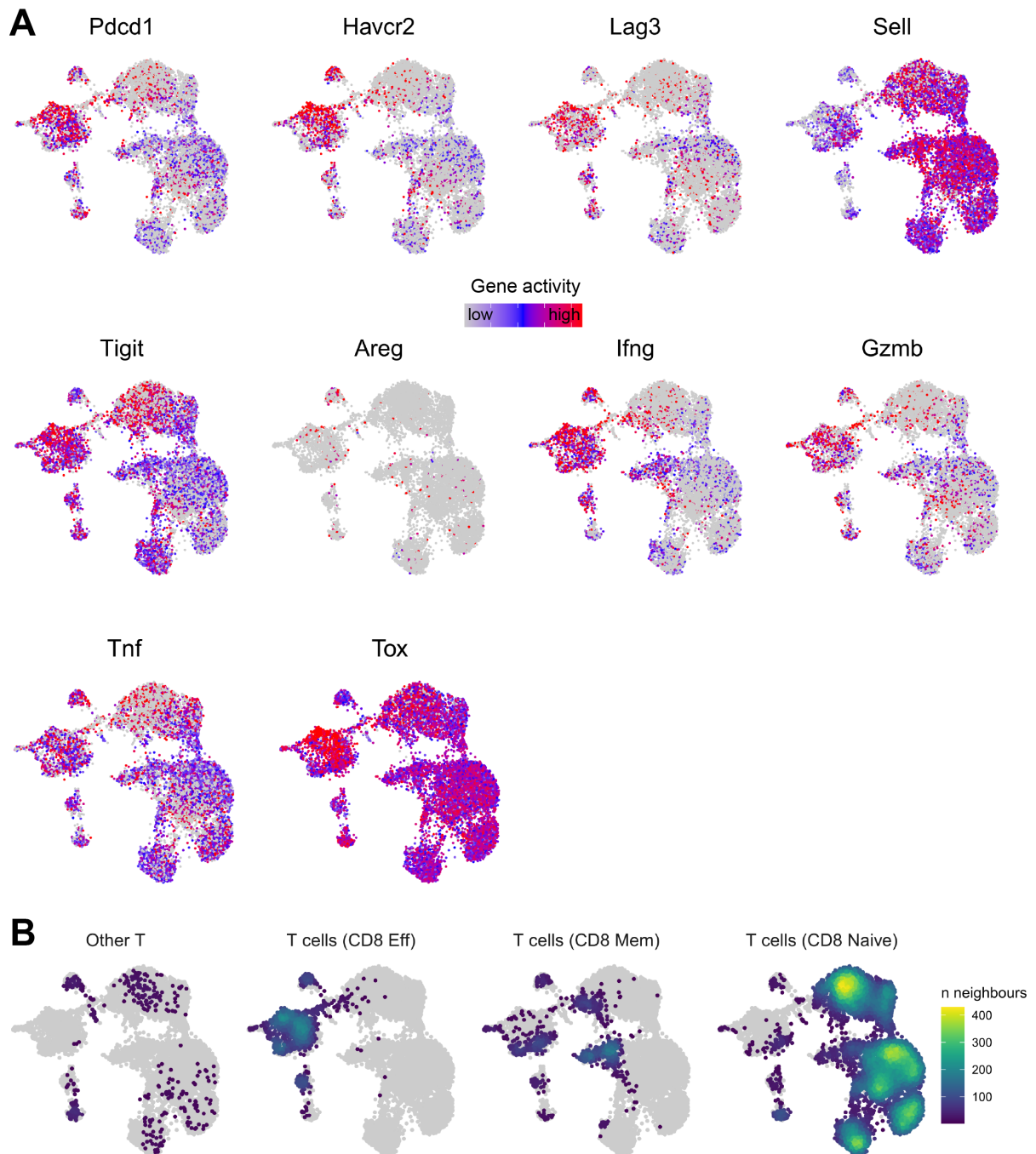


Figure S9: Mouse SPF CD8⁺ T cell markers. **A** UMAP colored by gene activities for exhausted T cells (*Pdcd1*, *Havcr2*, *Lag3*, *Tigit*, *Tox*), naive T cells (*Sell*) and effector T cells (*Areg*, *Ifng*, *Gzmb*, *Tnf*) are shown. **B** Number of nearest neighbors that received the indicated label by referenced-based annotation with SingleR. Grey dots indicate cells with another label. The CD8⁺ T cell subset from the ImmGen dataset provided in the cellDex R package was used as reference (Aran et al., 2019).

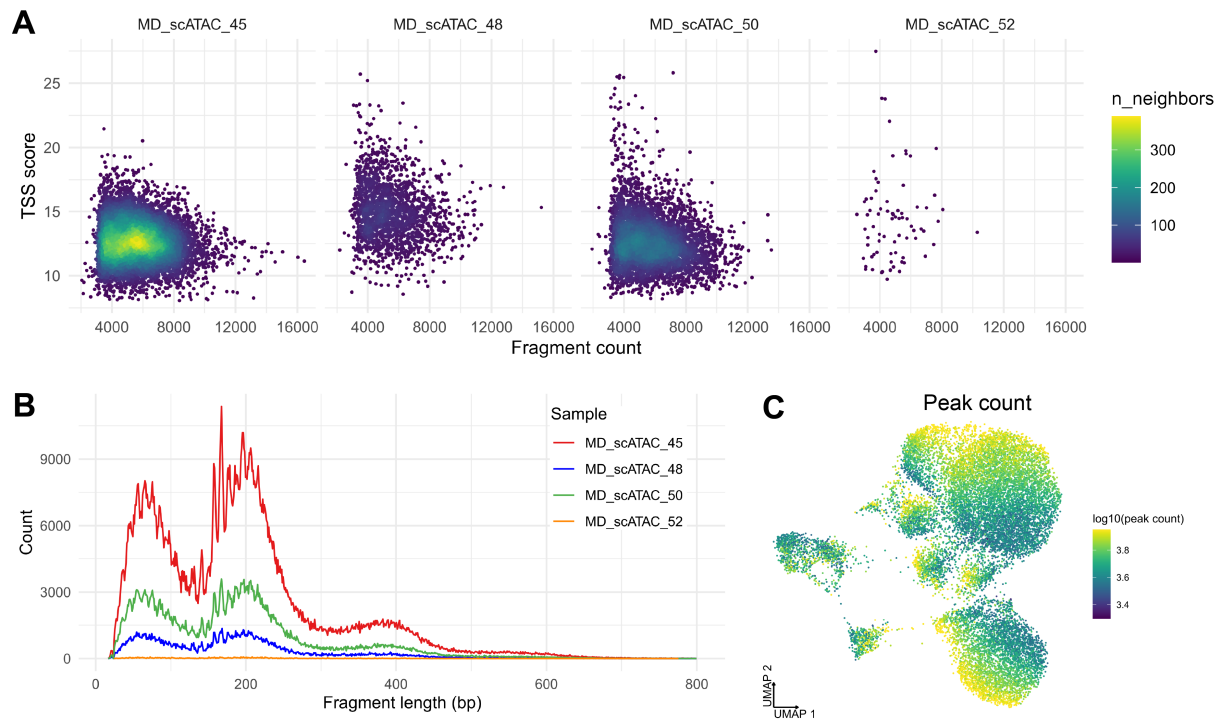


Figure S10: Mouse gnotobiotic CD8⁺ T cell quality control. **A** Scatter plot of TSS score over number of fragments for cells passing fragment and TSS filters. **B** Distribution of fragment lengths per sample. Due to a low number of cells in sample MD_scATAC_52 its fragment size periodicity is not visible on the absolute count scale. **C** Peak count per cell shown on the UMAP dimensionality reduction.

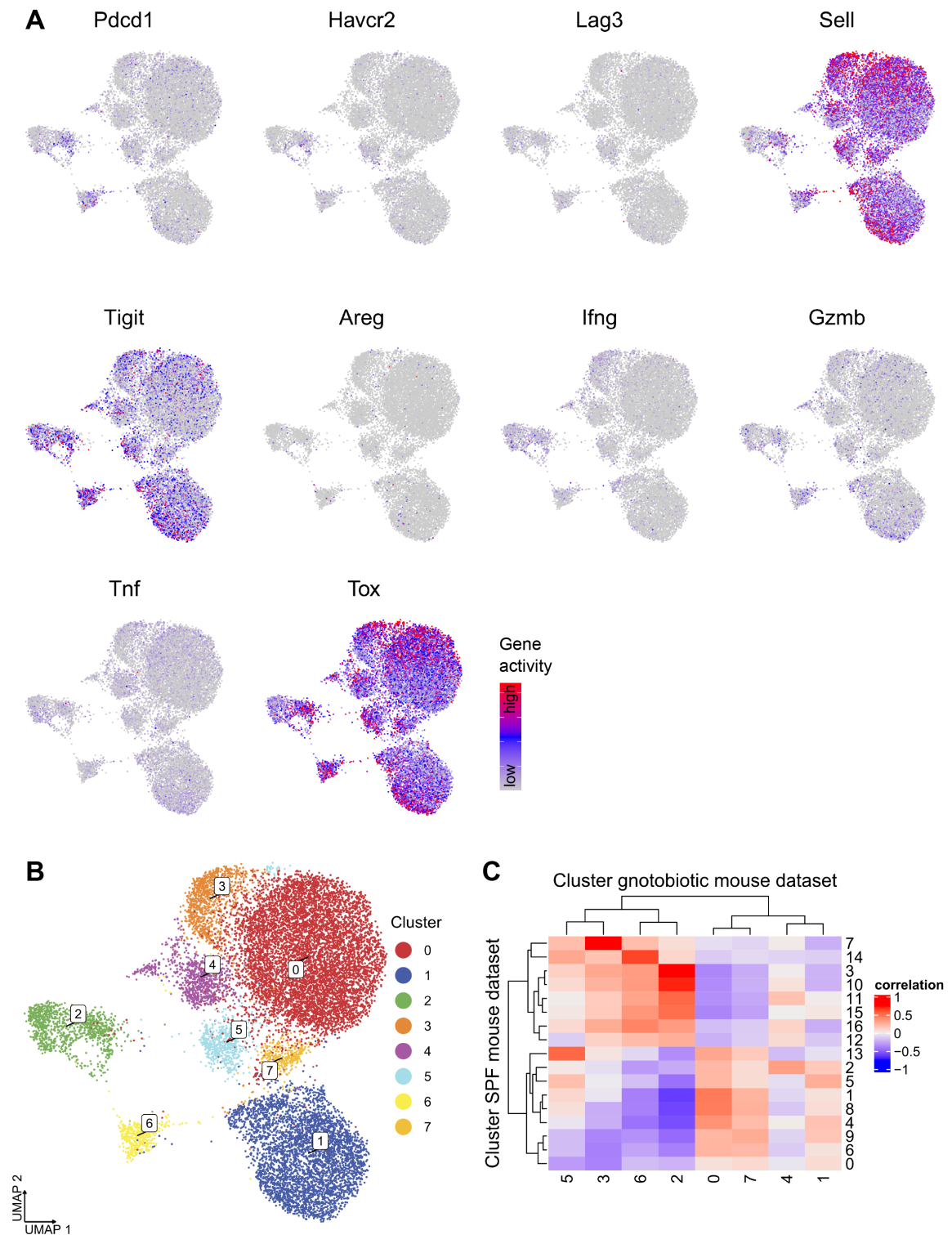
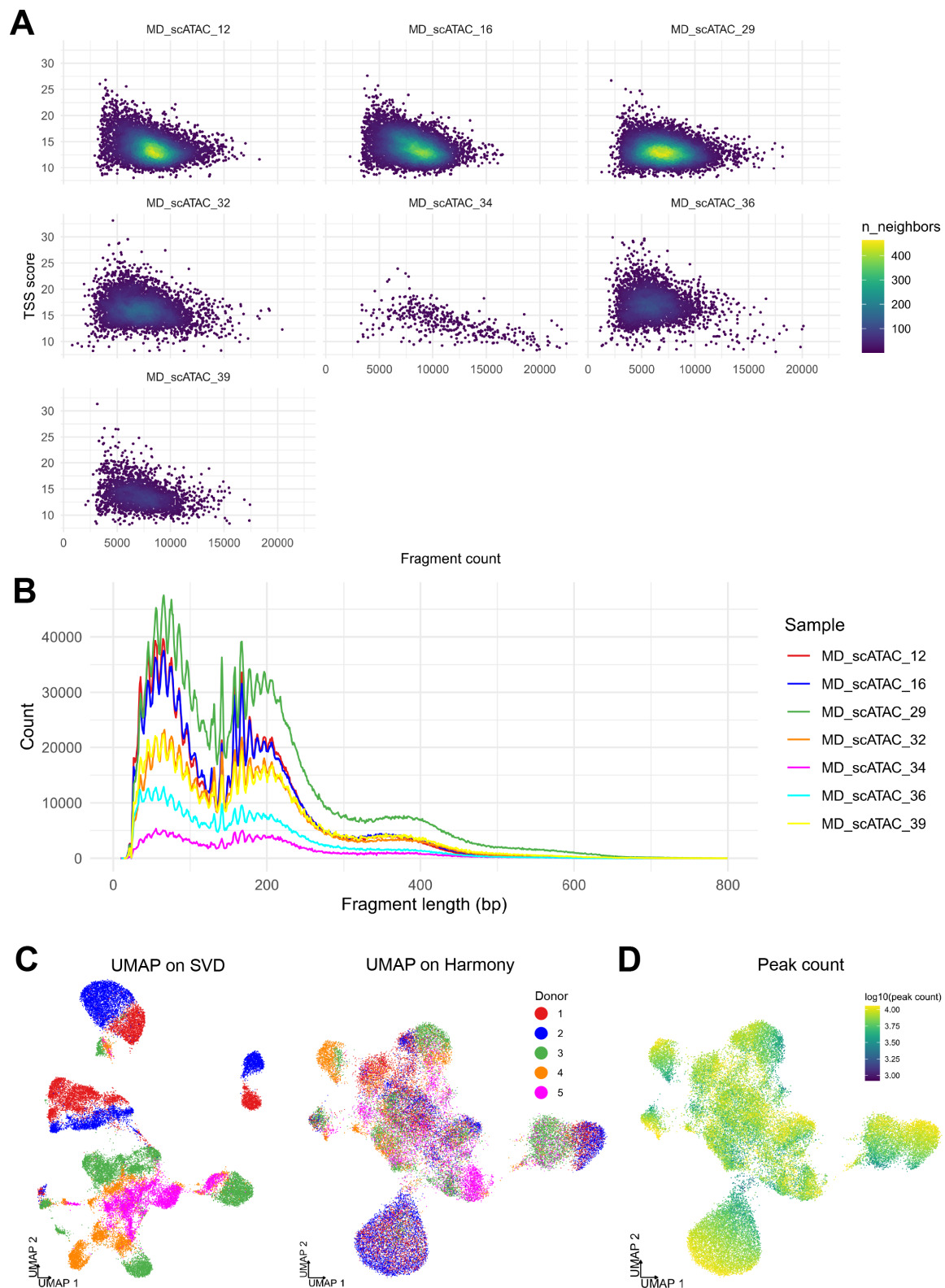


Figure S11: Independence of effector CD8⁺ T cells from microbiota. **A** Gene activities plotted on the UMAP representation of the gnotobiotic mouse CD8⁺ T cell dataset. Markers for exhausted T cells (*Pdcd1*, *Havcr2*, *Lag3*, *Tigit*, *Tox*), naive T cells (*Sell*) and effector T cells (*Areg*, *Ifng*, *Gzmb*, *Tnf*) are shown. **B** Clusters obtained by graph-based clustering. **C** Heatmap showing Spearman correlations between clusters from the SPF and gnotobiotic mouse CD8⁺ T cell datasets. Correlations were calculated based on the mean scaled gene activity by cluster considering the intersection between the 3,000 most variable gene activities in both datasets (1,481 common genes). SPF mouse clusters 14, 15 and gnotobiotic mouse clusters 2, 6 contain effector CD8⁺ T cells from the colon.



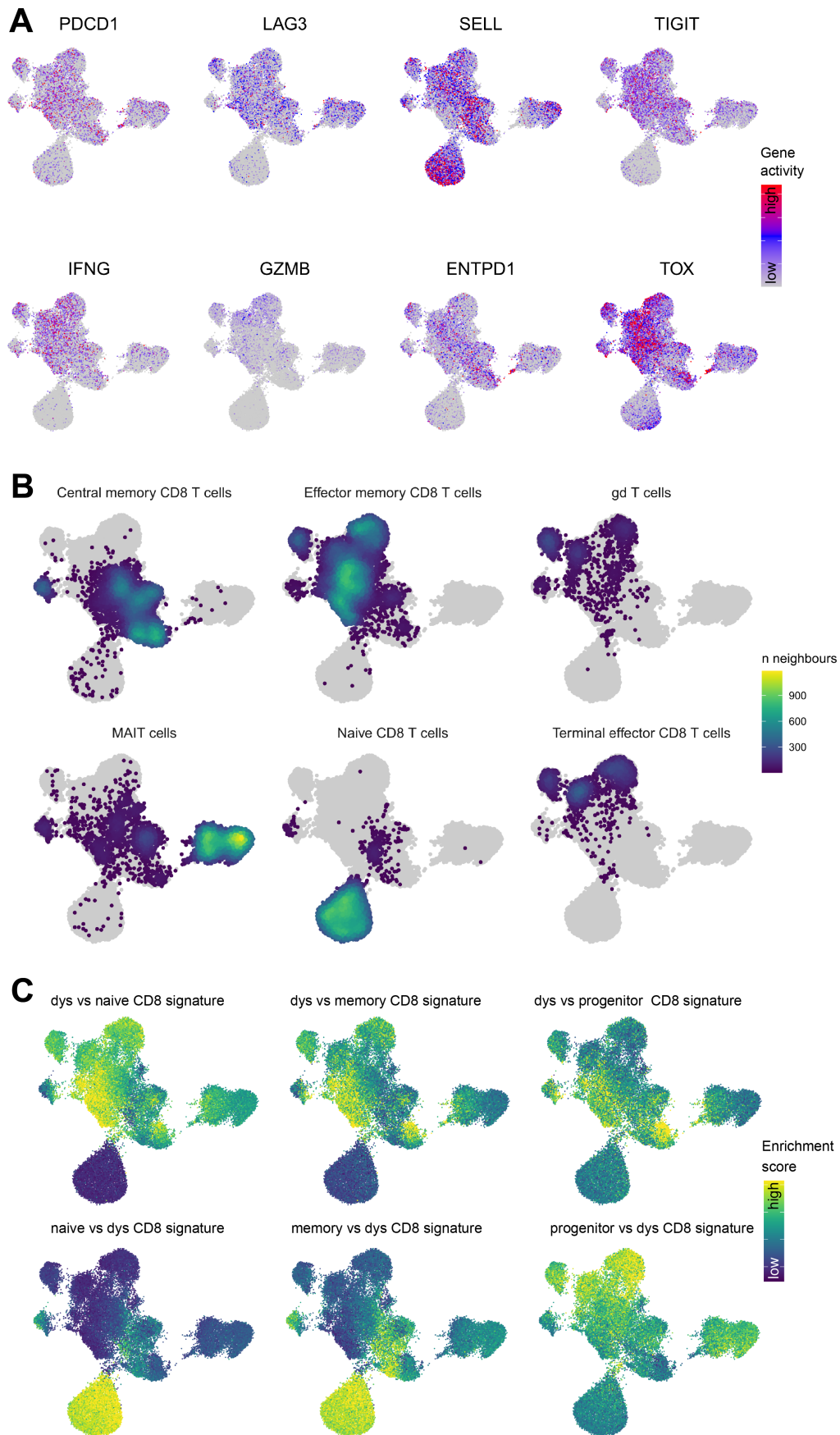


Figure S13: Human CD8⁺ T cell markers and cell type annotations. (Legend on the next page.)

Figure S13: Human CD8⁺ T cell markers and cell type annotations. **A** UMAP of human CD8⁺ T cells colored by gene activity scores for exhausted CD8⁺ T cells (*PDCD1*, *LAG3*, *TIGIT*, *ENTPD1*, *TOX*), naive T cells (*SELL*) and effector T cells (*IFNG*, *GZMB*). **B** Density of SingleR cell type annotations. Grey values indicate different cell type annotations. The CD8⁺ T cell samples from the Monaco immune cell atlas was used as reference (Aran et al., 2019). **C** Signature enrichment scores for differential peaks from pairwise comparisons of dysfunctional (dys) against naive, memory or progenitor dysfunctional CD8⁺ T cells provided by (Pritykin et al., 2021).

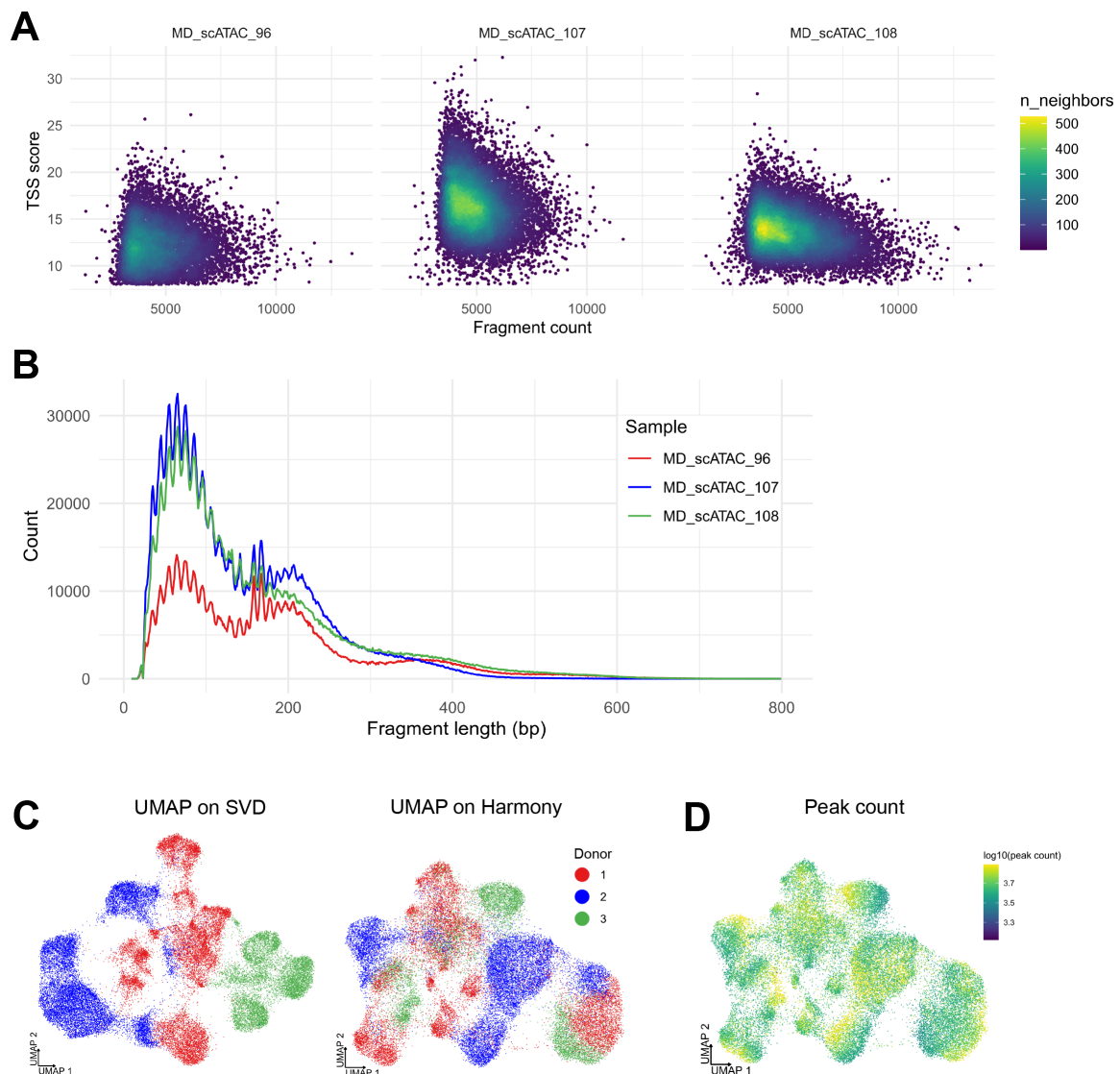


Figure S14: Human HCC CD3⁺ T cell quality control. **A** TSS score plotted over number of fragments. Prior to visualization, a minimum filter was applied to TSS score and fragment number. **B** Fragment size distribution per sample. **C** Left, UMAP based on first 20 score components from SVD. Right, UMAP on Harmony-corrected embedding with donor as batch variable. **D** UMAP colored by peak count.

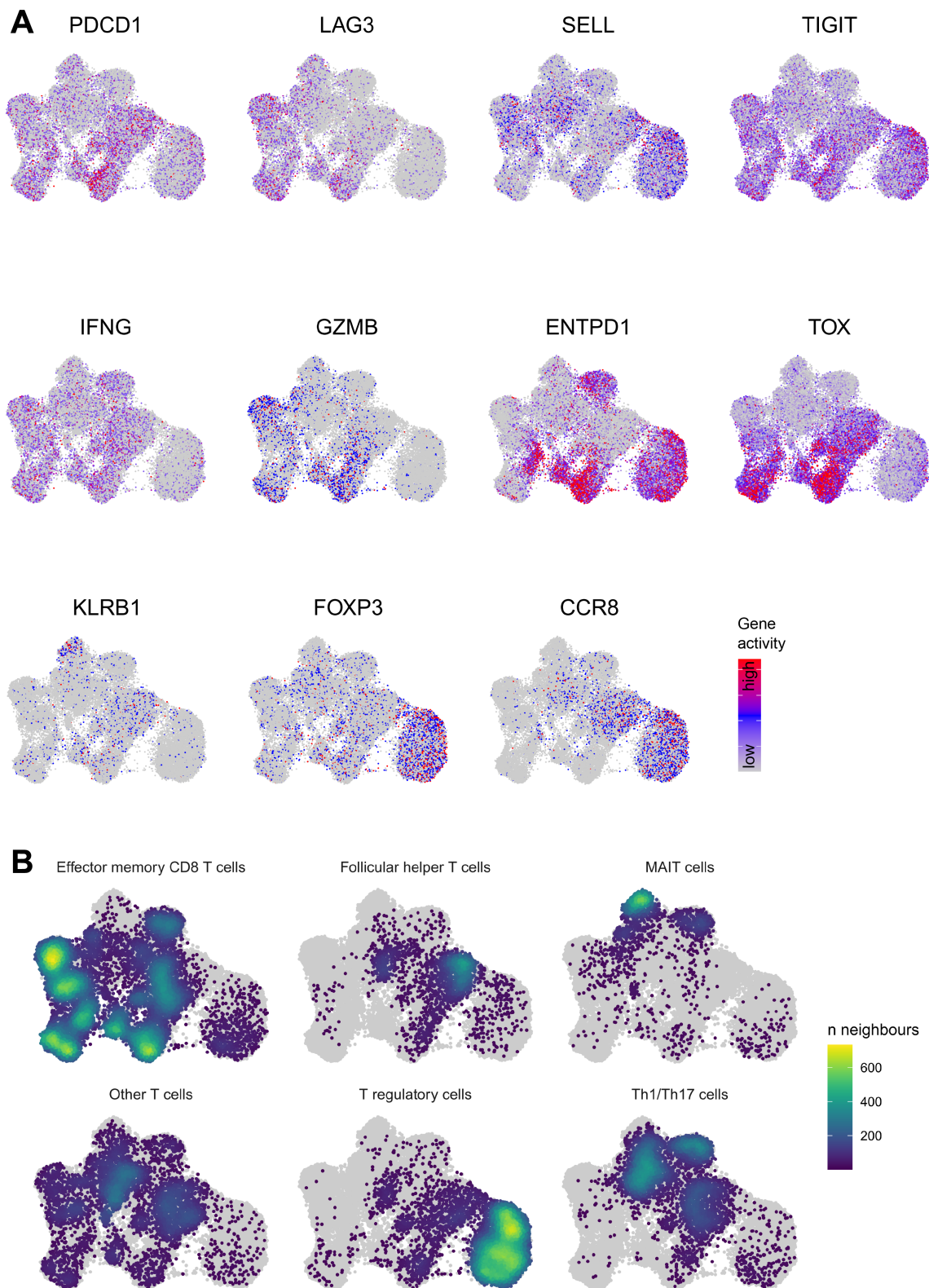


Figure S15: Human HCC CD3⁺ T cell markers and cell type annotations. **A** Marker gene activity visualized on UMAP. Markers are shown for exhausted CD8⁺ T cells (*PDCD1*, *LAG3*, *TIGIT*, *ENTPD1*, *TOX*), naive T cells (*SELL*), effector T cells (*IFNG*, *GZMB*), MAIT cells (*KLRB1*) and Treg cells (*FOXP3*, *CCR8*). **B** Density of SingleR cell type annotations plotted on UMAP. Color indicates the number of nearest neighbors sharing the respective label and grey dots represent cells with a different label. The Monaco immune cell atlas was used as reference (Aran et al., 2019).

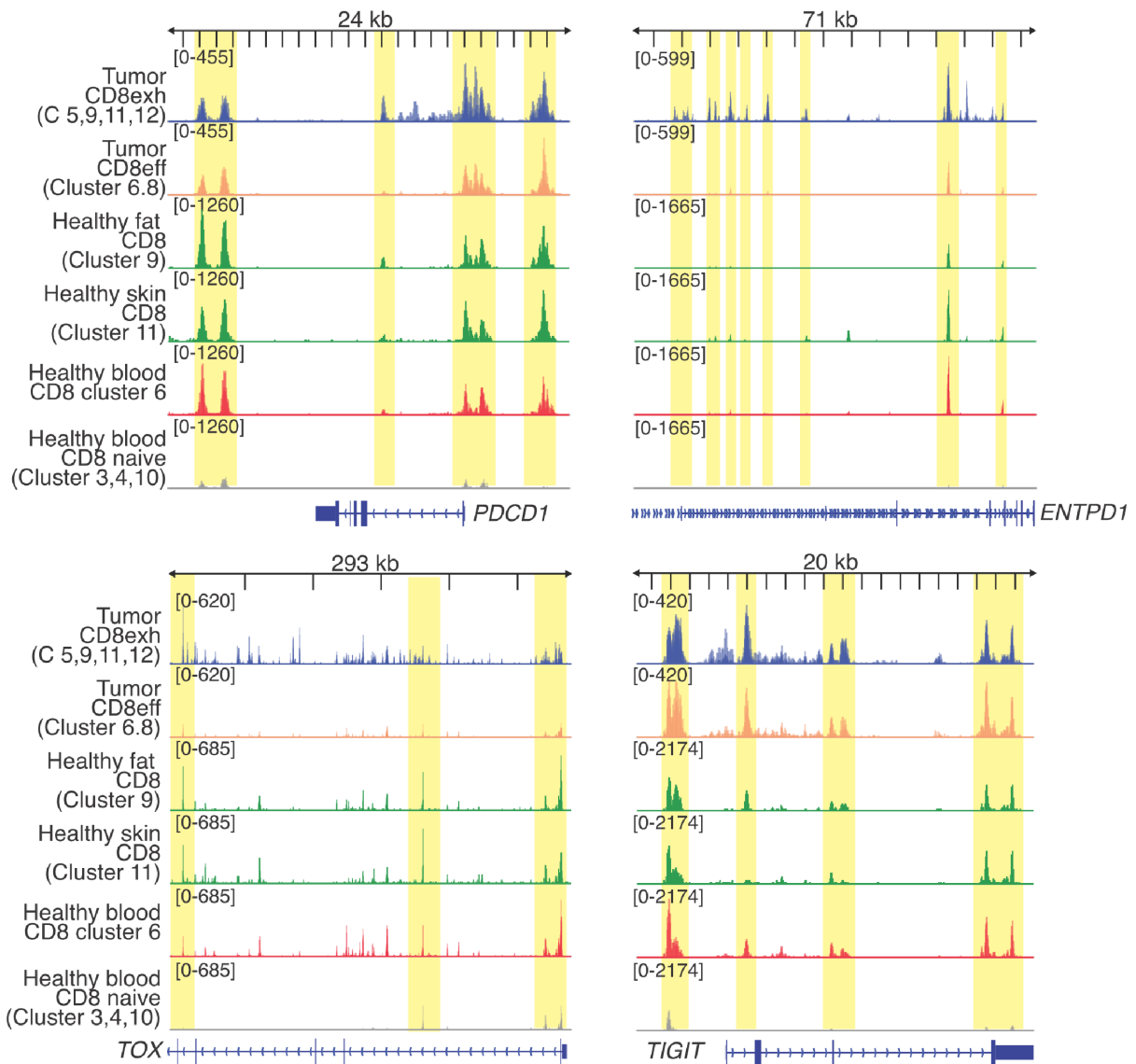


Figure S16: CD8⁺ T cell ATAC-profiles at exhaustion marker genes. Aggregated chromatin accessibility profiles for selected clusters from the human CD8⁺ T cell dataset and HCC CD3⁺ T cell dataset at the gene loci of CD8⁺ T cell exhaustion-associated genes *PDCD1*, *ENTPD1*, *TOX* and *TIGIT*. The figure was prepared by Prof. Dr. Michael Delacher and is adapted from Delacher et al. (nd).

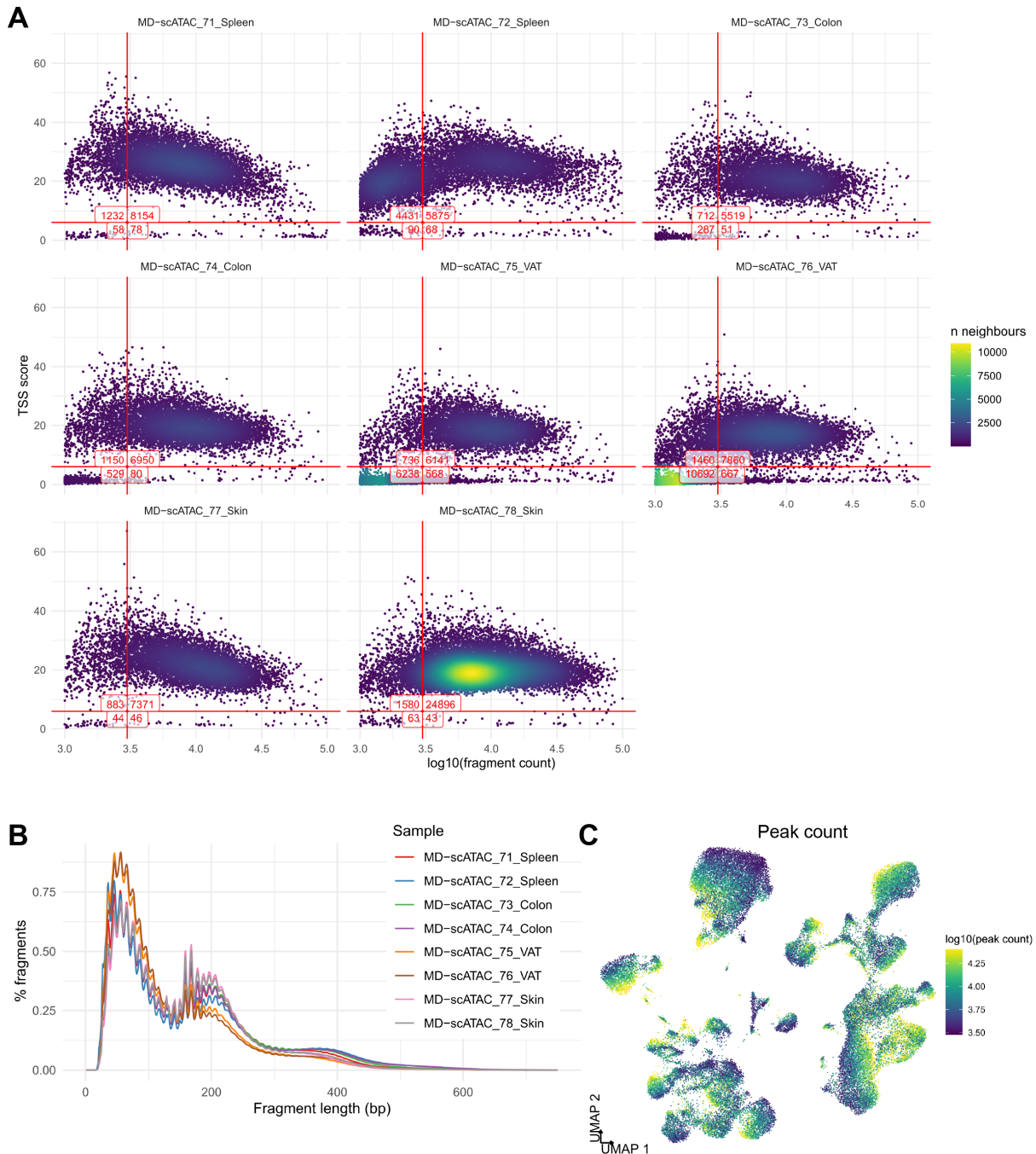


Figure S17: Mouse immune cell atlas quality control. **A** Number of unique fragments per cell compared with TSS score. Horizontal and vertical lines represent the applied filter thresholds and the number of barcodes in each quadrant is indicated. Only barcodes above both filter thresholds are annotated as high-quality cells for downstream analyses. **B** Fragment size distribution per sample. The y-axis shows the percentage of fragments with respective length of all fragments available for the sample. **C** Peak count per cell visualized on UMAP.

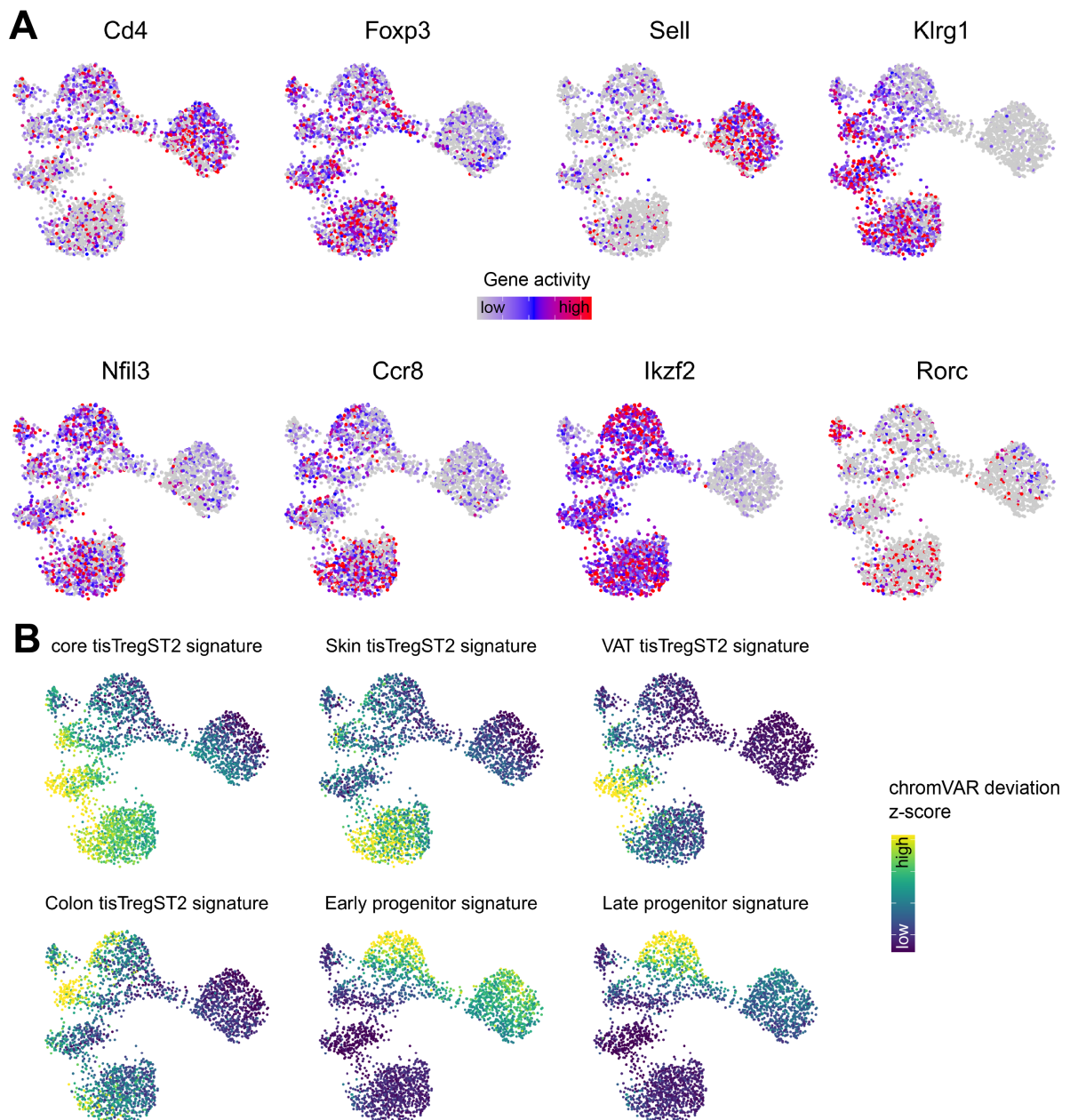


Figure S18: Confirmation of $Ccr8^+$ Treg cell marker in the mouse. **A** UMAP colored by gene activities. Markers for $CD4^+$ T cells (*Cd4*), Treg cells (*Foxp3*), antigen-naive cells (*Sell*), early and late tisTregST2 precursors (*Nfil3*, *Klrp1*, *Ccr8*), tisTregST2 cells (*Ccr8*), tTreg and pTreg cells (*Ikzf2*, *Rorc*) are shown. **B** chromVAR deviation z-scores of tisTregST2 signature peak sets from Delacher et al. (2020).

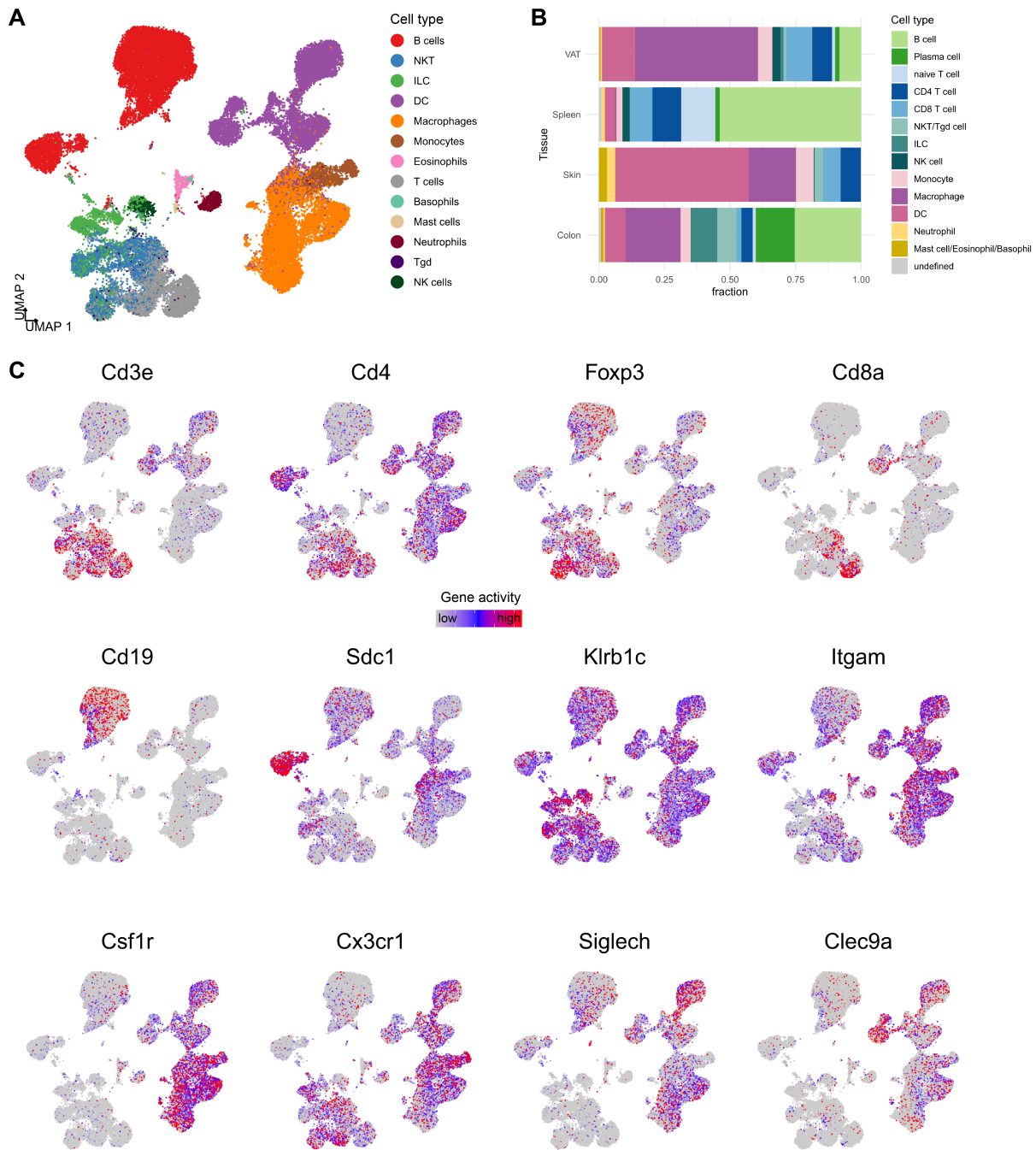


Figure S19: Mouse immune cell atlas cell type annotation and markers. **A** UMAP of murine immune cell atlas colored by SingleR cell type annotation. Samples from the ImmGen dataset served as reference (Aran et al., 2019). **B** Barplot of fractions of immune cell types per tissue based on the cluster annotation from Figure 26C. **C** UMAP of murine immune cells colored by gene activity scores. The following cell type markers are shown with corresponding cell type in brackets: *Cd3e* (T cells), *Cd4* (CD4⁺), *Foxp3* (Treg cell), *Cd8a* (Cd8 T cell), *Cd19* (B cell), *Sdc1* (Plasma cell), *Klrb1c* (NK cell), *Itgam* (myeloid cell), *Csf1r* (Monocyte/Macrophage), *Cx3cr1* (Monocyte), *Siglech* (pDC), *Clec9a* (cDC).

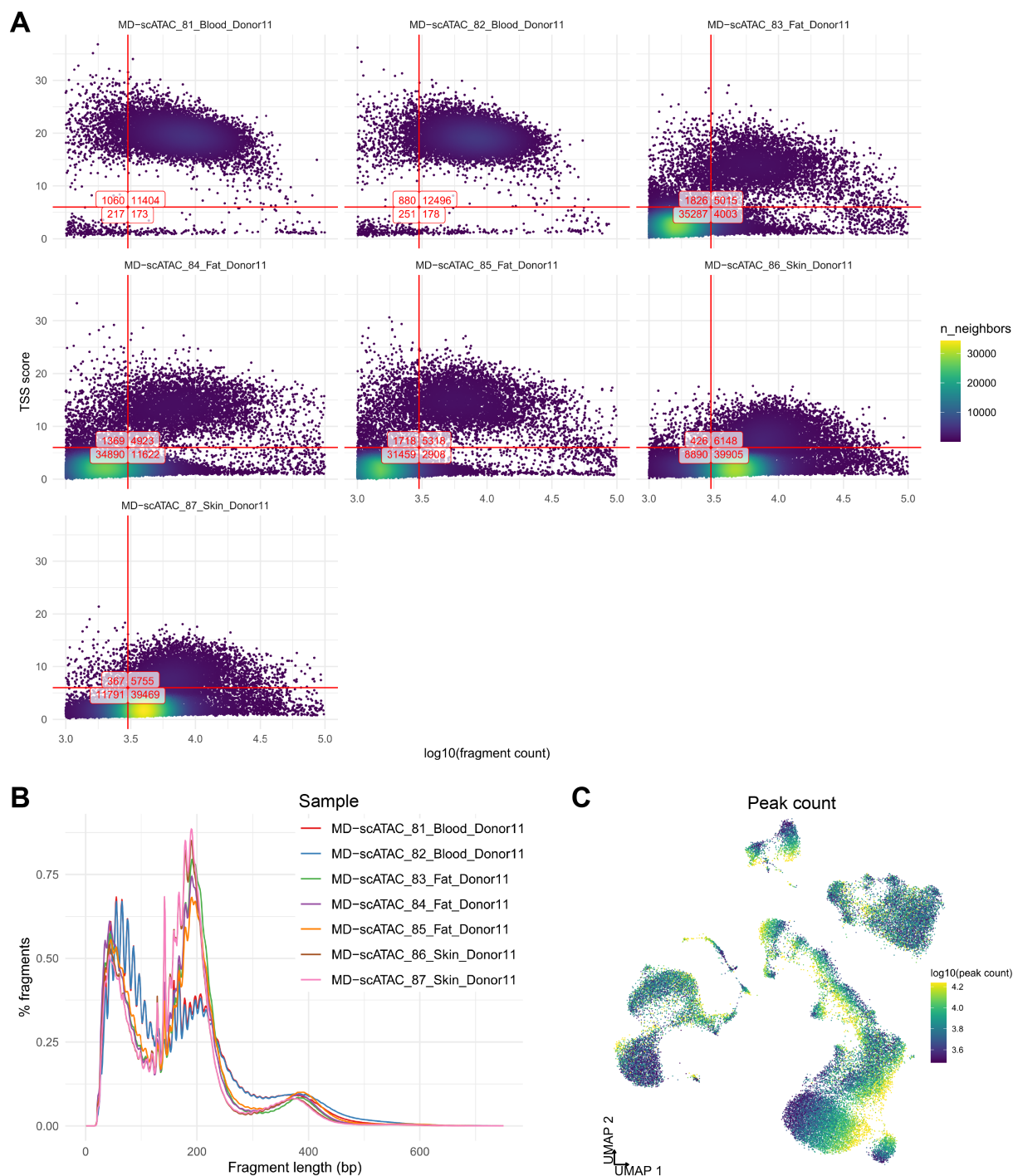


Figure S20: Human immune cell atlas quality control. **A** TSS score over number of unique fragments per cell. Filter thresholds are indicated by red lines and the number of barcodes in each quadrant is shown. Only barcodes in the first quadrant are used for further analyses. **B** Fragment length distribution for each sample in the dataset. **C** Peak count shown in UMAP space.

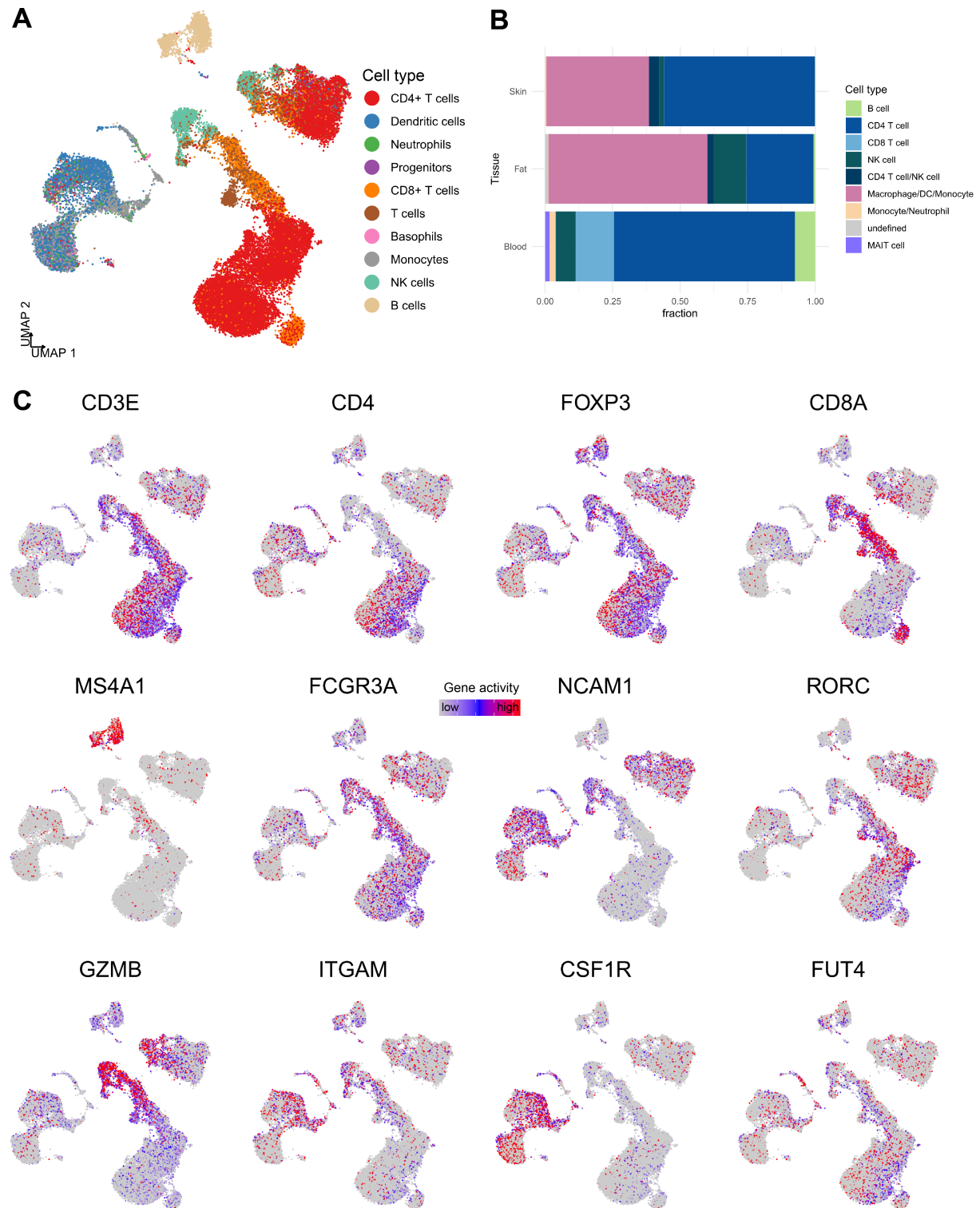


Figure S21: Human immune cell atlas cell type annotation and markers. scATAC-seq data of $CD45^+$ immune cells sorted from different human tissues. **A** UMAP colored by SingleR cell type annotation based on the Monaco reference dataset (Aran et al., 2019). **B** Fractions of annotated cell types by tissue. **C** Gene activity scores including markers for T cells ($CD3E$), $CD4^+$ T cells ($CD4$), Treg cells ($FOXP3$), $CD8^+$ T cells ($CD8A$, $GZMB$), B cells ($MS4A1$), NK cells ($FCGR3A$, $NCAM1$, $GZMB$), MAIT cells ($RORC$), myeloid cells ($ITGAM$), macrophages ($CSF1R$) and neutrophils ($FUT4$).

6.2 Supplementary Tables

Table S1: Dataset overview. Samples included in the indicated datasets of Project 1 (tisTreg cell analysis, Results Chapter 3.1), Project 2 (Tissue CD8⁺ T cell analysis, Results Chapter 3.2) and Project 3 (Immune cell atlas, Results Chapter 3.3). For murine samples, tissues from several mice were pooled. Mm, *Mus musculus*; Hs, *Homo sapiens*; gn, gnotobiotic.

Sample	Project	Dataset	Pool/Donor	Tissue	Celltype
MD_scATAC_1	1	Mm CD4 ⁺	1-5	Spleen	CD4 ⁺
MD_scATAC_4	1	Mm CD4 ⁺	1-5	Colon	CD4 ⁺
MD_scATAC_5	1	Mm CD4 ⁺	1-5	Fat	CD4 ⁺
MD_scATAC_8	1	Mm CD4 ⁺	6-10	Spleen	CD25 ⁺
MD_scATAC_9	1	Mm CD4 ⁺	6-10	Skin	CD4 ⁺
MD_scATAC_19	1	Mm CD4 ⁺	11-14	Fat	CD4 ⁺
MD_scATAC_21	1	Mm CD4 ⁺	11-14	Spleen	CD25 ⁺
MD_scATAC_40	1	Mm CD4 ⁺	40-41	Lung	CD4 ⁺
MD_scATAC_44	1	Mm gn CD4 ⁺	44-52	Spleen	CD4 ⁺
MD_scATAC_46	1	Mm gn CD4 ⁺	44-52	Spleen	CD25 ⁺
MD_scATAC_47	1	Mm gn CD4 ⁺	44-52	Fat	CD4 ⁺
MD_scATAC_49	1	Mm gn CD4 ⁺	44-52	Colon	CD4 ⁺
MD_scATAC_51	1	Mm gn CD4 ⁺	44-52	Skin	CD4 ⁺
MD_scATAC_11	1	Hs CD4 ⁺	1	Blood	CD4 ⁺
MD_scATAC_13	1	Hs CD4 ⁺	1	Blood	CD25 ⁺
MD_scATAC_14	1	Hs CD4 ⁺	1	Blood	CD25 ⁺
MD_scATAC_15	1	Hs CD4 ⁺	2	Blood	CD4 ⁺
MD_scATAC_17	1	Hs CD4 ⁺	2	Blood	CD25 ⁺
MD_scATAC_18	1	Hs CD4 ⁺	2	Blood	CD25 ⁺
MD_scATAC_28	1	Hs CD4 ⁺	3	Fat	CD4 ⁺
MD_scATAC_30	1	Hs CD4 ⁺	3	Fat	CD25 ⁺
MD_scATAC_31	1	Hs CD4 ⁺	4	Fat	CD4 ⁺
MD_scATAC_33	1	Hs CD4 ⁺	4	Skin	CD4 ⁺
MD_scATAC_35	1	Hs CD4 ⁺	5	Fat	CD4 ⁺
MD_scATAC_37	1	Hs CD4 ⁺	5	Fat	CD25 ⁺
MD_scATAC_38	1	Hs CD4 ⁺	5	Skin	CD4 ⁺
MD_scATAC_53	1	Hs CCR8 ⁺	3	Blood	CCR8 ⁺
MD_scATAC_54	1	Hs CCR8 ⁺	3	Blood	CCR8 ⁺
MD_scATAC_2	2	Mm CD8 ⁺	1-5	Colon	CD8 ⁺
MD_scATAC_3	2	Mm CD8 ⁺	1-5	Spleen	CD8 ⁺

Continued on next page

Sample	Project	Dataset	Pool/Donor	Tissue	Celltype
MD_scATAC_6	2	Mm CD8 ⁺	6-10	Fat	CD8 ⁺
MD_scATAC_10	2	Mm CD8 ⁺	6-10	Skin	CD8 ⁺
MD_scATAC_20	2	Mm CD8 ⁺	11-14	Fat	CD8 ⁺
MD_scATAC_41	2	Mm CD8 ⁺	40-41	Lung	CD8 ⁺
MD_scATAC_45	2	Mm gn CD8 ⁺	44-52	spleen	CD8 ⁺
MD_scATAC_48	2	Mm gn CD8 ⁺	44-52	fat	CD8 ⁺
MD_scATAC_50	2	Mm gn CD8 ⁺	44-52	colon	CD8 ⁺
MD_scATAC_52	2	Mm gn CD8 ⁺	44-52	skin	CD8 ⁺
MD_scATAC_12	2	Hs CD8 ⁺	1	Blood	CD8 ⁺
MD_scATAC_16	2	Hs CD8 ⁺	2	Blood	CD8 ⁺
MD_scATAC_29	2	Hs CD8 ⁺	3	Fat	CD8 ⁺
MD_scATAC_32	2	Hs CD8 ⁺	4	Fat	CD8 ⁺
MD_scATAC_34	2	Hs CD8 ⁺	4	Skin	CD8 ⁺
MD_scATAC_36	2	Hs CD8 ⁺	5	Fat	CD8 ⁺
MD_scATAC_39	2	Hs CD8 ⁺	5	Skin	CD8 ⁺
MD_scATAC_96	2	Hs HCC CD3 ⁺	HCC1	HCC	CD3 ⁺
MD_scATAC_107	2	Hs HCC CD3 ⁺	HCC2	HCC	CD3 ⁺
MD_scATAC_108	2	Hs HCC CD3 ⁺	HCC3	HCC	CD3 ⁺
MD_scATAC_71	3	Mm CD45 ⁺	53-57	Spleen	CD45 ⁺
MD_scATAC_72	3	Mm CD45 ⁺	53-57	Spleen	CD45 ⁺
MD_scATAC_73	3	Mm CD45 ⁺	53-57	VAT	CD45 ⁺
MD_scATAC_74	3	Mm CD45 ⁺	53-57	VAT	CD45 ⁺
MD_scATAC_75	3	Mm CD45 ⁺	53-57	Skin	CD45 ⁺
MD_scATAC_76	3	Mm CD45 ⁺	53-57	Skin	CD45 ⁺
MD_scATAC_77	3	Mm CD45 ⁺	53-57	Colon	CD45 ⁺
MD_scATAC_78	3	Mm CD45 ⁺	53-57	Colon	CD45 ⁺
MD_scATAC_81	3	Hs CD45 ⁺	11	Blood	CD45 ⁺
MD_scATAC_82	3	Hs CD45 ⁺	11	Blood	CD45 ⁺
MD_scATAC_83	3	Hs CD45 ⁺	11	Fat	CD45 ⁺
MD_scATAC_84	3	Hs CD45 ⁺	11	Fat	CD45 ⁺
MD_scATAC_85	3	Hs CD45 ⁺	11	Fat	CD45 ⁺
MD_scATAC_86	3	Hs CD45 ⁺	11	Skin	CD45 ⁺
MD_scATAC_87	3	Hs CD45 ⁺	11	Skin	CD45 ⁺

Table S2: Software used for data analysis. If different versions were used between projects, the project numbers are indicated in brackets.

Package	Version
Cell Ranger atac	1.1.0 (1, 2), 2.0.0 (3)
deepTools	3.5.1
Homer	4.11.1
R	3.6.0 (1, 2), 4.0.0 (3)
refdata-cellranger-atac-mm10-1.1.0	1.1.0
refdata-cellranger-atac-hg19-1.1.0	1.1.0
refdata-cellranger-arc-mm10-2020-A-2.0.0	2.0.0
refdata-cellranger-arc-GRCh38-2020-A-2.0.0	2.0.0
samtools	1.5
Sinto	0.7
UCSC liftOver	-

Table S3: R packages used for data analysis. If different versions were used between projects, the project numbers are indicated in brackets.

Package	Version
ArchR	1.0.1
biomaRt	2.40.5
BSgenome.Hsapiens.UCSC.hg19	1.4.0 (1, 2)
BSgenome.Hsapiens.UCSC.hg38	1.4.3 (3)
BSgenome.Mmusculus.UCSC.mm10	1.4.0
celldex	1.0.0
chromVAR	1.6.0 (1, 2), 1.10.0 (3)
cicero	1.2.0
EnsDb.Hsapiens.v86	2.99.0
EnsDb.Mmusculus.v79	2.99.0
GenomicFeatures	1.36.4
GenomicRanges	1.38.0 (1, 2), 1.40.0 (3)
harmony	1
Homo.sapiens	1.3.1
liftOver	1.12.0
monocle	2.12.0
org.Hs.eg.db	3.8.2
org.Mm.eg.db	3.8.2
Seurat	3.2.1
Signac	1.0.0
SingleCellExperiment	1.6.0
SingleR	1.0.6 (1, 2), 1.2.4 (3)
SummarizedExperiment	1.14.1 (1, 2), 1.18.2 (3)
tidyverse	1.3.0
TxDb.Hsapiens.UCSC.hg19.knownGene	3.2.2 (1, 2)
TxDb.Hsapiens.UCSC.hg38.knownGene	3.10.0 (3)
TxDb.Mmusculus.UCSC.mm10.knownGene	3.4.7

Table S4: Embeddings and resolutions per dataset. The listed embeddings were used for shared nearest neighbour graph calculation. (-) No cell clustering was performed. (*) Human CD4⁺ T cell clusters were used. (**) from Satpathy (2019).

Dataset	Embedding	Resolution
Mouse SPF CD4 ⁺ T cell	Harmony	1.7
Mouse tumor CD4 ⁺ T cell	SVD	0.5
Mouse gnotobiotic CD4 ⁺ T cell	SVD	1.7
Human CD4 ⁺ T cell	Harmony	1.0
Human CCR8 ⁺ T cell	Harmony	-
Human CD4 ⁺ with CCR8 ⁺ T cell	Harmony	*
Mouse SPF CD8 ⁺ T cell	SVD	1.3
Mouse gnotobiotic CD8 ⁺ T cell	SVD	0.5
Human CD8 ⁺ T cell	Harmony	1.0
Human HCC CD3 ⁺	Harmony	1.3
Human melanoma**	Harmony	0.7
Mouse immune cell atlas	IterativeLSI	0.5
Human immune cell atlas	IterativeLSI	0.5

7 List of Abbreviations

- AREG** amphiregulin
- ATP** adenosine triphosphate
- BAM** binary sequence alignment/map
- BATF** basic leucine zipper transcription factor, ATF-like
- bp** base pairs
- bZIP** basic leucine zipper
- cAMP** cyclic adenosine monophosphate
- CCL** CC chemokine ligand
- CCR** CC chemokine receptor
- CD** cluster of differentiation
- CD8^{exh}** exhausted CD8⁺ T cell
- ChIP-seq** chromatin immunoprecipitation following sequencing
- CLP** common lymphoid progenitor cell
- CMP** common myeloid progenitor cell
- CpG** cytosine-guanine dinucleotide
- CTLA4** cytotoxic T-lymphocyte antigen-4
- DC** dendritic cell
- DN** double-negative
- DP** double-positive
- ENTPD1** ectonucleoside triphosphate diphosphohydrolase-1
- FACS** fluorescence-activated cell sorting
- FOXP3** forkhead box P3
- GMP** granulocyte-monocyte progenitor cell
- HCC** hepatocellular carcinoma
- hg** human genome
- HSC** hematopoietic stem cell
- IDO** indoleamine 2,3-dioxygenase
- IFN γ** interferon gamma
- Ig** immunoglobulin
- IL** interleukin
- ILC** innate lymphoid cell
- iNKT** invariant natural killer T cell
- iTreg** induced regulatory CD4⁺ T cell

kb kilo base

Klrg1 killer cell lectin-like receptor subfamily G1

LAG3 lymphocyte-activation gene 3

LMPP lymphoid-primed multipotent progenitor cell

LSI latent semantic indexing

MAIT mucosal-associated invariant cell

mb mega base

MHC major histocompatibility complex

mm *Mus musculus*

MPP multipotent progenitor cell

mRNA messenger RNA

Nfil3 nuclear factor, interleukin 3 regulated

NK cell natural killer cell

PBMC peripheral blood mononuclear cell

PC principal component

PCA principal component analysis

PCR polymerase chain reaction

PD-1 programmed cell death protein 1

PD-L programmed death-ligand

PPAR γ peroxisome proliferator-activated receptor gamma

PRR pattern recognition receptor

pTreg peripherally induced regulatory CD4⁺ T cell

QC quality control

ROR γ RAR-related orphan receptor gamma

scATAC-seq single-cell assay transposase-accessible chromatin using sequencing

scRNA-seq single-cell RNA sequencing

SP single-positive

SPF specific-pathogen-free

ST2 interleukin 1 receptor-like 1

SVD singular value decomposition

Tcm central memory T cell

Tconv conventional CD4⁺ T cell

TCR T-cell receptor

TEC thymic epithelial cell

Tem effector memory T cell

Tfh T follicular helper cell

TF-IDF term frequency-inverse document frequency

TGF β transforming Growth Factor beta

Th cell T-helper cell

TIGIT T cell immunoreceptor with Ig and ITIM domains

tisTreg tissue regulatory CD4+ T cell

TME tumor microenvironment

TNF tumor necrosis factor

TOX thymocyte selection-associated high mobility group box protein

Treg regulatory CD4+ T cell

Trm tissue-resident memory T cell

TSS transcription start site

tTreg thymically derived regulatory CD4+ T cell

UMAP Uniform Manifold Approximation and Projection

VAT visceral adipose tissue

8 Acknowledgment

First, I would like to thank Prof. Dr. Benedikt Brors for giving me the opportunity to pursue a PhD in his group and for his valuable scientific and personal advice during the course of my doctorate.

I want to express my deepest gratitude to Dr. Charles Imbusch, who introduced me to bioinformatics and supported me all along the way, both as a friend and mentor.

Many thanks also to Prof. Dr. Markus Feuerer and Prof. Dr. Michael Delacher for the excellent collaboration and providing high-quality datasets, which enabled a successful analysis in my PhD project.

I would like to thank Prof. Dr. Brors and Prof. Dr. Feuerer for reviewing my dissertation. I also highly appreciate them and Prof. Dr. Stefan Fröhling for their input to my thesis project as members of my thesis advisory committee.

Thanks also to my brother, Dr. Sven Simon, for proofreading my thesis. I am most grateful to Yung Ping Chi, who has always been by my side and supported me in every possible way. Finally, I also want to thank my colleagues, family and friends for their support and making this time especially enjoyable.